EVALUATION OF ADSORBENTS FOR THE SEPARATION OF OLEFINS FROM MULTICOMPONENT PROCESS STREAMS

By

JAMES EARL GRAHAM

Bachelor of Science

Arkansas College

Lyon College

Batesville, Arkansas

1993

Submitted to the Faculty of the
Graduate College of the
Oklahoma State University
in partial fulfillment of
the requirements for
the Degree of
DOCTOR OF PHILOSOPHY
May, 1998

EVALUATION OF ADSORBENTS FOR THE SEPARATION OF OLEFINS FROM MULTICOMPONENT PROCESS STREAMS

Thesis Approved:

Thesis Adviser

Dean of the Graduate College

PREFACE

Currently, olefin/paraffin separation and recovery rely on traditional distillation techniques. These techniques are energy and capital intensive and limited to high capacity refinery crackers. Alternative techniques, based on physical and chemical adsorption, offer the potential to more efficiently and economically separate olefins from paraffin in off-gas purge streams.

Researchers have found that solid adsorbents have the greatest potential for application in industrial olefin separations. Adsorption studies and further research are required to improve adsorption capacities, stabilities, and selectivities of solid chemical adsorbents, design cost effective adsorption processes, and match adsorbents to process streams. The development of an experimental method for the direct measurement of the adsorption of gases from multicomponent streams, under conditions representative of industrial processes, is critical to the success of these efforts.

In this study, an improved laboratory scale technique, herein referred to as Multicomponent Desorption Analysis or MDA, has been developed to measure the adsorption of gases from multicomponent streams under conditions representative of industrial processes. Olefin adsorption capacities and olefin/paraffin selectivities of a family of solid chemical adsorbents, specifically Ag(I) exchanged Amberlyst 15 resins, have been determined as a function of multicomponent stream composition and Ag(I) loading. Adsorption studies indicate that reasonable olefin adsorption capacities are attained on extremely low Ag(I) loaded Amberlyst 15 resins, and that olefin/paraffin selectivities of the Ag(I) exchanged Amberlyst 15 resins increase as the concentration of olefin in the multicomponent decreases. Olefin adsorption capacities of Ca(II), Na(I), and Ni(II) exchanged Amberlyst 15 resins have been measured and show the unique role of

silver in olefin adsorption. The active site(s) for cation exchange on the Amberlyst 15 resin and the active site(s) for ethylene adsorption on cation exchanged Amberlyst 15 resins have been spectroscopically identified. Finally, an active site model for olefin adsorption on the Ag(I) exchanged Amberlyst 15 resin has been proposed.

In summary, a multicomponent desorption analyzer (MDA) for evaluating olefin and paraffin adsorption and olefin/paraffin selectivity under conditions representative of industrial process streams has been designed and constructed. The MDA offers chemists and engineers an improved technique for collecting adsorption data which can be used to better match adsorbents to process streams and design more applicable adsorber units. In addition, researchers have generally assumed that higher adsorption capacities and improved selectivities are achieved on adsorbents having increased and optimized metal loadings. In contrast, unexpectedly high olefin adsorption capacities and olefin/paraffin selectivities were achieved on Ag(I) exchanged Amberlyst 15 resins having extremely low Ag(I) loadings, and data conclusively support that Ag(I) exchanged Amberlyst 15 resins have chemically different Ag(I) exchanged active sites which adsorb olefin. These results should provide new routes for the design, development, and characterization of improved and more cost efficient adsorption technologies which may find commercial application in industrial olefin/paraffin separations.

ACKNOWLEDGMENTS

I would like to thank my advisor, Dr. Corinna Czekaj, for her assistance, unending patience, and direction over the last several years. I would like to thank the members of my graduate committee, Dr. Edward Knobbe, Dr. K. Darrell Berlin, Dr. Warren T. Ford, and Dr. Karen High, for their help and encouragement. I would like to thank Dr. Jan Wagner for the use of his engineering skills. I would like to thank Dr. Margaret Eastman for the use of her spectroscopic expertise. I would like to thank Don Yandle and Robert Parkhill for their time and efforts. I would also like to thank the Department of Chemistry at Oklahoma State University for granting this research opportunity.

In addition, I would like to thank my wife, Tammy Graham, for her patience, love, and understanding during my graduate career. I would like to thank my parents, Vernon and Fern Graham, for their continued love and support. I would like to thank my lab colleagues, Dr. Tammy Metroke and Lisa Phegley, for many graduate memories and deep intellectual conversations. Finally, I would like to thank GOD whom I owe my success.

I would like to acknowledge the Oklahoma State University Chemistry Department, Phillips Petroleum Company, and the Univerity Center for Energy Research at Oklahoma State University for providing the financial funding needed to conduct this study.

TABLE OF CONTENTS

LIST OF TABLES

Table

LIST OF FIGURES

Figure

NOMENCLATURE

a	adsorbent
CP	commercial purity
d	desorbed
EA	ethane
EE	ethylene
g	grams
K	Langmuir constant
m	moles
M	molarity
pa	GC peak area
P	pressure
P_a	atmospheric pressure
P_t	trap pressure
q_m	monolayer or saturated amount adsorbed
q_t	total equilibrium amount adsorbed
R	gas constant
STP	standard atmospheric temperature and pressure
T	temperature
UHP	ultra high purity
V_p	void space volume

V_s	syringe volume
V_t	trap volume
x	mole fraction in vapor phase
Δh_{ads}	heat of adsorption
δ	maximum error

CHAPTER I

INTRODUCTION

Background

Adsorption

History of Adsorption. Even though the term adsorption was not introduced until 1881 by Kayser (1881), the process of adsorption was first recognized by Fontana (1771) and Scheele (1780) while studying the interaction of gases with charcoal (Gregg and Sing, 1982). Fontana (1777) discovered that freshly calcined charcoal was able to adsorb several times its own volume in various gases, and Scheele (1780) discovered that air expelled from charcoal on heating was re-adsorbed on cooling. Today, adsorption is defined as the tendency for molecules from an ambient fluid phase to adhere to the surface of a solid (Ruthven, 1991). In contrast, absorption is defined as the tendency for molecules to only penetrate into the mass of a solid (Gregg and Sing, 1982)

Heat of Adsorption. Satterfield (1991) explained the equilibrium distribution of molecules between the fluid/vapor phase and adsorbed phase using equation 1 and thermodynamic arguments.

(1) $$\Delta G = \Delta H - T\Delta S$$

Since adsorption is a spontaneous process and combines two components, free energy (ΔG) is negative and entropy (ΔS) is reduced. Therefore, adsorption must be an exothermic process with enthalpy (ΔH) larger than $T\Delta S$. The heat released upon adsorption has routinely been calculated using the Clausius-Clapeyron equation 2 where P is pressure, T is temperature, ΔH is heat of adsorption, and R is the gas constant (Gregg and Sing, 1982; Joyner and Emmett, 1948).

(2) $$\left(\frac{\partial \ln p}{\partial T}\right)_v = \frac{-\Delta H}{RT^2}$$

Adsorption Forces. Adsorption is typically characterized as either physisorption or chemisorption (Ruthven, 1991, 1984; Gates, 1992; Satterfield, 1991). Physisorption is a weak interaction characterized by heats of adsorption less than 15 kcal/mol (Yang, 1987). It results from dispersion (London) forces which arise through the changing electron density within an adsorbate. The changing electron density creates a dipole moment within the adsorbate that leads to non-bonding interactions with the adsorbent. Physical adsorption is reversible and non site-specific (Satterfield, 1991). Furthermore, physisorption is of particular interest because it is routinely used in techniques which measure surface area and pore size distribution of materials (Gregg and Sing, 1982). Chemisorption, on the other hand, is a much stronger interaction having heats of adsorption greater than 20 kcal/mol (Yang, 1987). Chemisorption involves the sharing of electrons between adsorbent and adsorbate, resulting in the formation of a chemical bond. Chemisorption may or may not be reversible and is usually site specific (Satterfield, 1991).

Selecting Adsorbents for Application. According to Yang (1987) and Ruthven (1991), the most important adsorbent applications involve separating valuable components from multicomponent streams. Both authors stress that selecting the appropriate adsorbent for a given process stream is not a trivial task. The chosen adsorbent must selectively bind and/or retain the desired component without chemical modification. The adsorbent must also have a high adsorption capacity for the desired component, resist poisoning (i.e. adsorbing undesired components), remain stable under operating conditions, be environmentally friendly, and be easily regenerated (i.e. removal of desired components and/or poisons). As a result, the structure of the adsorbent, as well as the configuration of the adsorber unit, are critical to achieve efficient separations.

The structure of the adsorbent must have active sites (i.e. polar, non-polar, transition metal) for adsorption, high surface areas, and pore sizes greater than the size of the adsorbate (Ruthven, 1991; Yang, 1987). Molecules or atoms at active sites selectively trap and/or bond (physisorb or chemisorb) desired components. High surface areas maximize the number of available active sites. Pores regulate diffusion of the stream components into and out of the adsorbent.

Adsorbents must also have a high selectivity for the component to be separated. Defined by Yang (1987), selectivity is the ability of the adsorbent to selectively remove component *i* from a multicomponent stream. Taking into account the vapor phase and adsorbed phase, selectivity is calculated using equation 3, where $X_{i,j}$ and $Y_{i,j}$ are the equilibrium mole fractions of components *i* and *j*, respectfully, in the adsorbed and gas phase.

(3) $$selectivity = \frac{X_i / Y_i}{X_j / Y_j}$$

Since $X_{i,j}$ and $Y_{i,j}$ are not typically measured, selectivity has been most commonly expressed as an adsorption ratio (Yang and Kikkinides, 1995; Yang et al., 1997; Hirai et al., 1985). The adsorption ratio is based on total uptake of components *i* and *j* in a single component stream and is calculated using equation 4, where q_i and q_j are the total adsorbed quantities of components *i* and *j*, respectively.

(4) $$adsorption\ ratio = \frac{q_i}{q_j}$$

After adsorbent selection, the adsorber unit is designed. The unit design depends on the regeneration method (i.e. how the sorbate and/or poison are removed from the adsorbent), thermodynamics, and diffusion (Lukchis, 1973; Yang, 1987). Possible regeneration methods include temperature swings, pressure swings, and/or inert gas purges

(Ruthven, 1991; Yang, 1987). Selection of the most appropriate regeneration method rests on the strength of the adsorbent-adsorbate interaction, which is directly related to the thermodynamics of adsorption, as previously explained. Diffusion in and out of the pores (i.e. mass transfer) dictates the time needed to achieve maximum uptake and the time required for complete regeneration (Lukchis, 1973; Yang, 1987).

Adsorption Isotherms. Physical and chemical adsorption data are commonly reported in the form of isotherms (Ruthven, 1984, 1991; Knaebel, 1995; Yang, 1987; Satterfield 1991; Gregg and Sing, 1982). Adsorption isotherms express adsorption capacity of the adsorbent as a function of feed composition at constant temperature. The primary utility of the isotherm has been to evaluate the criteria needed for adsorbent selection and adsorber unit design.

Five types of adsorption isotherms have been classified by Brunauer, Emmett, Deming, and Teller (1940) and explained by Greg and Sing (1982). Of the five, type I isotherms are favorable for adsorption and are commonly curve fit using the Langmuir model (Langmuir, 1918).

The basic Langmuir model makes the following assumptions:

1. The adsorption system is in dynamic equilibrium,
2. Adsorbed molecules are held at a fixed number of well defined sites,
3. Each adsorption site can hold only one molecule,
4. The energy of adsorption is a constant over all sites, and
5. There are no interactions between molecules adsorbed on neighboring sites.

Using these assumption, it can be shown that

$$q = q_m \frac{KP}{1+KP}$$

where q is the adsorption capacity, q_m is the monolayer adsorption capacity, K is the Langmuir constant (which is directly related to the Henry constant), and P is the partial

pressure of adsorbate. The Toth isotherm (Toth, 1971) and Unilan isotherm (Honig and Reverson, 1952) are also routinely used to fit adsorption data (Myers and Valenzuela, 1989). The BET isotherm (Brunauer et al., 1938, 1940) is frequently used to evaluate surface area and pore size distribution of adsorbents. A more detailed discussion of isotherms is presented in Chapter V.

Experimental Techniques for Collecting Adsorption Data. Thermal gravimetric analysis (TGA) has been used to study the adsorption of gases on solids (Ackley, 1991; Ackley and Yang, 1991; Yang and Kikkinides, 1995; Yang et al., 1997; Buss, 1995; Vansant, 1994), desorption of gases from solids (Yang and Kikkinides, 1995), and the diffusion of gases through solids (Ackley, 1991; Ackley and Yang, 1991; Yang and Kikkinides, 1995). Even though TGA has been useful for studying single component adsorption, it does have limitations. First, since the masses of the adsorbed components cannot be differentiated, adsorption and desorption analyses are limited to single component streams which have been diluted with a second non-adsorbing gas. Second, since the interaction between the adsorbent and adsorbate cannot be directly characterized, distinguishing the type of adsorption (i.e. physisorption or chemisorption) is based solely on indirect observations. Finally, due to buoyancy, drag, flow, and thermal effects, investigation of adsorption and desorption under temperature and pressure swings representative of industrial processes is not routinely practiced.

Techniques for measuring adsorption in multicomponent streams have been developed. Yang (1987) has classified the techniques for measuring multicomponent gas adsorption into four categories: gravimetric methods, chromatographic methods, constant-volume methods, and dynamic methods. In gravimetric methods, adsorption capacities in multicomponent streams are measured by recording the mass increase of the adsorbent. The composition of the adsorbed phase is calculated using a rigorous thermodynamic technique, which requires measurements of the total mass adsorbed as a function of pressure at constant gas composition and temperature for both the pure gases and gas

mixtures (Van Ness; 1969). Unfortunately, collecting this adsorption data is very time consuming, and the gravimetric techniques, still plagued by the buoyancy, drag, and flow effects previously mentioned, cannot be adequately used to collect adsorption under conditions representative of industrial process streams .

Chromatographic methods involve analysis of breakthrough curves. Breakthrough curves are a time dependent measure of the composition of the gas mixture as it travels through and exits a clean adsorbent bed. In the technique, adsorption capacities are calculated by observing responses in the concentration of the effluent stream after a series of stepped changes in the feed. Unfortunately, these calculations, as noted by Yang (1987), are highly complicated, and the chromatographic methods, which are only accurate under idealized conditions (i.e. dilute mixtures, isothermal operation, and constant pressure), cannot be used to accurately collect adsorption data under conditions representative of industrial process streams.

In constant volume (static) methods, the amount and composition of the absorbed phase are approximated by the difference in the amount and composition of the gas phase mixture, before and after adsorption. The concentration of the gas phase mixture is calculated using pressure, volume, and temperature (PVT) relationships, while gas phase compositions are usually determined using gas chromatography. For example, Mathias and co-workers (1996) described a system for the measurement of oxygen/nitrogen adsorption equilibria on 5A-zeolite. The system consists of a closed loop, which is packed with adsorbent. A gas mixture of known quantity and composition is then introduced into the system and circulated over the adsorbent. After circulation, the quantity and composition of the gas mixture are re-evaluated. Adsorption capacities are calculated using mass balance (i.e. difference in quantity and composition of gas mixture before and after adsorption). Even though the constant volume method allows adsorption to be measured under conditions similar to industrial processes, the technique does not provide information

necessary for selecting regeneration methods such as heating, evacuation, and/or inert purge stream.

In dynamic (flow) methods, equilibrium is assumed to be attained after breakthrough, as indicated by the lack of change in the effluent gas composition. After breakthrough, the adsorbate mixture is quantitatively desorbed by evacuation and/or heating and trapped in nitrogen cooled and/or evacuated vessels. The total amount and composition of the desorbed mixture is measured directly using PVT relationships and gas chromatography, respectively. For example, Shu and co-workers (1990) have described a system for the measurement of propylene/propane adsorption on 13X zeolite. After loading the adsorbent with a compositional feed, the propylene and propane were desorbed at 160 °C, collected, and analyzed by gas chromatography. Even though dynamic flow methods provide data for selecting a regeneration methods, a dynamic flow method, which utilizes an inert purge stream for desorption, has not been recognized.

Thorough review of the methods (i.e. gravimetric, chromatographic, dynamic, and static) for measuring adsorption in multicomponent streams has indicated that an alternative experimental technique is needed which combines time efficiency, the ability to desorb gases under static vacuum, dynamic vacuum, and/or inert gas purge, and the opportunity to directly measure adsorption in multicomponent streams under conditions representative of industrial processes.

Classical Types of Adsorbents. According to Ruthven (1984, 1991) and Yang (1987), the classical types of industrial adsorbents are microporous materials with pore diameters ranging from a few Angstroms to tens of Angstroms. Silica gels, activated aluminas, activated carbons, and zeolites with high surface areas and controlled pore sizes are the most common adsorbents. Since these types of classical adsorbents have been modified for selective adsorption of olefin, a short description of each is presented below.

Silica gel is a polar, microporous adsorbent with a chemical composition expressed as $SiO_2 x H_2O$ (Ruthven, 1984). It is commonly synthesized by mixing sodium silicate solution with mineral acid (Iler, 1979). The reaction produces a concentrated dispersion of hydrated SiO_2. On standing, the SiO_2 polymerize and after drying and activation form linked SiO_4 tetrahedra. Depending on the preparation conditions (i.e. pH, concentration, drying), surface areas and pore sizes of silica gels range from 300-850 m^2/g and 2-15 nm, respectively (Yang, 1987). Silica gel is primary used as a drying agent (Ruthven, 1984, 1991; Yang, 1987).

Activated alumina is a highly polar adsorbent, consisting of linked AlO_4 tetrahedra. It is commercially produced by thermal dehydration or activation of aluminum trihydrate or gibbsite (MacZura et al., 1977). Depending on preparation conditions, typical surface areas of activated alumina range from 250-350 m^2/g (Yang, 1987). The primary uses of activated aluminas include drying agents and chromatography materials (Yang, 1987).

Activated carbon is a non-polar material with a structure consisting of graphite layers stacked together to form a porous framework (Ruthven, 1984). It is prepared by thermal degradation and stream activation of carbonaceous materials. The activation conditions control the pore structure and mechanical strength of the carbon (Yang, 1987). Typical surface areas of activated carbons range from 100-2500 m^2/g, and pore sizes may range from micropores (< 2 nm) to macropores (> 50 nm) (Yang, 1987). Several uses of activated carbon include removal of light organics from gas streams, water purification, and sugar decolorization (Ruthven, 1991)

Zeolites are crystalline materials with a charge balanced framework consisting of silica (SiO_4) and alumina (AlO_4) tetrahedra (Yang, 1987). Zeolites are characterized by a narrow size distribution of external pores that provide and/or restrict access to three-dimensional cavities (Yang, 1987). Zeolites are commercially prepared by mixing aluminum trioxide, silicon dioxide, water, and a charge balancing metal oxide in appropriate ratios (Breck, 1984). The materials copolymerize and crystallize in a

hydrothermal system. Using this technique, over 150 different zeolites, with specific pore sizes and continuous internal cavities, have been synthesized and are designated by numbers and letters (i.e. 5A, 4X, 10Y, ZSM5, etc.) (Yang, 1987). Zeolites are used primarily for separating components from multicomponent streams and catalytic cracking (Collins, 1968; Ruthven, 1991; Yang, 1987).

Olefin Separation and Recovery

Traditional Techniques. The separation and recovery of olefins from paraffin streams are important industrial processes (Eldridge, 1993) and currently rely on traditional techniques, such as low temperature (cryogenic) distillations (Stobaugh, 1966; Tucher, 1959; Chrones, 1961) and extractive distillations (Emmric, 1986: Kumar et al., 1972). Low temperature distillations are performed at elevated pressures in traditional trayed fractionators. A typical ethylene/ethane separation is performed at around -25 °C and 320 psi in a column with over 100 trays (Yang, 1997). Extractive distillations involve use of a polar solvent that changes the relative volatilities of the olefins and paraffins in the mixture, making their fractionation possible. Unfortunately, both techniques are energy and capital intensive, requiring equipment that is expensive to build, operate, and maintain. In addition, the techniques are only feasible for olefin separation and recovery from gas streams containing large quantities of olefins; hence, their utility is limited to high capacity refinery crackers. As a result, alternative technologies, based on physical and chemical adsorbents, have been investigated for separating olefin from paraffin streams.

Physical Adsorbents. Physical adsorbents, which have been studied for selective olefin adsorption, include the classical porous materials such as zeolites, activated carbon, etc. which were previously described. Olefin separation using these materials relies on differences in physisorption strengths and diffusion rates. For example, olefins can be separated from paraffins because the olefins, which replace adsorbed paraffins, diffuse into

the adsorbent at a faster rate; thus, a higher purity paraffin stream initially exits the adsorbent (Schoeller and Mueller, 1986; Shu et al., 1990). When the olefin concentration in the effluent stream breaks through, the adsorbent is regenerated, and the adsorbed olefin is recovered. Alternatively, olefins and paraffins, physisorbed with unequal strengths, can be selectivity removed using specific regeneration methods. For example, Shu et al. (1990) and Kulvaranon et al. (1990) have selectively removed mixtures of propane and propylene from zeolite using variable stepwise temperature desorption. In the system, the more weakly adsorbed paraffin was removed at low temperatures, and the more strongly adsorbed olefin was removed at elevated temperatures. These two studies as well as additional studies of physical adsorbents for selective olefin adsorption are discussed below.

Schoeller and Mueller (1986) demonstrated the utility of modified zeolites for the separation of ethylene and propylene from gas mixture streams containing 10% olefin, paraffin, and nitrogen carrier gas. By replacing Na^+ ion with larger K^+, Ba^{2+}, and Mg^{2+} ions, olefin adsorption and separation were accomplished by blocking the transport of paraffins through the zeolite. Based on breakthrough curves, retention times for ethane and ethylene at 25 °C were 3 min and 15 min respectfully for the Mg^{2+} zeolite. In the separation tests, the olefin was desorbed by heating to temperatures between 293 and 500 K and flowing nitrogen gas through the system. Olefin loadings per gram of adsorbent were shown to depend on the nature of the exchanged ions and were 1.35 mmol/g for K^+, 1.71 mmol/g for Ba^{2+}, and 1.93 mmol/g for Mg^{2+}.

Triebe et al. (1996) have investigated the utility of Ca^{2+} exchanged zeolites to separate ethylene from light paraffin streams. Separation studies on Ca^{2+} zeolite have shown that olefin/paraffin adsorption ratios, reported as ratios of Henry's law constants, range from 100 to 1100. The authors reported a heat of ethylene adsorption on the Ca^{2+} zeolite of 13.9 kcal/mol and attributed the separation to interaction between the olefin and the divalent cationic sites of the zeolite.

Shu et al. (1990) have investigated 13X zeolites in conjunction with variable temperature stepwise desorption (VTSD) for separation and recovery of propylene from streams containing both propylene and propane. The selectivity of the system primarily depends on VTSD, especially since adsorption studies (Danner and Chol, 1978), conducted at 1 atm in pure component streams, have shown that 13X zeolites adsorb approximately equal quantities of propane and propylene. In VTSD method, the zeolite is first exposed to a compositional feed of propylene and propane. Then, the propane is desorbed at 60-80 °C while the more strongly adsorbed propylene is removed at 120-160 °C. Using this system, Shu reported that 90% of the propylene from a 25% propylene/75% propane stream could be recovered.

Kulvaranon et al. (1990) have also investigated the separation and recovery of propylene using VTSD and a 5A zeolite adsorbent. The study reported that 85% of the propylene from a 25 mole% propylene/75 mole% propane stream was recovered with the method. In his report, a preliminary economic comparison between the VTSD method and typical distillation method(s) was also conducted. While operational costs of the VTSD method were found to be more economical, initial investments were twice that of distillation. Based on these results, he suggested that the VTSD method held promise for industrial application, but needed further evaluation.

Chemical Adsorbents. Chemical adsorbents, which have been investigated for selective olefin adsorption, include soluble metal complexes and solid materials both of which contain late transition metals (i.e. copper(I) and silver(I) that facilitate the formation of olefin-metal π-bonds (Blytas, 1990; Keller et al., 1990; Yang and Kikkinides, 1995; Yang et al., 1997; Eldridge, 1993). The olefin-metal π-bond has been explained by Dewar (1951), Chatt, and Duncanson (1953) and is illustrated in Figure 1.

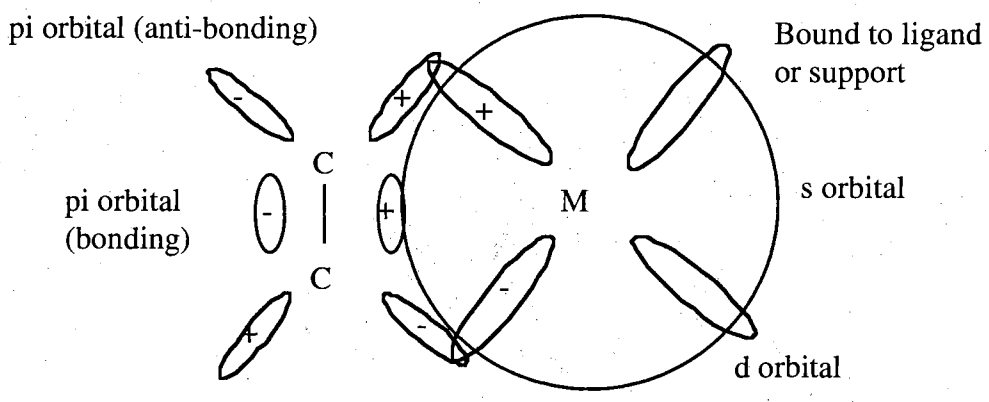

Figure 1. Olefin-metal π-bond.

In the bonding scheme, one metal center binds one olefin molecule through the following interactions: the olefin donates electron density from its π-orbital into the empty s orbital of the metal, and the filled d orbital of the metal donates electron density back (i.e. backbonding) into the empty anti-bonding orbital of the olefin.

The π-bond between olefins and transition metals has been characterized by infrared spectroscopy (Noltes et. al., 1970; Scott, 1973; Tsai and Quinn, 1969; Brandt, 1959). Upon coordination to transition metals, the infrared spectral data have shown that the band of the symmetric stretch of the olefin C=C bond shifts to lower wavenumbers and the band of the inactive CH_2 wag of ethylene shifts to higher wavenumber (Yates et al., 1966). The degree of C=C shift has routinely been correlated with olefin-metal bond strength (e.g. larger shift = stronger bond) (Elschenbroich and Salzer, 1992).

Since paraffins do not π-bond, the olefin-metal π -bond has provided a route to design more selective olefin adsorbent. As a result, a large number of chemical adsorbents have been investigated for selective olefin adsorption. A representative set of soluble and solid chemical adsorbents are listed in Table 1 and reviewed below.

Table 1. Chemical Adsorbents Investigated for Olefin Adsorption

adsorbent	references
Copper(I) Zeolites	Xie, 1990; Pearce, 1988; Cen, 1990
Copper(I) Activated Alumina	Linlin, 1984
Copper(I) Activated Carbon	Hirai, 1988
Copper(I) Clays	Yang, 1995
Copper(I) and Silver(I) soluble complexes	Blytas, 1990; Keller, 1990; Doyle, 1988; Komiyama, 1989; Tabler, 1985
Copper(I) and Silver(I) resins	Yang and Kikkinides, 1995; Yang et al., 1997; Hirai et al., 1985

Soluble Chemical Adsorbents. Blytas (1990) has reviewed the area of copper(I) salts dissolved in hydrocarbon solvents for separating olefins from paraffins. Adsorption studies, conducted at 1 atm and 50 °C, have shown that a 1 M xylene solution of copper (I) trifluoroacetate adsorbs 0.76 mmol of propylene per gram of solution, has a propylene/Cu(I) mole ratio of 0.8, and a propylene/propane adsorption ratio of 14. Adsorption studies, conducted on a series of the copper(I) salt solutions, pointed out that adsorption ratios increased at higher salt concentrations but dramatically decreased at pressures greater than 1 atm.

Keller et al. (1990) have reviewed aqueous silver(I) salts for separating olefins from paraffins. Adsorption studies, conducted at 1 atm and 25 °C, have demonstrated that a 3 M silver nitrate solution adsorbs 0.92 mmol of ethylene per gram of solution and has an ethylene/silver(I) mole ratio of 0.46. Additional studies determined a heat of olefin adsorption of 4.8 kcal/mol. The report also mentioned that olefin adsorption capacities of a

series of silver(I) nitrate solutions increased with increasing salt concentrations; however, this trend was paralleled by a dramatic drop in the ethylene/silver mole ratio.

Doyle et al. (1988) have investigated copper(I) diketonates, stabilized by coordinating olefinic solvent, for separating olefins from paraffins. Adsorption studies, conducted on copper(I)hexafluoroacetonate in α-methylstyrene at 1.18 atm and 28 °C, have shown that a copper diketonate solution has an ethylene/copper(I) mole ratio of 0.8 and has a ethylene/ethane adsorption ratio of 17. Based on Cu(I)-olefin interactions, the olefin was proposed to displace the coordinating solvent. In the studies, the olefin was recovered by heating or depressurization.

Methanol solutions of copper(I) chloride-ethylenediamine complex have been investigated by Komiyama (1989). Adsorption studies, conducted at 1 atm and 20 °C, have shown that a 1.3 M methanol solution of the copper complex adsorbs 0.52 mole ethylene and 0.03 mole of ethane per liter of solution, corresponding to an ethylene/ethane adsorption ratio of 17. The report also stated that the selectivity was greatly enhanced at higher concentrations of the copper(I) chloride-ethylenediamine complex; however, at higher concentrations, the salt was reported to precipitate out of solution.

Tabler (1985) has evaluated olefin adsorption in hydrocarbon solutions of copper(I) cyanide-aluminum chloride complex. Adsorption studies, conducted at 0.9 atm and 25 °C, have indicated that a 3 M xylene solution of copper cyanide-aluminum chloride complex adsorbs 2.94 mole of ethylene/1 L of solution, corresponding to an ethylene/copper mole ratio of 1.1. The report concluded that the expected 1:1 mole ratio of ethylene/copper(I) was exceeded due to alkylation of olefin with solvent. Olefin/paraffin selectivities of the complex were not evaluated in the study.

Solid Chemical Adsorbents. Hirai et al. (1985) reported the utility of copper(I) chloride immobilized on polystyrene resins having primary and secondary amino groups

for olefin separations. Adsorption studies at 20 °C and 1 atm in single component streams, have shown that the copper(I) chloride resin adsorbs 0.6 mmol/g of ethylene and 0.076 mmol/g of ethane corresponding to an ethylene/ethane adsorption ratio of 7.9. By studying a series of copper(I)chloride loaded resins, olefin adsorption capacities were found to increase to a maximum at a Cu(I)Cl loading of 15 mmol copper(I)chloride/g of resin, and the olefin/copper(I) mole ratios were shown to decrease as the copper(I)chloride loadings increased. Assuming maximum exchange capacity (3.85 meq/g) for the resins, the ethylene/copper(I) mole ratios for all samples were less than 0.16.

Olefin adsorption on activated carbon impregnated with copper(I) chloride has been investigated by Hirai et al. (1988). Adsorption studies conducted at 20 °C and 0.9 atm have shown that the copper(I) chloride activated carbon adsorbs approximately 0.31 mmol/g of ethylene, corresponding to an ethylene/copper mole ratio of 0.2.

Linlin et al. (1984) evaluated ethylene adsorption by copper(I) chloride dispersed on activated alumina. In studying a series of the different copper(I) chloride loaded alumina samples, it was shown that ethylene adsorption (4.95 ml/g) reached a maximum at a loading ratio of 0.31 g Cu(I)Cl/g alumina and that the ethylene/copper(I) mol ratio (0.19 at lowest copper(I)chloride loading) decreased with higher copper(I)chloride loadings.

Copper(I) zeolites have been investigated for olefin adsorption by Xie et al. (1990). Studies conducted in single component streams at 25 °C and 1 atm have shown that copper(I) zeolites have a large ethylene adsorption capacity (4.4 mmol/g). In addition, studies, conducted on the copper(I) zeolite in mixture streams composed of 10% ethylene and 90% inerts and hydrocarbons, have shown that the offgas in the first 20 min was only 10 ppm of ethylene and the total ethylene uptake was 2.2 mmol/g. In the system, ethylene was desorbed by heating and evacuating at 150 °C.

Yang and Cheng (1995) have investigated pillared interlayered clays impregnated with copper(I) chloride for the separation of ethylene and ethane. Adsorption studies, conducted at 1 atm and 25 °C in single component streams, have shown that the copper(I) chloride TiO_2-clay adsorbs 0.58 mmol/g of ethylene and 0.1 mmol/g ethane, corresponding to an adsorption ratio of 5.3. The authors reported a heat of ethylene adsorption on the copper(I) TiO_2-clay of 13.7 kcal/mol. Additional adsorption studies, conducted on a series of different copper(I)chloride loaded clay samples, indicated a maximum ethylene adsorption capacity on a clay with a copper(I)chloride/clay mole ratio of 0.38. In addition, it was shown that the ethylene/copper(I) mole ratio (0.38 at lowest copper(I) loading) steadily declined as the copper(I)chloride loadings increased.

The separation of ethylene from ethane using silver(I) exchanged sulfonated polystyrene divinylbenzene resins (Amberlyst 15 and 35) has been investigated by Yang and Kikkinides (1995) and Yang et al. (1997). Adsorption studies, conducted at 25 °C and 1 atm in single component streams, have shown that a 51.2% Ag(I) exchanged Amberlyst 15 resin adsorbs 1.15 mmol/g of ethylene and 0.125 mmol/g of ethane, corresponding to an adsorption ratio of 9.2 and an ethylene/Ag(I) mole ratio of 0.4. Adsorption studies, conducted at 25 °C and 1 atm in single component streams,indicated that a 36.5% Ag(I) exchanged Amberlyst 35 resin adsorbs 1.48 mmol/g of ethylene and 0.231 mmol/g of ethane, corresponding to a ethylene/silver adsorption ratio of 0.64 and ethylene/Ag(I) mole ratio of 0.78. In addition, a series of Ag(I) exchanged Amberlyst 35 resins (range: 31-64% of ex. capacity) were evaluated for ethylene and ethane adsorption at RT and 1.7 atm in single component streams. The data indicated that; the ethylene/ethane adsorption ratio was maximized on a 45% Ag(I) exchanged Amberlyst 35 resin and dropped afterwards; the ethylene adsorption capacity was maximized on a 36.5% Ag(I) exchanged Amberlyst 35 resin; and the ethylene/silver mole ratio (initially 0.97), dropped dramatically at higher Ag(I) loadings. On all the Ag(I) resins, the heat of ethylene adsorption ranged from 9-11

kcal/mol, and approximately 10% of the ethylene was irreversibly adsorbed. The authors reported that the irreversibly adsorbed ethylene was removed at 100 °C, restoring the adsorption capacities of the resin.

Statement of Problem

As presented, physical and chemical adsorbents are available for separating olefins from multicomponent streams; however, few have found industrial application in olefin separation. The physical adsorbents have large adsorption capacities but very poor selectivities, adsorbing both paraffins and olefins equally well (Hirai et al., 1985, 1988). The soluble chemical adsorbents have good selectivities but low adsorption capacities (Hirai et al., 1985, 1988). In addition, they are extremely sensitive to air, water, oxygen, and solvent and have a strong tendency to precipitate out of solution (Blytas, 1990; Keller et al., 1990; Tabler, 1985; Komiyama, 1989). The solid chemical adsorbents, as noted by Yang and Kikkinides (1995), Yang et al. (1997), Hirai et al. (1985, 1988), and Eldridge (1993), hold the most potential for application in industrial olefin separations; however, additional adsorption data and further research are required to improve adsorption capacities, stabilities, and selectivities of solid chemical adsorbents, design cost effective adsorption processes, and match adsorbents to process streams.

Research Goals

The main objective of this study has been to further evaluate olefin adsorption on cation exchanged Amberlyst 15 resins using improved experimental adsorption techniques and spectroscopic techniques. The cation exchanged Amberlyst 15 resins were chosen for this study because, when compared with other olefin adsorbents, the resins have been shown to offer increased olefin adsorption capacities, larger metal loadings, and stabilities required for adsorption and spectroscopic characterization. Since a commercially viable olefin adsorbent is not currently available, the goals of the study, listed below, focus on

introducing alternative techniques for characterizing adsorption and discovering new information which can be applied to the design and development of improved olefin adsorbents.

The goals of this study were:

(1) To develop and verify an improved method, which combines static and dynamic volumetric techniques to measure olefin and paraffin adsorption capacities and olefin/paraffin selectivities under conditions representative of industrial processes.

(2) To measure olefin adsorption capacities and determine olefin/paraffin selectivities of Ag(I) exchanged Amberlyst 15 resins as a function of multicomponent stream composition, cation exchange, and metal loading.

(3) To measure olefin adsorption capacities of Ca(II), Na(I), and Ni(II) exchanged Amberlyst 15 resins.

(4) To fit olefin adsorption data collected on Ag(I) exchanged Amberlyst 15 resins using the Yang and Kikkinides, Langmuir, Toth, and Unilan isotherms.

(5) To characterize the active site(s) for ion exchange on the Amberlyst 15 resin.

(6) To spectroscopically characterize olefin adsorption on Ag(I) exchanged Amberlyst 15 resin.

(7) To propose active sites for olefin adsorption on Ag(I) exchanged Amberlyst 15 resins.

Summary of Chapters

In Chapter II, a thermal gravimetric analyzer, which was used to collect temperature dependent ethylene and ethane adsorption isotherms, is described. An improved multicomponent desorption analyzer (MDA), which combines gas chromatography and volumetric methods to measure temperature dependent equilibrium adsorption of ethylene and ethane as a function of multicomponent stream composition under conditions representative of industrial processes, is described. The synthetic method used to prepare

the cation exchanged Amberlyst 15 resins is presented. Nitrogen adsorption, mercury porosimetry, scanning electron microscopy (SEM), energy dispersive x-ray adsorption spectroscopy (EDXAS), nuclear magnetic resonance spectroscopy (NMR), and diffuse reflectance infrared fourier transform spectroscopy (DRIFTS), which are used to characterize the unexchanged and cation exchanged Amberlyst 15 resins and the nature of the interaction between olefin and Ag(I) exchanged Amberlyst 15 resin, are presented.

In Chapter III, nitrogen adsorption data, mercury porosimetry data, scanning electron microscopy (SEM) images, energy dispersive x-ray adsorption spectroscopy (EDXAS) profiles, nuclear magnetic resonance spectroscopy (NMR) spectra, and diffuse reflectance infrared fourier transform spectroscopy (DRIFTS) spectra, collected on unexchanged and Ag(I) exchanged Amberlyst 15 resins, are presented and discussed. In agreement with previous reports, the DRIFTS and NMR spectra indicate; (1) the sulfonate groups are the active sites for ion exchange on the Amberlyst 15 resin; (2) the hydration structure of the Amberlyst 15 resin is reorganized by ion exchange; and (3) the Amberlyst 15 resins contain significant quantities of moisture even after extensive drying. The nitrogen adsorption data, mercury porosimetry data, and SEM images suggest that the physical structure of the Amberlyst 15 resin is not modified by Ag(I) exchange. The EDXAS profiles indicate that Ag(I) is homogeneously dispersed within the Amberlyst 15 resin bead.

In Chapter IV, temperature dependent ethylene and ethane adsorption data, collected on Ag(I) exchanged Amberlyst 15 resins as a function of binary stream composition and Ag(I) loading using the TGA and MDA, are reported and discussed. The extent of Ag(I) exchange on the Amberlyst 15 resins, estimated by weight analysis and determined by elemental analysis, is presented. DRIFTS-HTEC spectra, used to characterize the nature of the interaction between olefin and 61% Ag(I) exchanged Amberlyst 15 resin, are presented and discussed. When compared with elemental analysis, weight analysis shows to be highly inaccurate for measuring the extent of ion exchange on Amberlyst 15 resins. Gas

chromatography analysis of CP grade ethane sets precedence for the evaluation of gas purities in future adsorption studies. When compared with the TGA, the adsorption results indicate that the MDA is a comparable technique which collects adsorption data under conditions more representative of industrial processes. In agreement with previous predictions, the adsorption data indicate that ethylene/ethane selectivities of the Ag(I) exchanged Amberlyst 15 resins dramatically increase as the concentration of ethylene in a binary stream decreases. Although unprecedented in the literature, our adsorption data show that extremely low Ag(I) loaded Amberlyst 15 resins have surprisingly high olefin adsorption capacities and olefin/paraffin selectivities. Contradictory to previous infrared studies and adsorption predictions, the DRIFTS spectra and adsorption data suggest that ethylene is primarily physisorbed on the Ag(I) exchanged Amberlyst 15 resin. The combination of nitrogen adsorption data, mercury porosimetry data, EDXAS profiles, temperature dependent adsorption data collected as a function of Ag(I) loading, and DRIFTS-HTEC spectra suggest that the Ag(I) exchanged Amberlyst 15 resin contain unequivalent Ag(I) exchanged active sites for adsorption.

In Chapter V, curve fits of the ethylene adsorption data collected on 61% Ag(I) exchanged Amberlyst 15 resin are presented. In addition, the physisorbed and chemisorbed fractions of ethylene on 51.7% Ag(I) exchanged Amberlyst 15 resin, estimated from the previously reported Yang and Kikkinides isotherm equation, are reported. The curve fits indicate that the Langmuir, Toth, Unilan, and Yang and Kikkinides isotherm equations adequately represent the ethylene adsorption isotherm and that previously proposed models for ethylene adsorption on Ag(I) exchanged Amberlyst 15 resins do not adequately represent ethylene adsorption on Ag(I) exchanged Amberlyst 15 resin. As previously suggested, the curve fits provide no evidence to distinguish sites for ethylene adsorption on Ag(I) exchanged Amberlyst 15 resins.

In Chapter VI, ethylene adsorption isotherms, collected on Ca(II), Na(I), and Ni(II) exchanged Amberlyst 15 resin, are reported. In addition, DRIFTS spectra of Ca(II) and

Na(I) exchanged Amberlyst 15 resins are presented. The adsorption isotherms illustrate the unique role of silver in olefin adsorption on cation exchanged Amberlyst 15 resin. In agreement with conclusions in Chapter III, DRIFTS spectra indicate; (1) the sulfonate groups are the active sites for ion exchange on the Amberlyst 15 resin; (2) the hydration structure of the Amberlyst 15 resin is reorganized by ion exchange; and (3) the Amberlyst 15 resins contain significant quantities of moisture.

In Chapter VII, nuclear magnetic resonance spectroscopy (NMR) spectra of model compounds, which represent the monomer unit of the Amberlyst 15 resins, are presented and discussed, and an active site model for ethylene adsorption on Ag(I) exchanged Amberlyst 15 resins is proposed. Model compound studies show that Ag(I) does not preferentially interact with unsaturated systems of the Amberlyst 15 resins, ruling out possible Ag(I)-unsaturated sites for ethylene adsorption on the Ag(I) exchanged Amberlyst 15 resins. The experimental data indicate that ethylene is not physisorbed in pockets or trapped in isolated areas of the resin created during Ag(I) exchange. In agreement with previous ion exchange studies of macroreticular ion exchange resins, the experimental data indicate that Ag(I) exchanged Amberlyst 15 resins have different exchange sites which preferentially exchange Ag(I) cation resulting in Ag(I) sites which have different affinities for ethylene.

In Chapter VIII, future investigations of cation exchanged Amberlyst 15 resins are discussed.

Summary Statement

In summary, a multicomponent desorption analyzer (MDA) for evaluating olefin and paraffin adsorption and olefin/paraffin selectivity under conditions representative of industrial process streams has been designed and constructed. The MDA offers chemists and engineers an improved technique for measuring multicomponent adsorption data which can ultimately be used to better match adsorbents to process streams and design more

applicable adsorber units. In addition, researchers have generally assumed that higher adsorption capacities and improved selectivities are achieved on adsorbents having increased and optimized metal loadings. In contrast, unexpectedly high olefin adsorption capacities and olefin/paraffin selectivities are achieved on Ag(I) exchanged Amberlyst 15 resins having extremely low Ag(I) loadings and data conclusively support that Ag(I) exchanged Amberlyst 15 resins have chemically different Ag(I) exchanged active sites which adsorb olefin. These results should provide new routes for the design, development, and characterization of improved and more cost efficient adsorption technologies which may find commercial application in industrial olefin/paraffin separations.

CHAPTER II

EXPERIMENTAL METHODS AND PROCEDURES

Summary

In Chapter II, a thermal gravimetric analyzer, which was used to collect temperature dependent ethylene and ethane adsorption isotherms, is described. An improved multicomponent desorption analyzer (MDA), which combines gas chromatography and volumetric methods to measure temperature dependent equilibrium adsorption of ethylene and ethane as a function of multicomponent stream composition under conditions representative of industrial processes, is described. The synthetic method used to prepare the cation exchanged Amberlyst 15 resins is presented. Nitrogen adsorption, mercury porosimetry, scanning electron microscopy (SEM), energy dispersive x-ray adsorption spectroscopy (EDXAS), nuclear magnetic resonance spectroscopy (NMR), and diffuse reflectance infrared fourier transform spectroscopy (DRIFTS), which were used to characterize the unexchanged and cation exchanged Amberlyst 15 resins and the nature of the interaction between olefin and Ag(I) exchanged Amberlyst 15 resin, are presented.

Preparation of Ion Exchanged Amberlyst 15 Resins

Materials

$AgNO_3$, $NaNO_3$, $Ca(NO_3)_2 \cdot 4H_2O$, and $Ni(NO_3)_2 \cdot 6H_2O$, Amberlyst 15 resin, and methanol were purchased from Aldrich and used as received. Deionized (DI) water was prepared in-house using a Barnstead E-pure filter system. The conductivity of the DI water was 5.49×10^{-6} ohm·m (i.e. resistivity of 18.2 megohms·cm).

Ion Exchange

Ag(I), Ca(II), Ni(II) and Na(I) exchanged Amberlyst 15 resins were prepared following a procedure reported by Yang and Kikkinides (1995). Before exchange, 200 g of Amberlyst 15 resin was prepared by washing with 300 mL of DI water and 300 mL of methanol followed by drying in air at 100 °C for 24 h. In a typical exchange, a selected volume and molarity of aqueous metal salt was added to a preweighed quantity of prepared Amberlyst 15 resin and exchanged for 14 hr at RT. The solution was then decanted, and the exchange successively repeated. After a set number of exchanges, the cation exchanged Amberlyst 15 resin was washed with 100 mL of DI water and 100 mL of methanol, dried in air at 100 °C for 24 h, and stored in air. The extent of Ag(I) ion exchange was determined by elemental analysis and weight increase after exchange. The extent of Na(I), Ca(II), and Ni(II) ion exchange were not measured, because a significant weight increase was not observed after exchange. The details of the Ag(I), Ca(II), Na(I), and Ni(II) exchanges are summarized in Tables 2, 3, 4, and 5 respectfully.

Table 2. Synthesis of Ag(I) Exchanged Amberlyst 15 Resin

resin, g	$AgNO_3$ conc., M	$AgNO_3$ volume, mL	number of exchanges	extent of exchange, % elemental analysis	extent of exchange, % weight analysis	error, %
5.000	0.014	20.0	5	7.0	na	na
3.047	0.07	16.8	3	16	12.5	28
2.978	0.07	20.1	2	19.6	14	29
3.011	0.07	20.1	3	29	21.8	25
3.002	0.07	30.2	3	42.6	34.9	18
5.000	0.07	100	5	61	75.1	23

Table 3. Synthesis of Ca(II) Exchanged Amberlyst 15 Resin

resin, g	$Ca(NO_3)_2 \times 4H_2O$ conc., M	$Ca(NO_3)_2 \times 4H_2O$ volume, mL	number of exchanges
2.000	0.07	100	5

Table 4. Synthesis of Na(I) Exchanged Amberlyst 15 Resin

resin, g	$NaNO_3$ conc., M	$NaNO_3$ volume, mL	number of exchanges
1.030	0.014	100	4

Table 5. Synthesis of Ni(II) Exchanged Amberlyst 15 Resin

resin, g	$Ni(NO_3)_3 \times 6H_2O$ conc., M	$Ni(NO_3)_3 \times 6H_2O$ volume, mL	number of exchanges
2.069	0.07	100	2

Thermal Gravimetric Analysis

Thermal Gravimetric Analyzer. Temperature dependent pure gas adsorption and desorption isotherms of ethylene and ethane were collected using a Cahn System 113 Microgravimetric 2000 Balance (TGA), displayed in Figure 2.

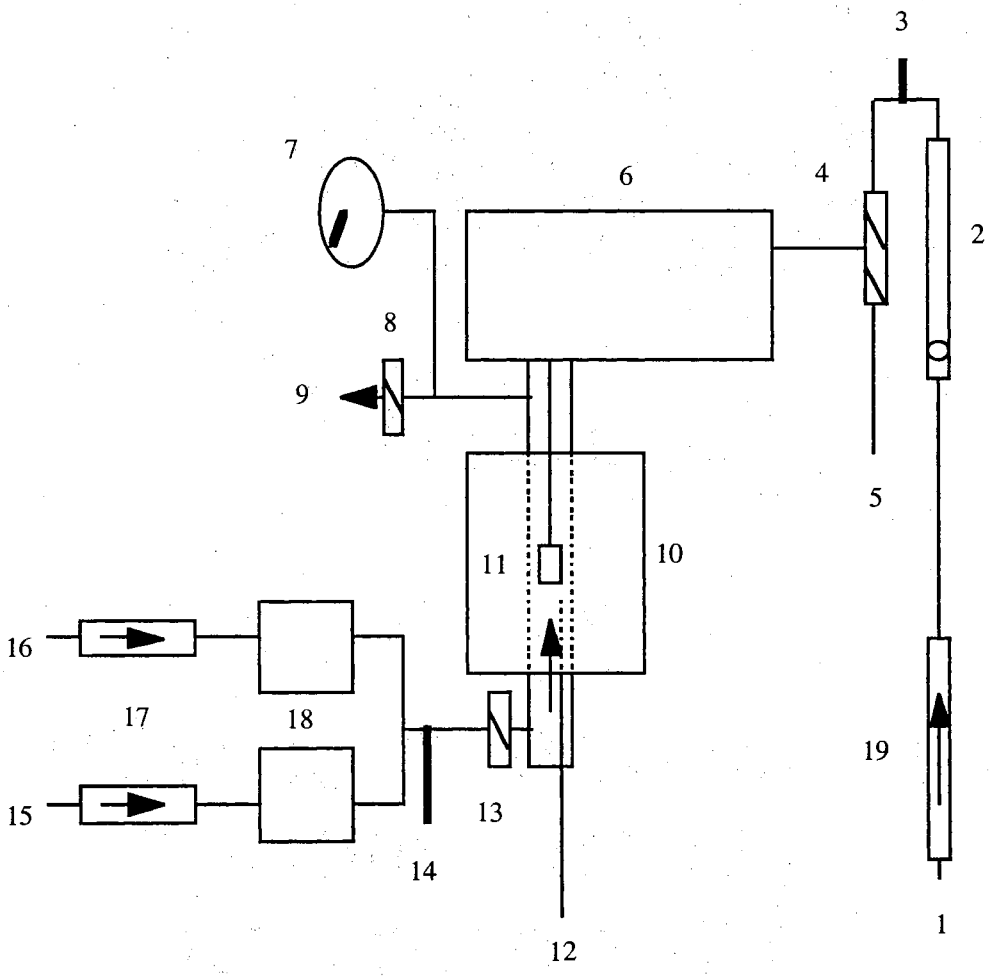

Figure 2. Thermal gravimetric analyzer. 1. Helium feed. 2. Manual flowmeter. 3. Blowoff valve. 4. 3-way valve. 5. Vacuum pump. 6. Balance. 7. Pressure gauge. 8. 3-way valve. 9. Vent. 10. Furnace. 11. Sample pan. 12. Thermocouple. 13. 2-way valve. 14. Blowoff valve. 15. Hydrocarbon feed. 16. Helium feed. 17. Drying column. 18. Electronic flow controllers. 19. Drying column.

The TGA consists of two Brooks 5890C electronic flow controllers, which regulate and maintain the flow of helium and hydrocarbon mixtures in the sample chamber at 500 mL/min; a manual flowmeter, which regulates and maintains helium purge flow at 100 mL/min; a Micricon 823 temperature program controller, a furnace, and a J-type thermocouple, which monitor and regulate the temperature of the sample; a microbalance, which measures the weight of the sample on a 100 μg scale; and a Precision Scientific D-75 vacuum pump.

Materials. CP grade ethane, CP grade ethylene, and UHP grade helium were purchased from Sooner Air. Gas chromatography (GC) was used to determine the purity of the hydrocarbons. While the ethylene was found to be pure, chromatography results indicated that the ethane was contaminated with 1% residual ethylene. For moisture removal, ethylene and ethane were passed through an Alltech gas purifier drying column, and helium was passed through an Alltech hydro-purge drying column.

Buoyancy and Drag. Buoyancy and drag of the sample in different compositional streams of helium and hydrocarbon create variations in sample weight due to changes in the density and viscosity of the gas mixture. Therefore, buoyancy corrections and drag corrections, which are required to accurately calculate total uptake, were evaluated for each compositional stream.

Buoyancy corrections were collected using the following procedure. A 50.0 mg non-adsorbing blank was placed in the sample cup, the balance was outgassed (2.6×10^{-5} Torr), and the sample weight recorded. Helium purge was then used to return the balance to atmospheric pressure, and the sample weight was recorded. Then, the first compositional stream of helium and hydrocarbon was introduced into the sample chamber. After the compositional stream was interrupted, the weight of the sample fell compared to the starting weight. The difference between the starting weight and final weight was the buoyancy correction for this compositional stream. The procedure was repeated for each

compositional stream of helium and hydrocarbon. The buoyancy corrections for all the compositional streams of helium and hydrocarbon are presented in Appendix A.

Drag corrections were collected using the following procedure. A 50.0 mg non-adsorbing blank was placed in the sample cup, the balance was outgassed (2.6×10^{-5} Torr), and the sample weight recorded. Helium purge was then used to return the balance to atmospheric pressure and the sample weight recorded. Then, the first compositional stream of helium and hydrocarbon was introduced into the sample chamber, and the weight of the sample was observed to drop. The difference between the starting weight and the final weight was the drag correction for this compositional stream. The procedure was repeated for each compositional stream of helium and hydrocarbon. The drag corrections for all the compositional streams of helium and hydrocarbon are presented in Appendix A.

Ethylene and Ethane Adsorption Isotherms Collected at RT. In a typical analysis, approximately 50 mg of sample was placed in the sample pan and outgassed to a constant weight. Helium purge was used to return the balance to atmospheric pressure and maintained. A compositional stream of helium and hydrocarbon gas was then introduced into the sample chamber and maintained until an equilibrium weight was achieved. In a typical run, equilibrium was achieved in approximately 5-10 min. Hydrocarbon flow into the sample chamber was then stopped, the total weight gain recorded, and the subsequent compositional flow of helium and hydrocarbon initiated. The procedure was repeated for each compositional stream of helium and hydrocarbon. Uptake of hydrocarbon was calculated using equation 5.

(5) uptake = (weight gain + buoyancy correction) - initial vacuum weight

Sample TGA calculations are presented in Appendix A.

Ethylene Desorption Isotherms Collected at RT. After equilibrium adsorption was attained in a pure hydrocarbon stream at RT and 1.0 atm, equilibrium desorption was achieved by repeating the adsorption procedure in reverse order and eventually outgassing

to constant weight. Equilibrium desorption typically required 10-15 min while complete outgassing required 2-4 h. Desorption of hydrocarbon was calculated using equation 6.

(6) desorption = (weight gain + buoyancy correction) - final vacuum weight

Ethylene Adsorption Isotherms Collected at 60 °C. The RT adsorption procedure was slightly modified since erratic weight fluctuations occurred when sample flow was interrupted at 60 °C. As reported by Ackley (1991), erratic weight fluctuations, resulting from convection currents in the sample tube and temperature overshoot of the furnace, are a common problem in gravimetric analyses at elevated temperature. In a typical analysis at 60 °C, approximately 50 mg of sample was placed in the sample pan and outgassed to a constant weight. Helium purge was then used to return the balance to atmospheric pressure at which point the temperature was adjusted to 60 °C, and the sample weight was recorded. A compositional stream of helium and hydrocarbon was then introduced into the sample chamber and maintained until an equilibrium weight was achieved. The weight was recorded, and the next compositional stream of helium and hydrocarbon was initiated. The procedure was repeated for each compositional stream of helium and hydrocarbon. Hydrocarbon uptake was calculated using equation 7.

(7) uptake = flow weight - (helium weight - buoyancy weight - drag weight)

Heats of Ethylene Adsorption. Knowing equal volumes of ethylene adsorbed at two different partial pressures and two different temperatures allowed the heat of ethylene adsorption (ΔH_{ads}) to be calculated using equation 8.

(8) $$-\Delta H_{ads} = Ln\frac{P_2}{P_1}R\left(\frac{T_1T_2}{T_2 - T_1}\right)$$

Multicomponent Desorption Analysis

Multicomponent Desorption Analyzer. An in-house constructed, multicomponent desorption analyzer (MDA), displayed in Figure 3, was used to measure temperature dependent equilibrium adsorption of ethylene and ethane on the cation exchanged Amberlyst 15 resins as a function of binary stream composition and metal loading.

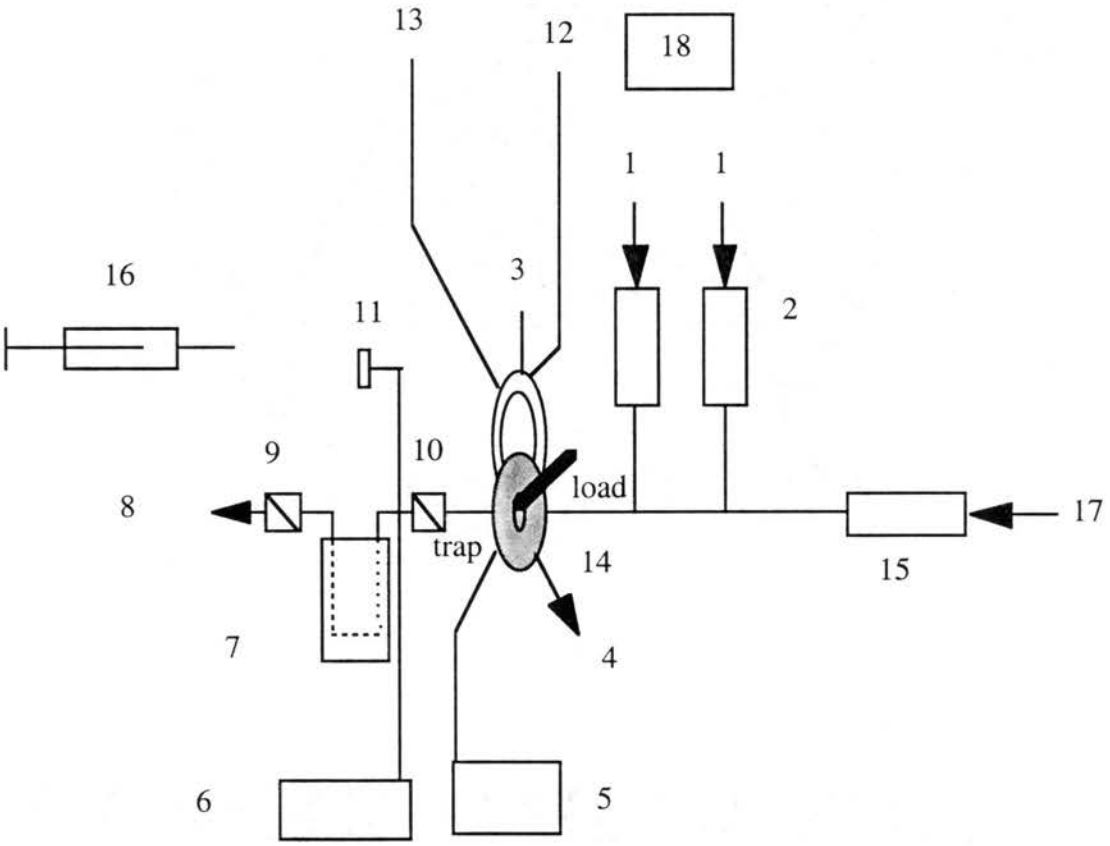

Figure 3. Multicomponent desorption analyzer. 1. Hydrocarbon feed. 2. Electronic flow controllers. 3. Adsorbent loop. 4. Vent. 5. Vacuum gauge. 6. Pressure transducer. 7. Cold trap. 8. Vacuum. 9. 2-way valve. 10. 2-way valve. 11. Septum. 12. Heating cord. 13. Thermocouple. 14. 6-way valve. 15. Electronic flow controller. 16. GC syringe. 17. Argon. 18. Variac.

The MDA consists of a variac, heating cord, and +/- 1 °C J-type thermocouple, which regulate and monitor the temperature of the adsorbent loop; a +/- 0.05% sensitivity 0-50.00 psi Sensotech pressure transducer, which provides the pressure of desorbed components; a gas chromatograph, which analyzes the composition of the desorbed components; an Alltech 6-way valve, a cold trap section, a Welch 1405 vacuum pump, and two Brooks 5890C electronic flow controllers, which regulate the composition of the binary gas mixture and maintain the binary gas mixture flow at 50 mL/min.

Materials. CP grade ethane, CP grade ethylene, UHP grade argon, zero grade air, UHP grade hydrogen, and CP grade nitrogen were purchased from Sooner Air and used as received. As discussed previously, GC analysis indicated that the ethane was contaminated with residual ethylene.

Ethylene and Ethane Calibration Curves. For analyzing gas mixture compositions, ethylene and ethane calibration curves were prepared using the MDA cold trap and a Hewlett Packard 5890 Series 2 Plus Chemstation Gas Chromatograph (GC). For collecting the calibration data, the MDA cold trap was outgassed, isolated, and filled with ethylene or ethane to approximately 1.00 atm at RT. Then, a 10.0 µl sample of the gas in the cold trap was injected into the GC using a gas tight syringe. Knowledge of the volume, pressure, and temperature of the gas allowed the total moles of the gas injected to be calculated using equations 9 or 10.

(9) $$\text{total mEE injected} = P_t \cdot V_s / R \cdot T$$

(10) $$\text{total mEA injected} = P_t \cdot V_s / R \cdot T$$

The procedure was repeated 4 times at 1 atm and 5 times at trap pressures of 0.61, 0.41, 0.20, & 0.12 atm, providing 25 ethylene and 25 ethane calibration points.

For the GC analyses, a (50 m x .53 mm x 15 mm) Hewlett Packard P-PLOT Al_2O_3 capillary column (80 °C oven), split/splitless inlet (120 °C), and flame ionization detector (120 °C) were employed. Helium was used as the inert carrier gas. Column flow was 1.0 mL/min; the split ratio was 100:1; and the purge flow was 1.0-3.0 mL/min. Detector flows were constant at 19.0 mL/min of make-up helium, 400 mL/min of air, and 30.0 mL/min of hydrogen. An Alltech digital flow check meter was used to measure GC flows.

The integrated peak areas of the injections were plotted against the corresponding moles of ethylene and ethane. Linear regression analyses of the calibration points, conducted using Excel 5.0, provided calibration curves, which are presented in Appendix B, and equations 11 and 12, which were used to calculate moles of ethylene and ethane in all GC analyses.

(11) $mEE = (pa + 18270.97536)/4.47886537832 \times 10^{11}$ [R = 0.998]

(12) $mEA = (pa + 11544.446449)/3.68207038303 \times 10^{11}$ [R = 0.988]

Trap Volume Determination. The trap volume of the MDA, which is used in conjunction with pressure and temperature to calculate the moles of desorbed gas, was determined by outgassing and isolating the trap section between valves 9 and 10. Samples of gaseous nitrogen (100 mL), obtained at STP, were then injected into the cold trap using a gas tight syringe, and the pressures recorded. The trap volume (4.485 mL), based on an average of 10 injections, was calculated using equation 13.

(13) $$V_t = (P_a \cdot 100)/P_t$$

Sample Loop Preparation. A pre-weighed 3.94" x 1/8" stainless steel loop was loosely packed with adsorbent (150-200 mg) to minimize diffusion limitations. Weighing the loop before and after packing provided the mass of the adsorbent in the loop. After packing the ends of the loop with glass wool, the loop was re-weighed and attached to the 6-way Alltech valve. The 6-way valve was then positioned to trap, isolating the loop for

adsorbate removal, and the adsorbent was outgassed (6.6 x 10^{-5} Torr) overnight at 100 °C. Weight loss of the adsorbent during outgassing was measured by removing the loop and re-weighing. Depending on moisture content of the sample, the % weight loss ranged from 3-15%.

Void Space Determination. To account for components trapped in the void space of the adsorbent loop, the void space of the packed loop was determined. In the procedure, the 6-way valve was positioned to load, and the adsorbent charged for 10 min with argon at 80 ml/min. Under static vacuum, the 6-way valve was then switched to trap; the argon flow terminated; and the argon collected in the cold trap at liquid N_2 temperature. The cold trap was then isolated and warmed to RT, and then the pressure was recorded. Keeping the loop isolated, the cold trap was outgassed. A considerable portion of argon, having a vapor pressure of 0.33 atm (Lide, 1990) at liquid N_2 temperature, remained in the loop. The residual argon was removed by repeated trapping under static vacuum until 0.00 atm was attained. The valve was then re-positioned to trap and the adsorbent outgassed (6.6 x 10^{-5} Torr) overnight at 100 °C. The void space was calculated using equation 14.

(14) $$V_p = V_t \cdot P_t / P_a$$

Sample void space calculations are presented in Appendix B.

Adsorption of Ethylene and Ethane Mixtures at RT. For adsorption of ethylene and ethane mixtures, a binary stream was introduced into the loop by positioning the 6-way valve to load. The binary stream flowed over the adsorbent and exited the vent at RT and 1 atm. The adsorbent was in contact with the binary stream for 20 min, which, as estimated by TGA analysis, was sufficient to achieve adsorption equilibrium. During the last minute of adsorption, a 10.0 µl sample of the binary stream exiting the vent was injected into the GC using a gas tight syringe to determine the composition. The ethylene/ethane mole ratio of the stream was calculated using equations 15 and 16.

(15) % ethylene vent = mEE vent/(mEE vent + mEA vent)

(16) % ethane vent = mEA vent/(mEEvent + mEA vent)

Desorption of Ethylene and Ethane Mixtures at RT and 100 °C. The ethylene and ethane mixtures, adsorbed on the sample, were removed, analyzed, and calculated using the following procedure. Under static vacuum, the 6-way valve was positioned to trap, and the mixture stream terminated. The ethylene and/or ethane in the loop was desorbed using static vacuum and collected in the cold trap at liquid N_2 (77 °K) temperature. At this point, the variac was activated for desorption at 100 °C. After 0.00 psi was attained, indicating that the gases had solidified (ethylene and ethane have 0.0 vapor pressures at liquid N_2 temperature; Lide. 1990), dynamic vacuum was initiated and maintained for 10 min. The cold trap was then isolated and warmed to RT, and the pressure was recorded. Using a gas tight syringe, a 10.0 µl sample of the gas in the cold trap was then injected into the GC. Keeping the loop isolated, the septum was replaced, and the cold trap outgassed. The desorption sequence was then successively repeated to remove any residual fraction of adsorbates remaining in the loop. Next, the variac was switched off (if 100 °C desorption was utilized), and the adsorbent cooled to RT. Finally, the flow controllers were adjusted to establish the next composition of the binary stream; the loop re-positioned to load, and the procedure repeated.

Total moles of gas collected in the trap were calculated using equation 17.

(17) $\text{total } m = \sum P_t \cdot (V_t / R \cdot T)$

The ethylene/ethane mole ratio in the trap was calculated directly from GC data using equations 18 and 19.

(18) $\%\ \text{ethylene } V_t = mEEV_t / (mEEV_t + mEAV_t)$

(19) $\%\ \text{ethane } V_t = mEAV_t / (mEEV_t + mEAV_t)$

The moles of ethylene and ethane in the trap were calculated using equations 20 and 21.

(20) $mEEV_t$ = total mEEEA·(% ethylene V_t)

(21) $mEAV_t$ = total mEEEA·(% ethane V_t)

The moles of ethylene and ethane in the void space were calculated using equations 22 and 23.

(22) $mEEV_p = [P_a \cdot V_p/R \cdot T] \cdot$(% ethylene vent)

(23) $mEAV_p = [P_a \cdot V_p/R \cdot T] \cdot$(% ethane vent)

The moles of ethylene and ethane desorbed/gram of adsorbent were calculated using equations 24 and 25.

(24) $mEEdga = [(mEEV_t - mEEV_p)/ga]$

(25) $mEAdga = [(mEAV_t - mEAV_p)/ga]$

Selectivities of the adsorbent in the multicomponent streams were calculated using equation 26.

(26) mEE/mEA = (mEEdga/XEE)/(mEAdga/XEA) \

Sample MDA calculations on 61% Ag(I) exchanged 15 resin in a binary stream approximately composed of 20% ethylene and 80% ethane are presented in Appendix B.

Propagation of Error Analysis. Propagation of error analysis (Jenson and Jefferys, 1963) was conducted on MDA calculations. The maximum syringe error was estimated at 0.1 µl; the maximum temperature error was 1 °C; and the maximum pressure error was 0.02 psi. Plugging maximum error values (δ) into equation 27 resulted in a +/- 2.5% error in calculations.

(27) $$Maximum\,error = \frac{\delta P}{P} + \frac{\delta V}{V} + \frac{\delta T}{T}$$

Curve Fitting

A fitting program (Jackson, 1974), based on Marquardt's method, was employed to nonlinear least squares fit ethylene adsorption data using the Yang and Kikkinides isotherm equation (1995), the Langmuir isotherm equation, the Toth isotherm equation, and the Unilan isotherm equation. Single component adsorption isotherms and binary desorption data, which were not nonlinear least squares fit, are plotted as experimental data points connected with straight lines.

Characterization of Unexchanged and Cation Exchanged Amberlyst 15 Resins

Scanning Electron Microscopy and Energy Dispersive X-ray Adsorption Spectroscopy

Scanning electron micrographs (SEM) and Energy Dispersive X-ray Adsorption (EDXAS) Spectra were collected using a Leica Cambridge Stereoscan 360FE 03.03. Voltage was 20 kV; field emission was 360; probe current was 100.02 pA; and the working distance was 9-10 mm. The x-ray unit was an Oxford Link eXLII. Samples were mounted on aluminum supports using silver paste. Before analysis, the mounted samples were carbon coated. The SEM and EDXAS analyses were conducted by Robert Parkhill at Wright Patterson Research Facility located in Dayton, Ohio.

Elemental Analysis

Elemental analyses of the Ag(I) exchanged Amberlyst 15 resin for silver content were conducted by Galbraith Laboratories located in Knoxville, TN.

Nitrogen Adsorption and Mercury Porosimetry

Nitrogen adsorption data were collected using a Quantachrome Autosorb Automated Adsorption System (version 2.30). Mercury porosimetry data were collected using a Micrometritics Autopore 9220. Prior to analysis, samples were degassed overnight at 100 °C. The nitrogen adsorption and mercury porosimetry analyses were conducted by Don Yandle at Phillips Petroleum Research Facility located in Bartlesville, OK.

Diffuse Reflectance Infrared Fourier Transform Spectroscopy

Infrared data were collected using a Nicolet Magna 750 Fourier transform infrared spectrometer (FTIR). For characterization of cation exchange sites, unexchanged and cation exchanged Amberlyst 15 resin samples were dried in air at 110 °C overnight, mixed with oven dry KBr (10%), and analyzed directly using a Spectra Tech diffuse reflectance accessory (DRIFTS). In addition, selected samples were also dried in vacuo at 120 °C overnight and analyzed using DRIFTS. For characterization of ethylene adsorption on cation exchanged Amberlyst 15 resin, the resin sample was dried in vacuo at 120 °C for 12 h and analyzed in a Spectra Tech high temperature environmental chamber (HTEC). The HTEC, illustrated in Figure 4, allowed in-situ infrared analysis of the cation exchanged Amberlyst 15 resin in an inert (N_2 gas) or ethylene environment.

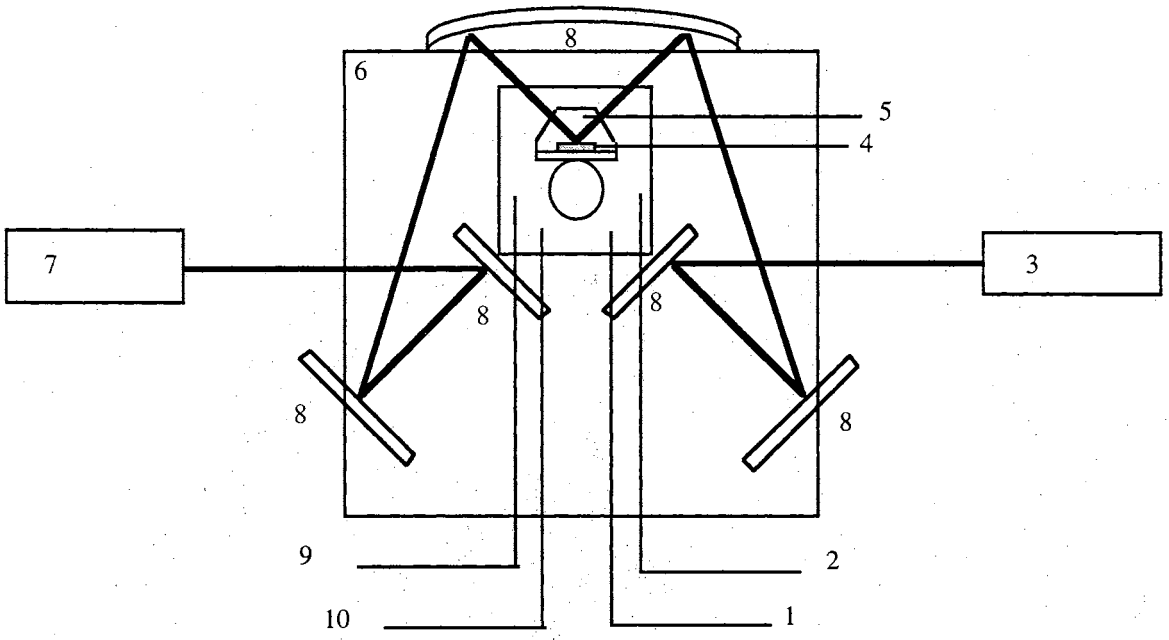

Figure 4. High temperature environmental chamber. 1. Water in. 2. Gas in. 3. IR beam. 4. Sample. 5. HTEC. 6. DRIFTS base. 7. Detector. 8. Mirrors. 9. Gas out. 10. Water out.

All DRIFTS spectra were obtained using 256 scans at 4 cm^{-1} resolution, a 4000-400 cm^{-1} spectral width, and Kubella Munk processing. GRAMS32® software was used for spectral subtraction. Prior to analyses, all unexchanged and cation exchanged Amberlyst 15 resin samples were ground in a Wiggle Bug to improve spectral resolution. TGA measurements confirmed that the adsorption capacities of the unexchanged and cation exchanged Amberlyst 15 resins were not effected by grinding.

Nuclear Magnetic Resonance Spectroscopy

Solid state single pulse ^{1}H MAS NMR spectra and ^{13}C CP-MAS NMR spectra of the unexchanged and cation exchanged Amberlyst 15 resins were collected using a Chemagnetics 300 MHz solid state NMR spectrometer. Single pulse ^{1}H spectra were collected using 256 acquisitions, a 6.0 μs pulse width, and a 1.0 s pulse delay. ^{13}C CP-

MAS NMR spectra were collected using 64,800 acquisitions, a 3.9 μs pulse width, a 1.0 ms contact time, and a 1.0 s pulse delay. In all analyses, the pulse width was maximized to 90°, and magic angle spinning was carried out in 5 mm zirconia rotors spinning at 2-5 kHz. Before packing, samples were ground in a Wiggle Bug. All spectra were referenced to tetramethylsilane (TMS),

^{1}H and ^{13}C NMR spectra of the model compounds were collected using a Varian 300 MHz liquid NMR spectrometer. ^{1}H NMR spectra were collected using 16 acquisitions and a 3.0 μm pulse width. All liquid ^{1}H NMR spectra were referenced to TMS. Due to poor intensity, the ^{13}C NMR spectrum of silver trifluoroacetate was collected using 3600 acquisitions and a 3.0 μs pulse width. ^{13}C NMR spectra of the model compounds were collected using 112 acquisitions and a 3.8 μs pulse width. All liquid ^{13}C NMR spectra were referenced to acetonitrile at 1.3 ppm (Kegley and Pinhas, 1986).

Model Compounds

p-Toluenesulfonic acid, 4-styrenesulfonic acid sodium salt, silver trifluoroacetate, acetonitrile-d_3, and deuterium oxide were purchased from Aldrich. All chemicals were used as received. For ^{1}H and ^{13}C NMR analyses, 100 mg of each compound was dissolved separately in 500 μl of an 80% acetonitrile-d_3/20% deuterium oxide mixture. After NMR spectra were collected, 100 μl of the silver trifluoroacetate mixture was added to each of the test samples and NMR analyses were repeated.

CHAPTER III

CHARACTERIZATION OF UNEXCHANGED AND Ag(I) EXCHANGED AMBERLYST 15 RESINS

Summary

In Chapter III, nitrogen adsorption data, mercury porosimetry data, scanning electron microscopy (SEM) images, energy dispersive x-ray adsorption spectroscopy (EDXAS) profiles, nuclear magnetic resonance spectroscopy (NMR) spectra, and diffuse reflectance infrared fourier transform spectroscopy (DRIFTS) spectra, collected on unexchanged and Ag(I) exchanged Amberlyst 15 resins, are presented and discussed. In agreement with previous reports, the DRIFTS and NMR spectra indicate; (1) the sulfonate groups are the active sites for Ag(I) exchange on the Amberlyst 15 resin; (2) the hydration structure of the Amberlyst 15 resin is reorganized by Ag(I) exchange; and (3) the Amberlyst 15 resins contain a significant quantity of moisture. The nitrogen adsorption data, mercury porosimetry data, and SEM images suggest that the physical structure of the Amberlyst 15 resin is not modified by Ag(I) exchange. The EDXAS profiles indicate that Ag(I) is homogeneously dispersed within the Amberlyst 15 resin bead.

Background

Ion Exchange

History of Ion Exchange. Ion exchange, defined by Wheaton and Hatch (1969), is the reversible exchange of ions between solids and liquids in which there is no substantial change in the structure. A general ion exchange is illustrated in equation 28.

(28) $$\text{metal-Y}_{(Aq)} + \text{H-resin}_{(s)} \longrightarrow \text{metal-resin}_{(s)} + \text{H-Y}_{(aq)}$$

Ion exchange was first recognized by H. S. Thompson (1850) after observing that soil treated with ammonium sulfate liberated calcium sulfate. Way (1850) attributed this observation to ion exchange involving complex silicates present in the soil. Ion exchange was first employed by Harm (1896) to remove sodium and potassium from sugar beet juice. The first industrial scale application of cation exchange for water softening and sugar treatment was developed by Gans (1905).

Unfortunately, the inorganic ion exchange compounds were not acid resistant and thus could not be used in reactions containing hydrogen ion. After the development of synthetic resins by Holmes and Adams (1935) and the first polystyrene resin by D'Alelio (1944), ion exchange applications grew rapidly since the resins were more stable. Synthetic resins are among the most important ion exchange materials (Albright and Yarnell, 1987).

Preparation of Ion Exchange Resins. Ion exchange resins are commercially prepared by suspension copolymerization of styrene with varying amounts of crosslinking divinylbenzene (DVB) (Tooper and Wirth, 1956). Depending on the reaction conditions (i.e. DVB content, solution mixture, reactor design, and dispersion agents), spherical particles with varying pore sizes and stabilities are produced. The ion exchange functionalities are introduced into the aromatic system by typical organic aromatic substitution reactions: sulfonation (Kressman and Tye, 1955), phosphonation (Alexandratos et al., 1985), phosphination (Abrams, 1958), chloromethylation (Olah et al., 1976), or aminomethylation (Corte and Netz, 1966; Wuchter, 1974).

Classification of Ion Exchange Resins. According to Albright and Yarnell (1987), ion exchange resins are classified according to their functionalities (i.e. cation exchange resin or anion exchange resin) and properties (i.e. regeneration, leakage, exhaustion, ion exchange capacity, selectivity, moisture retention, density, particle size, porosity, swelling, and stability). The most critical property, according to Albright and Yarnell (1987), is the

exchange capacity. Exchange capacity is defined as the number of exchangeable sites per unit mass or volume of resin. Kitchener (1957) has explained that the exchange capacity relies on the position of the equilibrium of ions in solution. The position of the equilibrium depends on the relative concentrations of the ions in solution and on the resin. Using the law of mass action, Kitchener (1957) defined the selectivity coefficient (K_{ab}) of cation exchange resin for ion B^+ in equation 29, where subscript r denotes ions bound to the resin.

(29) $$K_{ab} = \frac{[B_r^+][A^+]}{[A_r^+][B^+]}$$

Using this principle, selectivities of 8-10% DVB sulfonated polystyrene resins for specific metal ions were reported and are listed in Table 6.

Table 6. Selectivity Coefficients of Sulfonated Polystyrene (8-10% divinylbenzene) Resin[a]

ion A	ion B	K_{ab}
H^+	Li^+	0.8
H^+	Na^+	1.5
H^+	K^+	3
H^+	NH_4^+	3
H^+	Ag^+	18
H^+	Tl^+	24
Na^+	K^+	1.8
H^+	Ca^{2+}	42
Ni^{2+}	Ca^{2+}	2.5

[a] Kitchener, 1957.

Structure and Properties of the Amberlyst 15 Resin

The ion exchange resin in this study is a sulfonated polystyrene resin crosslinked with 20% divinylbenzene (Albright and Yarnell, 1987). The resin is commercially produced by Rohm and Haas and goes by the commercial name of Amberlyst 15. The

structure of the Amberlyst 15 resin is represented in Figure 5, and the physical properties of the Amberlyst 15 resin, as reported by Rohm and Haas, are listed in Table 7 (Pitochelli, 1980).

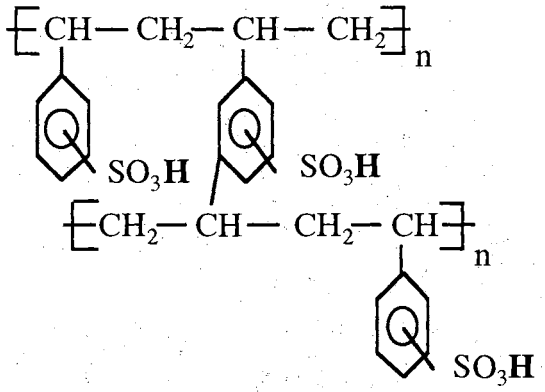

Figure 5. Structure of Amberlyst 15 resin.

Table 7. Physical Properties of Amberlyst 15 Resin[a]

exchange capacity, meq/g	4.7
divinylbenzene, %	20
bead size, mm	500
surface Area, m^2/g	55
pore volume, mL	0.35
temperature stability, °C	120

[a] Pitochelli, 1980.

The classical sites for ion exchange on the sulfonated polystyrene-divinylbenzene resins are the sulfonate groups (Albright and Yarnell, 1987). Quantitative studies, based on a statistical distribution, have indicated an average of one sulfonate group per phenyl ring (Albright and Yarnell, 1989).

Structural Studies of Sulfonated Polystyrene-Divinylbenzene Resins

Dixit and Yadav (1996) have used nitrogen adsorption (BET analysis), mercury porosimetry, and SEM to investigate deactivation of Amberlyst 15 resin during alkylation of xylene. The data indicated that the pore size and surface area of the resin decreased and pore cavities became blocked during the reaction. Based on these results, the authors concluded that the activity of the Amberlyst 15 resin was reduced because reaction by-products blocked access to the active sites. Dixit and Yadav's (1996) nitrogen adsorption and mercury porosimetry results, collected on the untreated Amberlyst 15 resin, are presented in Table 8.

Table 8. Mercury Porosimetry and Nitrogen Adsorption Results Collected on Amberlyst 15 Resin[a]

pore volume, mL/g	mean pore size, nm	bulk density, g/mL	skeletal density, g/mL	porosity, %	BET surface area, m^2/g
0.34	17	0.99	1.5	34	45

[a] Dixit and Yadav, 1996.

Burford et al. (1994) have used EDXAS to characterize sulfonic acid dispersion in polystyrene-divinylbenzene (DVB) membranes. The top surfaces of four different membranes, containing varying degrees of DVB, were analyzed after an 8 h treatment with sulfuric acid. EDXAS data demonstrated the following; (1) the highest levels of sulfur occurred at the top surface, with reduced levels at lower surfaces and (2), the amount of sulfur incorporated into the membrane increased with increasing DVB content.

^{1}H NMR Studies of Sulfonated Polystyrene-Divinylbenzene Resins

Sulfonated polystyrene-divinylbenzene resins swollen in water have been characterized by ^{1}H NMR (Gordon, 1962; Smith et al., 1996) and ^{1}H MAS NMR (Smith et at., 1996). In the ^{1}H NMR solution spectrum of sulfonated polystyrene-divinylbenzene

resin, a resonance at 4.7 ppm was attributed to external water and a downfield resonance to that of internal (adsorbed) water (Gordon, 1962). In ^{1}H MAS NMR studies, Smith et al. (1996) demonstrated that the external water peak was removed by MAS and the internal (adsorbed) water resonance was governed by the degree of divinylbenzene (DVB) crosslinking and the acidic character of the sulfonate groups. Decreasing the DVB content caused the internal (adsorbed)water resonance to shift upfield. Titration experiments with NaOH, which were assumed to remove the acidic proton, indicated that the internal (adsorbed) water resonance shifted upfield with increasing pH.

^{13}C NMR Studies of Polystyrene-Divinylbenzene Resins

Ford et al. (1989a, 1989b) studied macroporous polystyrene-divinylbenzene (DVB) resins by ^{13}C CP-MAS NMR. In the study, resins with vinyl ^{13}C labeled DVB groups were polymerized in suspension using 2,2'-azobisisobutyronitrile (AIBN) as initiator. After heating the polymers to 135-155 °C, the ^{13}C CP-MAS NMR spectra indicated that resins with greater than 1% DVB contained unpolymerized vinyl groups characterized by resonances at 137 ppm and 109 ppm. In the study, commercially available XAD-1, XAD-2, and XAD-4 resins (Rhom and Haas) were also characterized. The XAD-1, XAD-2, and XAD-4 resins contained 20%, 50%, and 80% DVB respectively. Similar to Sherrington, the ^{13}C CP-MAS NMR spectra of the 50% and 80% DVB resins had residual vinyl resonances at 137 ppm and 109 ppm as well as the ethyl-aromatic resonances at 12 ppm and 26 ppm. In the spectrum of the 10% DVB, only a very weak 137 ppm resonance was observed. No data were reported on the XAD-1 resin.

Sherrington et al. (1995) have investigated both gel and macroporous commercially available polystyrene-divinylbenzene (DVB) resins by solid state ^{13}C CP-MAS NMR. In the study, the gels contained 0.5% DVB and 3.5% of DVB and the macroporous resins contained 3.5% DVB and 7.5% of DVB. In the ^{13}C CP-MAS NMR spectrum of the 7.5% DVB macroporous resin, resonances at 37-55 ppm were attributed to the aliphatic CH and

CH_2 carbons of the polymer backbone. The resonance at 127 ppm was assigned to the protonated carbons of the benzene ring, and the resonance at 147 ppm was assigned to the quaternary carbon connected to the backbone. While not observed in ^{13}C CP-MAS NMR spectrum of the macroporous resins, a very weak resonance at 137 ppm appeared in the ^{13}C CP-MAS NMR spectrum of 3.5% gel. In agreement with Ford et al. (1989a, 1989b), the 137 ppm resonance of the 3.5% gel was assigned to unpolymerized vinyl groups of DVB.

Sherrington et al. (1997) have also conducted solid ^{13}C CP-MAS NMR studies of highly crosslinked (35-55%) polystyrene-divinylbenzene (DVB) resins. In addition to the peaks characterized in the earlier study (1995), resonances at 112.4, 29.7, and 14.5 ppm were observed in the ^{13}C CP-MAS NMR spectrum of the resins. In agreement with Ford et al. (1989a, 1989b), the 112.4 ppm resonance was assigned to the methylene carbons of unreacted DVB vinyl groups, while the 29.7 and 14.5 ppm resonances were assigned to ethyl-aromatic residues.

A compiled list of ^{13}C resonances of polystyrene-divinylbenzene resins from the ^{13}C CP-MAS NMR studies are provided in Table 9.

Table 9. Carbon Resonance Assignments of Polystyrene-Divinylbenzene Resin[a,b]

carbon	moiety	resonance, ppm
Ar-**C**H, -**C**H_2	Backbone	37-55
C$_{ar}$-CH	Phenyl	145-148
C$_{ar}$-H	Phenyl	126-129
C$_{ar}$-S	Phenyl	135-138
Ar-**C**H=CH_2	Vinyl	135-138
Ar-CH=**C**H_2	Vinyl	112-109
Ar-**C**$H_2$$CH_3$	Ethyl	29-26
Ar-CH_2**C**H_3	Ethyl	12-17

[a] Ford et al., 1989a, 1989b.
[b] Sherrington et al., 1995, 1997.

Infrared Spectroscopy Studies of Polystyrene-Divinylbenzene Resins and Sulfonated Polystyrene Resins

Zundel (1969) has published a complete review on the characterization of polystyrenesulfonic acids and their metal salts by infrared spectroscopy. Bartholin et al. (1981) have studied styrene-divinylbenzene (DVB) co-polymer by infrared, and Bazuin and Fan (1995) have reported an infrared study on sulfonated polystyrene ionomers. Compiled lists of the infrared band assignments are presented in Tables 10 and 11; detailed discussions of band changes which occur due to cation exchange and water of hydration follow.

Table 10. Infrared Band Assignments of Polystyrenesulfonic Acid and its Salts[a,b,c]

vibration	moiety	band, cm^{-1}
-O-H stretch	Water	3700-2500
=C-H stretch	Phenyl	3065, 3030
-C-H anti, sym stretches	Backbone	2928, 2856
H-O-H scissor	Water	1690-1640
-C-H skeleton	Phenyl	1601, 1495, 1413
-C-H scissor	Backbone	1451
-S=O antisym. stretch	$-SO_3H$	1350
-S-O antisym. stretch	$-SO_3^-$	1200 (split)
-S=O sym. stretch	$-SO_3H$	1172
-S-O sym. stretch	$-SO_3^-$	1134
-C-H in-plane skeleton	Phenyl	1128
-C-H in-plane skeleton	Phenyl	1097
-S-O sym. stretch	$-SO_3^-$	1034
-C-H in-plane bend	Phenyl	1011-1001
-S-O stretch	$-SO_3H$	907
-C-H out-of-plane bend	Phenyl	838
-C-H out-of-plane bend	Phenyl	777
-C-C ring vibration	Phenyl	671

[a] Zundel, 1969.
[b] Bazuin and Fan, 1995.
[c] Burford et al. 1994.

Table 11. Infrared Band Assignments of Polystyrene-Divinylbenzene Resin[a]

vibration	moiety	band, cm^{-1}
-C=C	Vinyl	1680-1630
H-O-H	Water	1600-1602
-C-C, -C-H	Phenyl	1600-1602
-C-C	Phenyl	1510
-C-C	Phenyl	1492
-C-C	Phenyl	1484-1488
-C-C	Phenyl	1451
-C-C	Phenyl	1443
-C-H	Vinyl	1410
-C-H	Phenyl	1026
=C-H	Phenyl	1015-1018
=C-H	Vinyl	990-985
-C-H	Phenyl	905
-C-H	Phenyl	838, 830
-C-H	Phenyl	795-797
-C-H	Phenyl	760

[a] Bartholin et al., 1981.

Zundel (1969) and Bazuin and Fan (1995) have assigned two bands at 1172 cm^{-1} and 1350 cm^{-1} to the symmetric and antisymmetric stretching vibrations of the S=O bonds with double bond character. A band at 900 cm^{-1} was assigned to the stretching vibration of the S-O bond with single bond character. Upon removal of the acidic proton, the intensity of the 900 cm^{-1} band was observed to decrease dramatically, due to the elimination of the S-O single bond character. The intensities of the 1350 cm^{-1} and 1172 cm^{-1} bands, which are masked by overlapping polystyrene bands and sulfonate anion band, decreased as well.

Changes related to the antisymmetric and symmetric vibrations of the polystyrene sulfonate anion and its interaction with metal cation were also observed. According to Zundel (1969) and Bazuin and Fan (1995), the sulfonate anion, having C_{3v} symmetry, is double degenerate; hence, it has only one band centered at 1200 cm^{-1}. Interaction of the sulfonate anion with the electrostatic field of a metal cation changes the sulfonate group to C_S symmetry, causing the 1200 cm^{-1} peak to split. After studying a series of different cations, Zundel (1969) noted that cations having stronger electrostatic fields increased the amount of the splitting. The split was observed to increase with drying, due to the removal of waters of hydration.

Zundel (1969) observed that the exact position of these water bands as well as the sulfonic acid bands, sulfonate anion bands, and selected polystyrene bands depended on the degree of hydration and the metal cation. These observations were explained using the series of structures shown in Figures 6, 7, and 8.

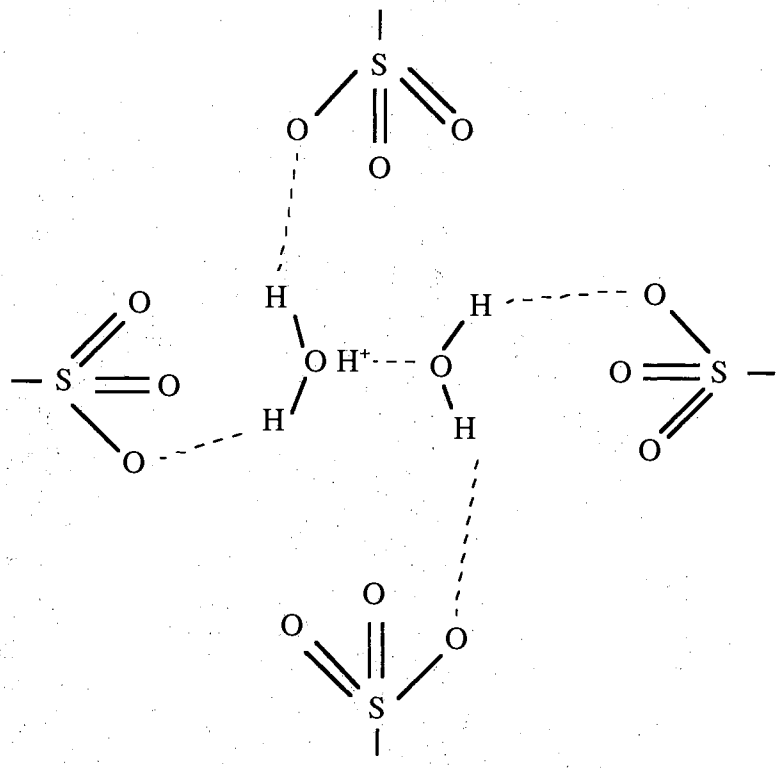

Figure 6. Proposed structure of hydrated polystyrenesulfonic acid.

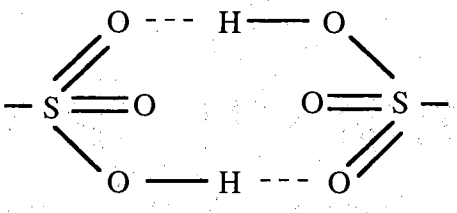

Figure 7. Proposed structure of thoroughly dried polystyrenesulfonic acid.

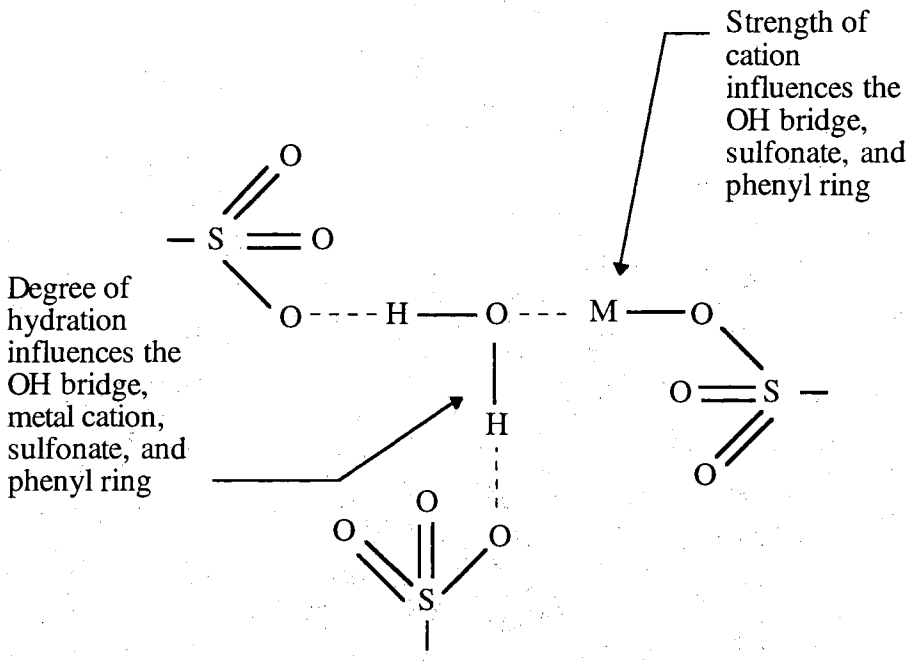

Figure 8. Proposed structure of cation exchanged polystyrenesulfonic acid.

At increased degrees of hydration, Zundel (1969) suggested that the protons are removed from the anions, forming hydrate structures (i.e. $H_5O_2^+$ and/or $H_9O_4^+$ species), with hydrogen bridged to surrounding anions. The hydrate structures, illustrated in Figure 6, were characterized by a continuous and very broad OH vibrational stretch ranging from 3700-2000 cm^{-1} and an intense scissor vibration of water at 1690-1640 cm^{-1}.

Zundel (1969) suggested that the acid groups in the thoroughly dried polystyrenesulfonic acid are hydrogen bridged as illustrated in Figure 7. Zundel (1969) assigned bands at 2950 cm^{-1} and 2405 cm^{-1} to the vibrational stretch of the bridging OH groups. Zundel (1969) suggested that formation of the bridge weakens the OH bond strength, causing the OH vibrations to shift to lower wavenumber.

In the salts of polystyrenesulfonic acid, Zundel (1969) suggested that the cations were bound to surrounding anions by water bridges, as depicted in Figure 8. Zundel (1969) demonstrated that as the electrostatic field (based on size and charge) of the cation increased, the OH vibrations shifted to lower wavenumber as the strength of the OH bond was reduced. Shifts of the OH stretching vibrations to higher wavenumber were observed

at higher degrees of hydration, suggesting that excess water reduced the electrostatic strength of the cation and strengthened the OH bond.

Zundel (1969) reported corresponding wavenumber shifts for SO_3^- anion and phenyl ring vibrations. The amount of splitting of the SO_3^- anion vibration at 1200 cm^{-1} was observed to decrease with increasing hydration. The intensities of the in-plane C-H vibrations of the phenyl ring at 1128 cm^{-1} and 1097 cm^{-1} were observed to increase and decrease with hydration. The in-plane C-H bending vibrations of the ring at 1011 cm^{-1} were observed to shift to 1001 cm^{-1} with hydration. To explain these observations, Zundel (1969) postulated that larger amounts of water reduced the electrostatic strength of the cation, making OH bonds stronger. This, in turn, reduced the perturbation of the SO_3^- anion, affecting the splitting of the 1200 cm^{-1} band and the intensities and positions of SO_3^- bands coupled to vibrations of the phenyl ring.

In an infrared study on the sulfonation of polystyrene-divinylbenzene (DVB) membranes, Burford et al. (1994) attributed a band at 1680 cm^{-1} to the C=C stretch of the unpolymerized vinyl group of DVB. Other researchers (Ford, 1989; Sherrington, 1995, 1997) have assigned an infrared band at 1630 cm^{-1} to the unpolymerized vinyl groups of DVB. Burford also demonstrated; (1) Membranes with higher degrees of crosslinking have more sulfonate groups and higher exchange capacities; (2) Increasing DVB content reduced the swelling ability of the membrane, and (3) Hydrophilicity of the membranes increased as the number of sulfonate groups increased.

Raman Spectroscopy Studies of Sulfonated Polystyrene-Divinylbenzene Resin

Vickers et al. (1995) studied cation exchanged polystyrene-divinylbenzene resins (Dowex 50W-X16) by Raman spectroscopy. Changes in the sulfonic acid vibrations and ring vibrations were observed after cation exchange, as summarized in Table 12.

Table 12. Effects of Cation Exchange on Raman Bands of Sulfonated Polystyrene-Divinylbenzene Resin[a]

cation	sulfonate band, cm^{-1}	ring band, cm^{-1}
H^+	1126.1	1598.6
Na^+	1130.4	1599.9
NH_4^+	1124.0	1598.0
K^+	1127.7	1599.3
Ag^+	1122.7	1596.9
Mg^{2+}	1131.1	1599.2
Ca^{2+}	1131.9	1599.0
Sr^{2+}	1129.6	1599.1
Ba^{2+}	1127.7	1597.8
La^{3+}	1130.4	1598.6
Average	1128.2	1598.5
Range	9.2	3.0

[a] Vickers er al. 1995.

Even though the spectra were of low resolution, Vickers et al. (1995) stated that the changes of the sulfonate features in the 1000-1200 cm^{-1} region could be used to identify the cation. Since bands associated with the ring features were unaffected by cation exchange, the authors suggested that the ring bands could be used as internal standards for quantitative analysis.

Nitrogen Adsorption and Mercury Porosimetry Results

Nitrogen adsorption data and mercury porosimetry data, collected on unexchanged, 7% exchanged, and 61% Ag(I) exchanged Amberlyst 15 resins, are presented in Tables 13 and 14 respectfully and are in agreement with previous reports (Dixit and Yadav, 1996; Pitochelli, 1980).

Table 13. Nitrogen Adsorption Results Collected on Unexchanged, 7% Exchanged, and 61% Ag(I) Exchanged Amberlyst 15 Resins

property	resin	7% Ag(I) exchanged 15 resin	61% Ag(I) exchanged 15 resin	weight corrected 61% Ag(I) exchanged 15 resin
BET surface area, m^2/g	38.4	38.6	29.22	38.0
pore volume, mL/g	0.30	0.30	0.22	0.29
avg. pore size, nm	16	16	15	15

Table 14. Mercury Porosimetry Results Collected on Unexchanged, 7% Exchanged, and 61% Ag(I) Exchanged Amberlyst 15 Resins

property	resin	7% Ag(I) exchanged 15 resin	61% Ag(I) exchanged 15 resin	weight corrected 61% Ag(I) exchanged 15 resin
total intrusion volume, ml/g	0.34	0.34	0.27	0.35
median pore radius, nm	11	13	13	13
bulk density, g/ml	1.0	1.0	1.3	1.0
skeletal density, g/ml	1.5	1.5	2.0	1.6
porosity, %	33	34	35	35

For comparison, the 61% Ag(I) exchanged Amberlyst 15 resin data was weight corrected based on the elemental analysis results to reflect the increase in sample weight after Ag(I) exchange. The surface areas of the resins ranged from 38 to 39 m^2/g. The pore size and pore volume of the resins ranged from 16 to 11 nm (mesoporous) and 0.30 to 0.35 mL/g, respectfully. Porosity of the resins ranged from 33 to 35%.

SEM Images

SEM images of the surface and inner core of the unexchanged Amberlyst 15 resin are presented in Figures 9 and 10. SEM images of the surface and inner core of the 7% Ag(I) exchanged Amberlyst 15 resin are presented in Figures 11 and 12. The SEM images of the surface and inner core of the 61% Ag(I) exchanged Amberlyst 15 resin are presented in Figures 13 and 14. The surface images of the resin samples (5 micron resolution) show residual dust particles and grain boundaries. The inner core images of the resin samples (500 nm resolution) show a porous network of interwoven polymer. In conclusion, the SEM show no change in appearance of the Amberlyst 15 resin after Ag(I) exchange.

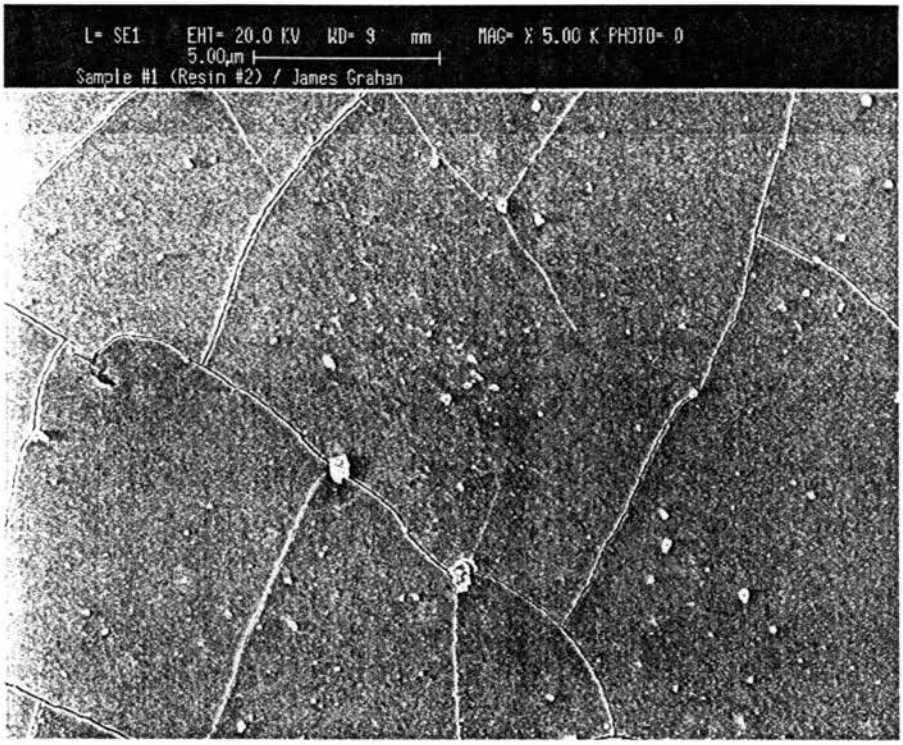

Figure 9. SEM surface image of unexchanged Amberlyst 15 resin.

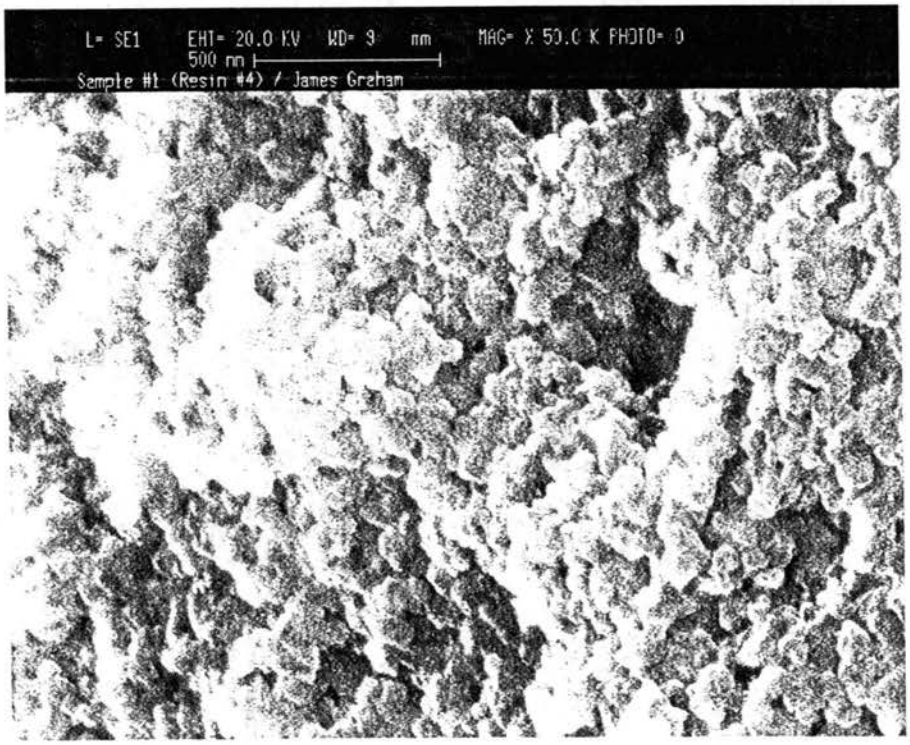

Figure 10. SEM inner core image of unexchanged Amberlyst 15 resin.

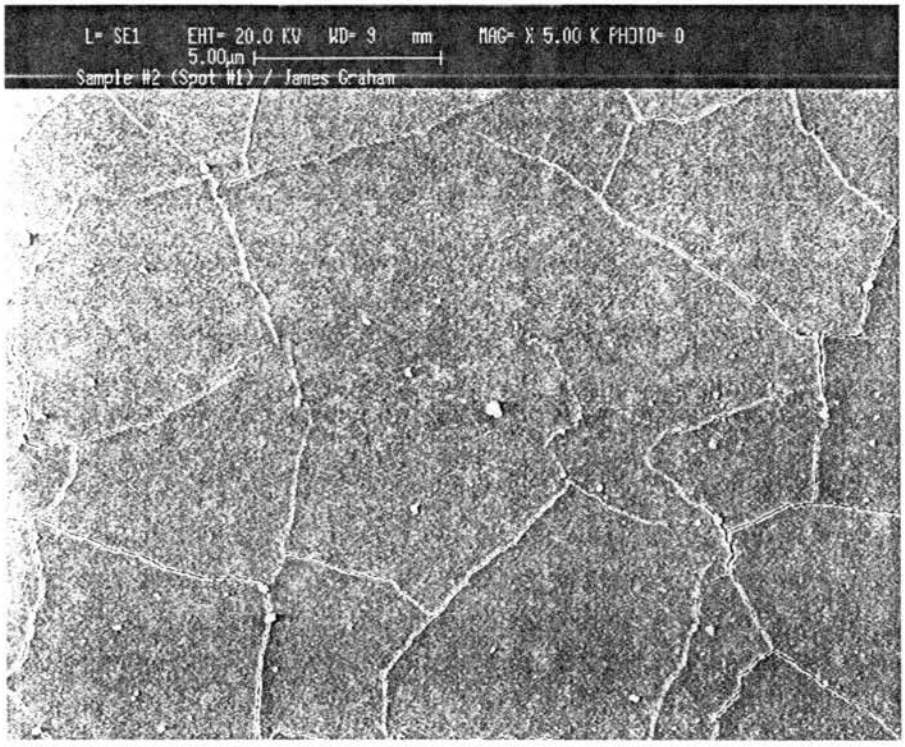

Figure 11. SEM surface image of 7% exchanged Amberlyst 15 resin.

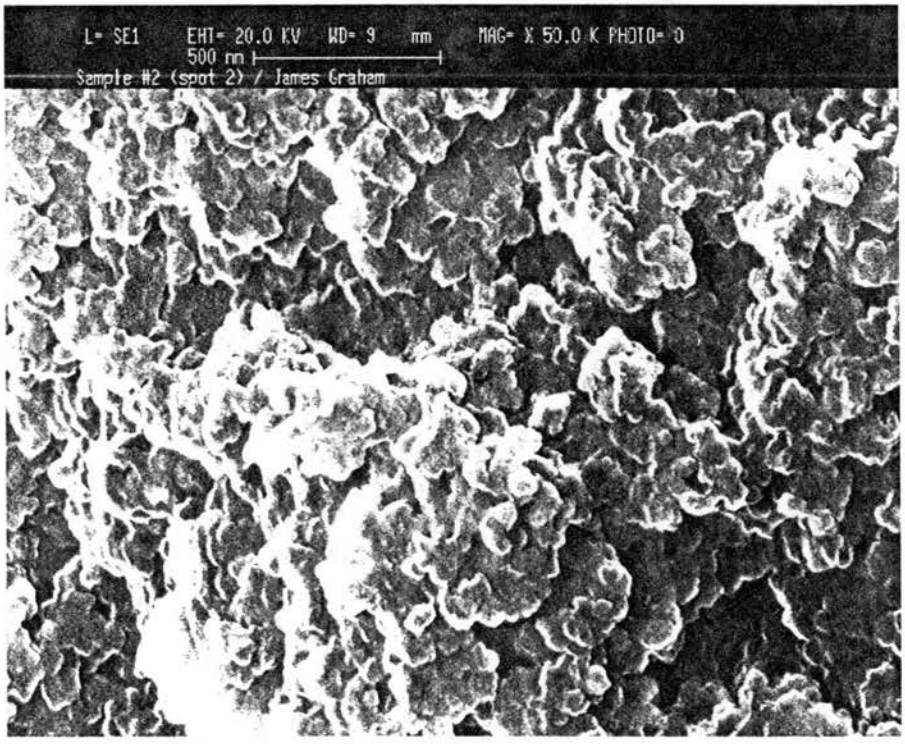

Figure 12. SEM inner core image of 7% Ag(I) exchanged 15 resin.

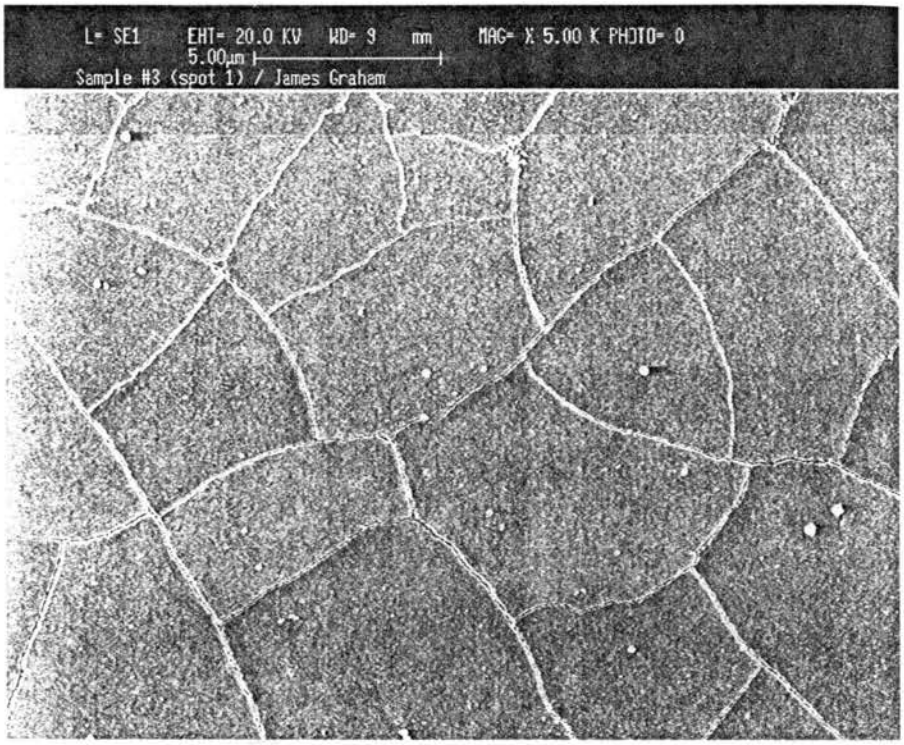

Figure 13. SEM surface image of 61% Ag(I) exchanged Amberlyst 15 resin.

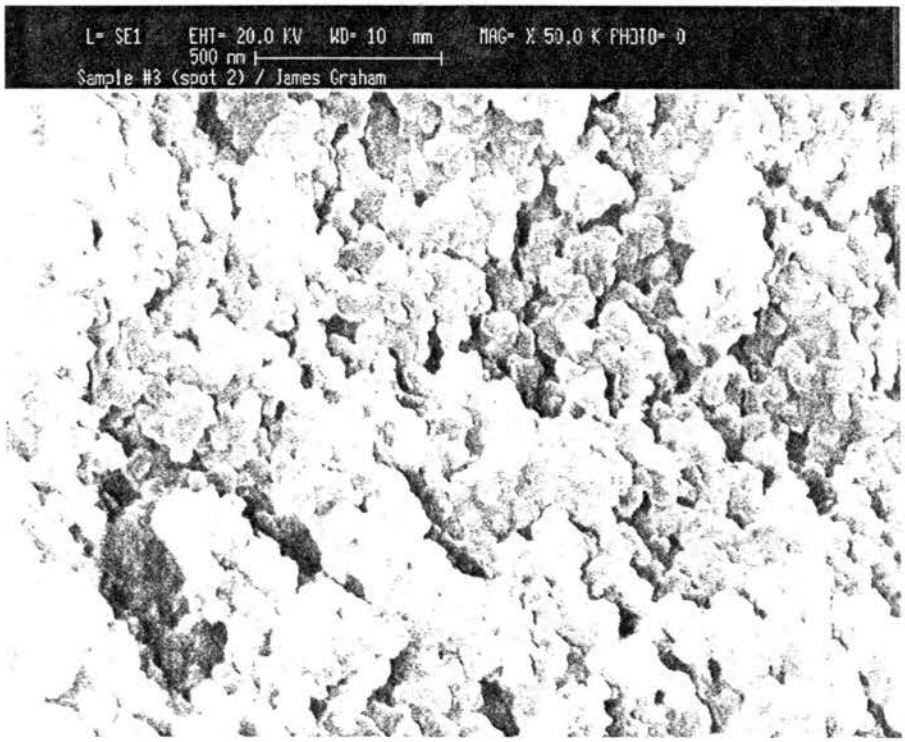

Figure 14. SEM inner core image of 61% Ag(I) exchanged Amberlyst 15 resin.

EDXAS Profiles

EDXAS profiles were taken of three different areas (e.g. surface, inner surface and inner core) of the unexchanged, 7% Ag(I) exchanged, and 61% Ag(I) exchanged Amberlyst 15 resin beads to investigate Ag(I) dispersion. The profiles of the unexchanged Amberlyst 15 resin are presented in Figures 15, 16, and 17; the profiles of the 7% Ag(I) exchanged Amberlyst 15 resin are presented in Figures 18, 19, and 20; and the profiles of the 61% Ag(I) exchanged Amberlyst 15 resins are presented in Figures 21, 22, 23. In the profiles of the unexchanged Amberlyst 15 resin, bands representative of carbon, sulfur and oxygen are present. In addition to carbon, oxygen, and sulfur, the profiles of the 7% and 61% Ag(I) exchanged Amberlyst 15 resins show bands of equal intensity that represent Ag(I) in the three regions of the Amberlyst 15 beads.

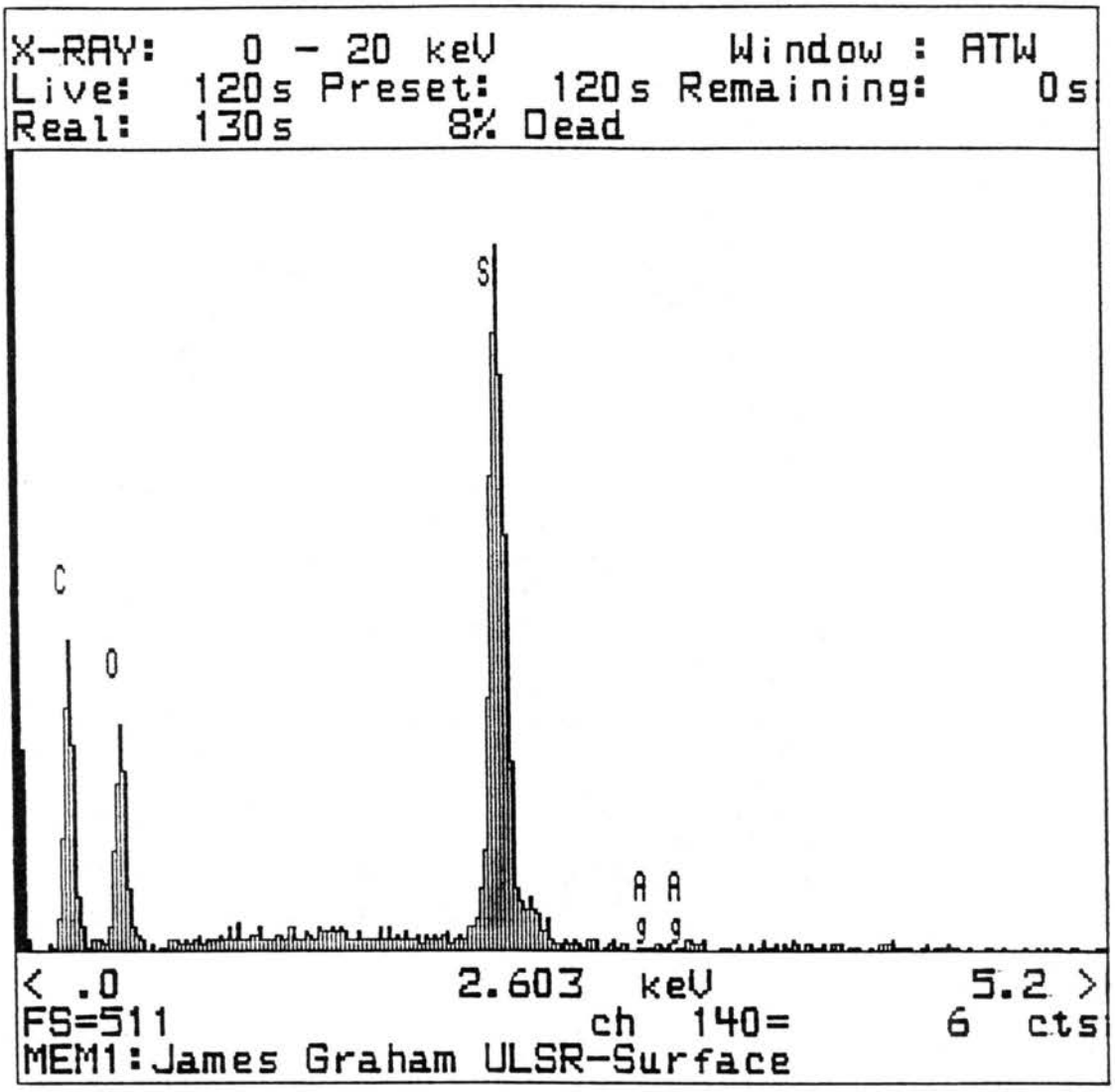

Figure 15. EDXAS surface profile of unexchanged Amberlyst 15 resin.

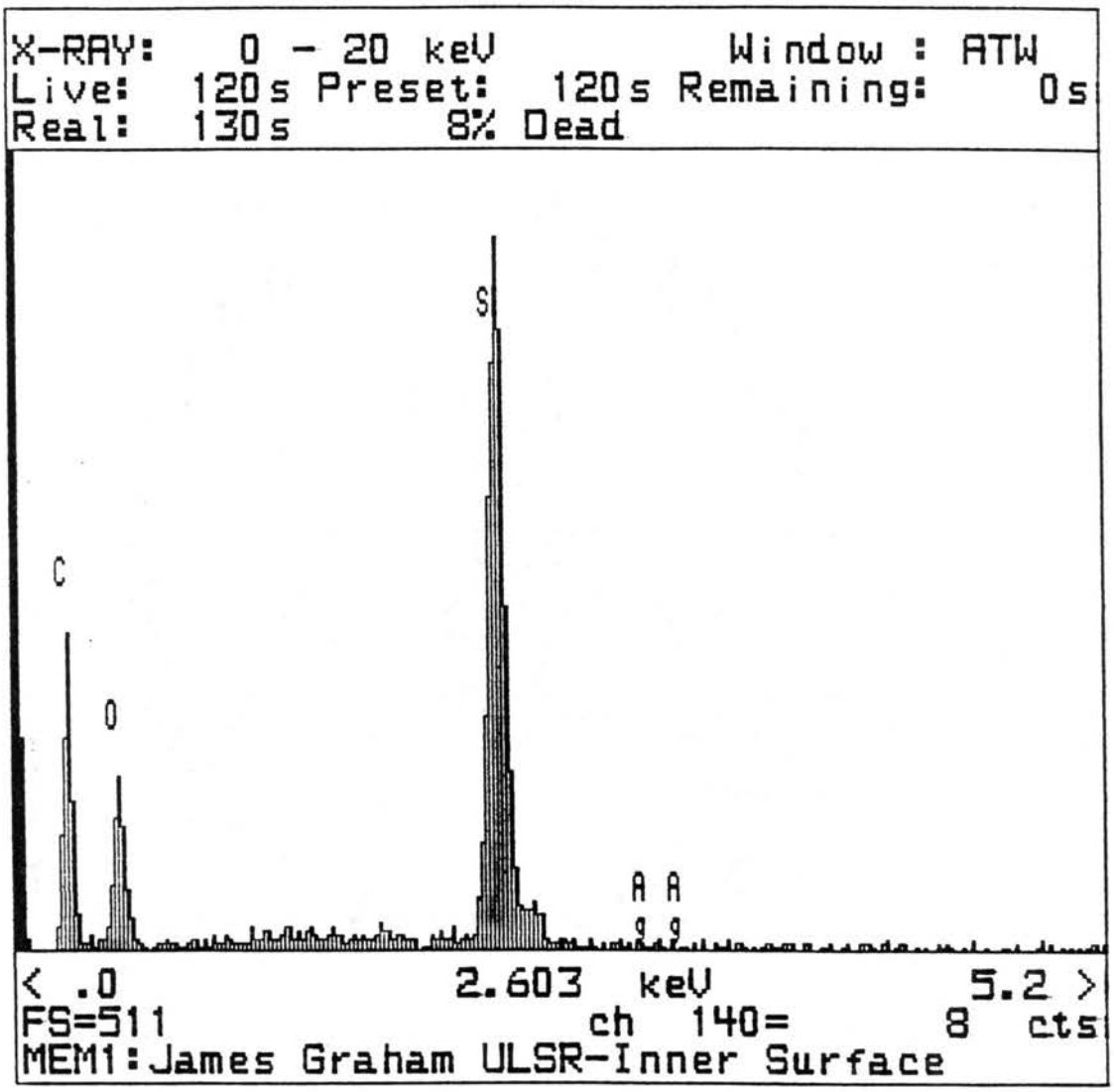

Figure 16. EDXAS inner surface profile of unexchanged Amberlyst 15 resin.

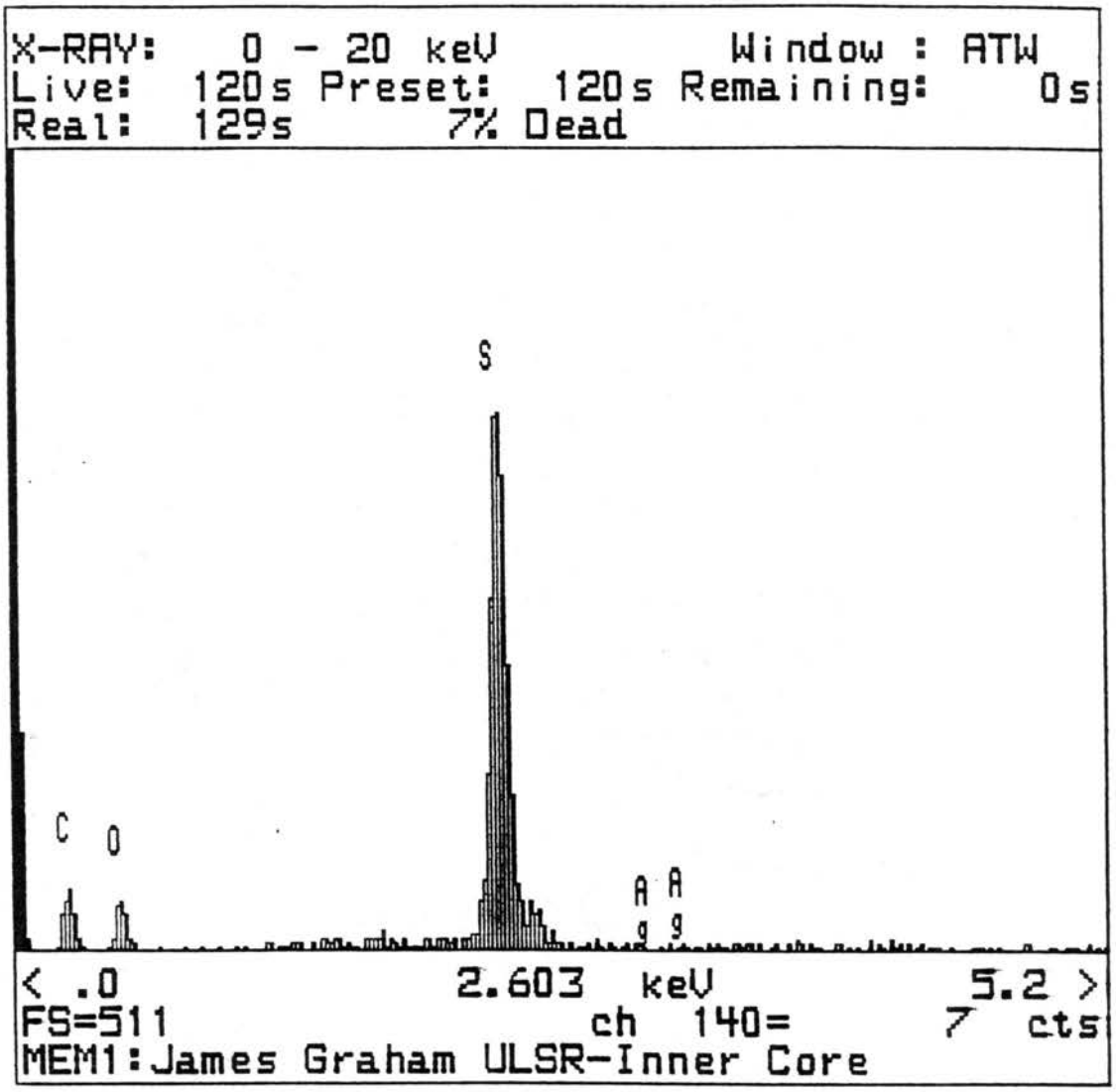

Figure 17. EDXAS inner core profile of unexchanged Amberlyst 15 resin.

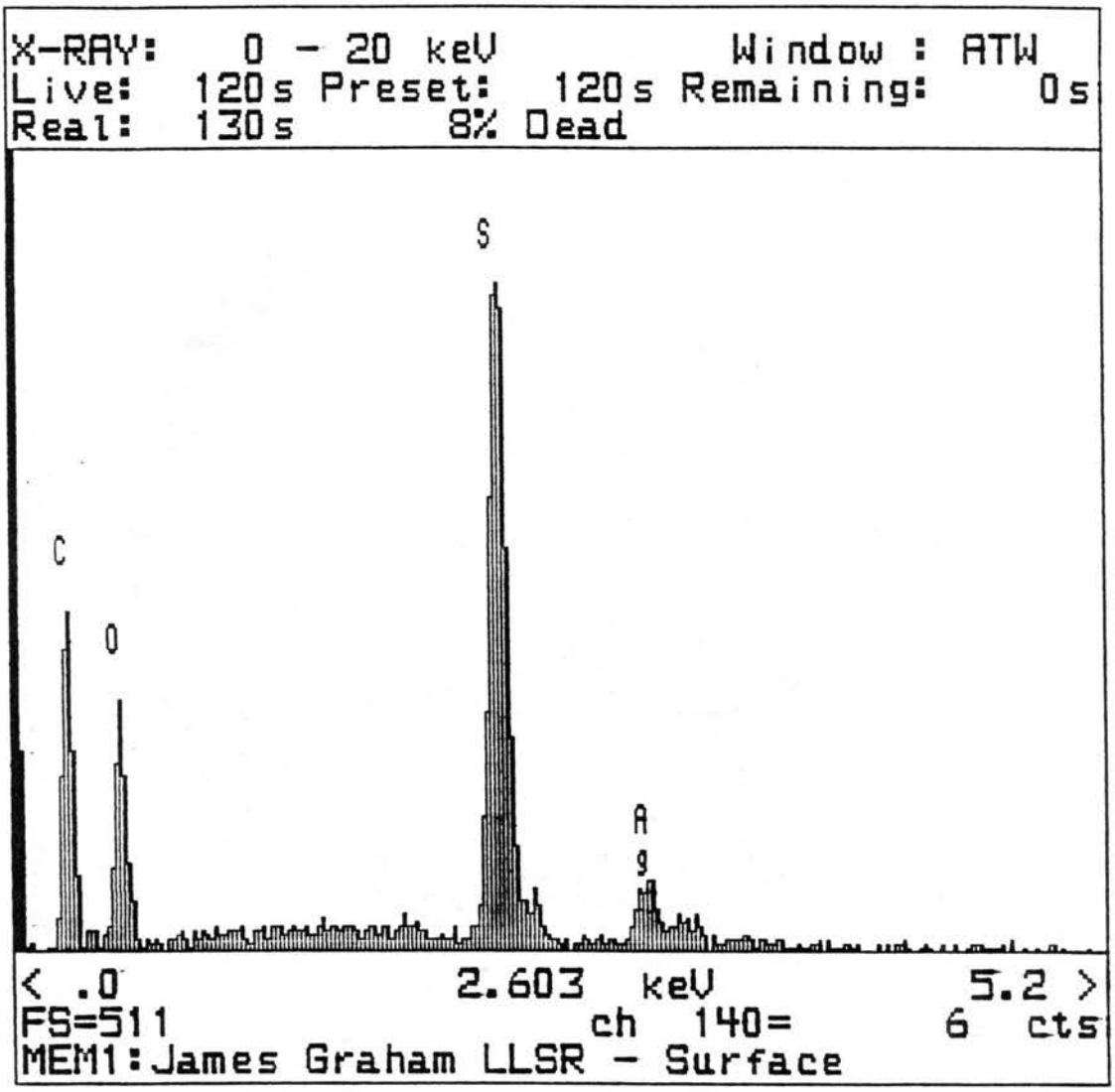

Figure 18. EDXAS surface profile of 7% Ag(I) exchanged Amberlyst 15 resin.

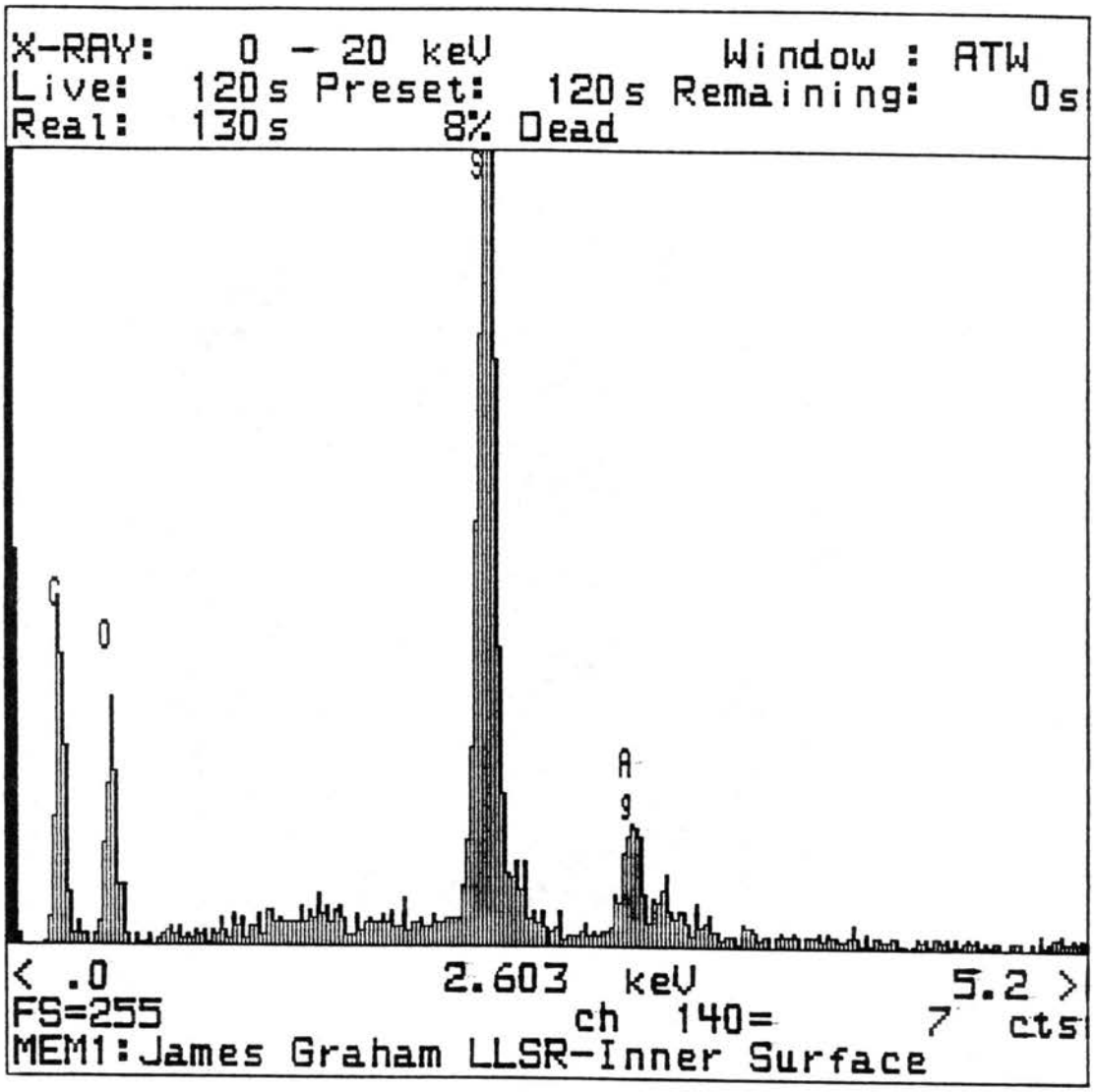

Figure 19. EDXAS inner surface profile of 7% Ag(I) exchanged Amberlyst 15 resin.

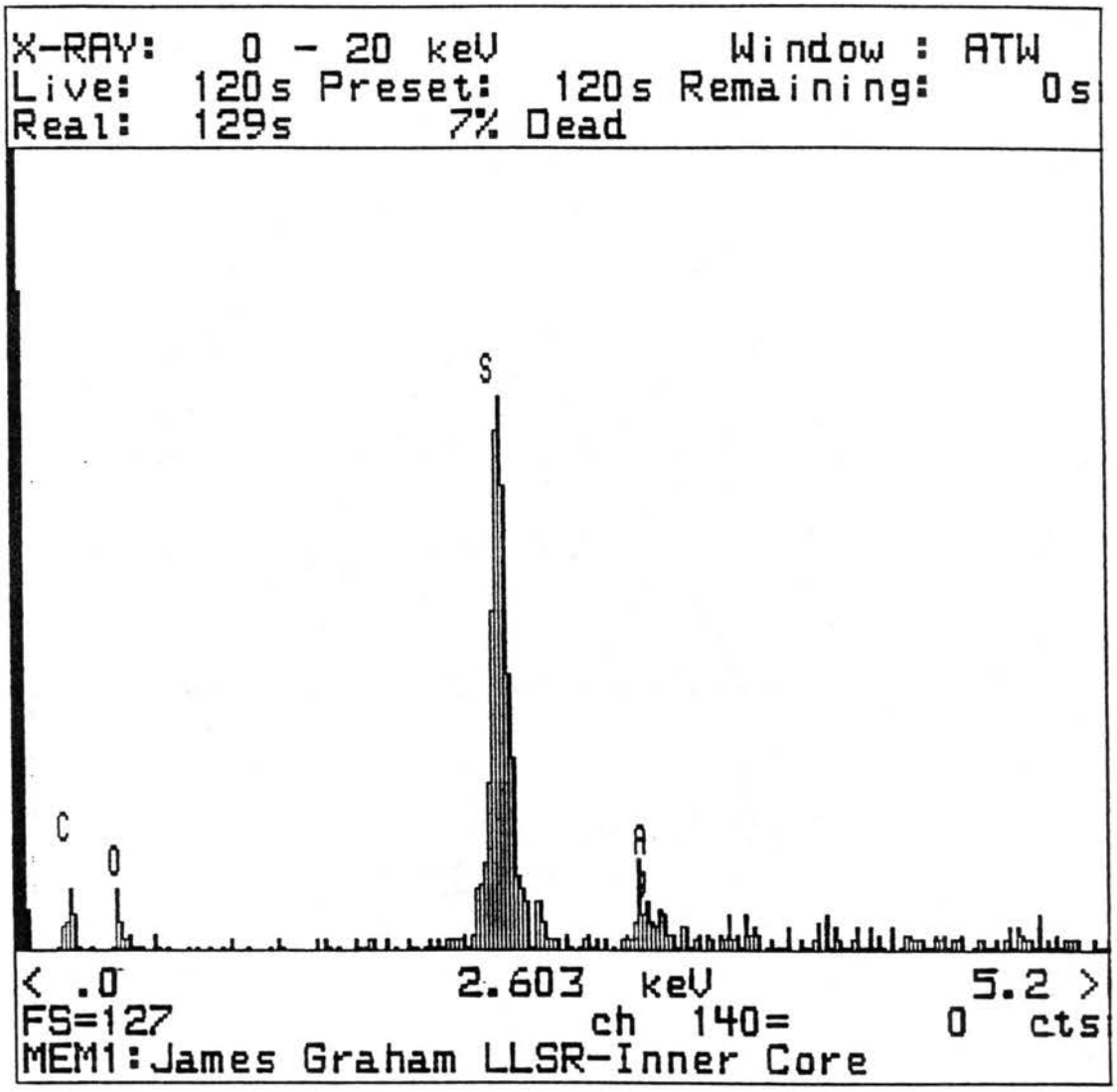

Figure 20. EDXAS inner core profile of 7% Ag(I) exchanged Amberlyst 15 resin.

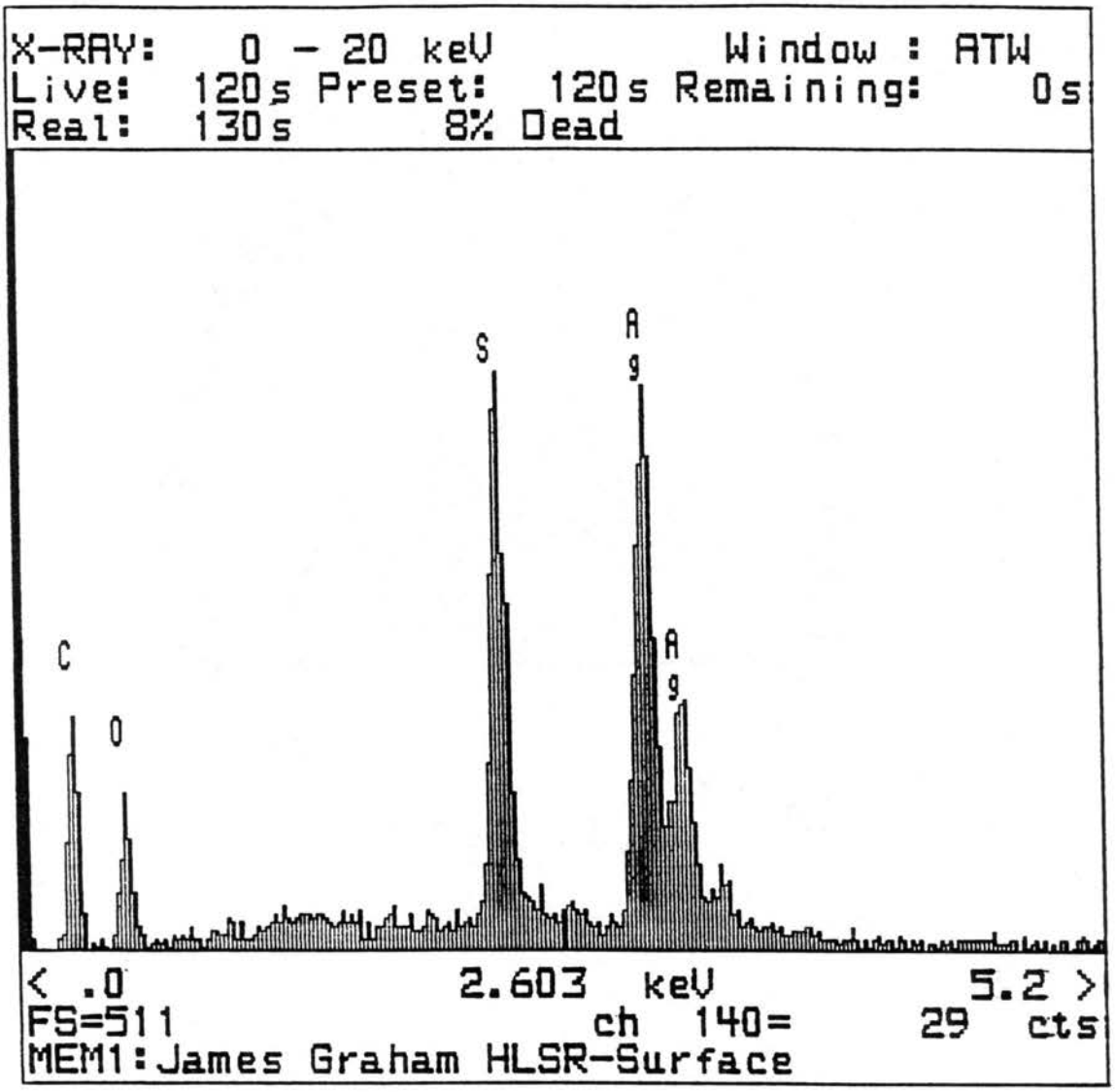

Figure 21. EDXAS surface profile of 61% Ag(I) exchanged Amberlyst 15 resin.

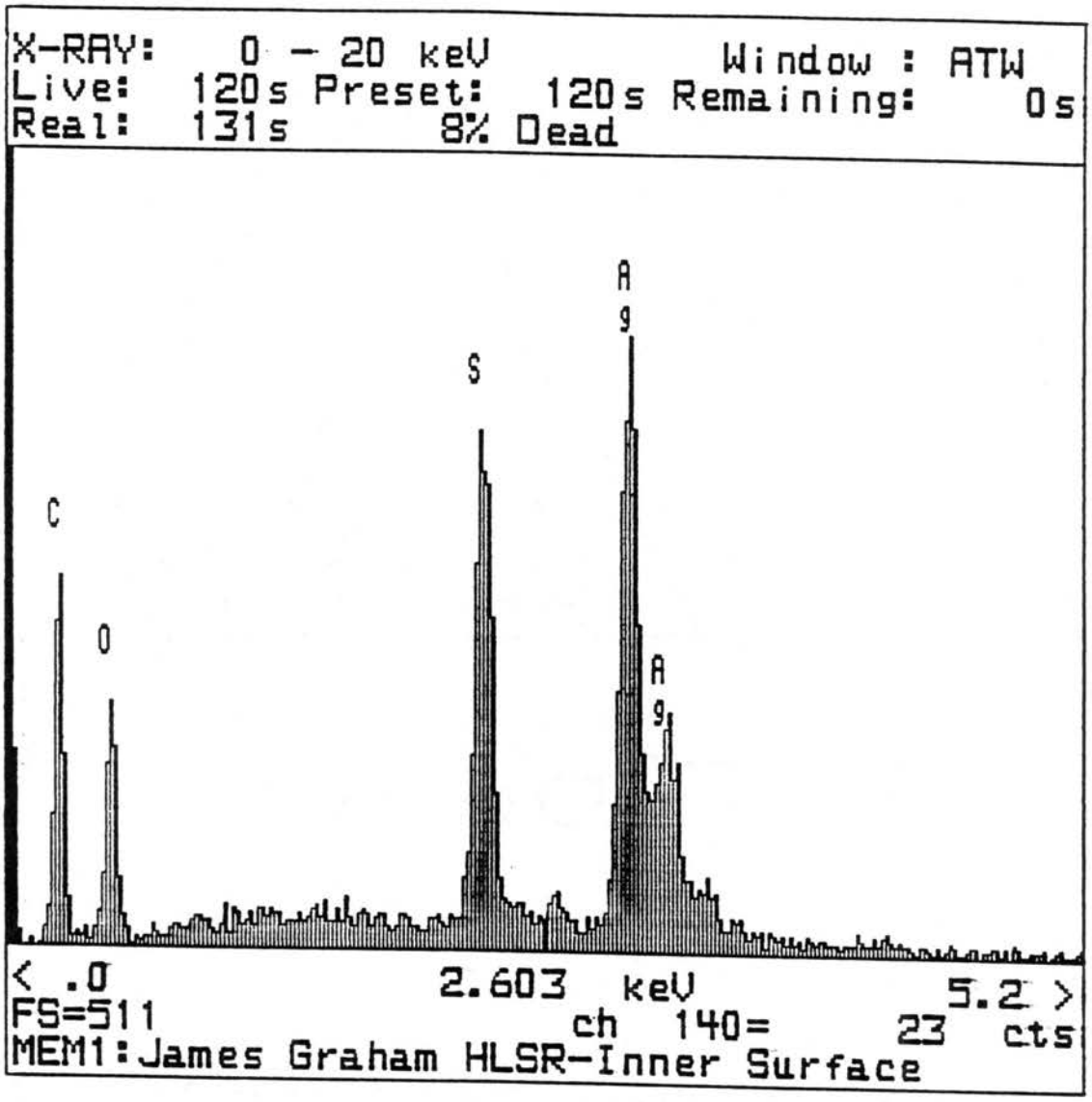

Figure 22. EDXAS inner surface profile of 61% Ag(I) exchanged Amberlyst 15 resin.

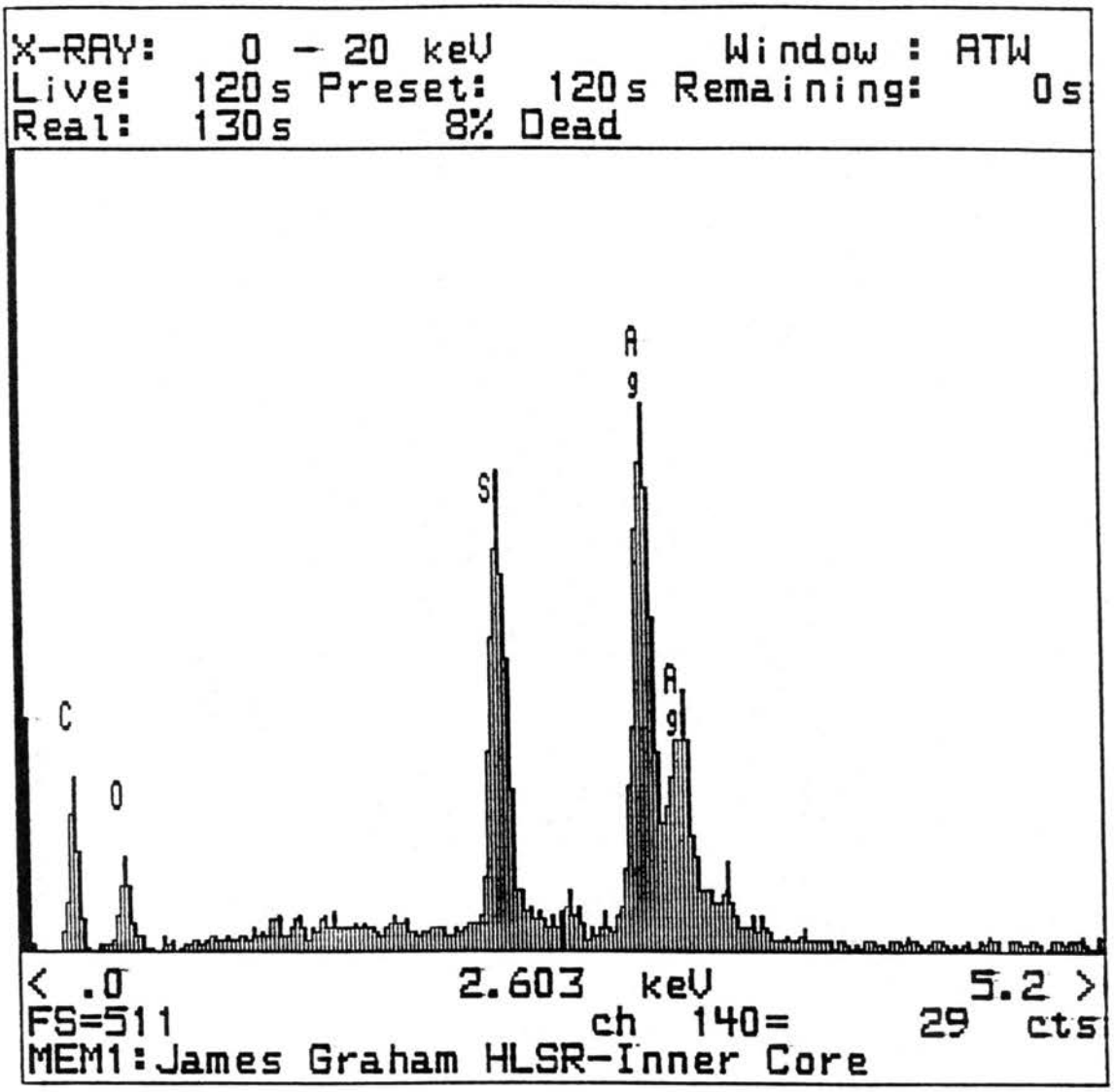

Figure 23. EDXAS inner core profile of 61% Ag(I) exchanged Amberlyst 15 resin.

^{1}H MAS NMR Spectra

The ^{1}H single pulse MAS NMR spectrum of the unexchanged Amberlyst 15 resin is presented in Figure 24. In the spectrum, a broad resonance is observed downfield at 9.9 ppm. In agreement with Gordon (1962) and Smith et al. (1996), the 9.9 ppm resonance is attributed to adsorbed water in the resin. The ^{1}H single pulse MAS NMR spectra of the 7 to 61% Ag(I) exchanged Amberlyst 15 resins are presented in Figures 25 to 30. The broad ^{1}H resonances in the spectra are also attributed to adsorbed water in the Amberlyst 15 resin.

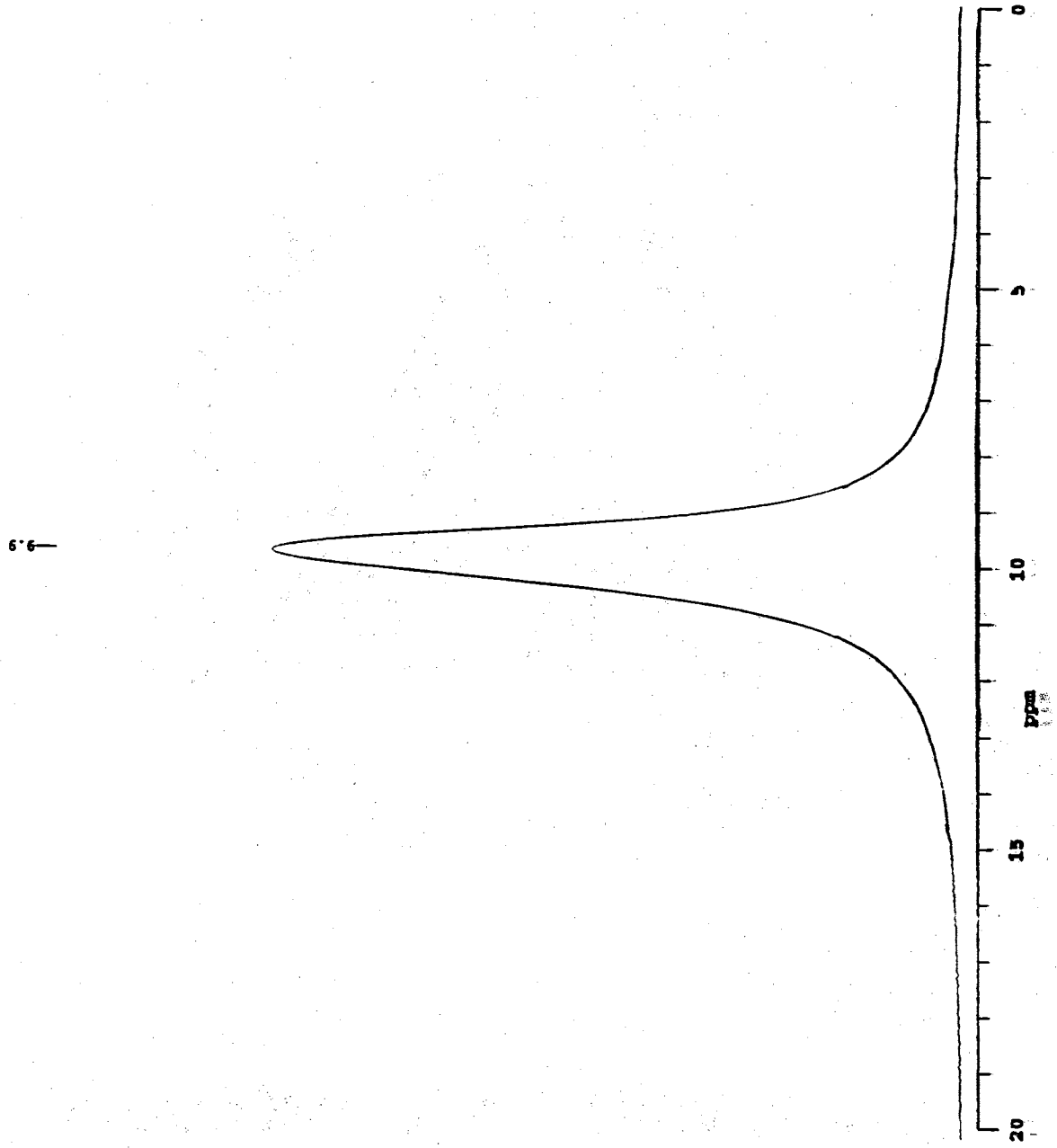

Figure 24. ^{1}H MAS NMR spectrum of unexchanged Amberlyst 15 resin.

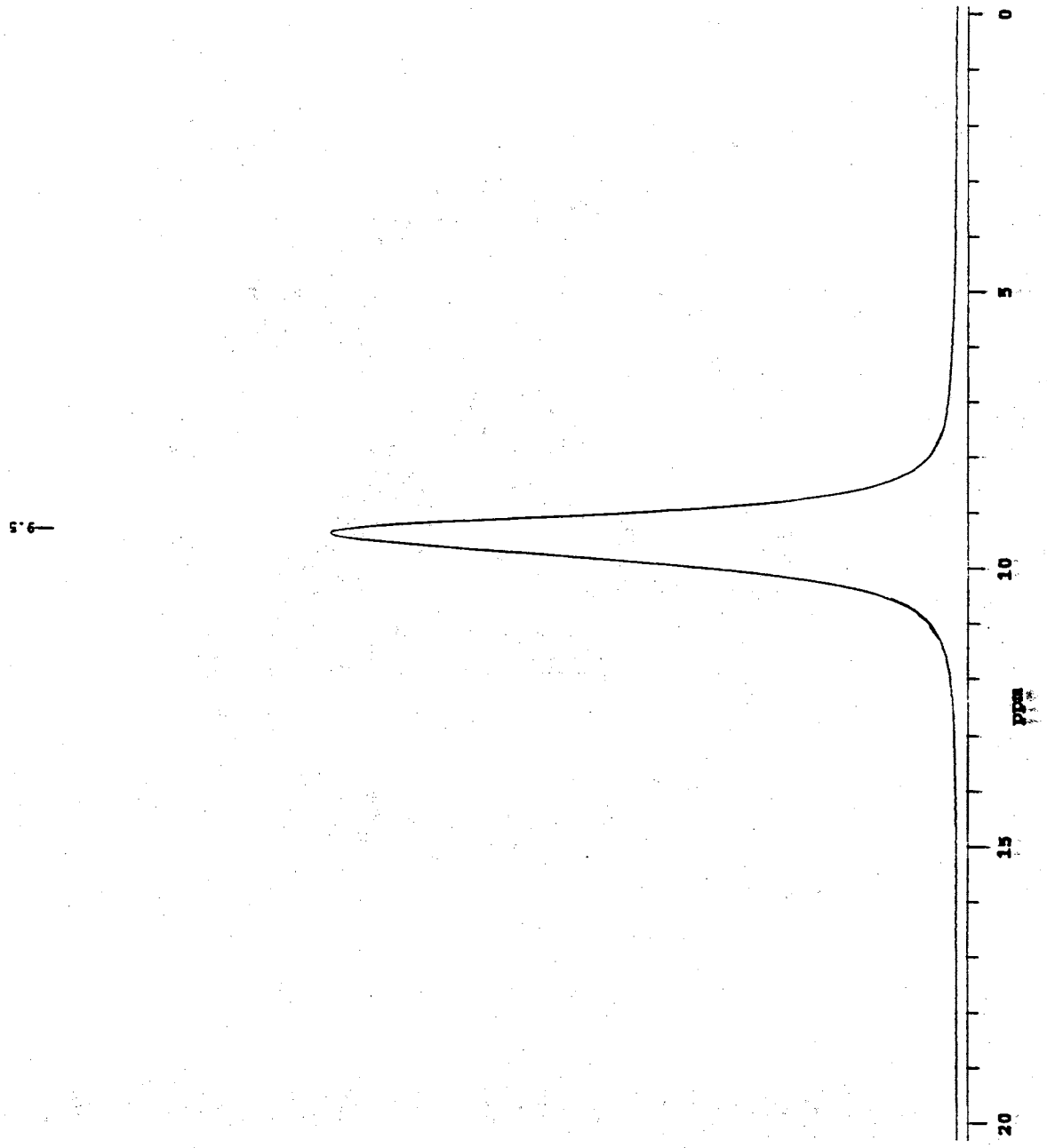

Figure 25. ^{1}H MAS NMR spectrum of 7% Ag(I) exchanged Amberlyst 15 resin.

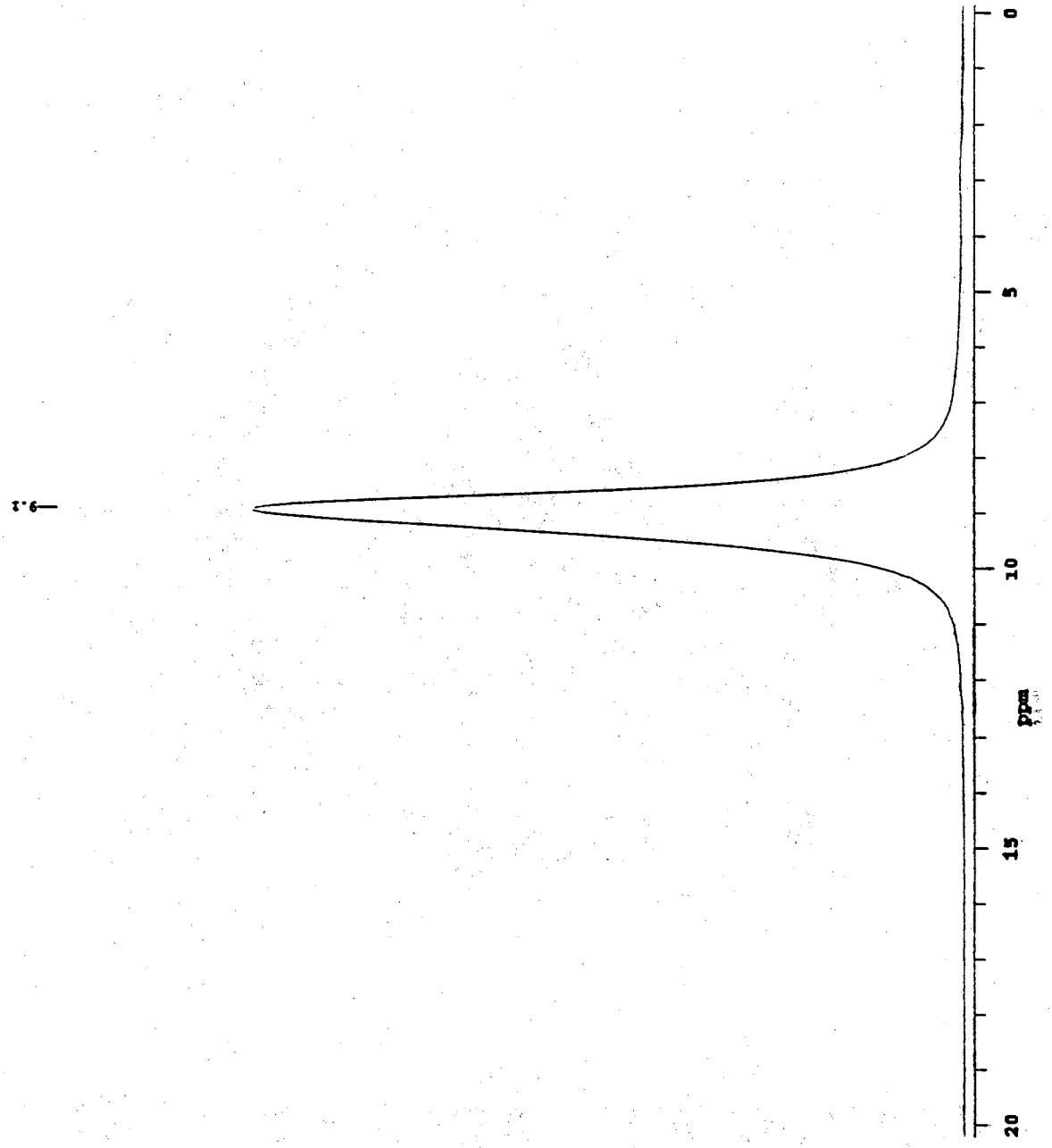

Figure 26. ^{1}H MAS NMR spectrum of 16% Ag(I) exchanged Amberlyst 15 resin.

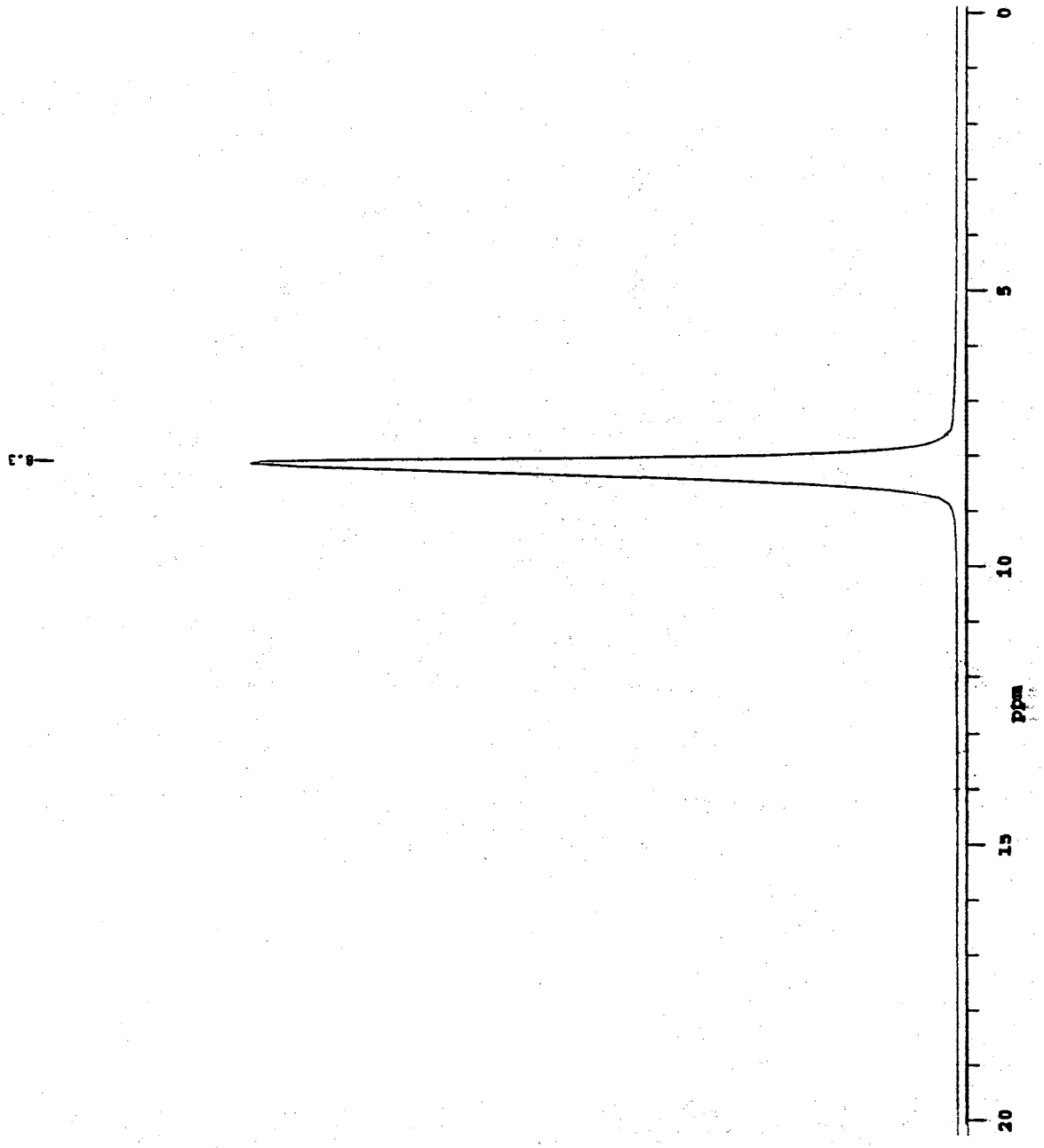

Figure 27. ^{1}H MAS NMR spectrum of 19.6% Ag(I) exchanged Amberlyst 15 resin.

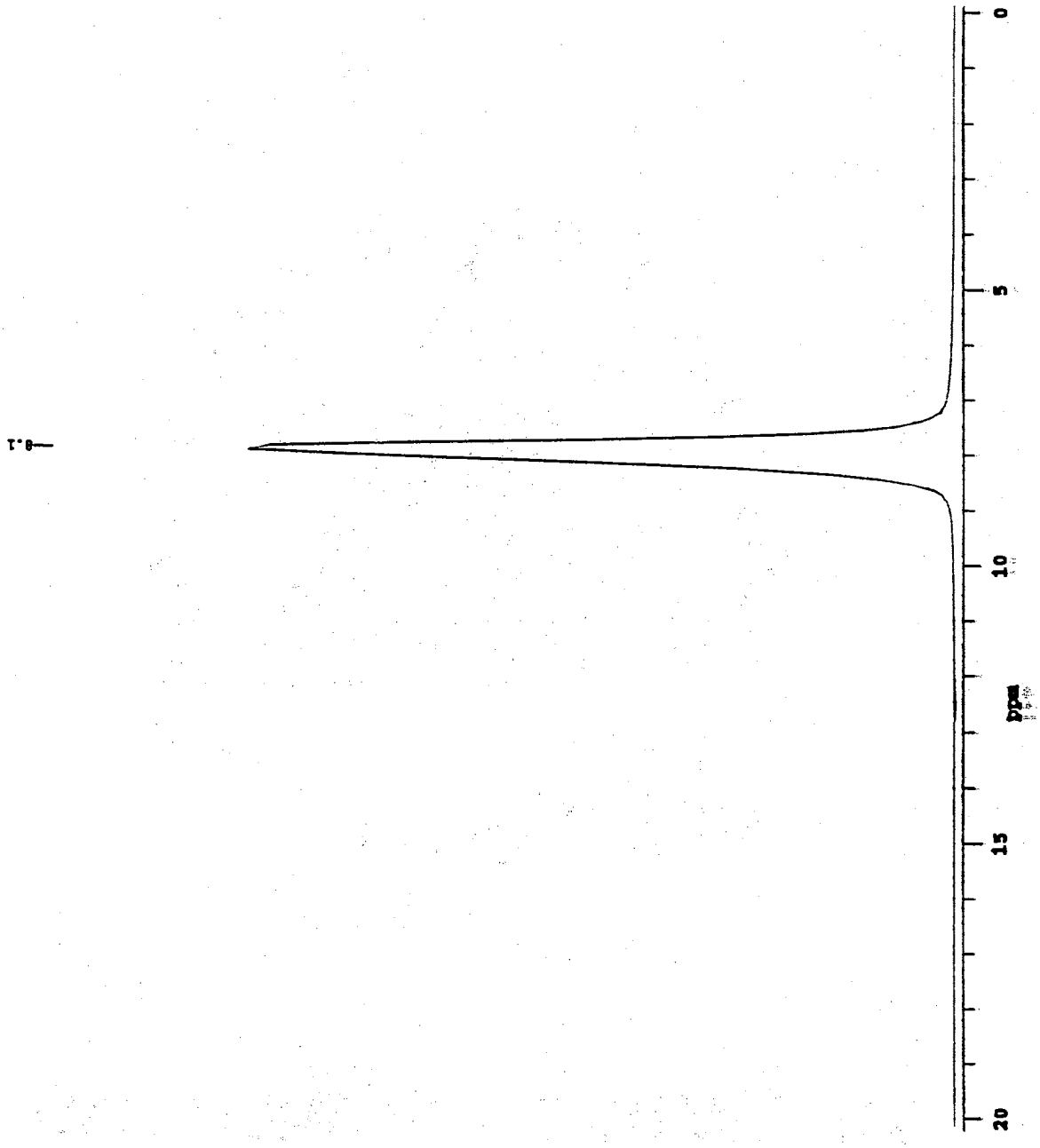

Figure 28. ^{1}H MAS NMR spectrum of 29% Ag(I) exchanged Amberlyst 15 resin.

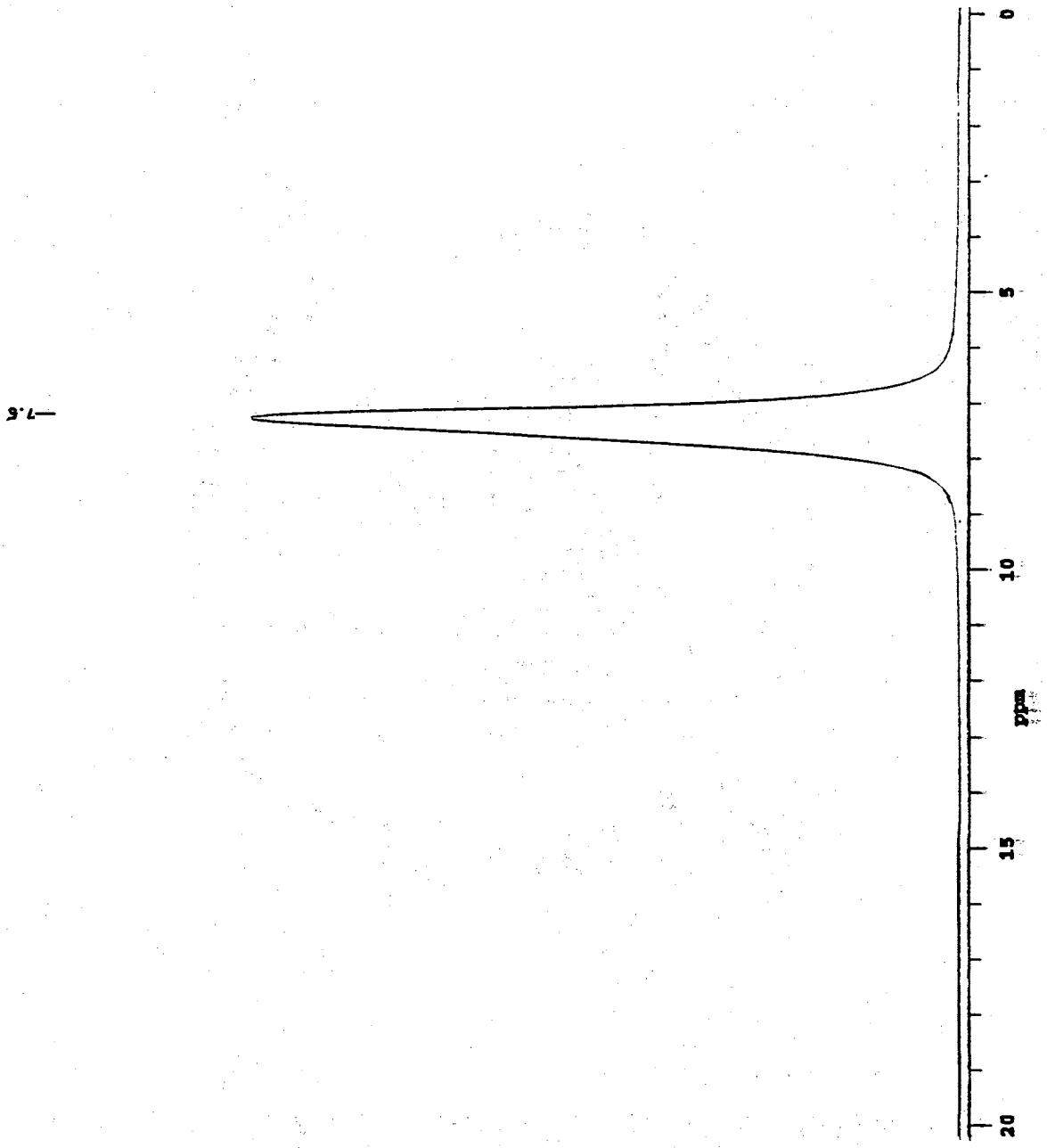

Figure 29. ^{1}H MAS NMR spectrum of 42.6% Ag(I) exchanged Amberlyst 15 resin.

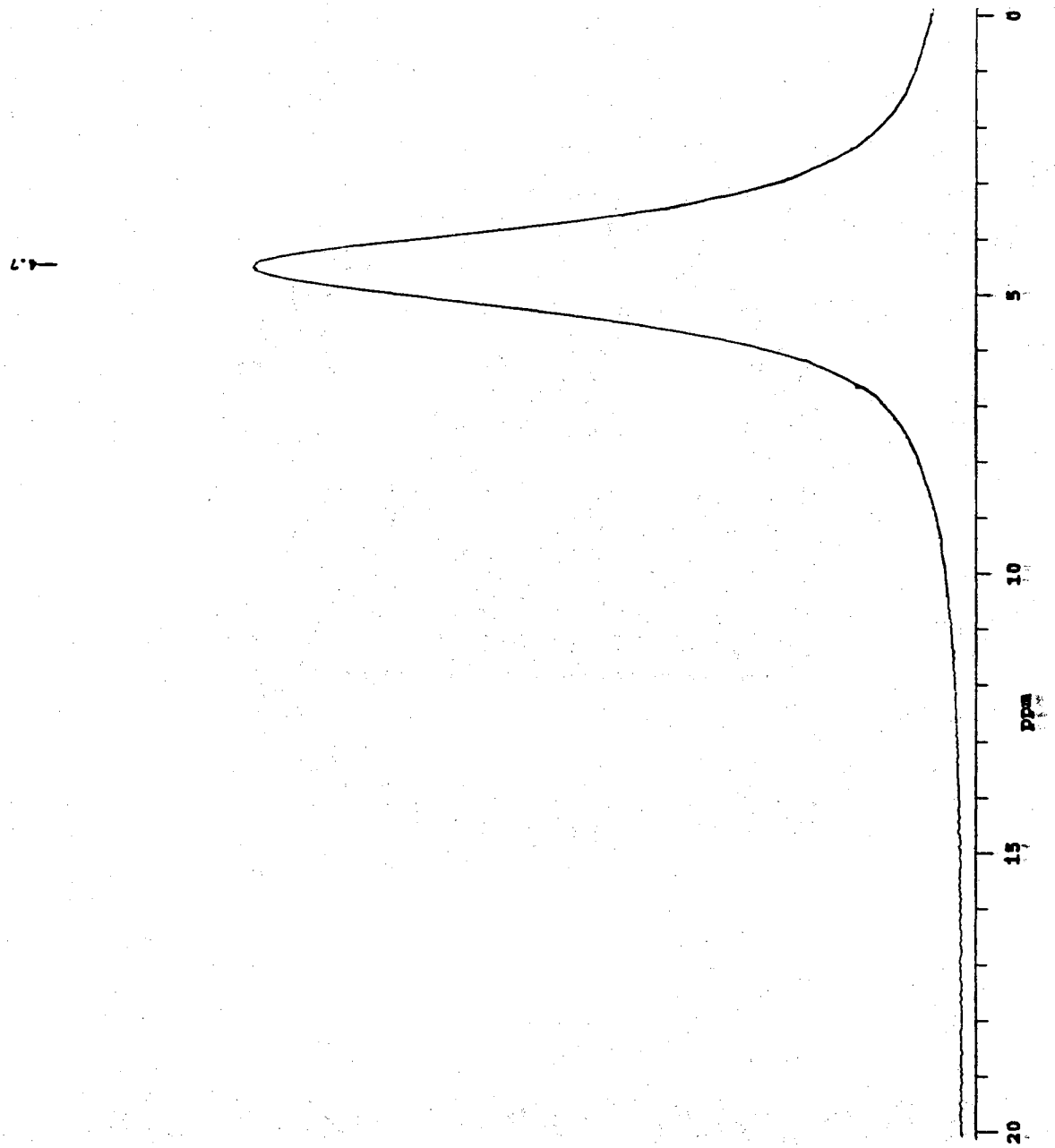

Figure 30. ^{1}H MAS NMR spectrum of 61% Ag(I) exchanged Amberlyst 15 resin.

^{13}C CP-MAS NMR Spectra

The ^{13}C CP-MAS NMR spectrum of the unexchanged Amberlyst 15 resin is presented in Figure 31. Resonances, differentiated by MAS spinning at 2,3 and 4 kHz, are observed at 147, 137, 127, 40, 27, and 14 ppm and spinning side bands are noted with asterisks. Based on previous assignments (Ford et al., 1989a, 1989b; Sherrington et al., 1996, 1997), the 147 ppm resonance is assigned to the quaternary carbon of the phenyl ring; the 127 ppm resonance is assigned to the CH groups of the phenyl ring; and the 40 ppm resonance is assigned to the aliphatic carbons of the polymer backbone. The 137 ppm resonance, which may overlap umpolymerized vinyl groups, is assigned to the sulfonated phenyl carbon. The 27 and 14 ppm resonances are assigned to ethyl-aromatic residues which overlap 2nd order spinning sidebands.

The ^{13}C CP-MAS NMR spectrum of the 7% exchanged and 61% Ag(I) exchanged Amberlyst 15 resins are presented in Figures 32 and 33. In the spectra, resonances at 147, 137, 127, 40, 27, and 14 ppm are observed. These resonances coincide with resonances observed in the ^{13}CP-MAS NMR spectrum of the unexchanged Amberlyst 15 resin.

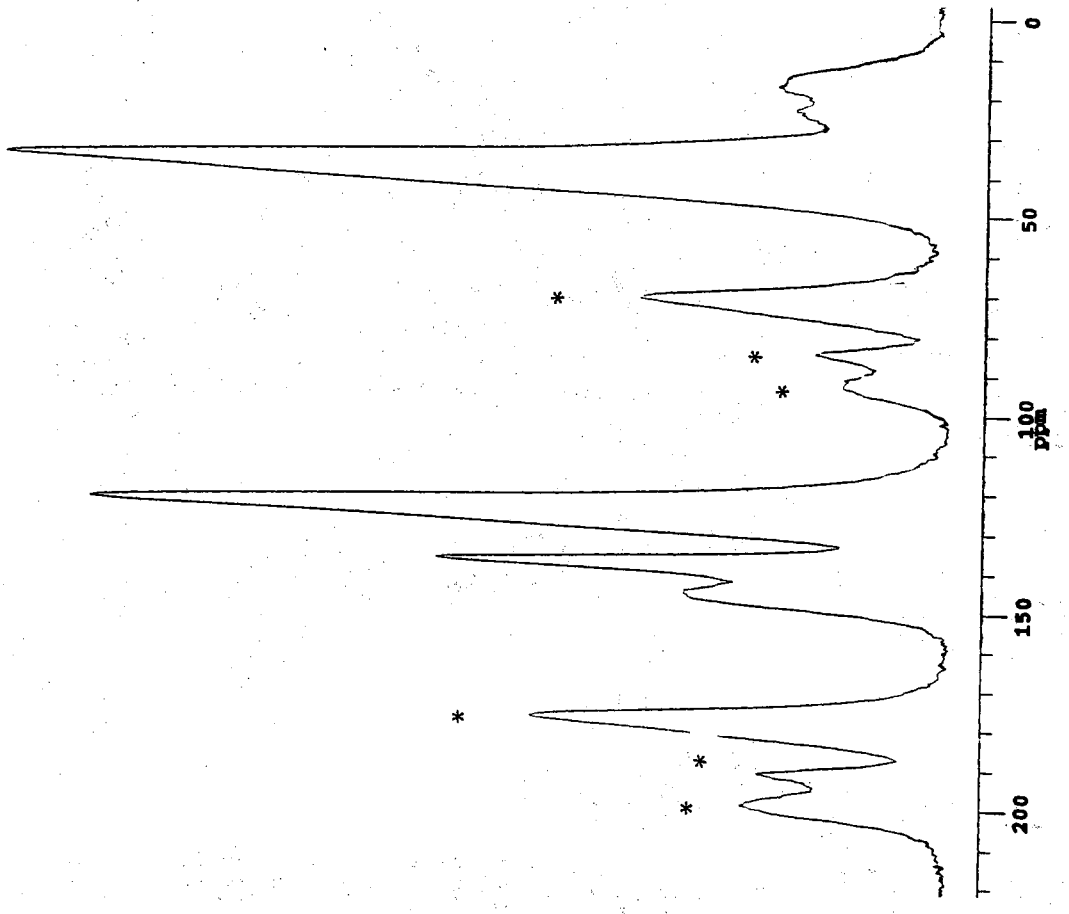

Figure 31. ^{13}C CP-MAS NMR spectrum of unexchanged Amberlyst 15 resin.

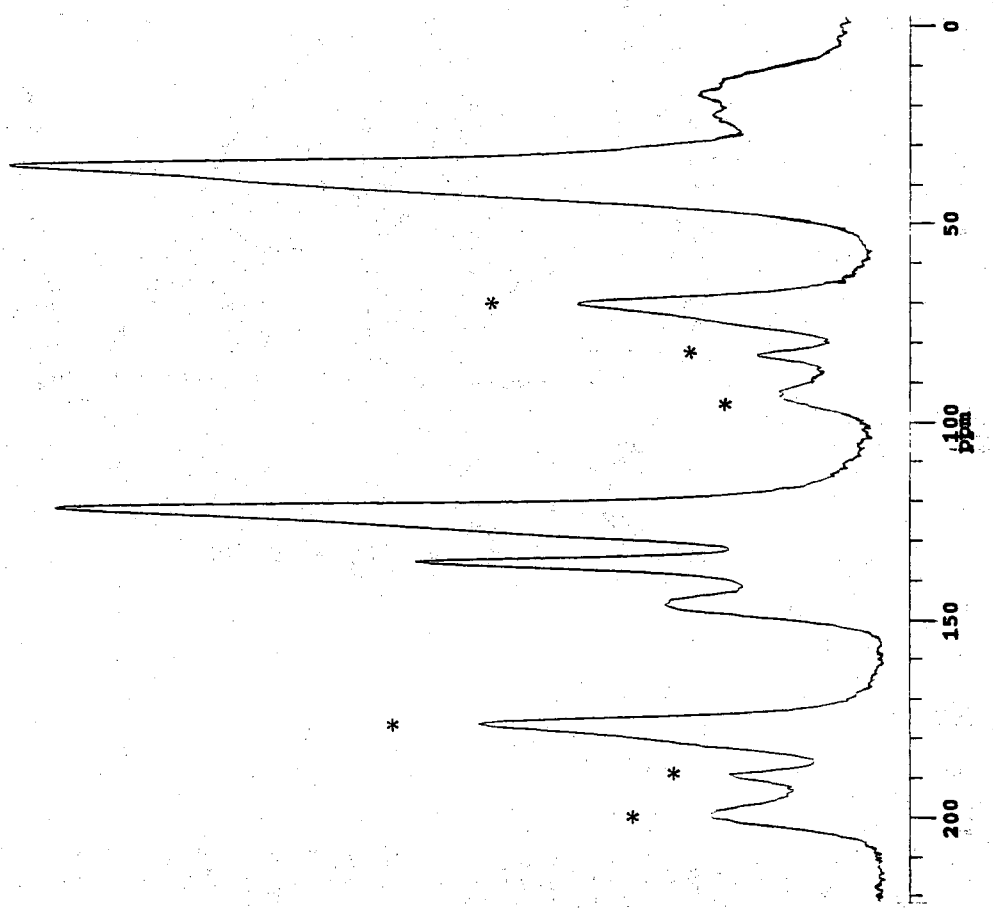

Figure 32. ^{13}C CP-MAS NMR spectrum of 7% Ag(I) exchanged Amberlyst 15 resin.

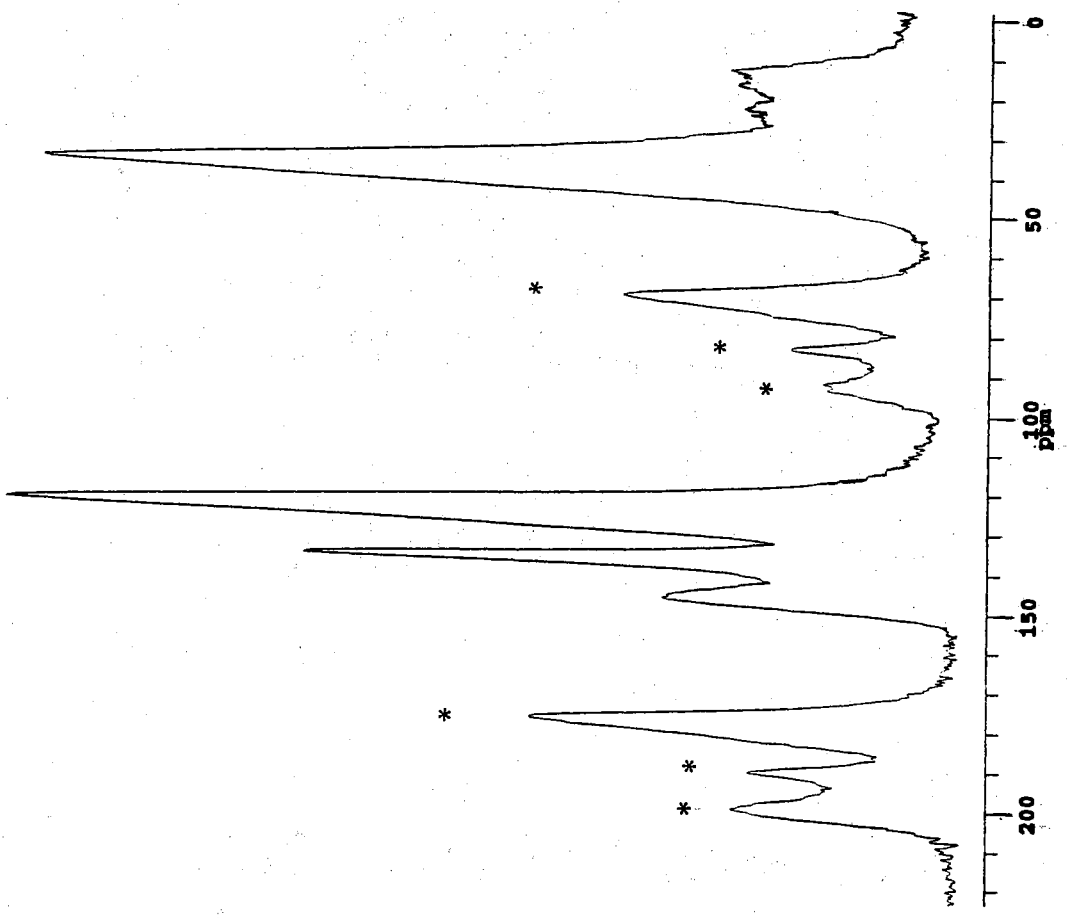

Figure 33. ^{13}C CP-MAS NMR spectrum of 61% Ag(I) exchanged Amberlyst 15 resin.

DRIFTS Spectra

The DRIFTS spectrum of the 110 °C air dried unexchanged Amberlyst 15 resin and the DRIFTS spectrum of the 120 °C vacuo dried unexchanged Amberlyst 15 resin are presented in Figures 34 and 35 respectfully, and band assignments are based on previous reports (Zundel, 1969; Bartholin et al., 1981; Bazuin and Fan; 1995). In both spectra, intense bands at 900 cm^{-1} and 1350 cm^{-1} are assigned to the S-O vibrational stretch and S=O antisymmetrical stretch of the sulfonic acid respectfully. The bands of polystyrene-divinylbenzene, listed in Table 11, are observed. In the spectrum of the 110 °C dried sample, a broad 1690-1640 cm^{-1} band and continuous 2500-3600 cm^{-1} band, assigned respectfully to the scissor vibration and OH stretch of water, are observed. In addition, a band at 1128 cm^{-1}, assigned to the in-plane vibration of the phenyl ring, is observed. In the spectrum of the 120 °C vacuo dried sample, the 2000-3600 cm^{-1} band of water is still observed; however, the intensity of the 1690-1640 cm^{-1} band of water is reduced, and a band at 2209 cm^{-1}, assigned to the OH stretch of the hydrogen bridge, is resolved. In both spectra, the band, assigned to the in-plane bending vibration of the phenyl ring, is observed at 1006 cm^{-1}.

The DRIFTS spectrum of the 110 °C air dried 61% Ag(I) exchanged Amberlyst 15 resin and the DRIFTS spectrum of 120 °C vacuo dried 61% Ag(I) exchanged Amberlyst 15 resin are presented in Figures 36 and 37 respectfully, and band assignments are based on previous reports (Zundel, 1969; Bartholin et al., 1981; Bazuin and Fan, 1995). In both spectra, unchanged bands of polystyrene-divinylbenzene are observed. A strong band, centered at 1200 cm^{-1} (i.e. split at 1215 cm^{-1} and 1185 cm^{-1}), which is assigned to the S-O symmetric stretch of the sulfonate anion, and a band at 1006 cm^{-1}, which is assigned to the in-plane bending vibration of the phenyl ring, are also observed. In the spectrum of the

110 °C air dried sample, the band, assigned to the in-plane skeleton vibration of the phenyl ring, is observed at 1126 cm^{-1} and is overlapped by the intense sulfonate anion band at 1200 cm^{-1}. In the spectrum of the 120 °C vacuo dried sample, the intensity of the 1126 cm^{-1} band is reduced and overlapped by the sulfonate anion band, and the intensities of the 3420 cm^{-1} and 1640 cm^{-1} bands of water are reduced.

The DRIFTS spectra of the 110 °C dried unexchanged and 0 to 61% Ag(I) exchanged Amberlyst 15 resins are overlayed in Figures 38, 39, and 40, and band assignments are based on previous reports (Zundel, 1969; Bartholin et al., 1981; Bazuin and Fan, 1995). The spectra are characterized by intensity shifts of the 900 cm^{-1} and 1350 cm^{-1} bands of sulfonic acid, the 1200 cm^{-1} band of the sulfonate anion, and the 1640-1690 cm^{-1} and 2500-3600 cm^{-1} bands of water. In the series of spectra, the band assigned to in-plane vibration of the phenyl ring is observed at 1126 cm^{-1}, and the band assigned to the bend of the phenyl ring is observed at 1006 cm^{-1}.

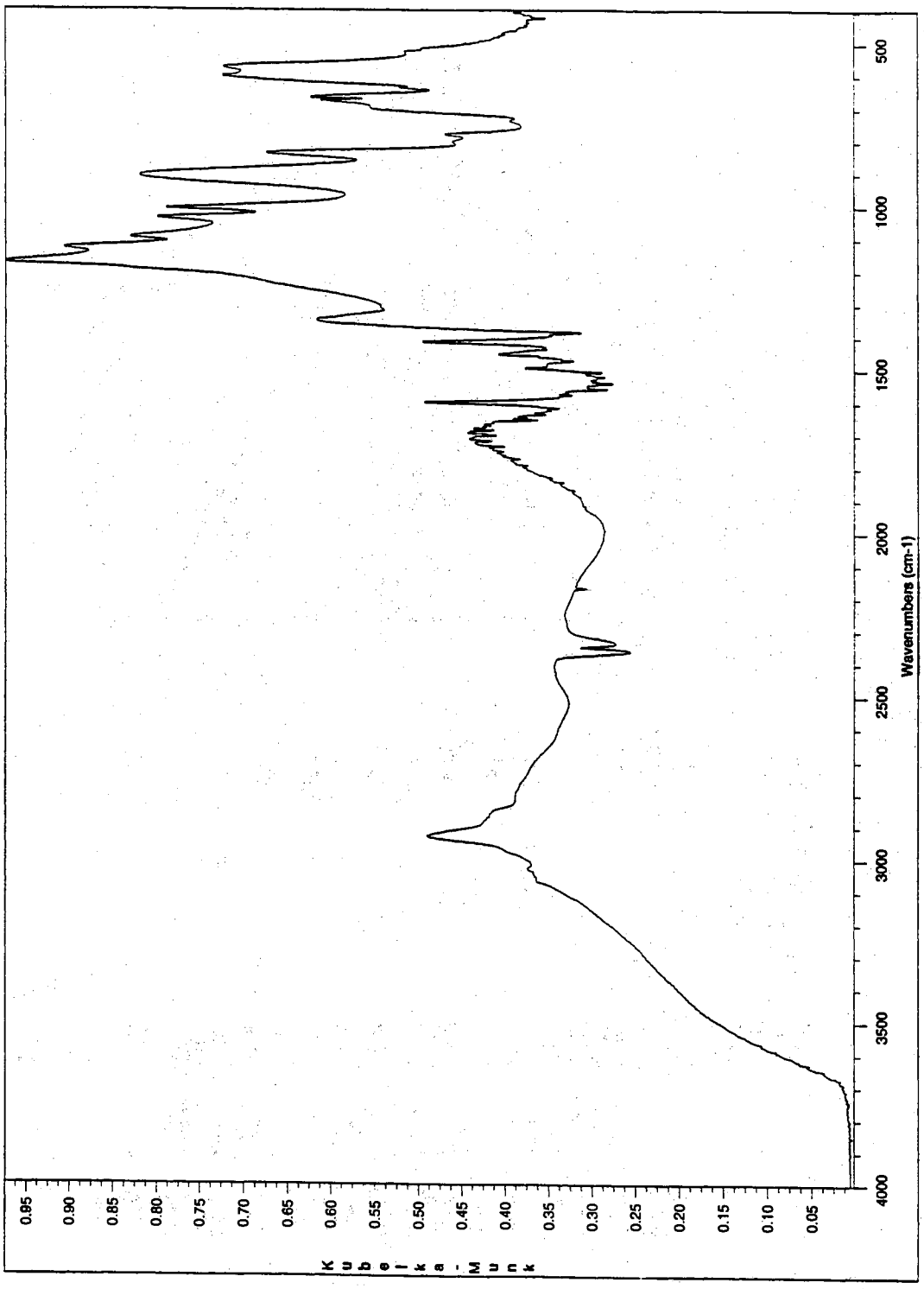

Figure 34. DRIFTS spectrum of 110 °C air dried unexchanged Amberlyst 15 resin.

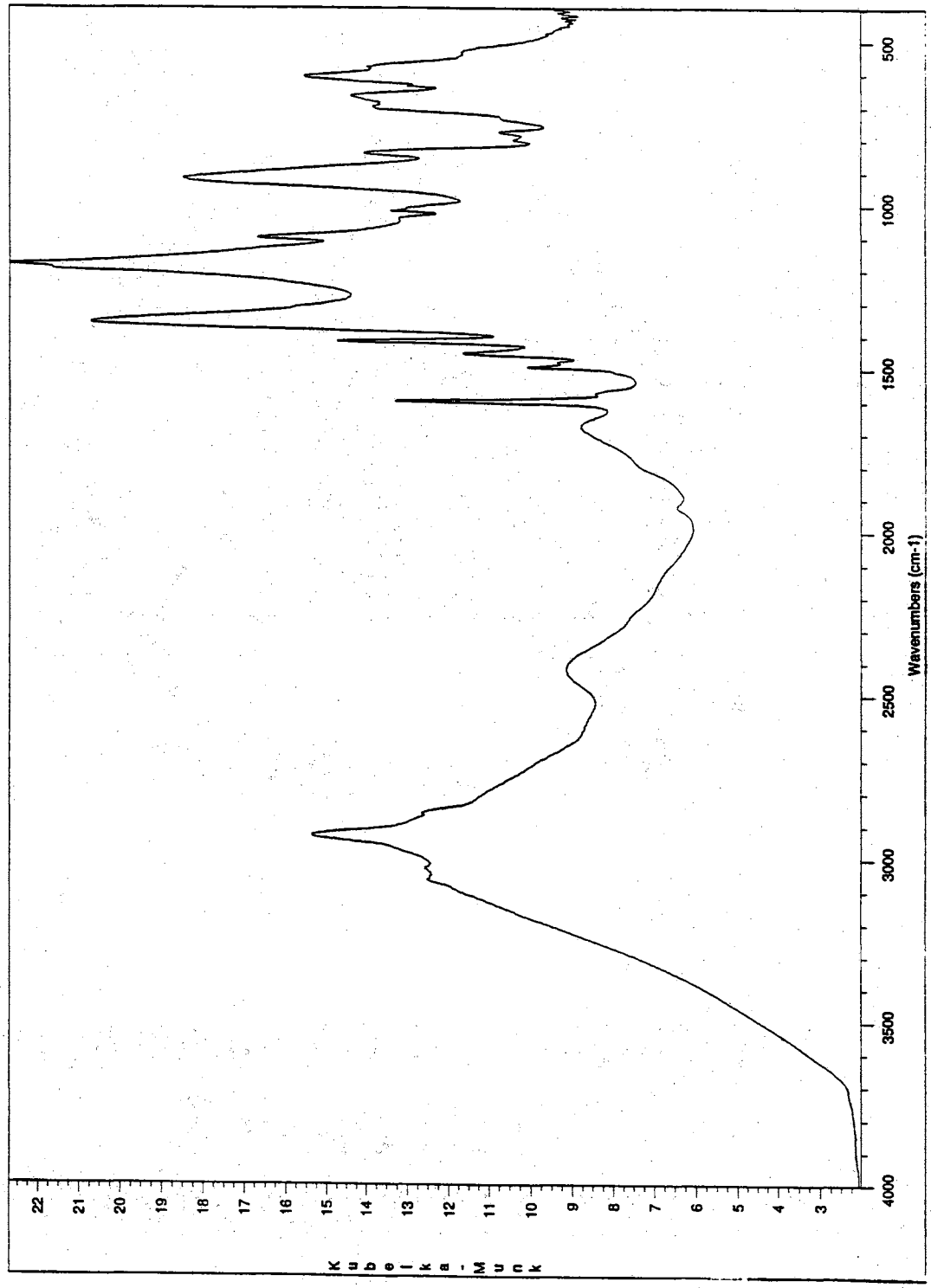

Figure 35. DRIFTS spectrum of 120 °C vacuo dried unexchanged Amberlyst 15 resin.

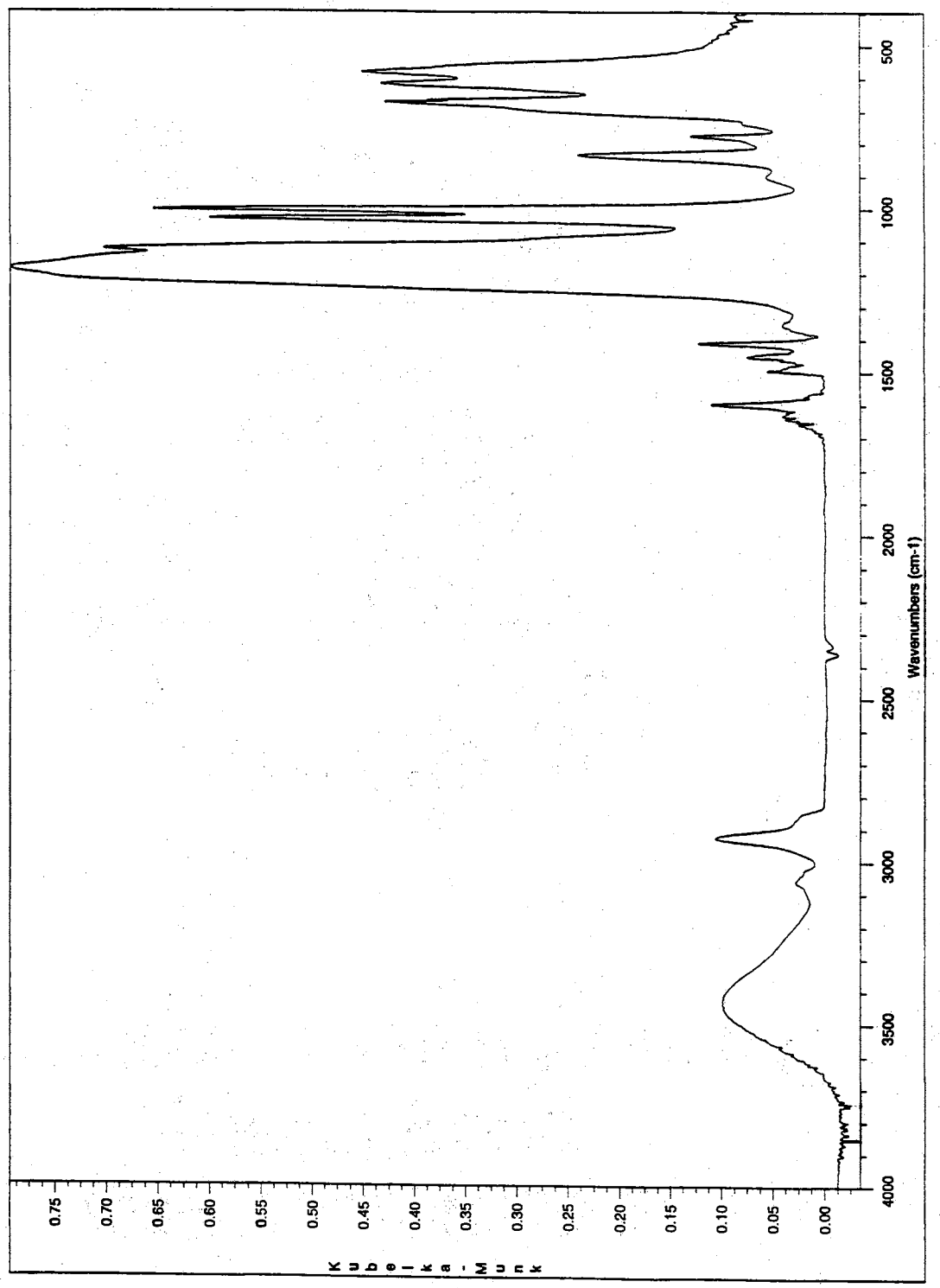

Figure 36. DRIFTS spectrum of 110 °C air dried 61% Ag(I) exchanged Amberlyst 15 resin.

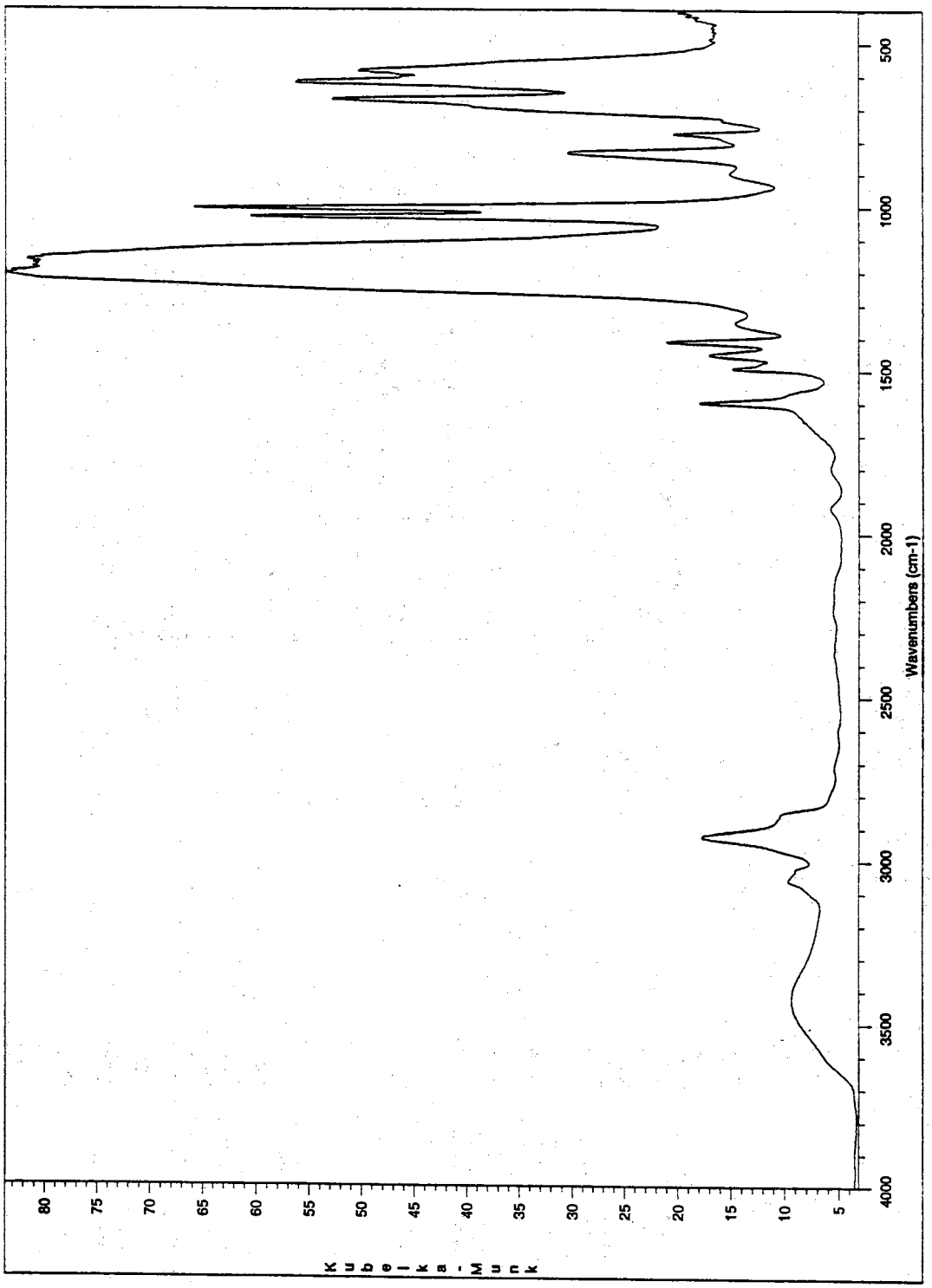

Figure 37. DRIFTS spectrum of 120 °C vacuo dried 61% Ag(I) exchanged Amberlyst 15 resin.

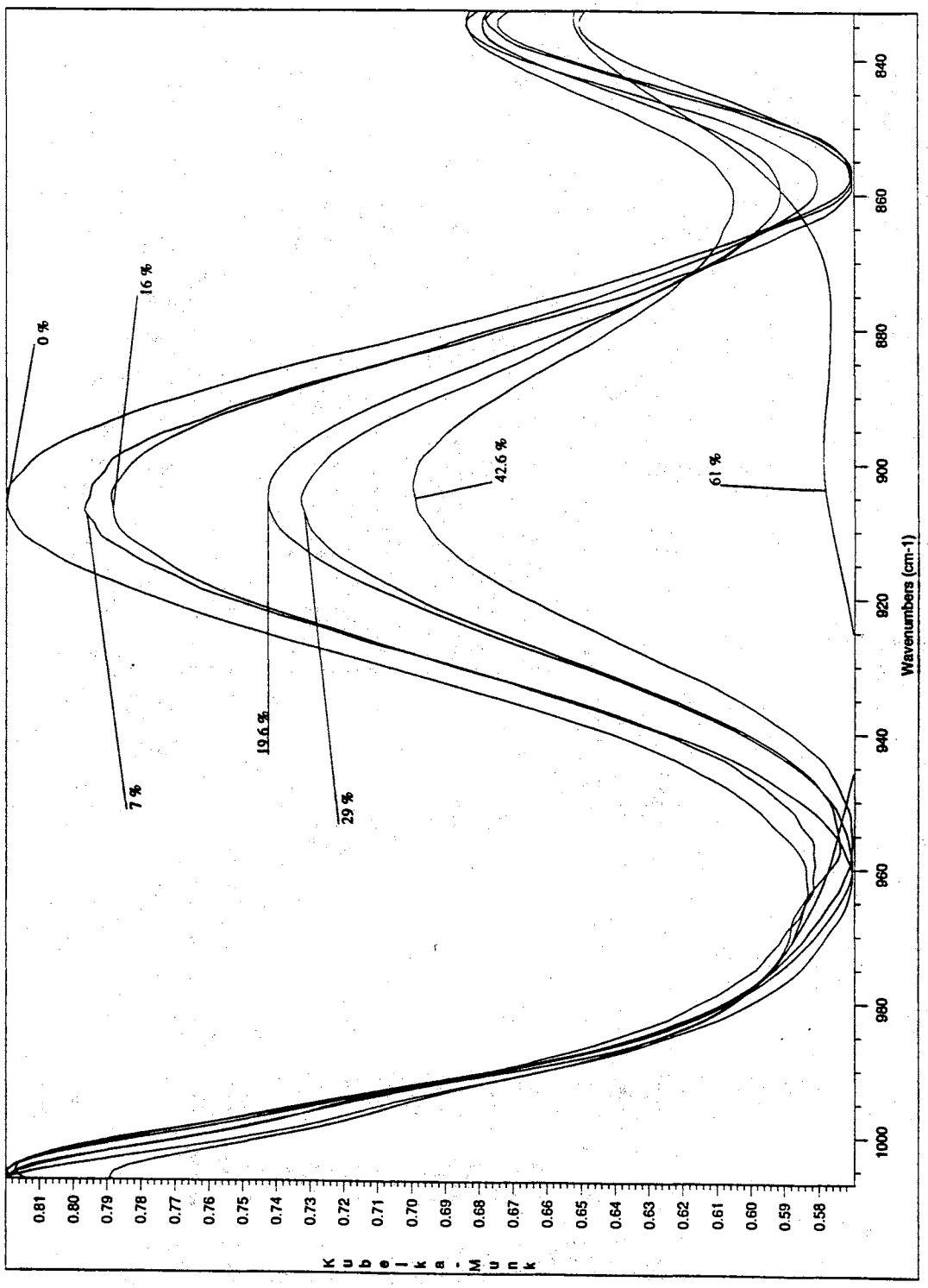

Figure 38. Overlaid DRIFTS spectra of 110 °C air dried 0-61% Ag(I) exchanged Amberlyst 15 resins.

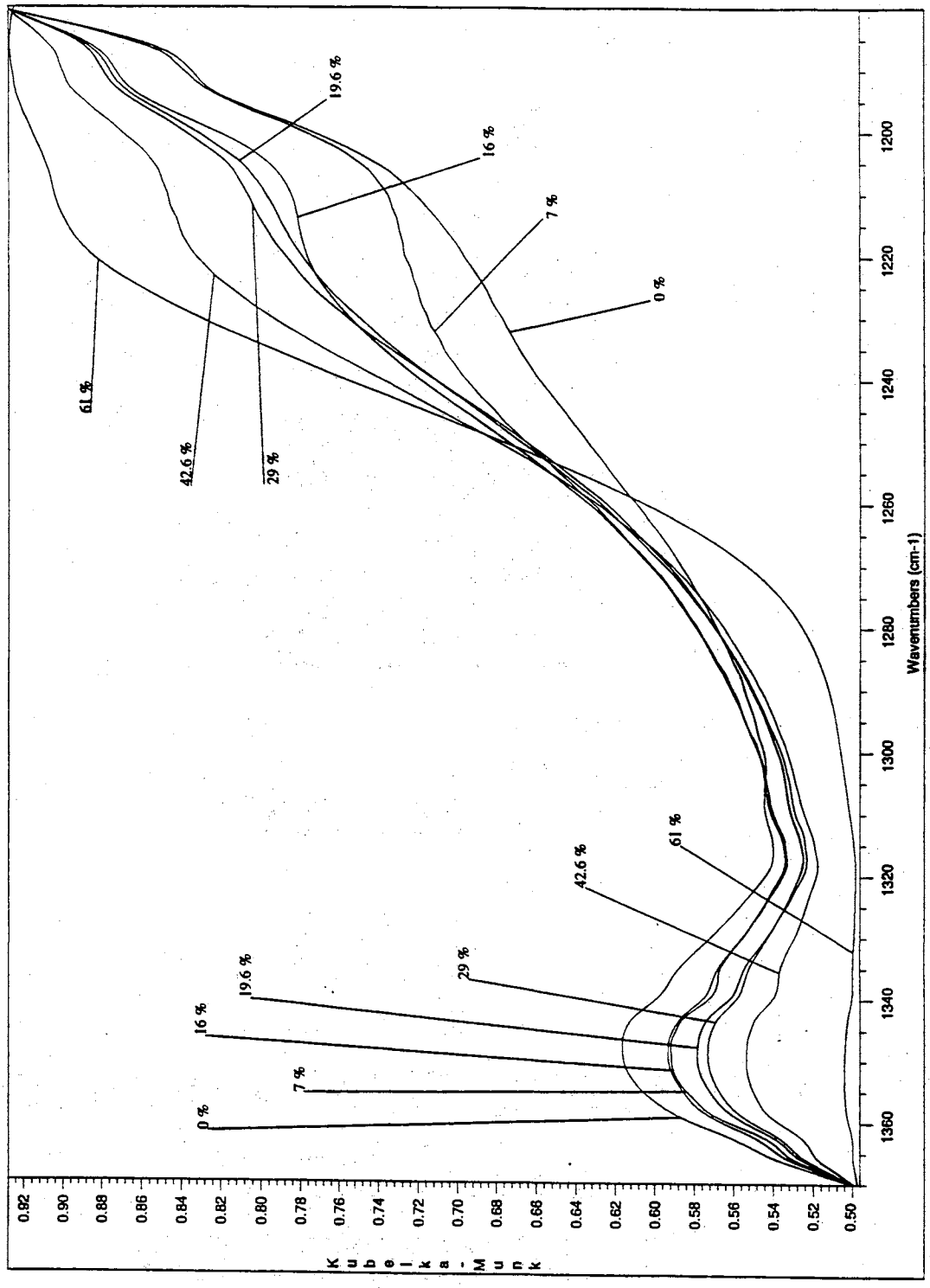

Figure 39. Overlaid DRIFTS spectra of 110 °C air dried 0-61% Ag(I) exchanged Amberlyst 15 resins.

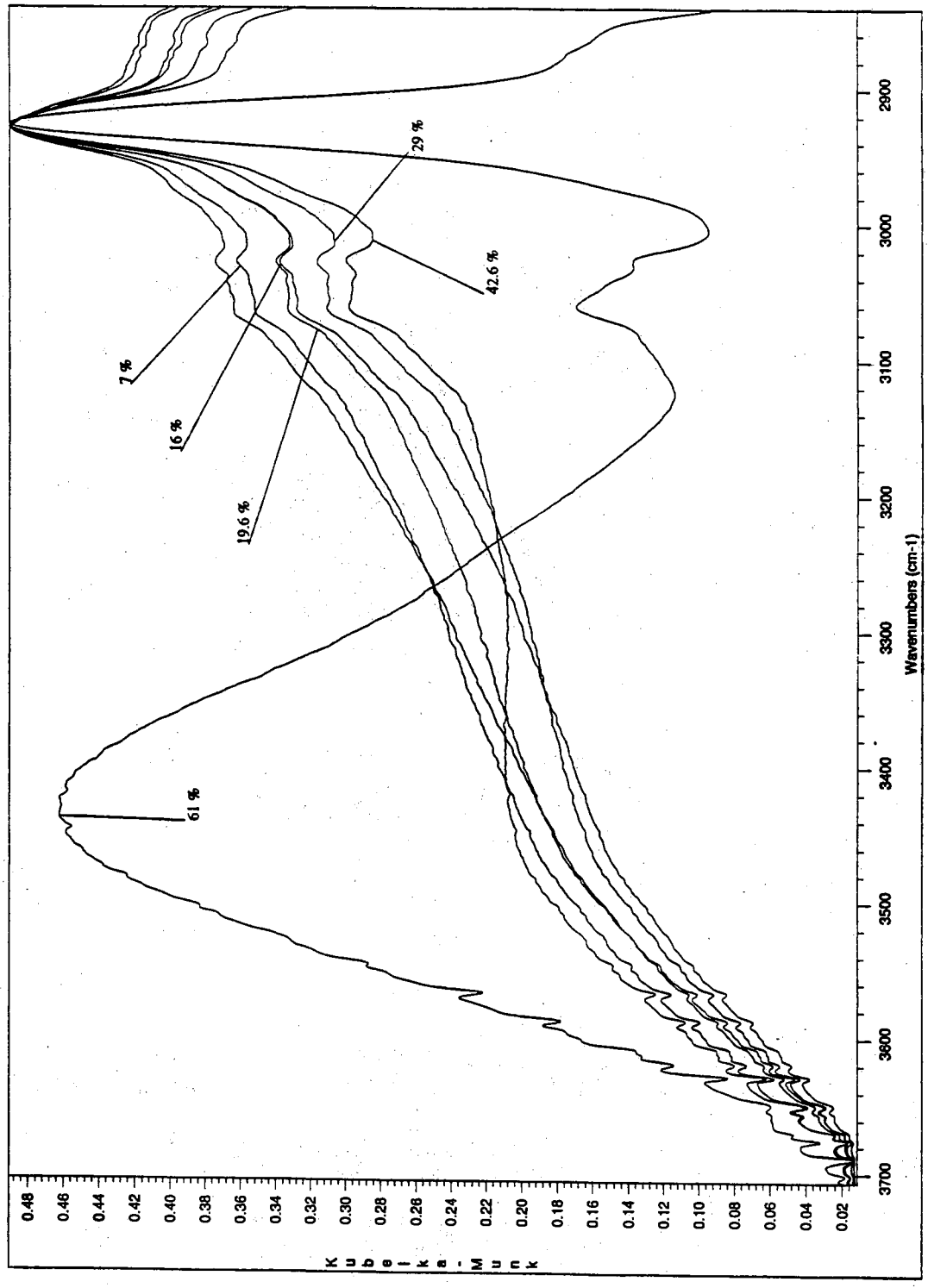

Figure 40. Overlaid DRIFTS spectra of 110 °C air dried 0-61% Ag(I) exchanged Amberlyst 15 resins.

Discussion

The nitrogen adsorption data, mercury porosimetry data, SEM images and ^{13}C CP-MAS NMR spectra, collected on the unexchanged, 7% Ag(I) exchanged, and 61% Ag(I) exchanged Amberlyst 15 resins, indicate that the physical structure and/or physical properties of the Amberlyst 15 resin are not modified by Ag(I) exchange. For example, the BET analysis and porosimetry data show no deviation in the surface area, pore volume, pore size, and porosity of the Amberlyst 15 resin after Ag(I) exchange. The SEM images of the resin samples, which were of poor resolution and magnification, show no deviations in the physical structure after exchange. The ^{13}C CP-MAS NMR spectra of the samples, revealing no additional resonances and/or shifted resonances after exchange, indicate that the carbon backbone of the Amberlyst 15 resin is not affected by Ag(I) exchange. These results are easily rationalized by the smaller hydration sphere of the hydrated Ag(I) cation (Bonner and Rhett, 1953). For example, due to the smaller hydration sphere, the Ag(I) cation easily migrates through the pore structure of the Amberlyt 15 resin without modifying the physical properties or blocking the pores of the Amberlyst 15 resin.

The Ag(I) intensities, observed in the EDXAS profiles of the unexchanged and Ag(I) exchanged Amberlyst 15 resin samples, indicate that Ag(I) is homogeneously dispersed throughout the Amberlyst 15 resin bead. For example, equal intensities of the Ag(I) peaks were observed for the surface, inner surface, and core of the Ag(I) exchanged Amberlyst 15 resins. Yasuda et al. (1997), based on EDXAS profiles of Y_2O_3 in carbon fiber, have made similar conclusions about the dispersion of Y_2O_3 within the fiber. This result is in agreement with the nitrogen adsorption results, mercury porosimetry data, SEM images, and ^{13}C CP-MAS NMR spectra which indicate that Ag(I) cation readily diffuses through the Amberlyst 15 resin.

The infrared band changes and ^{1}H resonance shifts observed in the DRIFTS and ^{1}H NMR spectra of the unexchanged and Ag(I) exchanged Amberlyst 15 resins indicate that Ag(I) displaces the acidic proton associated with the sulfonic acid. For example, an

upfield shift of the adsorbed water resonance was observed in the ^{1}H NMR spectra of the unexchanged and Ag(I) exchanged Amberlyst 15 resins as Ag(I) loading increased. Smith et al. (1996), observing similar shifts in the ^{1}H NMR solution spectra of sulfonated polystyrene divinylbenzene resins after neutralization with base, have attributed the shift to removal of the acidic proton of the sulfonic acid. A gradual decrease in intensities of the 900 cm^{-1} and 1350 cm^{-1} bands were observed in the DRIFTS spectra of unexchanged and Ag(I) exchanged Amberlyst 15 resins as the Ag(I) loading increased. Zundel (1969) has similarly observed these bands of polystyrenesulfonic acid to decrease during ion exchange, and Bazuin and Fan (1996) have observed these bands of sulfonated polystyrene ionomers to decrease after the addition of base. Based on these observations, both authors assigned the 900 cm^{-1} and 1350 cm^{-1} bands to the vibrations of the sulfonic acid and attributed the decrease in the band intensities to the displacement of the acidic proton of the sulfonic acid.

The infrared band changes observed in the DRIFTS spectra of the unexchanged and Ag(I) exchanged Amberlyst 15 resins indicate that Ag(I) interacts with the oxygen of the sulfonate anion. For example, in the DRIFTS spectra of Ag(I) exchanged Amberlyst 15 resins, the intensity of a split band, centered at 1200 cm^{-1}, was observed to increase at higher Ag(I) loadings. Zundel (1969) has similarly observed this split band at 1200 cm^{-1} during ion exchange of polystyrenesulfonic acid. Based on these changes, Zundel assigned the 1200 cm^{-1} band to the symmetric stretch of the S-O bond of the sulfonate anion and attributred the split to the interaction of the metal cation with the oxygen of the sulfonate anion.

Consistent with Zundel (1969) and Bazuin and Fan (1996), the changes of the sulfonate bands, characterized in the DRIFTS spectra of the Ag(I) exchanged Amberlyst 15 resins and the shifts of the ^{1}H resonances observed in the NMR spectra of the Ag(I) exchanged Amberlyst 15 resins, indicate that the active sites for Ag(I) interaction on the Amberlyst 15 resin are the sulfonate groups. Even though literature reports have suggested

that Ag(I) interacts with the phenyl rings of polystyrene (Donovan and Mowat, 1995) and/or unpolymerized vinyl groups within the polystyrene divinylbenzene resins, these spectroscopic studies provide no evidence to support Ag(I) interaction on these alternative sites.

The infrared bands observed in the DRIFTS spectra of the unexchanged and Ag(I) exchanged Amberlyst 15 resins indicate that Ag(I) exchange reorganizes the hydration structure of the Amberlyst 15 resin. For example, very broad water bands at 3600-2500 cm^{-1} and 1690-1640 cm^{-1} are observed. As proposed by Zundel (1969), these broad and continuous water bands suggest that the Amberlyst 15 resins are hydrated and contain significant quantities of the hydrogen bonded $H_5O_2^+$ and $H_9O_4^+$ species. At increased Ag(I) loadings, the water bands of the Ag(I) exchanged Amberlyst 15 resins are observed to gradually decrease, and eventually, a flat baseline and an isolated OH band of water at 3420 cm^{-1} are observed in the spectra of the 61% Ag(I) exchanged Amberlyst 15 resin. In accord with the postulated structures reported by Zundel (1969), the isolated OH band of water at 3420 cm^{-1} in the 61% Ag(I) exchanged Amberlyst 15 resin implies that the hydration structure of the Amberlyst 15 is progressively more organized at higher Ag(I) loadings and that the structure may consist of water molecules which are bound to Ag(I) cation and hydrogen bonded to surrounding unexchanged sulfonate groups.

The infrared bands observed in the DRIFTS spectra of the 110 °C air dried and 120 °C vacuo dried unexchanged and 61% Ag(I) exchanged Amberlyst 15 resins indicate that the Amberlyst 15 resins retain significant quantities of moisture even after extensive drying. For example, the 1001 cm^{-1} band, assigned to the in-plane bend of the phenyl ring and reported to shift to 1011 cm^{-1} on drying (Zundel, 1969), is observed at 1006 cm^{-1} in both spectra. In both the air dried and vacuo dried spectra, OH vibrational bands of water are observed after extensive drying.

Conclusion

In agreement with previous reports, the DRIFTS and NMR spectra of the unexchanged and Ag(I) exchanged Amberlyst 15 resins conclusively indicate; (1) the sulfonate groups are the active sites for ion exchange on the Amberlyst 15 resin; (2) the hydration structure of the Amberlyst 15 resin is reorganized by ion exchange; and (3) the Amberlyst 15 resins contain significant quantities of moisture even after extensive drying. The nitrogen adsorption data, mercury porosimetry data, and SEM images, collected on the unexchanged, 7% exchanged, and 61% exchanged Amberlyst 15 resins, suggest that the physical structure and physical properties of the Amberlyst 15 resin are not modified by Ag(I) exchange. The EDXAS profiles of the unexchanged, 7% exchanged, and 61% exchanged Amberlyst 15 resins indicate that Ag(I) is homogeneously dispersed within the Amberlyst 15 resin bead.

CHAPTER IV

ADSORPTION OF ETHYLENE AND ETHANE ON UNEXCHANGED AND Ag(I) EXCHANGED AMBERLYST 15 RESINS

Summary

In Chapter IV, temperature dependent ethylene and ethane adsorption data, collected on Ag(I) exchanged Amberlyst 15 resins as a function of binary stream composition and Ag(I) loading using the TGA and MDA, are reported and discussed. The extent of Ag(I) exchange on the Amberlyst 15 resins, estimated by weight analysis and determined by elemental analysis, are presented. DRIFTS-HTEC spectra, used to characterize the nature of the interaction between olefin and 61% Ag(I) exchanged Amberlyst 15 resin, are presented and discussed. When compared with elemental analysis, weight analysis shows to be highly inaccurate for measuring the extent of ion exchange on Amberlyst 15 resins. Gas chromatography analysis of CP grade ethane sets precedence for the evaluation of gas purities in future adsorption studies. When compared with the TGA, the adsorption results indicate that the MDA is a comparable technique which collects adsorption data under conditions more representative of industrial processes. In agreement with previous predictions, the adsorption data indicate that ethylene/ethane selectivities of the Ag(I) exchanged Amberlyst 15 resins dramatically increase as the concentration of ethylene in the binary stream decreases. Although unprecedented in the literature, adsorption data show that extremely low Ag(I) loaded Amberlyst 15 resins have surprisingly high olefin adsorption capacities and olefin/paraffin selectivities. Contradictory to previous infrared studies and adsorption predictions, the DRIFTS spectra and adsorption data suggest that ethylene is primarily physisorbed on the Ag(I) exchanged Amberlyst 15 resin. The combination of nitrogen adsorption data, mercury porosimetry data, EDXAS profiles, temperature dependent adsorption data collected as a function of Ag(I) loading, and

DRIFTS-HTEC spectra suggest that the Ag(I) exchanged Amberlyst 15 resin contain chemically different adsorption sites.

Background

Ag(I) Exchanged Amberlyst 15 Resins

Employing ion exchange from aqueous $AgNO_3$ solutions, Yang and Kikkinides (1995) prepared a 51.7% Ag(I) exchanged sulfonated polystyrene divinylbenzene resin (Amberlyst 15). The extent of Ag(I) exchange on the Amberlyst 15 resin was estimated by weight gain after exchange. The accuracy for determining ion exchange by this procedure was reported to be within 0.1%.

Yang and Kikkinides (1995) collected temperature dependent pure component adsortion and desorption isotherms of ethylene and ethane on the 51.7% Ag(I) exchanged Amberlyst 15 resin by TGA. The isotherm data indicated that the 51.7 Ag(I) exchanged Amberlyst 15 resin selectivity adsorbs 1.15 mmol/g of ethylene and 0.125 mmol/g of ethane, corresponding to an ethylene/Ag(I) mole ratio of 0.4 and an olefin/paraffin adsorption ratio of 9.2. In addition, the heat of ethylene adsorption (10 kcal/mol) was calculated from the temperature dependent adsorption data. The desorption isotherm indicated that 10-15% of the ethylene was irreversibly adsorbed on the 51.7 Ag(I) exchanged Amberlyst 15 resin. The authors reported that the irreversibly adsorbed ethylene was removed at 100 °C, restoring the adsorption capacity of the 51.7% Ag(I) exchanged Amberlyst 15 resin. Finally, Yang and Kikkinides suggested that the olefin selectivities of the 51.7% Ag(I) exchanged Amberlyst 15 resins would increase in binary streams dilute in olefin; however, binary adsorption and/or binary selectivity data were not collected.

Based on these adsorption observations and the olefin-metal π-bond model (Chatt and Duncanson, 1953; Dewar, 1951), Yang and Kikkinides (1995) attributed the selectivity

of the 51.7% Ag(I) exchanged Amberlyst 15 resin to chemisorption of ethylene on the exchanged Ag(I) sites. To support the assertion that ethylene was chemisorbed on the Ag(I) sites, Yang and Kikkinides (1995) performed Extended Huckel Molecular Orbital (EHMO) calculations on a Ag(I)-olefin π–bond. In the calculations, ethylene was bonded to the Ag(I) salt of benzenesulfonic acid, the model compound chosen to represent the resin. Based on the calculations, Yang and Kikkinides concluded that sigma donation accounted for 84% of the bond where as π-backbonding accounted for only 16%. In addition, the calculations yielded a theoretical heat of ethylene adsorption of 29.6 kcal/mole.

Ag(I) Exchanged Amberlyst 35 Resins

Yang et al. (1997) have also prepared Ag(I) exchanged Amberlyst 35 resins having Ag(I) loadings ranging from 31% to 64% of the exchange capacity. Ethylene and ethane adsorption isotherms were collected on the 31 to 64% Ag(I) exchanged Amberlyst 35 resins at RT, 60 °C, and 1 to 1.7 atms by TGA. Adsorption data showed that the a 36.5% Ag(I) exchanged Amberlyst 35 resin adsorbs 1.48 mmol/g of ethylene on a 36.5% and that the ethylene adsorption capacities decrease at higher Ag(I) loadings. Yang proposed that the ethylene adsorption capacities fell at higher loadings becase the additional Ag(I) blocked the pores, preventing access to active sites and reducing olefin adsorption. The heat of ethylene adsorption on the 36.5% Ag(I) exchanged Amberlyst 35 resin (9.35 kcal/mol) was calculated using the temperature dependent adsorption results. The adsorption isotherms indicated that the ethylene/ethane adsorption ratio was maximized at 7.8 on a 45% Ag(I) exchanged Amberlyst 35 resin. The adsorption isotherms also established that the ethylene/Ag(I) mole ratio of the Ag(I) exchanged Amberlyst 35 resins (initially 0.97 at 31% exchange capacity) fell at higher Ag(I) loadings.

Physical and Chemical Adsorbents

In addition to the Ag(I) exchanged resins, physical (i.e. based on physisorption) and chemical (i.e. based on chemisorption) adsorbents have also been investigated for olefin adsorption. As discussed in Chapter I, the physical adsorbents rely on physisorption strengths and diffusion rates to separate olefins from paraffins. The physical adsorbents include zeolites (Shu et al., 1990; Kulvaranon et al., 1990) activated carbon (Ruthven, 1991; Yang, 1987), activated alumina (Ruthven, 1991; Yang, 1987), and alkali metal exchanged zeolites (Schoeller and Mueller, 1986). The chemical adsorbents, on the other hand, rely on the formation of olefin-metal π-bonds for olefin separation. They include soluble metal complexes (Blytas, 1990; Keller et al., 1990) and transition metal supported solids (Yang and Kikkinides, 1995; Yang et al., 1997; Hirai et al., 1985, 1987; Eldridge, 1993). For reference, a thorough review of physical and chemical olefin adsorbents was provided in Chapter I.

Adsorption as a Function of Metal Loading

Tamon et al. (1996) have investigated the adsorption of CO_2 on activated carbon impregnated with copper(I) chloride as a function of metal halide loading. Results indicated that the adsorption capacity of CO_2 increased with copper(I) chloride loading. Plotting the CO_2/copper(I) chloride ratio revealed that the CO_2/copper(I) chloride ratio was maximized at 0.8 on extremely low loaded samples and decreased as copper(I) chloride was added. The authors suggested that the copper(I) chloride at low loadings was highly dispersed, resulting in high CO_2/copper(I) chloride mole ratios. In contrast, at higher copper(I) chloride loadings, the authors proposed that the metal was poorly dispersion resulting in the lower CO_2/copper(I) chloride ratios.

Linlin et al. (1984) have evaluated ethylene adsorption by copper(I) chloride dispersed on activated alumina. Adsorption results indicated that the ethylene adsorption

capacity (4.95 ml/g) reached a maximum at a sample with a loading ratio of 0.31 g copper(I) chloride/g alumina. At higher loadings, the data indicated that the ethylene/copper(I) chloride mole ratio (0.19 at lowest copper(I) loading) decreased. The authors attributed the decrease in the mole ratio to poor dispersion of the copper(I) chloride on the alumina surface.

Yang and Cheng (1995) have investigated pillared interlayered clays impregnated with copper(I) chloride for the separation of ethylene and ethane. Adsorption studies, conducted at 1 atm and 25 °C in single component streams as a function of copper(I) loading, showed that ethylene adsorption capacity was maximized on a clay with a copper(I) chloride/clay mole ratio of 0.38. In addition, the data indicated that the ethylene/copper(I) chloride mole ratio (0.38 at lowest copper(I) loading) steadily declined as the copper(I) chloride loadings increased. Yang et al. (1995) attributed the reduction in the mole ratio at higher loadings to poor dispersion of the copper(I) chloride in the clay lattice.

Adsorption Studies Conducted in Binary Streams

Buss (1996) has measured binary adsorption of CO_2/methane mixtures on activated carbon over a wide range of compositions at 20 °C. In the studies, the CO_2/methane selectivities of the activated carbon, measured at 0.99 atm, ranged from 3.2 in a 94% CO_2/6% methane stream to 5.0 in a 9% CO_2/91% methane stream. In the report, Buss explained that the CO_2 was the more strongly adsorbed component. Therefore, the CO_2, when in low concentration, was preferred by high-energy active sites, and the selectivity was high. At higher concentrations, the CO_2 had to compete with the weaker component (i.e. methane) for energetically weaker active sites, and the selectivity dropped.

Mathias et al. (1996) have evaluated the binary adsorption of nitrogen/oxygen mixtures on 5A zeolite. Adsorption results, collected at 9 atm and 23 °C on the zeolite,

indicated that the nitrogen/oxygen selectivities increased from 1.8 in nitrogen rich streams to 3 for compositions rich in oxygen. In agreement with Buss (1996), Mathias et al. also observed an increase in selectivity as the concentration of the more strongly adsorbed component (i.e. N_2) in the binary stream was reduced.

Infrared Spectroscopy

The infrared bands of ethylene, listed in Table 16, have been reported by Herzberg (1945) and Busca et al.(1996).

Table 15. Infrared Band Assignments of Gas Phase Ethylene[a,b]

vibration	band, cm^{-1}	intensity
$=CH_2$ anti. sym. stretch	3105.5	strong
$=CH_2$ combination	3067[1]	
$=CH_2$ sym. stretch	2989.5	strong
$=CH_2$ combination	2325	weak
$=CH_2$ combination	2047	weak
$=CH_2$ combination	1889.6	medium
C=C sym. stretch	1625[1], inactive	strong
$=CH_2$ in-plane wag	1443	strong
$=CH_2$ in-plane wag	1342.4 inactive	very strong
$=CH_2$ in-plane bend	949	very strong

[a] Herzberg, 1945.
[b] Busca et al. 1996.

Activation of the inactive ethylene bands at 1625 cm^{-1} and 1342.4 cm^{-1} have been shown to indicate formation of olefin-metal π-bonds. For example, Busca et al. (1992) have reported that the C=C symmetrical stretch of ethylene decreases to 1599 cm^{-1} when bonded to ZnO. In an organosilver review by Noltes et al. (1970), coordination of the C=C bond to Ag(I) cation was reported to lower the frequency of the infrared band assigned to the symmetrical C=C bond stretch by 50-60 cm^{-1}. Scott (1972) reported the results of an infrared study on the interaction between cyclooctadiene and $Ag(I)BF_4^-$. In the study, the

infrared spectra indicated that the infrared band assigned to the olefin C=C symmetrical stretch shifted from 1650 cm^{-1} to 1602 cm^{-1} upon coordination to Ag(I) cation. Nagakura and Hosoya (1963) have studied the interaction between cyclohexene and $AgClO_4^-$. The symmetrical stretch of the infrared band assigned to C=C bond of free cyclohexene was reported at 1640 cm^{-1}. Complexation with Ag(I) was observed to shift the frequency of the C=C band to 1585 cm^{-1}. Yates et al. (1966) investigated ethylene adsorbed on Ag(I) zeolite by infrared analysis. Spectra indicated that the band assigned to the inactive C=C symmetrical stretching mode of ethylene was activated and shifted to 1580 cm^{-1} upon complexation with Ag(I) in the zeolite. The band assigned to the inactive wag of ethylene at 1342 cm^{-1} was also activated and reported to shift upfield when complexed with Ag(I) in the zeolite. Nagendrappa and Devaprabhakara (1968) have characterized cis,cis-1,5-cyclononadiene complexes of silver(I) by infrared. Infrared spectra established that the bands assigned to the symmetrical stretches of the C=C bonds of the diene, which appeared at 1646 cm^{-1} and 1653 cm^{-1}, respectfully, shifted to 1592 cm^{-1} and 1602 cm^{-1} upon complexation with Ag(I).

Elemental Analysis and Weight Analysis of Ag(I) Exchange

The extent of Ag(I) exchange on the Amberlyst 15 resin, estimated by weight analysis and calculated by elemental analysis, is presented in Table 17.

Table 16. Extent of Ag(I) Exchange on Amberlyst 15 Resin[a]

weight analysis, %	elemental analysis, %	difference, %
--	7.0	--
12.5	16.0	28
14.0	19.6	29
21.8	29.0	25
34.9	42.6	18
75.1	61.0	23

[a]Total weight gain based on 4.7 meg/g = 0.507 g Ag(I)/g resin.

Adsorption and Desorption of Ethylene and Ethane

Ethylene and ethane adsorption isotherms of unexchanged and 61% Ag(I) exchanged Amberlyst 15 resins are presented in Figure 41. The isotherms were collected at 1 atm and RT using the TGA. As shown, the unexchanged Amberlyst 15 resin adsorbs 0.18 mmol/g of ethylene and 0.18 mmol/g of ethane. The 61% Ag(I) exchanged Amberlyst 15 resin selectively adsorbs 1.15 mmol/g of ethylene and 0.26 mmol/g of ethane, corresponding to an adsorption ratio of 4.4.

Ethylene adsorption and desorption isotherms of 61% Ag(I) exchanged Amberlyst 15 resin are presented in Figure 42. The isotherms was collected at 1 atm and RT using the TGA. As indicated, the 61% Ag(I) exchanged Amberlyst 15 resin irreversibly adsorbs 14% of the 1.15 mmol/g of ethylene.

The ethylene adsorption isotherm of 7% Ag(I) exchanged Amberlyst 15 resin ispresented in Figure 43. The isotherm was collected at 1 atm and RT using the TGA. As

shown, the 7% Ag(I) exchanged Amberlyst 15 resin selectively adsorbs 0.83 mmol/g of ethylene. As discussed in Chapter II, ethane adsorption isotherms were not collected due to ethylene contaminant in the ethane feed.

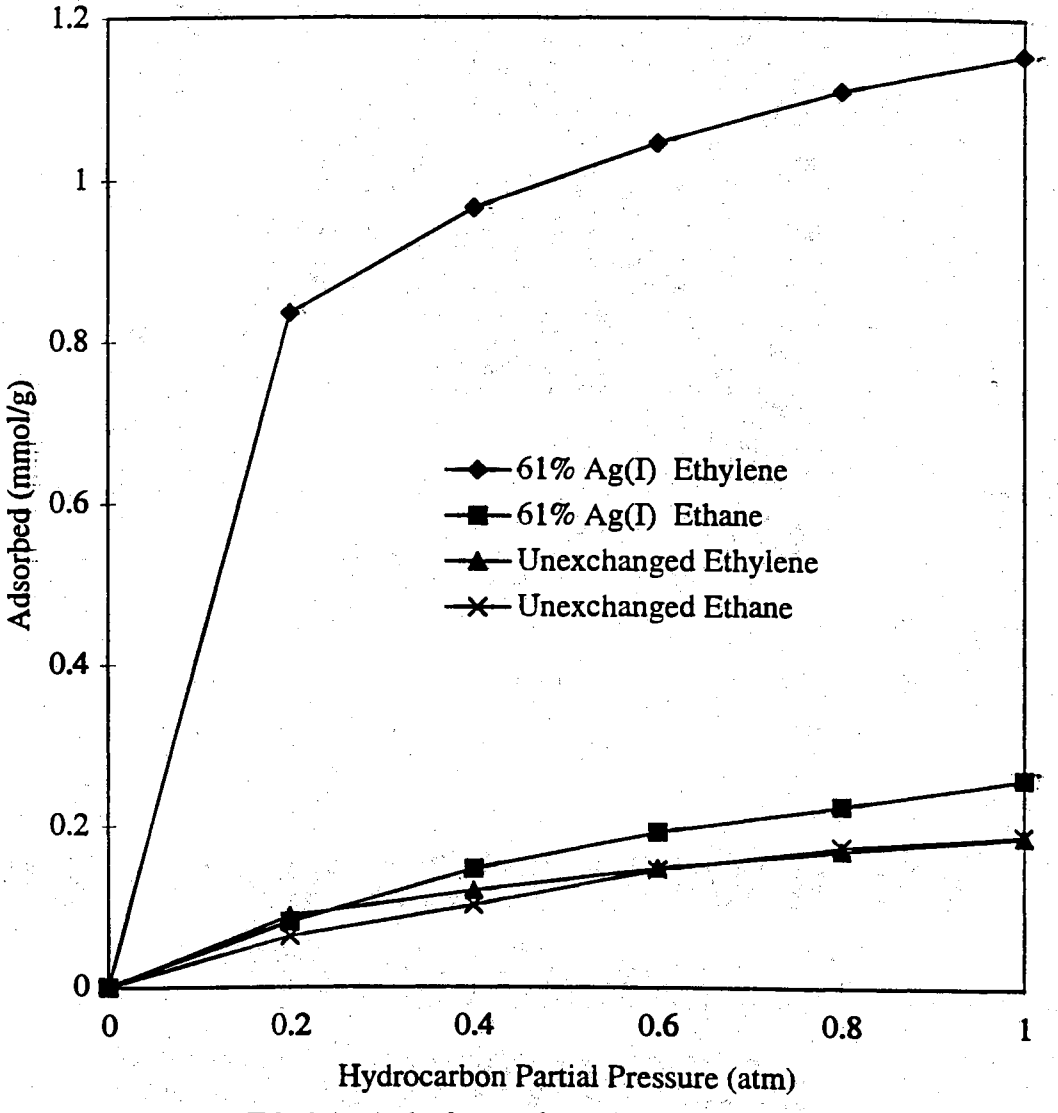

Figure 41. Ethylene and ethane adsorption isotherms of unexchanged and 61% Ag(I) exchanged Amberlyst 15 resins.

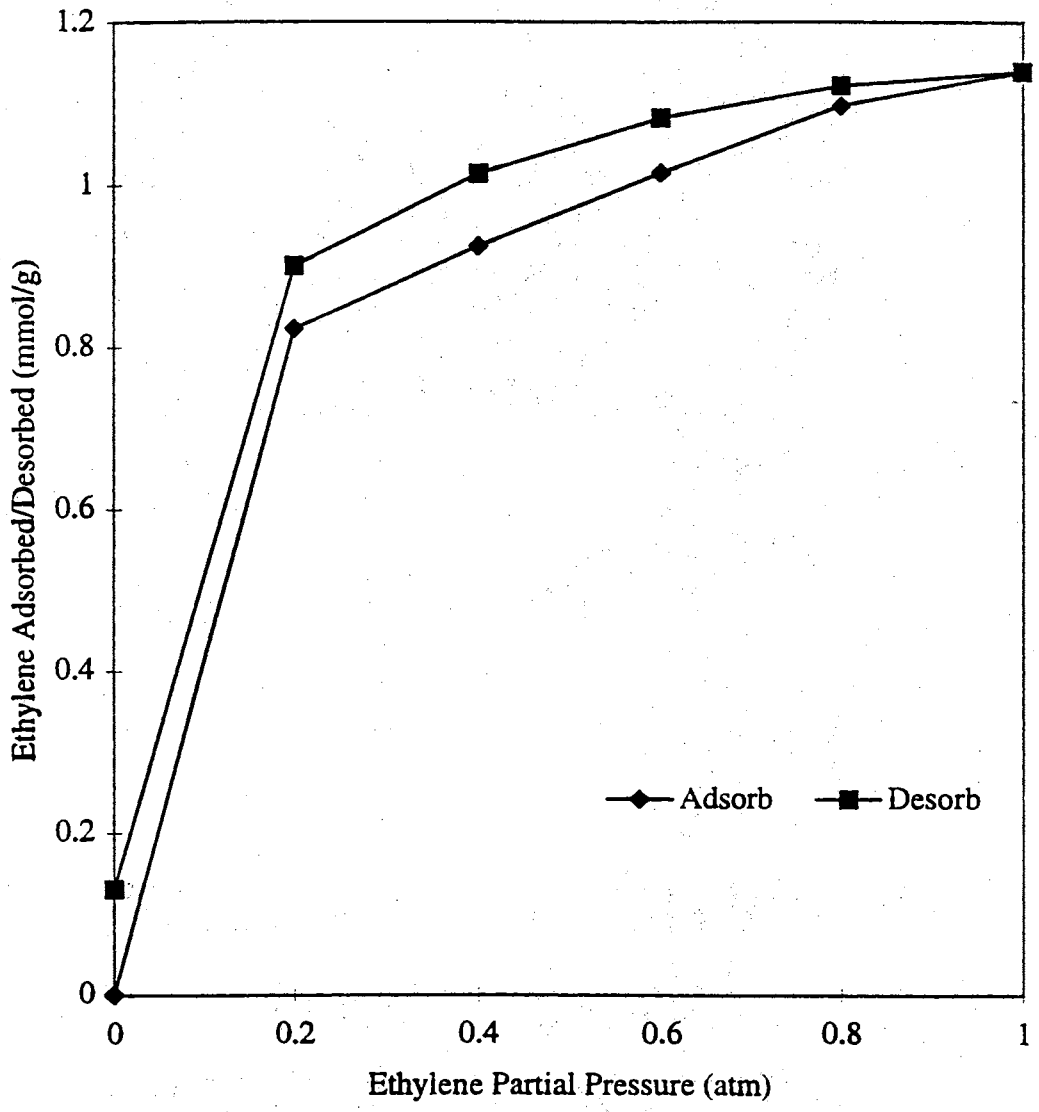

Figure 42. Ethylene adsorption and desorption isotherms of 61% Ag(I) exchanged Amberlyst 15 resin.

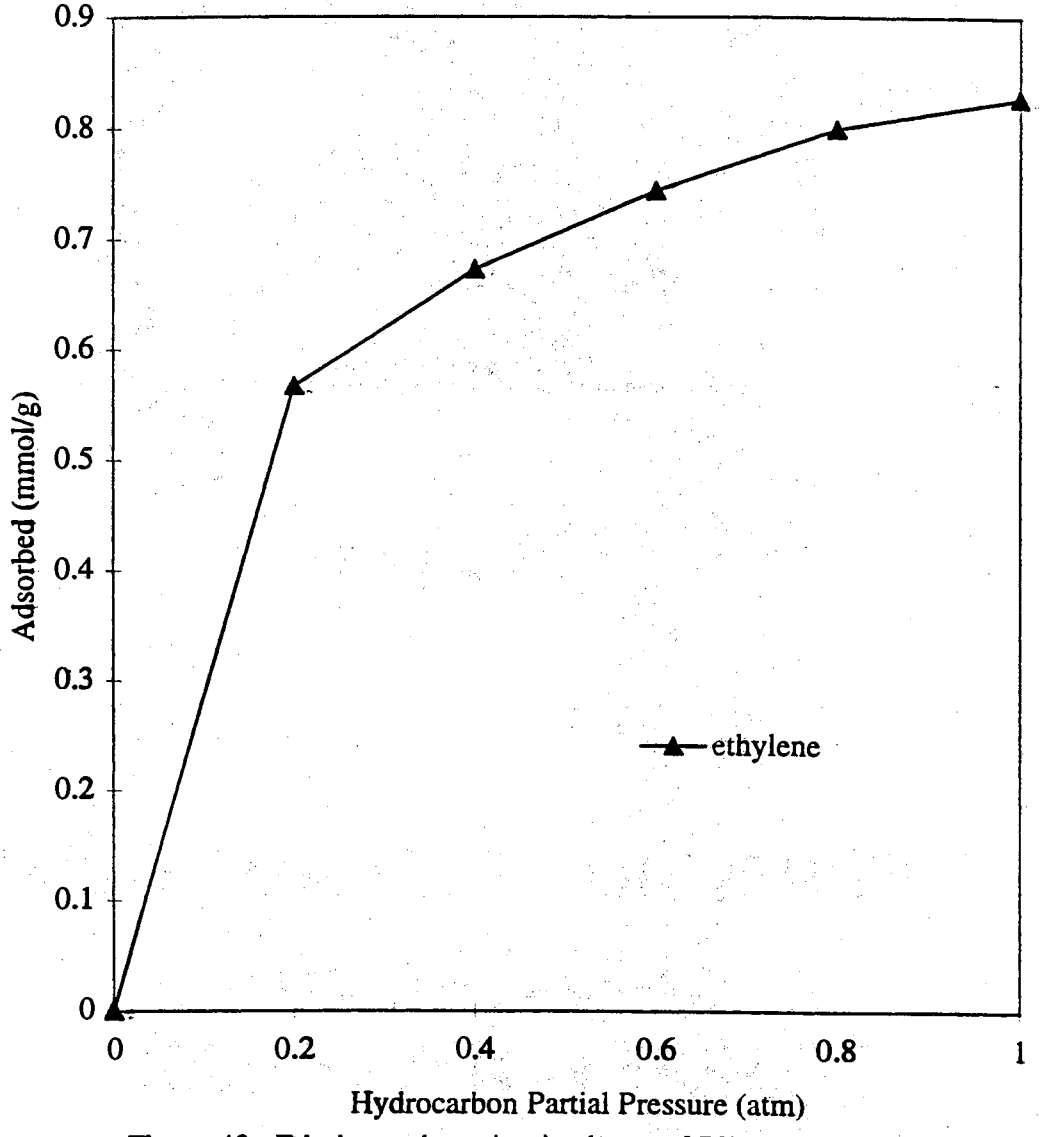

Figure 43. Ethylene adsorption isotherm of 7% Ag(I) exchanged Amberlyst 15 resin.

Ethylene adsorption of Ag(I) exchanged Amberlyst 15 resins as a function of Ag(I) loading is presented in Figure 44. The data were collected at RT and 1 atm using the TGA. As shown, ethylene adsorption capacities initially increase at low Ag(I) loadings and reach a maximum of 1.42 mmol/g on the 29% Ag(I) exchanged Amberlyst 15 resin. At higher Ag(I) loadings, the olefin adsorption capacities of the Ag(I) exchanged Amberlyst 15 resins decrease by over 20%.

Ethylene/Ag(I) mole ratios of the Ag(I) exchanged Amberlyst 15 resins as a function of Ag(I) loadings are presented in Figure 45. The mole ratios were calculated from the results in Figure 44. As shown, the ethylene/Ag(I) mole ratios of the 42.6% and 61% Ag(I) exchanged Amberlyst 15 resins are less than 1. For example, the 42.6% Ag(I) exchanged Amberlyst 15 resin has an ethylene/Ag(I) mole ratio of 0.7. Conversely, the ethylene/Ag(I) mole ratios of the 7-29% Ag(I) exchanged Amberlyst 15 resins exceed 1. For example, the 19.6% Ag(I) exchanged Amberlyst 15 resin has an ethylene/Ag(I) mole ratio of 1.4, and the 7% Ag(I) exchanged Amberlyst 15 resin has an even larger ethylene/Ag(I) mole ratio of 2.5.

Temperature dependent ethylene adsorption isotherms of 7% and 61% Ag(I) exchanged Amberlyst 15 resins are presented in Figures 46 and 47. The isotherms were collected at 1 atm and 60 °C. From the temperature dependent adsorption data, the heats of ethylene adsorption on the 7% and 61% Ag(I) exchanged Amberlyst 15 resins were calculated. The heats of ethylene adsoption on both resins were 10 kcal/mol.

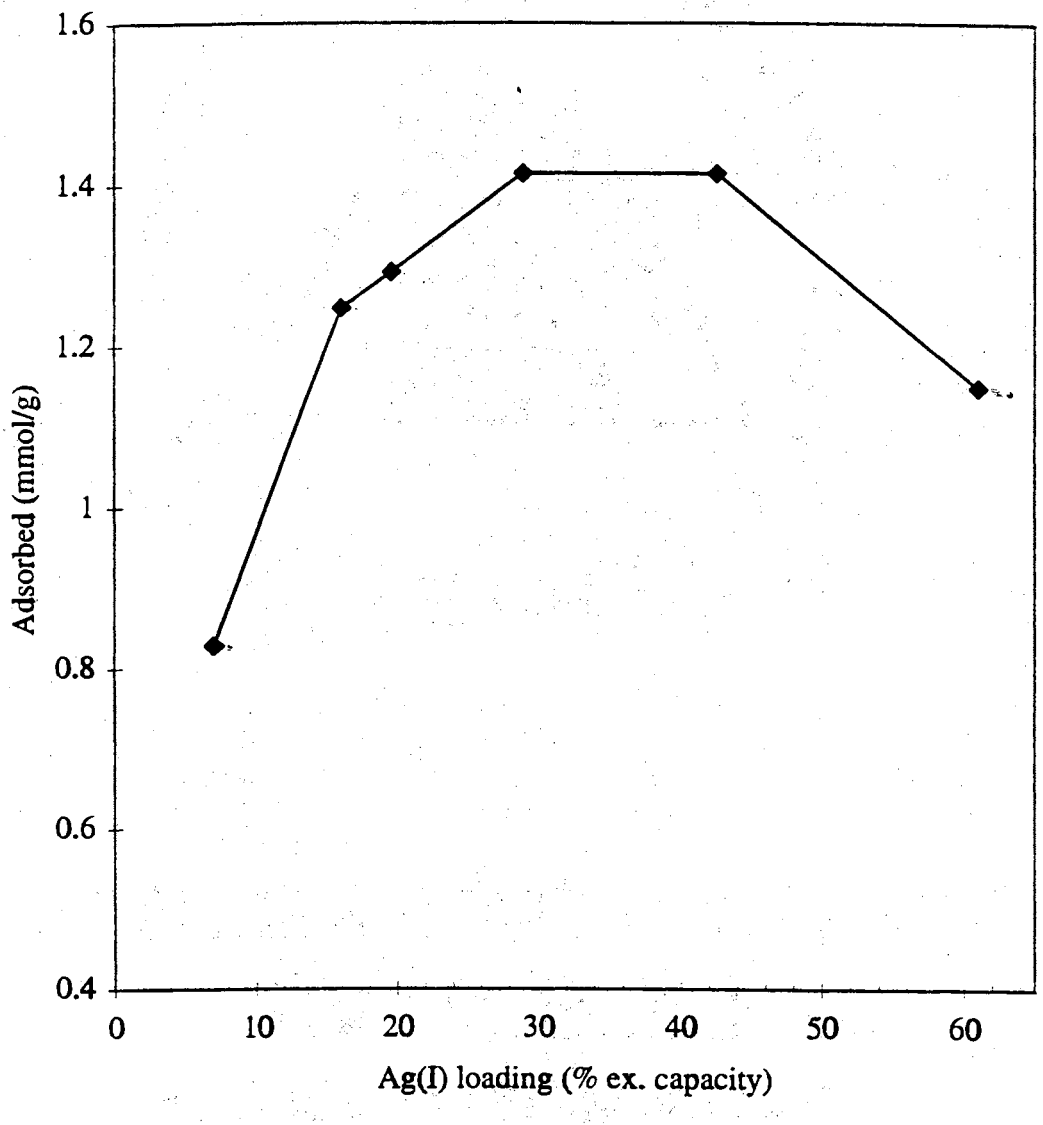

Figure 44. Ethylene adsorption of Ag(I) exchanged Amberlyst 15 resins as a function of Ag(I) loading.

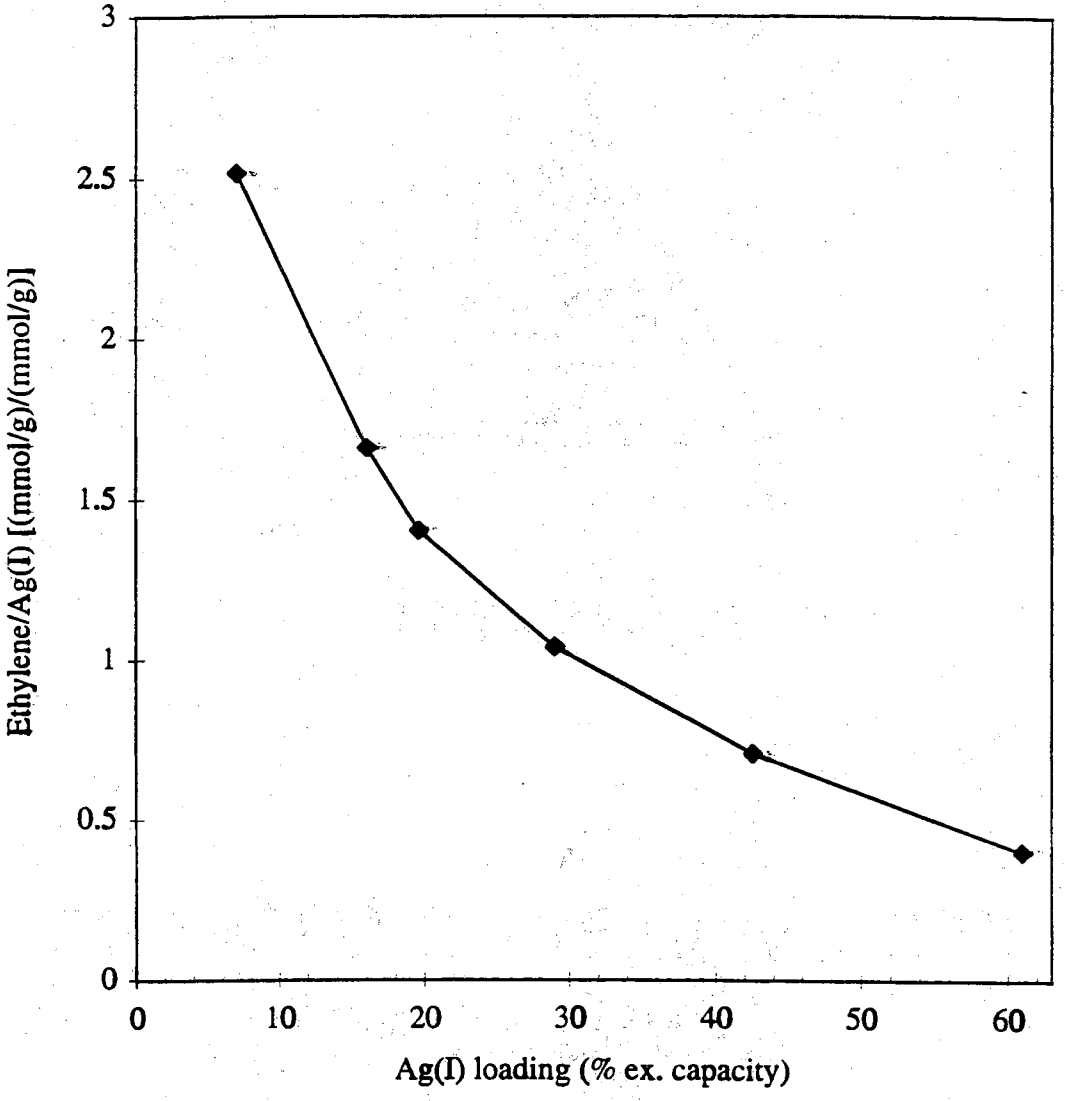

Figure 45. Ethylene/Ag(I) mol ratios of Ag(I) exchanged Amberlyst 15 resin as a function of Ag(I) loading.

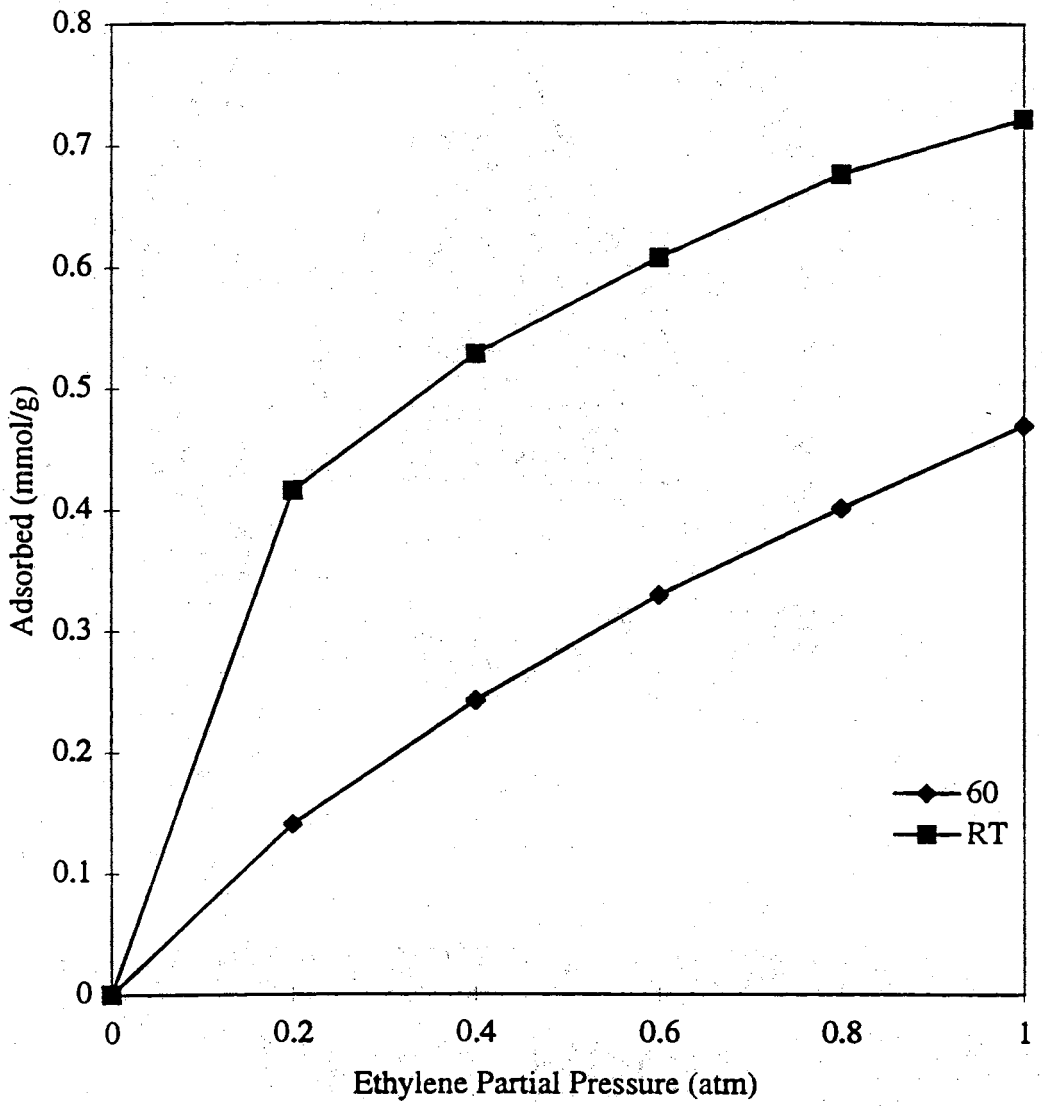

Figure 46. Temperature dependent ethylene adsorption isotherms of 7% Ag(I) exchanged Amberlyst 15 resin.

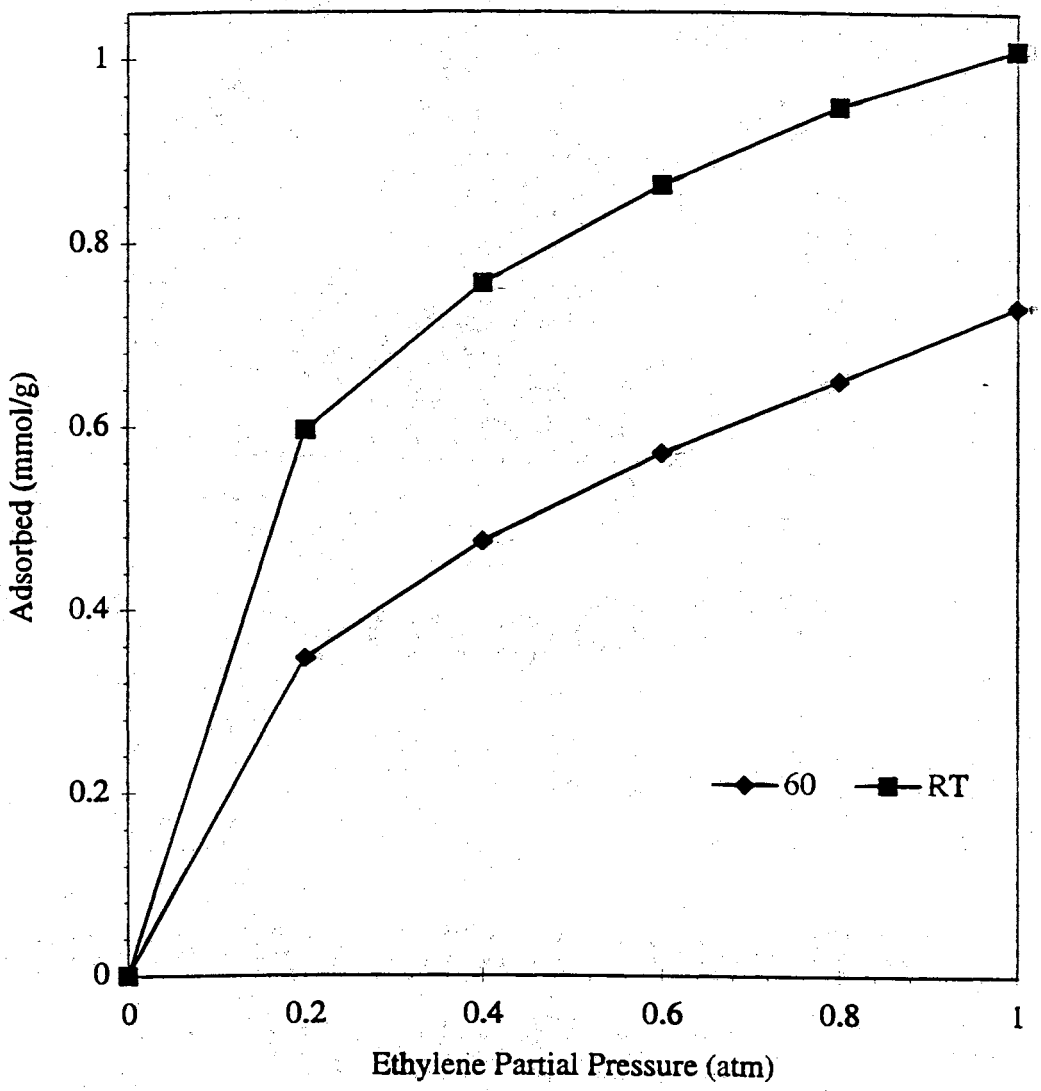

Figure 47. Temperature dependent ethylene adsorption isotherms of 61% Ag(I) exchanged Amberlyst 15 resin.

Temperature dependent desorption of ethylene from 61% Ag(I) exchanged Amberlyst 15 is presented in Figure 48. For adsorption, the sample was charged at RT and 1 atm with a pure stream of ethylene for 20 min. Desorption was carried out at RT and 100 °C using the MDA. As shown, desorption at 100 °C removes 1.15 mmol/g of ethylene and desorption at RT removes 0.98 mmol/g of ethylene.

Adsorption and Desorption of Ethylene and Ethane Mixtures

Temperature dependent desorption of ethylene and ethane mixtures from 61% Ag(I) exchanged Amberlyst 15 resin as a function of binary stream composition is presented in Figure 49. For adsorption, the sample was charged for 20 min at RT and 1 atm with a binary stream of ethylene and ethane. Desorption was carried out at RT and 100 °C using the MDA. As shown, the desorption of ethylene from the 61% Ag(I) exchanged Amberlyst 15 resin increases as the concentration of ethylene in the binary stream increases. For example, after loading the 61% Ag(I) exchanged Amberlyst 15 resin in a binary stream composed of 40% ethylene and 60% ethane, desorption at 100 °C removes 0.79 mmol/g ethylene and desorption at RT removes 0.48 mmol/g. After loading the same sample with a binary stream composed of 97% ethylene and 3% ethane, desorption at 100 °C removes 1.03 mmol/g of ethylene and 0.69 mmol/g of ethylene at RT. The desorption data also indicate that the desorption of ethylene is temperature dependent. For example, after loading, desorption at 100 °C removes an additional 33-39% of ethylene from the 61% Ag(I) exchanged Amberlyst 15 resin. Data indicate that the desorption of ethane from the 61% Ag(I) exchanged Amberlyst 15 resin is not temperature dependent.

Temperature dependent desorption of ethylene and ethane mixtures from 7% Ag(I) exchanged Amberlyst 15 resin as a function of binary stream composition is presented in Figure 50. For adsorption, the sample was charged for 20 min at RT and 1 atm with a

binary stream of ethylene and ethane. Desorption was carried out at RT and 100 °C using the MDA. As shown, the desorption of ethylene from the 7% Ag(I) exchanged Amberlyst 15 resin increases as the concentration of ethylene in the binary stream increases. For example, after loading the 7% Ag(I) exchanged Amberlyst 15 resin in a binary stream composed of 40% ethylene and 60% ethane, desorption at 100 °C removes 0.51 mmol/g ethylene and desorption at RT removes 0.45 mmol/g. After loading the same sample with a binary stream composed of 80% ethylene and 20% ethane, desorption at 100 °C removes 0.63 mmol/g of ethylene and 0.55 mmol/g of ethylene at RT. The desorption data also show that removal of ethylene is slightly temperature dependent. For example, after loading, desorption at 100 °C removes an additional 11-15% of ethylene from the 7% Ag(I) exchanged Amberlyst 15 resin. Data indicate that the desorption of ethane from the 7% Ag(I) exchanged Amberlyst 15 resin is not temperature dependent, but does increase in streams higher in ethane concentration. For example, in the stream composed of 20% ethane and 80% ethylene, desorption removes 0.02 mmol/g of ethane while in a stream composed of 80% ethylene and 20% ethane, desorption removes 0.09 mmol/g of ethane.

Temperature dependent desorption of ethylene and ethane mixtures from Ag(I) exchanged Amberlyst 15 resins as a function of Ag(I) loading is presented in Figure 51. For adsorption, the samples were charged for 20 min at RT and 1 atm with a binary stream composed of 20% ethylene and 80% ethane. Desorption was carried out at RT and 100 °C using the MDA. As shown, desorption of ethylene significantly increases in going from the 7% Ag(I) exchanged Amberlyst 15 resin to the 16% Ag(I) exchanged Amberlyst 15 resin. At the higher Ag(I) loadings, the data show that the desorption of ethylene is constant and eventually diverges at the 61% Ag(I) loading. The data also show that the desorption of ethylene is temperature dependent at high Ag(I) loadings. For example, desorption at 100 °C removes 0.67 mmol/g of ethylene, while desorption at RT is shown

to remove only 0.39 mmol/g of ethylene. In contrast, at low Ag(I) loading, this temperature dependence is not observed. The data also indicate that the desorption of ethane is not temperature dependent but does fall at high Ag(I) loadings. For example, desorption at RT removes 1.2 mmol/g of ethane from the 7 % Ag(I) exchanged Amberlyst 15 resins while desorption at RT only removes 0.8 mmol/g of ethane from the 61% Ag(I) exchanged Amberlyst 15 resin.

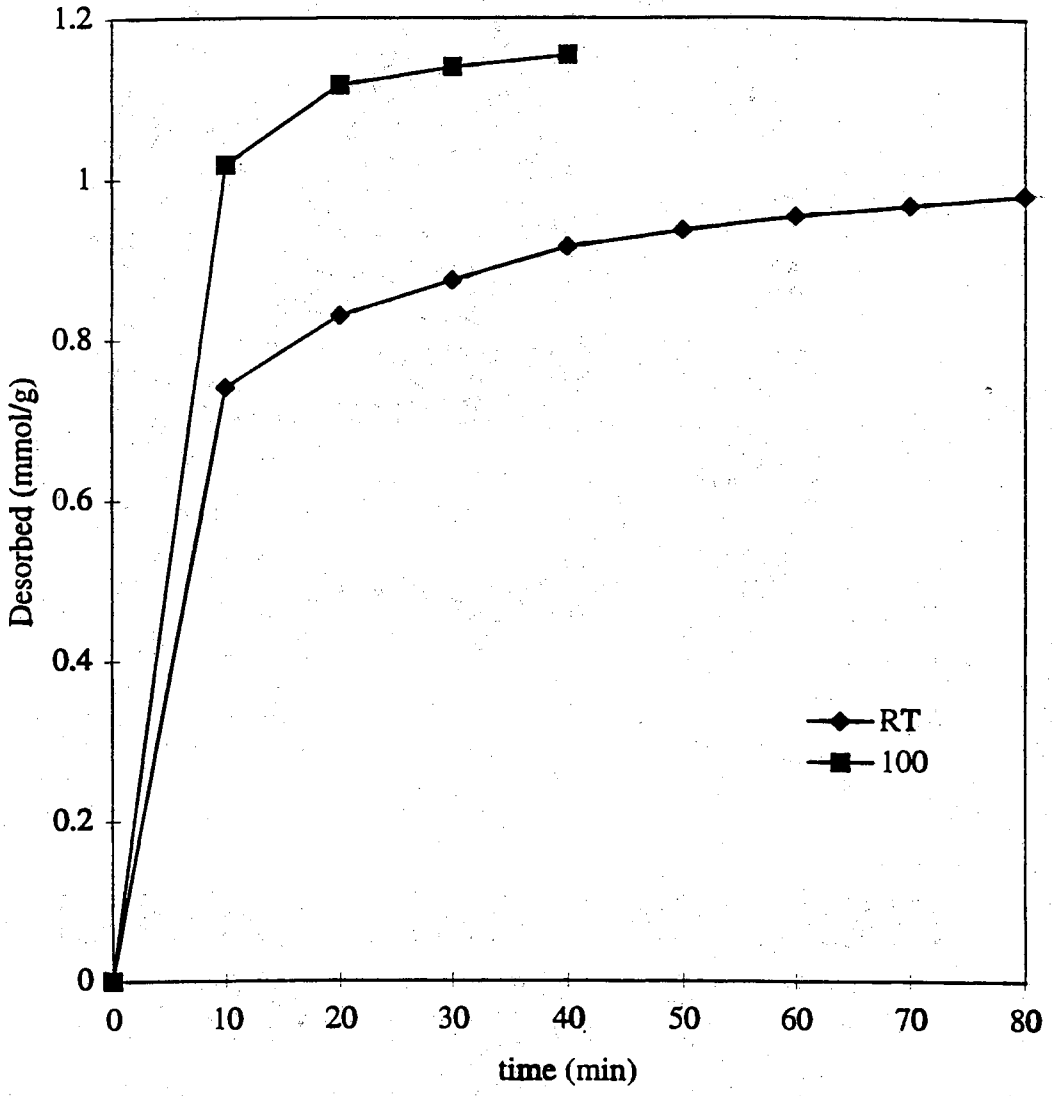

Figure 48. Temperatue dependent desorption of ethylene from 61% Ag(I) exchanged Amberlyst 15 resin.

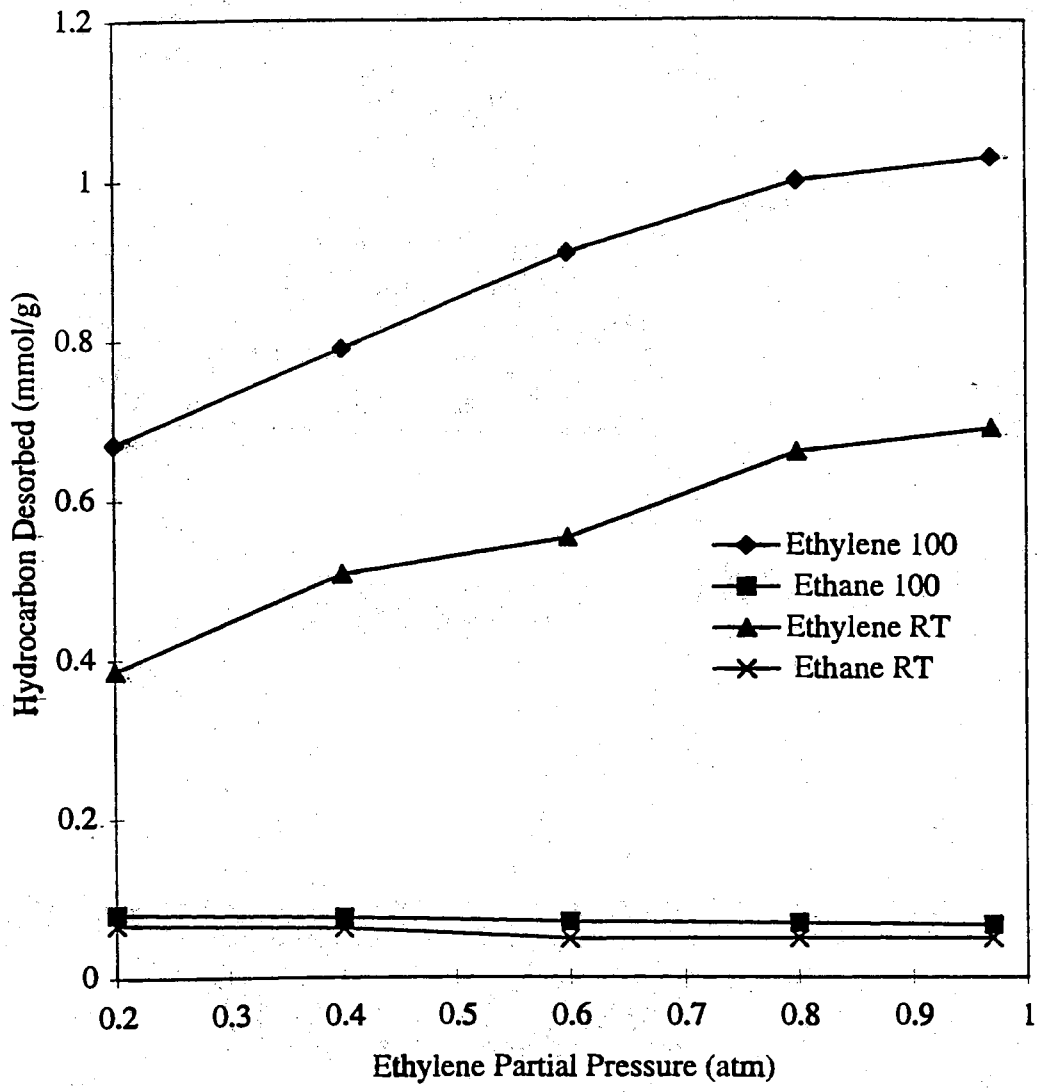

Figure 49. Temperature dependent desorption of ethylene and ethane mixtures from 61% Ag(I) exchanged Amberlyst 15 resin as a function of binary stream composition.

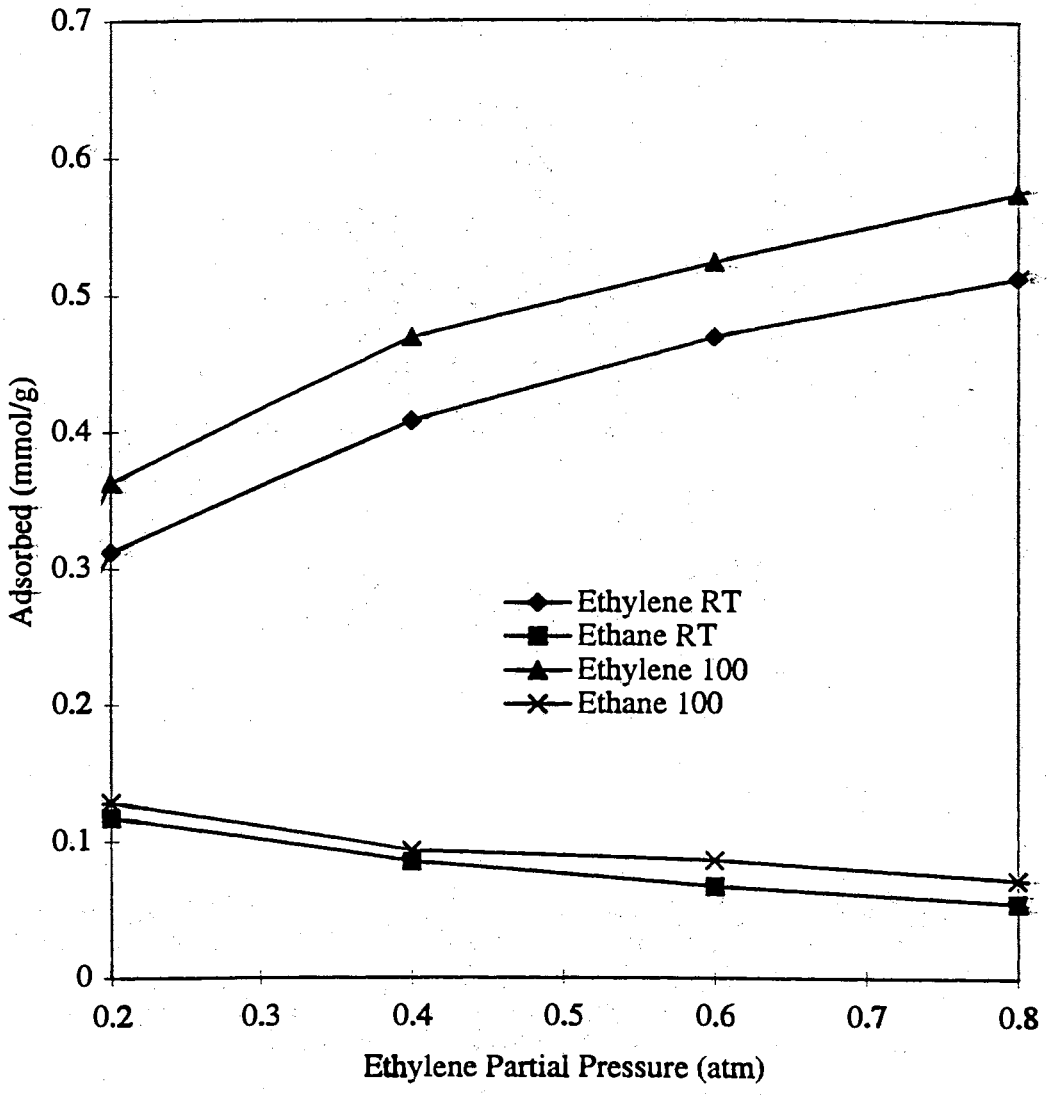

Figure 50. Temperature dependent desorption of ethylene and ethane mixtures from 7% Ag(I) exchanged Amberlyst 15 resin as a function of binary stream composition.

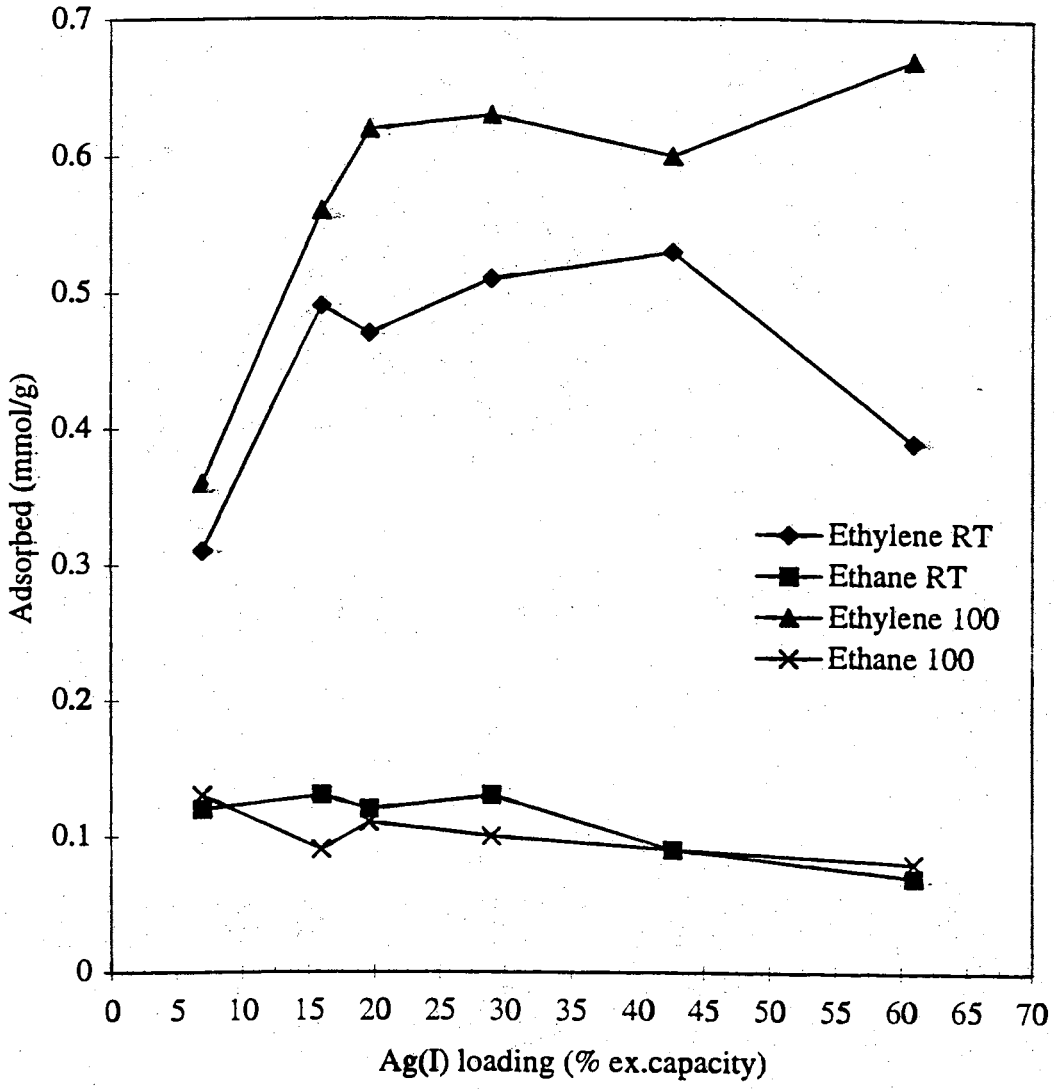

Figure 51. Temperature dependent desorption of ethylene and ethane mixtures from Ag(I) exchanged Amberlyst 15 resins as a function of Ag(I) loading.

Temperature Dependent Ethylene/Ethane Selectivities

Temperature dependent ethylene/ethane selectivities of 61% Ag(I) exchanged Amberlyst 15 resin as a function of binary stream composition are presented in Figure 52. The binary selectivities were calculated from the binary desorption data presented in Figure 49. As shown, the selectivities increase at higher desorption temperatures and as the concentration of ethylene in the binary stream decrease. For example, in a binary stream composed of 20% ethylene and 80% ethane, the selectivities are 29.7 at 100 °C and 19.8 at RT, while in a binary stream composed of 80% ethylene and 20% ethane, the selectivities are 6 at 100 °C and 5 at RT.

Temperature dependent ethylene/ethane selectivities of 7% Ag(I) exchanged Amberlyst 15 resin as a function of binary stream composition are presented in Figure 53. The binary selectivities were calculated from the binary desorption data presented in Figure 50. As shown, the selectivities increase as the concentration of ethylene in the binary stream decrease but show little variation with temperature. For example, in a binary stream composed of 20% ethylene and 80% ethane, the selectivities are 9.6 at 100 °C and 8.9 at RT, while in a binary stream composed of 80% ethylene and 20% ethane, the selectivities are 2.81 at 100 °C and 3.21 at RT.

Temperature dependent ethylene/ethane selectivities of the Ag(I) exchanged Amberlyst 15 resins as a function of Ag(I) loading are presented in Figure 54. The selectivities were calculated from the binary desorption data in Figure 51. As shown, the selectivities initially increase as the Ag(I) loadings increase. For example, the selectivities of the 7% Ag(I) exchanged 15 resin are 9 at RT and 10 at 100 °C while the selectivities of the 16% Ag(I) exchanged 15 resin are 14 at RT and 24 at 100 °C. At intermediate and higher Ag(I) loadings, the data only show a gradually increase in selectivity. On the 61%

Ag(I) exchanged Amberlyst 15 resin, the data show that the selectivity continue to rise at 100 °C but falls at RT. The data also show that the selectivities of the 16-61% Ag(I) exchanged Amberlyst 15 resins are temperature dependent. For example, the selectivities of the 16% Ag(I) exchanged Amberlyst 15 resin were 16 at RT and 24 at 100 °C, corresponding to an increase of 8 at 100 °C. In contrast, the data indicate that the selectivity of the low Ag(I) loaded samples are not temperature dependent. For example, the selecivitiy of the 7% Ag(I) exchanged Amberlyst 15 resin increases only by 1 after desorption at 100 °C.

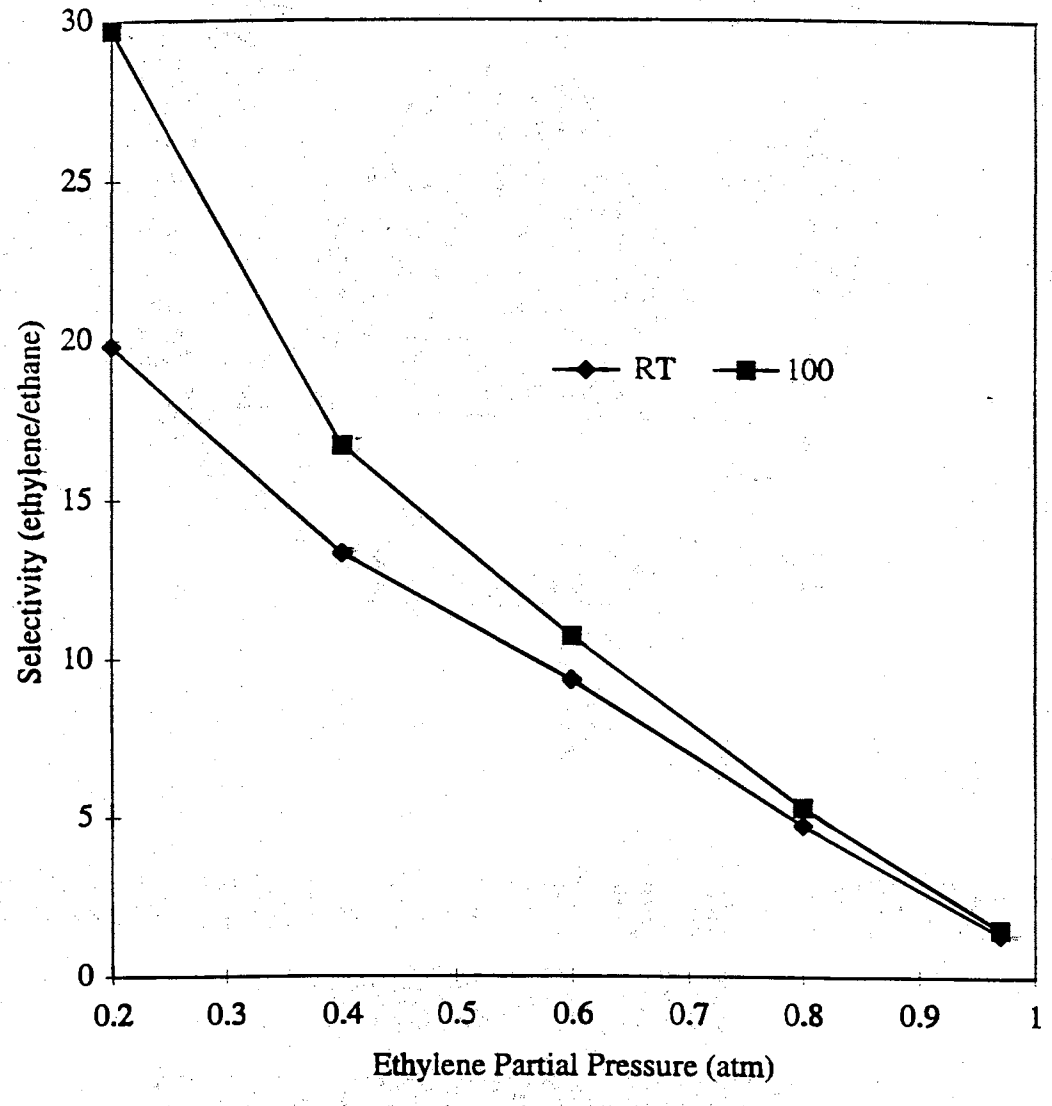

Figure 52. Temperature dependent ethylene/ethane selectivities of 61% Ag(I) exchanged Amberlyst 15 resin as a function of binary stream composition.

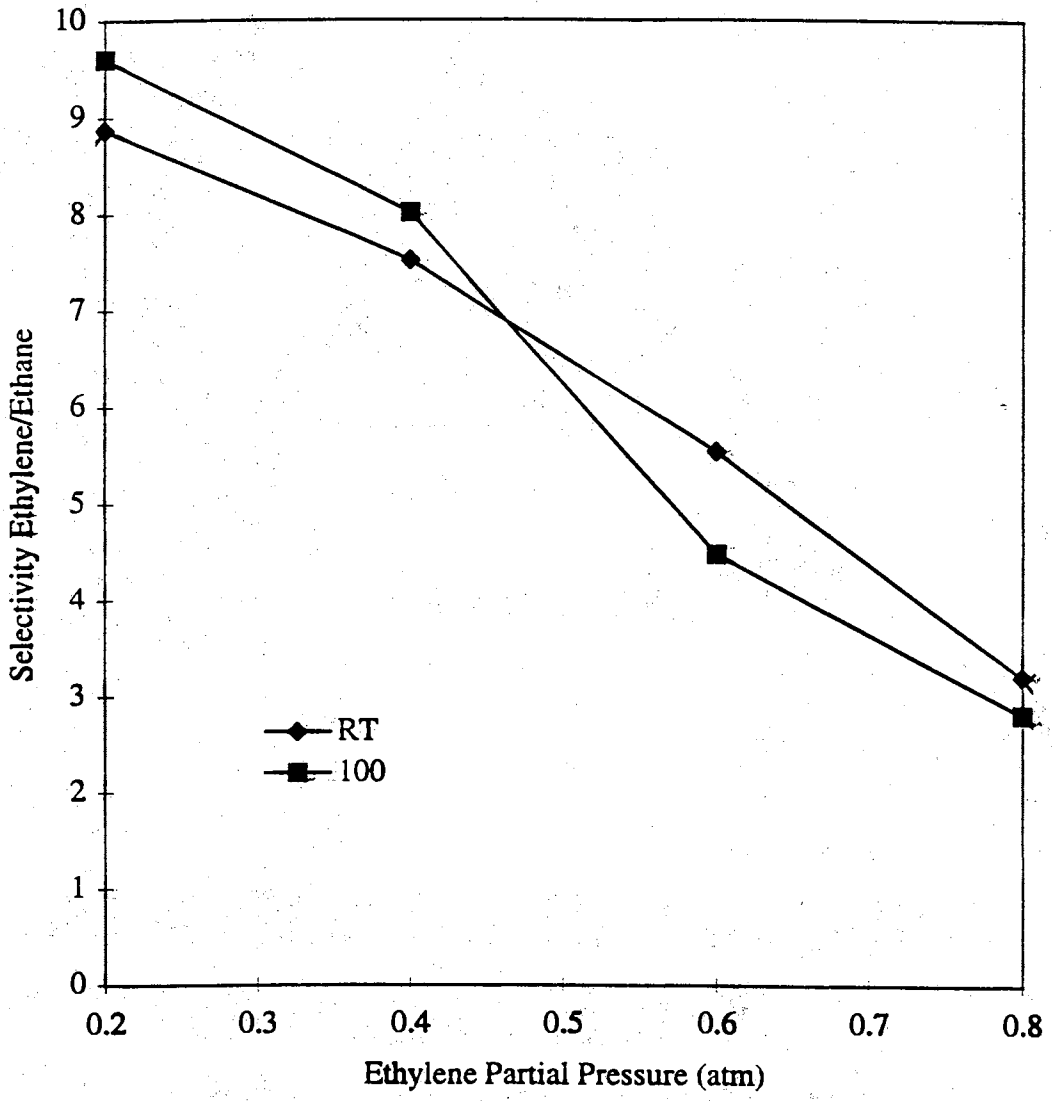

Figure 53. Temperature dependent ethylene/ethane selectivities of 7% Ag(I) exchanged Amberlyst 15 resin as a function of binary stream composition.

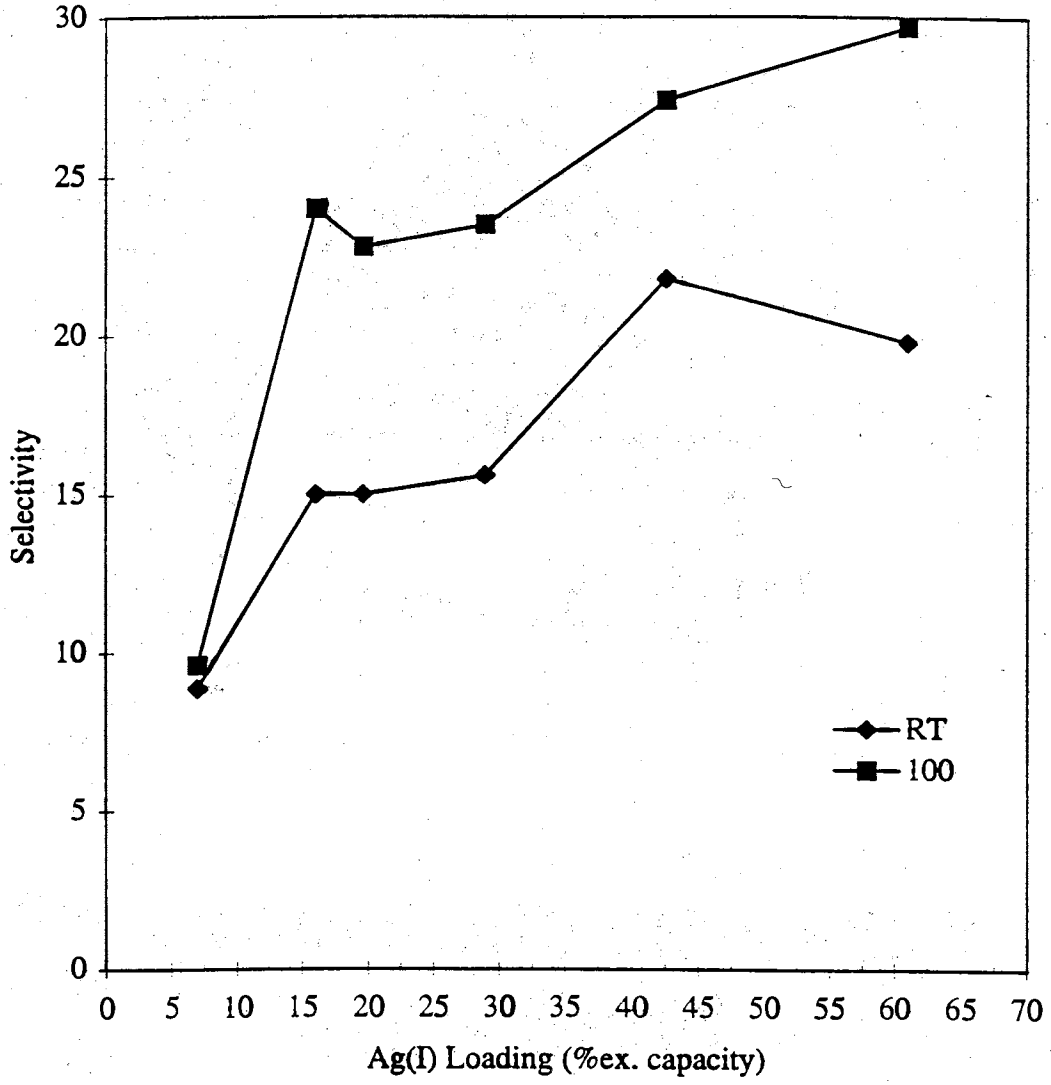

Figure 54. Temperature dependent ethylene/ethane selectivities of Ag(I) exchanged Amberlyst 15 resin as a function of Ag(I) loading.

DRIFTS Spectra

The DRIFTS-HTEC spectrum of gas phase ethylene is presented in Figure 55, and the bands are assigned based on previous reports (Herzberb, 1945; Busca et al., 1992). In the spectrum, ethylene bands along with fine structure are observed at 949 cm^{-1}, 1445 cm^{-1}, 1889 cm^{-1}, 2042 cm^{-1}, 2989 cm^{-1}, 3067 cm^{-1}, and 3105 cm^{-1}. In agreement with previous reports (Herzberb, 1945; Busca et al., 1992), the band at 949 cm^{-1} is assigned to the in-plane CH_2 bend; the band at 1445 cm^{-1} is assigned to the in-plane CH_2 wag; the weak bands at 1889 cm^{-1} and 2042 cm^{-1} are assigned to the CH_2 combination bands; the band at 2989 cm^{-1} is assigned to the CH_2 symmetric stretch; the band at 3067 cm^{-1} is assigned to a CH^2 combination; and the band at 3105 cm^{-1} is assigned to the antisymmetric CH_2 stretch. As expected, the inactive in-plane wag of the CH_2 and the inactive C=C stretch, respectfully assigned to bands at 1342 cm^{-1} or 1625 cm^{-1}, are not observed in the spectra. In addition, the CH_2 combination band, previously characterized at 2325 cm^{-1}, is not observed due to its weak intensity.

The overlay of the DRIFTS-HTEC spectra of the 61% Ag(I) exchanged Amberlyst 15 resin and the ethylene exposed 61% Ag(I) exchanged Amberlyst 15 resin is presented in Figures 56. In both spectra, the bands previously assigned to the Ag(I) exchanged Amberlyst 15 resin in Chatper III are observed. In the spectrum of the ethylene exposed 61% Ag(I) exchanged Amberlyst 15 resin, the following bands of ethylene are observed and are assigned based on previous reports (Herzberb, 1945; Busca et al., 1992). The band at 949 cm^{-1} is assigned to the in-plane CH_2 bend; the band at 1445 cm^{-1} is assigned to the in-plane CH_2 wag; and the band at 2989 cm^{-1} is assigned to the CH_2 symmetric stretch.

The overlays of the time elapsed DRIFTS-HTEC spectra of the ethylene exposed 61% Ag(I) exchanged Amberlyst 15 resin under nitrogen purge are presented in Figures 57, 58, and 59. The series was collected in 5 minute intervals. In the series, the intensities of the active CH_2 bend, CH_2 wag, and CH_2 symmetric stretch of ethylene, were observed respectfully at 950 cm^{-1}, 1443 cm^{-1} and 2989 cm^{-1}, decrease under nitrogen purge.

Eventually, the spectrum correlates with that of unexposed 61% Ag(I) exchanged Amberlyst 15 resin.

The subtracted DRIFTS-HTEC spectrum (neat DRIFTS-HTEC spectrum of ethylene exposed 61% Ag(I) exchanged Amberlyst 15 resin subtracted from the neat DRIFTS-HTEC spectrum of 61% Ag(I) exchanged Amberlyst 15 resin) is presented in Figure 60. Subtraction, revealing only infrared active bands of ethylene, provided no evidence for the activation of ethylene bands which have been assigned to metal-olefin π-bond.

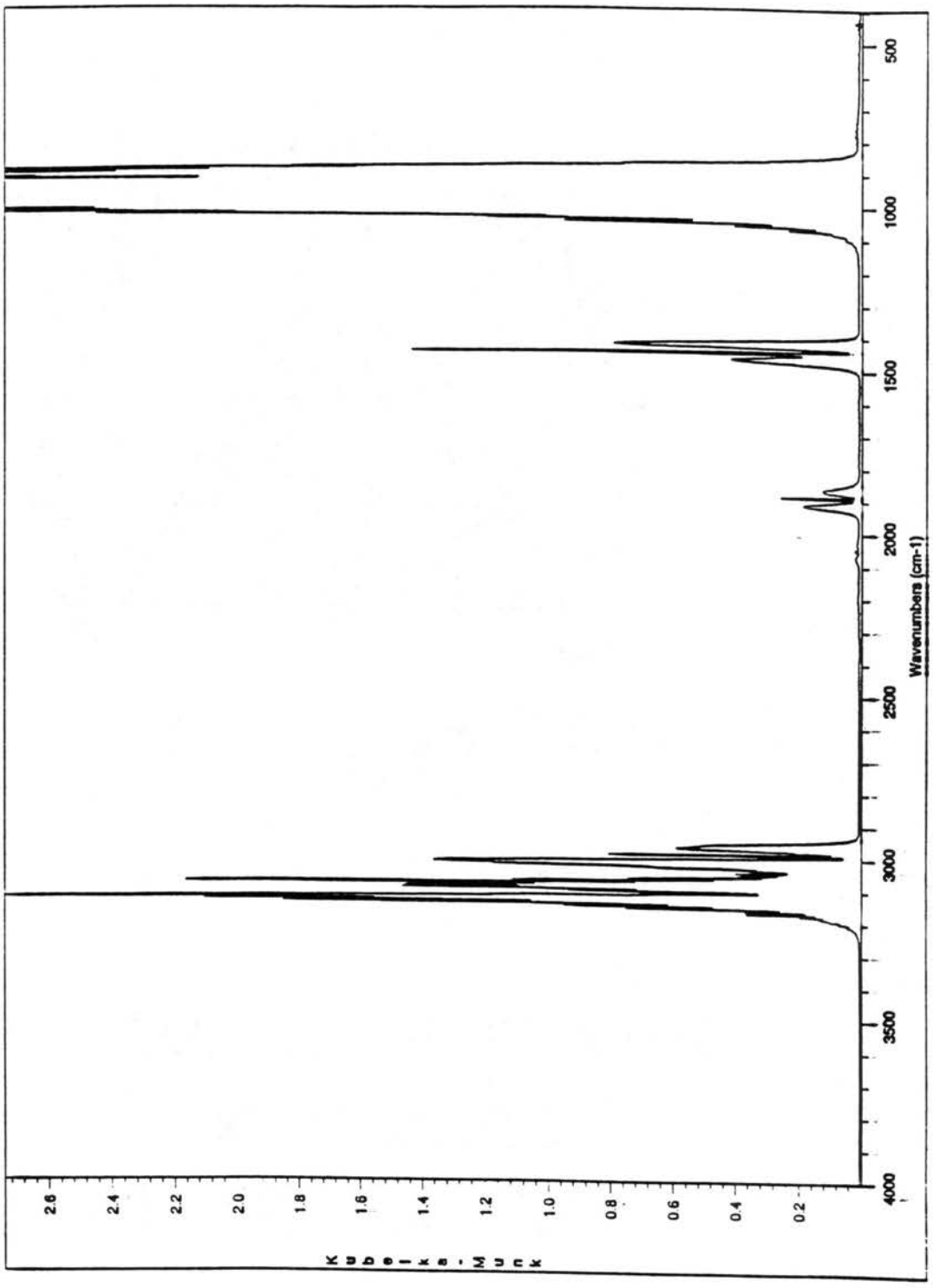

Figure 55. DRIFTS-HTEC spectrum of gas phase ethylene.

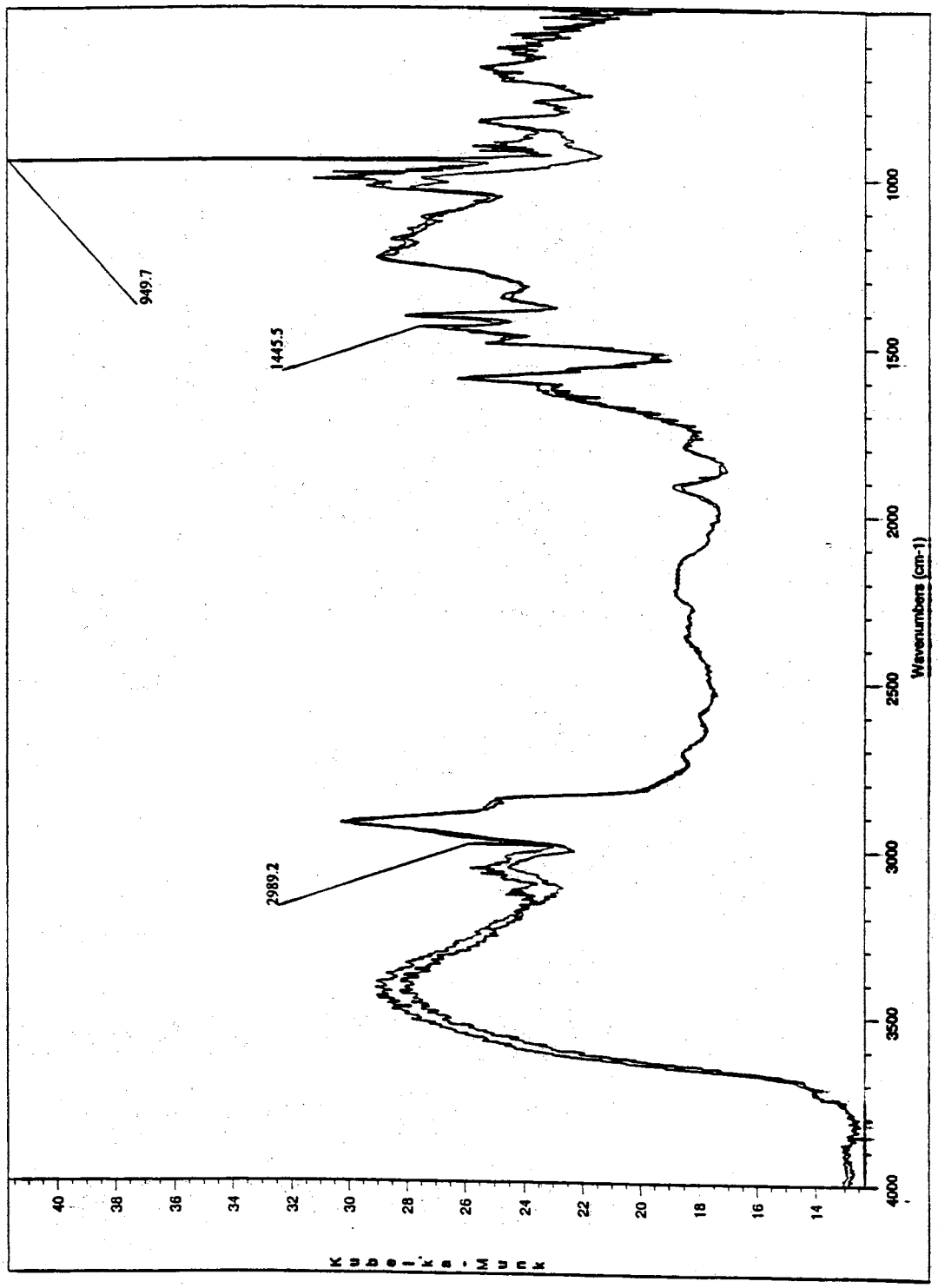

Figure 56. Overlaid DRIFTS-HTEC spectra of 61% Ag(I) exchanged Amberlyst 15 resin and ethylene exposed 61% Ag(I) exchanged Amberlyst 15 resin.

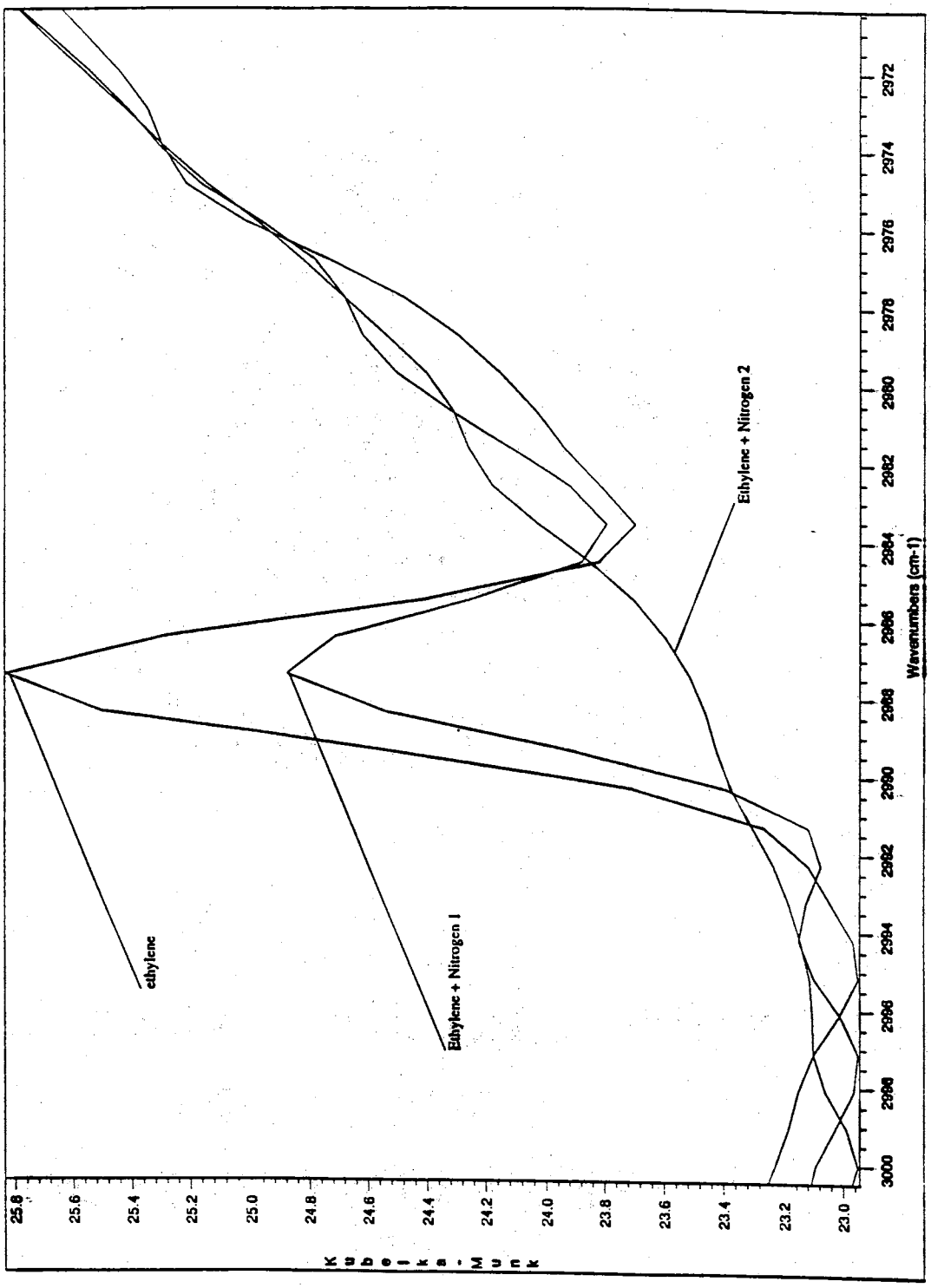

Figure 57. Overlaid DRIFTS-HTEC spectra of ethylene exposed 61% Ag(I) exchanged Amberlyst 15 resin in nitrogen purge.

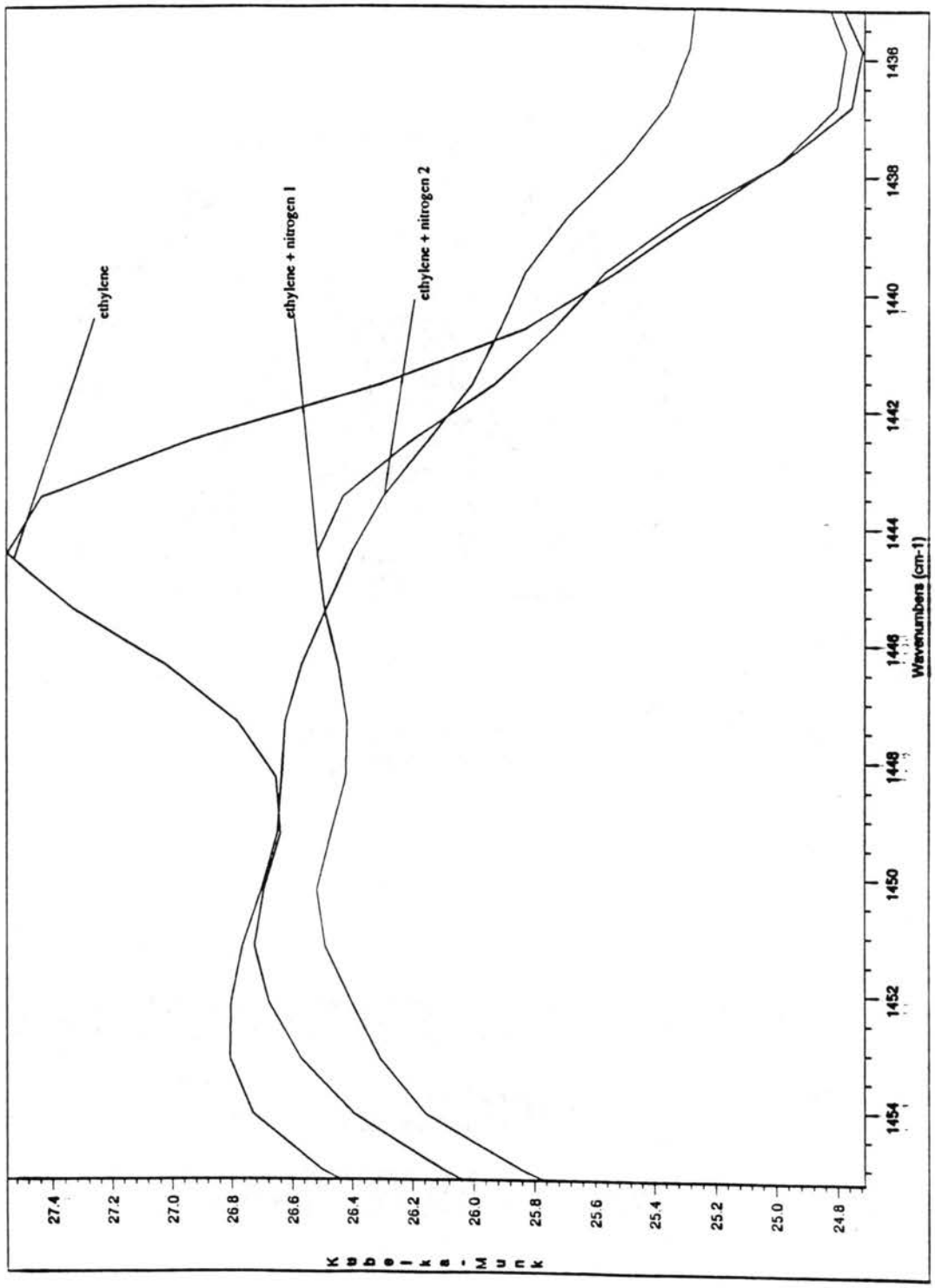

Figure 58. Overlaid DRIFTS-HTEC spectra of ethylene exposed 61% Ag(I) exchanged Amberlyst 15 resin in nitrogen purge.

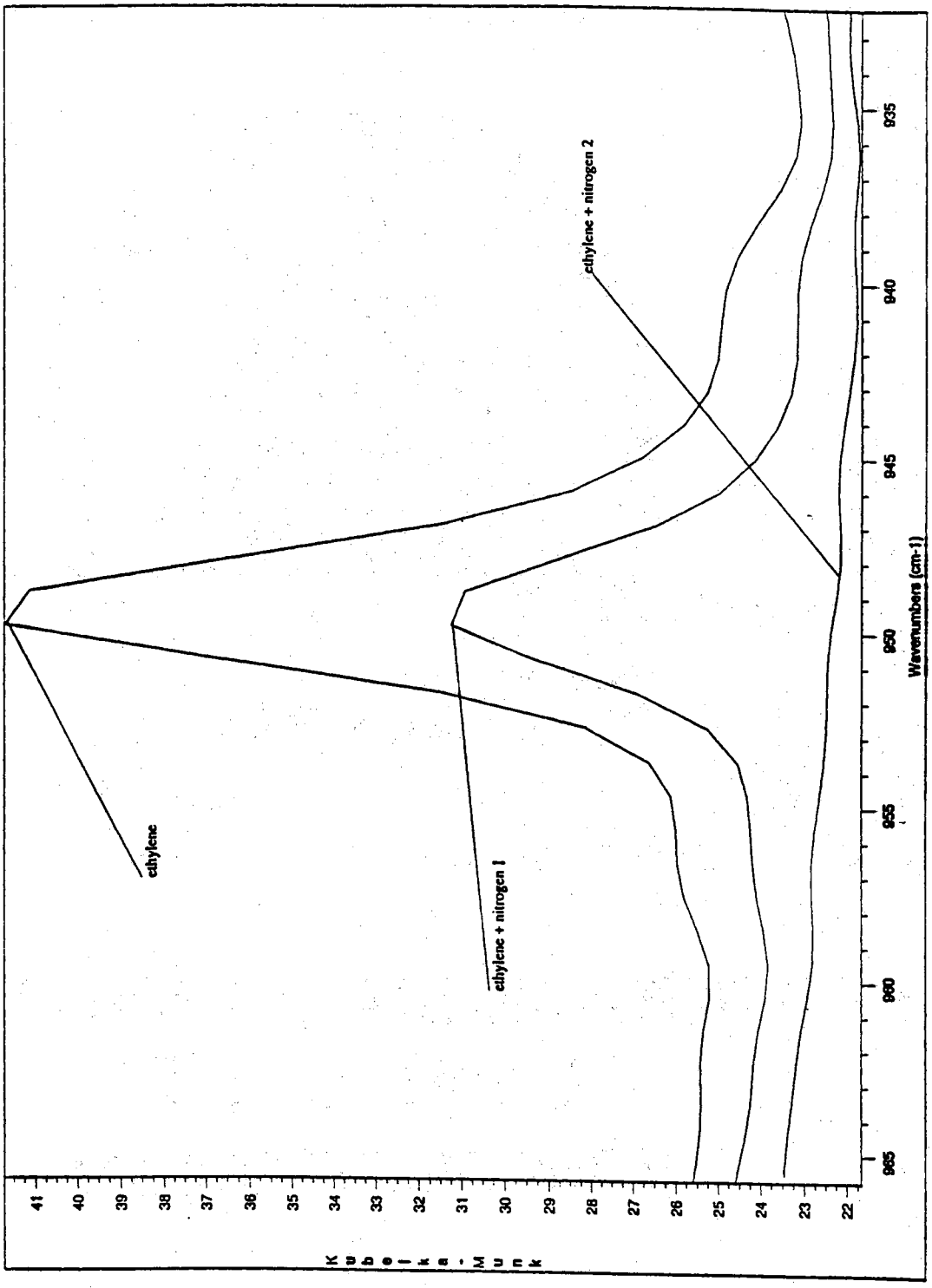

Figure 59. Overlaid DRIFTS-HTEC spectra of ethylene exposed 61% Ag(I) exchanged Amberlyst 15 resin in nitrogen purge.

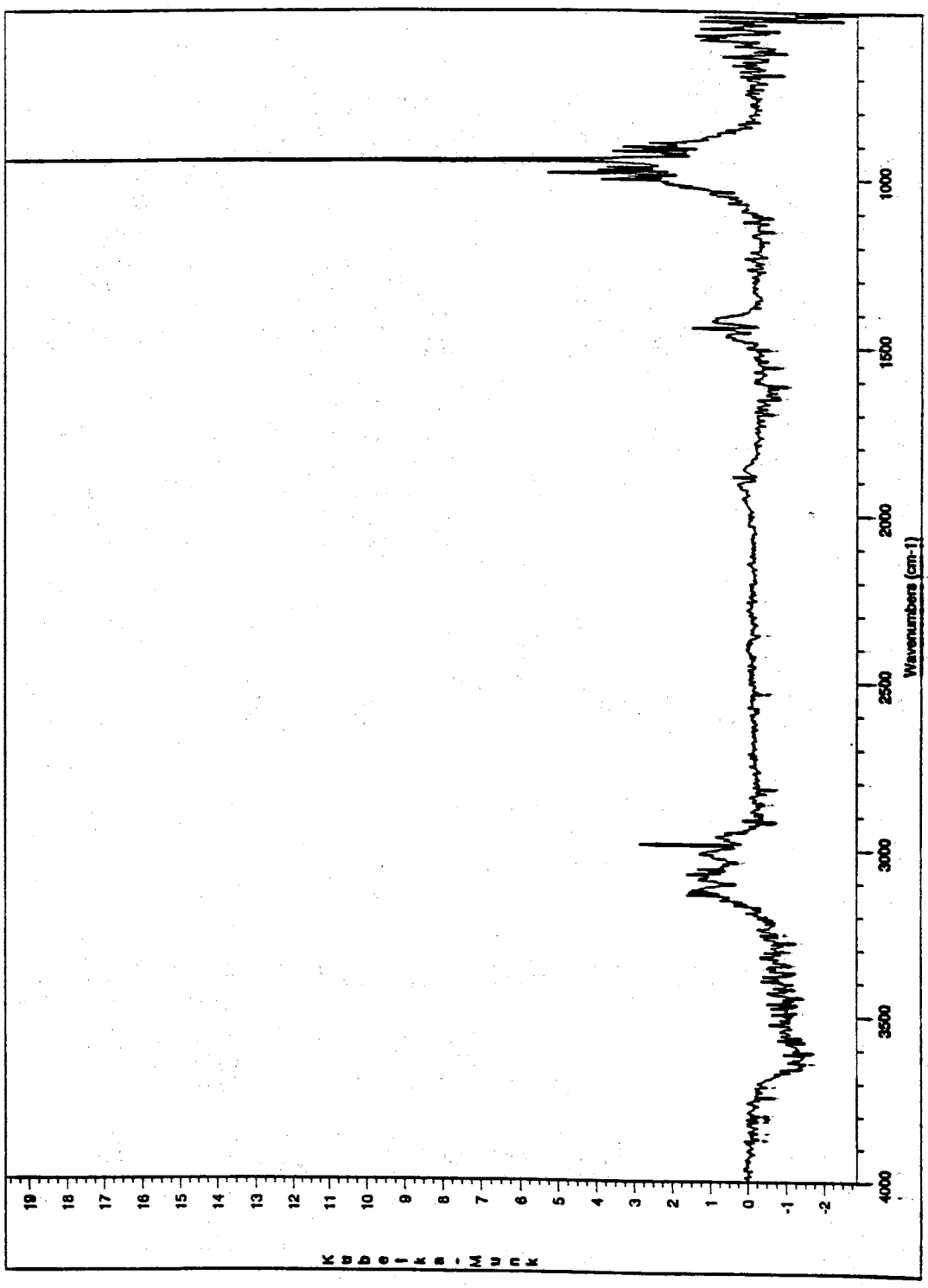

Figure 60. DRIFTS-HTEC spectrum of 61% Ag(I) exchanged Amberlyst 15 resin subtracted from ethylene exposed 61% Ag(I) exchanged Amberlyst 15 resin.

Discussion

When compared with elemental analysis, weight analysis is highly inaccurate for measuring the extent of ion exchange on Amberlyst 15 resins. For example, errors in the extent of ion exchange measured by weight analysis range from 19-29%. Based on spectroscopic results in Chapter III, the error of the weight analysis method can be attributed to varying amounts of moisture in the Amberlyst 15 resin. As indicated by DRIFTS spectra in Chapter III, the Amberlyst 15 resins contain residual moisture which varies with cation exchange and is not removed by extensive drying. In conclusion, the extent of ion exchange on Amberlyst 15 resin should not be inferred by weight gain measurements.

Ethylene adsorption and desorption data, collected on the unexchanged and 61% Ag(I) exchanged Amberlyst 15 resin in single component streams, agree with previous reports (Yang and Kikkinides, 1995), verifying the adsorption capacities of the Ag(I) exchanged Amberlyst 15 resins. However, ethane adsorption data, collected on the 61% Ag(I) exchanged Amberlyst 15 resin, do not agree with previous reports (Yang and Kikkinides, 1995). Results show the 61% Ag(I) exchanged Amberlyst 15 resin adsorbs an additional 50% of ethane. During attempts to reconcile the deviations, gas chromatography analysis of the ethane revealed that the ethane feed was contaminated with residual ethylene. Hence, deviations in ethane results were attributed to the slow and continual adsorption of ethylene contaminant in the ethane stream. Efforts were undertaken to purchase a higher purity ethane feed, but suppliers were not found. Due to the ethylene contaminant, ethane adsorption and ethylene/ethane adsorption ratios were not measured by TGA in subsequent studies. Additional literature review revealed that many adsorption studies have reportedly used CP grade ethane without verifying its purity. Therefore, the residual ethylene, characterized in the CP grade ethylene, sets precendence for the evaluation of gas purities in future adsorption studies.

The ethylene adsorption/desorption data, measured on the 61% Ag(I) exchanged Amberlyst 15 resin by MDA, corroborate the adsorption data collected using the TGA. For example, adsorption data, collected using both techniques, indicate that the 61% Ag(I) exchanged Amberlyst 15 resin adsorbs 1.15 mmol/g of ethylene and irreversibly adsorbs 14% of the ethylene at RT. The binary adsorption/desorption data also highlight the additional utility of the MDA. For example, instead of calculating an adsorption ratio, which is based solely on pure stream adsorption data, the binary desorption data allow selectivities to be calculated in multicomponent streams. The buoyancy, drag, and thermal effects, which plague the weight measurement in the TGA, are not a limitation of the MDA; and therefore, collecting temperature dependent adsorption data using the MDA is an easier and more accurate process. The variety of desorption techniques, provided by the MDA, allows the collection of adsorption data needed to select more appropriate adsorber units and more applicable regeneration method(s).

Adsorption data show that ethylene adsorption capacities of the Ag(I) exchanged Amberlyst 15 resins decrease at higher Ag(I) loadings. For example, the ethylene adsorption capacity falls 20% in going from the 42.6% to 61% Ag(I) exchanged Amberlyst 15 resin. Previous adsorption studies (Tamon et al. 1996; Yang and Cheng, 1995; Linlin et al. 1984; Yang et al., 1997) have attributed this decline at high metal loading to poor metal dispersion and/or pore blockage. Poor metal dispersion has primarily been based on surface studies of catalysts, which have shown that metals aggregate at high loadings reducing available sites for reaction (Linlin et al. 1984; Somorjai, 1994; Youchang, et al. 1981). Pore blockage has primarily been based on studies of zeolites which have shown that metals block pore cavities, preventing access to adsorption sites (Schoeller and Mueller, 1986). However, in disagreement with poor metal dispersion and pore blockage, the EDXAS profiles, nitrogen adsorption data, and mercury porosimetry results in Chapter III indicate; (1) Ag(I) is homogeneously dispersed throughout the Amberlyst 15 resin bead; (2) Ag(I) does not modify the physical properties or structure of the Amberlyst 15 resins;

and (3) Ag(I), having the smaller hydration sphere, easily migrates through the pore structure of the Amberlyst 15 resin. Based on these data, poor metal dispersion and pore blockage do not explain the decreased adsorption capacities at high Ag(I) loading. It is therefore proposed that the high Ag(I) loaded samples have a high concentration of active sites which inefficiently adsorb ethylene.

Adsorption/desorption data and ethylene/Ag(I) mole ratios indicate that extremely low Ag(I) loaded Amberlyst 15 resins have surprisingly large ethylene adsorption capacities and ethylene/etahne selectivities. For example, when compared with the ethylene adsorption on the 61% Ag(I) exchanged Amberlyst 15 resin, the 29% Ag(I) exchanged Amberlyst 15 resin adsorbs an additional 0.27 mmol/g of ethylene with 32% less Ag(I) loading. More surprisingly, the 7% Ag(I) exchanged Amberlyst 15 resin maintains 75% of the ethylene adsorption capacitiy of the 61% Ag(I) exchanged Amberlyst 15 resin with 54% less Ag(I) loading. This corresponds to an ethylene/Ag(I) ratio of 2.5. In addition, the desorption data show that the 7% Ag(I) exchanged Amberlyst 15 resin has ethylene/ethane selectivities which are only 1/3-1/2 less than the selectivities of the 61% Ag(I) exchanged Amberlyst 15 resin. Literature precedence for these surprisingly large ethylene adsorption capacities, ethylene/ethane selectivities, and ethylene/Ag(I) mole ratios at low metal loadings has not been recognized. However, EDXAS profiles, nitrogen adsorption data, mercury porosimetry data indicate that Ag(I) exchange does not promote physical modifications of the resin which facilitate these large ethylene adsorption capacities. Therefore, based on these data, the low Ag(I) exchanged Amberlyst 15 resins are proposed to have active sites which more efficiently adsorb olefins. The combination of the reduced ethylene adsorption capacities at high Ag(I) loading and surprisingly high ethylene adsorption capacities at low Ag(I) loadings suggest that the Ag(I) exchanged resins have two different Ag(I) active sites for olefin adsorption. As suggested, the efficient active site predominates at low Ag(I) loading, while the inefficient sites predominate at higher Ag(I) loading. This hypothesis is further investigated in subsequent Chapters.

In agreement with Yang and Kikkinides' prediction (1995), the ethylene/ethane selectivities of the 61% Ag(I) exchanged Amberlyst 15 resin increase as the concentration of ethylene in the binary stream decreases. For example, compared to the 9.2 adsorption ratio reported by Yang and Kikkinides (1995), the temperature dependent desorption data show that selectivities as high as 19 and 29 are achieved on the 61% Ag(I) exchanged Amberlyst 15 in a binary stream composed of 20% ethylene and 80% ethane. These selectivity observations are in agreement with Buss (1996) who has stated at low concentrations of the more strongly adsorbed component (i.e. ethylene), the ethylene is preferred by the high-energy active sites, and the selectivity is high. However, at higher concentrations of the more strongly adsorbed component, ethylene must compete with the ethane for energetically weaker active sites, and the selectivity is lowered.

The ethylene/ethane selectivities of the Ag(I) exchanged Amberlyst 15 resin as a function of Ag(I) loading are shown to drastically increase at low metal loadings. This is easily rationalized by the increased amount of ethylene desorbed. The ethylene/ethane selectivities of the intermediate Ag(I) loadings also increase even though the desorption of ethylene remains fairly constant on the 16 to 42.6% Ag(I) exchanged Amberlyst 15 resins. This can be rationalized by the fact that the higher Ag(I) exchanged Amberlyst 15 resins desorb 44% less ethane. Since selectivity is a mole fraction calculation, reduction in the amount of ethane desorbed at higher Ag(I) loading provides the higher selectivites. The diverging selectivities, observed on 61% Ag(I) exchanged 15 resin, are attributed to the irreversibly adsorbed ethylene, which is removed at 100 °C.

Irreversible adsorption has been attributed to chemisorption (Satterfield, 1991). Infrared reports (Noltes et al., 1970; Scott, 1972; Nagakura and Hosoya, 1963; Yates et al., 1966; Nagendrappa and Devaprabhakara, 1968) on the interaction of Ag(I) with olefins have shown that the inactive infrared bands of olefin are activated (i.e. chemisorbed) when complexed (i.e. chemisorbed) with Ag(I). For example, Yates et al. (1966) have spectroscopically shown that the inactive band assigned to the C=C symmetrical stretching

mode of ethylene is activated and shifted to 1580 cm^{-1} upon complexation with Ag(I) in zeolite. Yates et al. (1955) also reported that the inactive band assigned to the CH_2 wag of ethylene is activated and shifted to higher wavenumber upon complexation with Ag(I) in zeolite. In contrast with these reports, a chemisorbed fraction of ethylene, characterized by the activation and shift of the band assigned to the C=C stretch and/or CH_2 wag of ethylene, was not observed in the DRIFTS-HTEC spectra of the ethylene exposed 61% Ag(I) exchanged Amberlyst 15 resin. The DRIFT-HTEC spectra therefore indicate that ethylene is not chemically modified when adsorbed on 61% Ag(I) exchanged Amberlyst 15 resin. Hence, in conflict with Yang and Kikkinides (1995), the DRIFTS-HTEC spectra imply that a large fraction of ethylene is physisorbed on the 61% Ag(I) exchanged Amberlyst 15 resin. Since a small fraction of ethylene, based on irreversible adsorption (5-15% at RT), is attributed to chemisorption, this fraction falls below infrared detection limits.

Yang (1987) has stated that heats of adsorption below 15 kcal/mole are characteristic of physisorption. Furthermore, the heats of olefin adsorption on physical adsorbents such as zeolites and alkali metal exchanged zeolite (Triebe et al. 1996), both of which are incapable of chemisorption, have been in excess of 13 kcal/mole. Based on these observations, it can be postulated that the heats of ethylene adsorption calculated from adsorption data collected on the 7% (10 kcal/mol), and 61% Ag(I) exchanged Amberlyst 15 resins (10 kcal/mol), suggest that a large fraction of ethylene is physisorbed on the Ag(I) exchanged Amberlyst 15 resins.

Conclusion

When compared with elemental analysis, weight analysis shows to be highly inaccurate for measuring the extent of ion exchange on Amberlyst 15 resins. Thus, the extent of ion exchange on Amberlyst 15 resins should not be determined by weight gain measurements.

Gas Chromatography analysis of CP grade ethane indictes that the CP grade ethylene contains residual ethylene. This result sets precedence for the evaluation of gas purities in future adsorption studies.

When compared with the TGA, the adsorption results indicate that the MDA is a comparable technique which collects adsorption data under conditions more representative of industrial processes.

In agreement with previous predictions, the adsorption data indicate that ethylene/ethane selectivities of the Ag(I) exchanged Amberlyst 15 resins dramatically increase as the concentration of ethylene in the binary stream decreases.

Even though unprecedented in the literature, adsorption data show that extremely low Ag(I) loaded Amberlyst 15 resins have surprisingly high olefin adsorption capacities and olefin/paraffin selectivities.

Contradictory to previous infrared studies and adsorption predictions, the DRIFTS spectra and adsorption data suggest that ethylene is primarily physisorbed on the Ag(I) exchanged Amberlyst 15 resin.

The combination of nitrogen adsorption data, mercury porosimetry data, EDXAS profiles, temperature dependent adsorption data collected as a function of Ag(I) loading, and DRIFTS-HTEC spectra suggest that the Ag(I) exchanged Amberlyst 15 have different types of Ag(I) active sites which adsorb ethylene.

CHAPTER V

CURVE FITTING ETHYLENE ADSORPTION ISOTHERMS

Summary

As reported in Chapter IV, the Yang and Kikkinides isotherm equation for ethylene adsorption on 51.7% Ag(I) exchanged Amberlyst 15 resin was derived based on the assumption that ethylene was chemisorbed on the Ag(I) sites. However, DRIFTS spectra and adsorption data in Chapter IV show that ethylene is primarily physisorbed on active sites of Ag(I) exchanged Amberlyst 15 resins. As pointed out by Do and Do (1997), Knaebel (1995), and Rudzinski et al. (1996), many isotherms have been curve fit with the purpose of estimating fitting parameters that provide information on the surface structure of the adsorbent and the interactions between adsorbates and adsorbents. The curve fitting equations have been derived based on assumptions about the surface structure of the adsorbent, the nature of the active sites, and the nature of adsorption. This suggests curve fitting isotherm data with equations might provide fitting parameters from which infomation about the active sites for ethylene adsorption on the Ag(I) exchanged Amberlyst 15 resins could be inferred.

In Chapter V, curve fits of the ethylene adsorption isotherm of the 61%Ag(I) exchanged Amberlyst 15 resin are presented and discussed. The curve fits are obtained by nonlinear least square fitting the experimental adsorption data to the Langmuir, Toth, Unilan, and Yang and Kikkinides isotherm equations. The fractions of chemisorbed and physisorbed ethylene on the 51.7% Ag(I) exchanged Amberlyst 15 resin, respectfully, evaluated using the Yang and Kikkinides isotherm equation, are also reported. Results indicated; (1) the Yang and Kikkinides, Langmuir, Toth, and Unilan isotherm equations all fit the ethylene adsorption isotherm of the 61% Ag(I) exchanged Amberlyst 15 resin, (2) the two site model, proposed by Yang and Kikkinides, and the Yang and Kikkinides isotherm equation do not adequately represent ethylene adsorption on Ag(I) exchanged

Amberlyst 15 resin, and (3) as suggested by Rudzinski, the heterogeneity fitting parameters of the Toth, Unilan, and Yang and Kikkinides isotherm equations provide no evidence to distinguish the heterogeneity of the active sites of the Ag(I) exchanged Amberlyst 15 resin.

Background

Adsorption Isotherms

Physical and chemical adsorption data are commonly reported in the form of isotherms (Albright and Yarnell, 1987; Knaebel, 1995; Yang, 1987; Satterfield 1991; Ruthven 1984, 1991; Gregg and Sing, 1982). Adsorption isotherms graphically express adsorption capacity as a function of feed composition at constant temperature. The isotherms are commonly nonlinear least squares curve fit to isotherm eqautions. Nonlinear least square curve fitting is a process which uses an algorithm in combination with independent variables (i.e. adsorption capacities and partial pressures) and a previously derived equation to determine dependent variables (i.e. fitting parameters of the eqaution) which minimize the sum of squared differences between the independent variables and the variables predicted by the equation. The process is iterative, which means initial guesses and constraints are put into the algorithm, and the algorithm continually makes better estimates until the difference between the residual sum of squares no longer decreases significantly. When a tolerance level (i.e. maximum error of residual sum of squares input into the algorithm) is achieved, the data are said to converge (i.e. equation and fitting parameters adequately represent the experimental data). The correlation of the fit with the values of the nonlinear least squares fitting parameters can be used to infer adsorbent properties such as pore shape, pore size distribution, surface area, and surface heterogeneity (Satterfield, 1991).

The theoretical derivations of isotherm equations are based on kinetics, statistics, and thermodynamics (Satterfield, 1991; Ruthven, 1984, 1991). Using these principles, a large number of isotherm equations have been developed. Several are listed and explained

herein; Langmuir, Henry's law, Brunauer-Emmett-Teller (BET), Toth, and Unilan (Knaebel, 1995; Ruthven, 1984, 1991).

In the most idealistic case (i.e. adsorption at very low partial pressure on a homogeneous surface), the simplest adsorption isotherm equation is Henry's law where adsorption approaches a linear form with a slope of K' (Gregg and Sing, 1982; Ruthven, 1991). Henry's law constant (K') is a simple thermodynamic equilibrium constant with a temperature dependence that follows the integrated form of the van't Hoff equation 30

(30) $$\lim\left(\frac{\partial q}{\partial p}\right)_T = K' = Ke^{-\Delta H_o / RT}$$

where q is the adsorbed phase concentration, p is the partial pressure of adsorbate, K is a pre-exponential factor, R is the gas constant, T is temperature, and $-\Delta H_o$ is the heat of adsorption.

Since adsorption is exothermic, $-\Delta H_o$ is a positive quantity and K' therefore decreases with increasing temperature. Henry's law breaks down at higher pressures, as molecules compete for surface sites or interact with other adsorbed molecules. At increased pressures these molecular interactions become important and the isotherm equations become more complex (Knaebel, 1995; Do and Do, 1996; Ruthven, 1991).

Brunauer, Emmett, Teller, and Deming (1940) classified five types of physical adsorption isotherms, pictured in Figure 61, that occur at higher partial pressures (Greg and Sing, 1982; Yang, 1987).

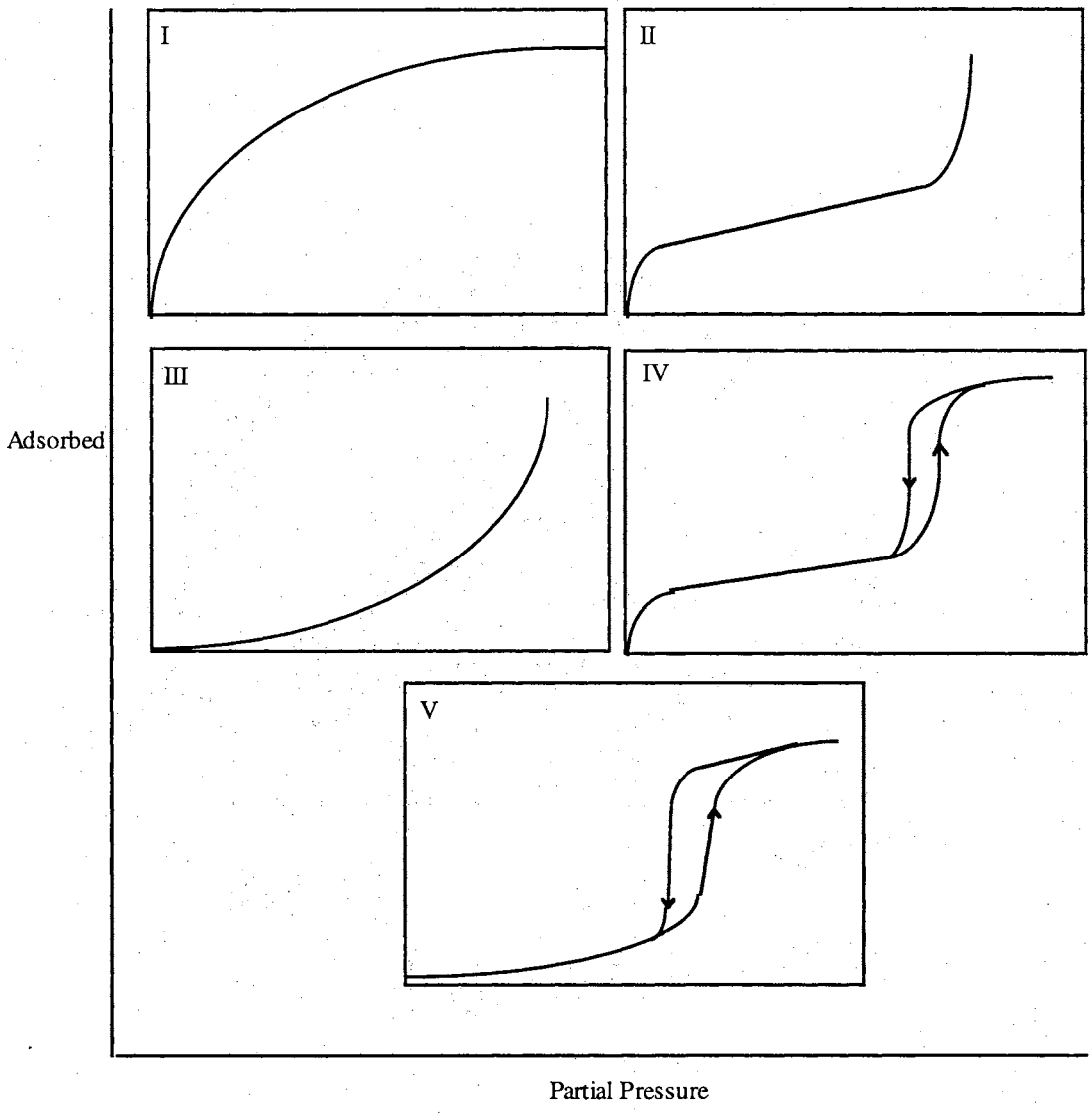

Figure 61. Brunauer, Emmett, Teller, and Deming (1940) classification of adsortion isotherms.

Adsorption isotherm variations reflect differenes in the porous structures of adsorbents (Satterfield, 1991). For example, Type II is typically called the S-shaped isotherm and is characteristic of solid non-porous materials. Type III is rare, very unfavorable for adsorption, and typical of systems in which adsorption forces are extremely weak. Type IV and V are more complex isotherms, with hysteresis effects characteristic of condensation and diffusion limitations in pores. Type I isotherms are the most common, most favorable for adsorption, and characteristic of microporous materials.

Of the many available isotherm equations, the Langmuir (1918) adsorption isotherm equation is the simplest and most commonly used equation for curve fitting both physical and chemical adsorption of Type I isotherms (Rudzinski, 1996; Ruthven, 1984, 1991; Knaebel, 1995). The basic Langmuir model makes the following assumptions (Langmuir, 1918):

1. The adsorption system is in dynamic equilibrium
2. Adsorbed molecules are held at a fixed number of well defined sites
3. Each adsorption site can hold only one molecule
4. The energy of adsorption is a constant over all sites
5. There are no interactions between molecules adsorbed on neighboring sites

Based on these assumptions, the Langmuir equation 34 can be derived using equations 31-33. The rate of adsorption $\left(\frac{d_{na}}{d_t}\right)_{ads}$ and rate of desorption $\left(\frac{d_{na}}{d_t}\right)_{des}$ on available and unavailable surface sites Θ are directly proportional as a function of the partial pressure P.

(31) $$\left(\frac{d_{na}}{d_t}\right)_{ads} = k(1-\Theta)P$$

(32) $$\left(\frac{d_{na}}{d_t}\right)_{des} = k'\Theta$$

(33) $$k(1-\Theta)P = k\Theta$$

(34) $$\Theta = \frac{q}{q_m} = \frac{kP}{k+P} = \frac{KP}{1+KP}$$

In the Langmuir equation 34, q is the adsorption capacity, q_m is the monolayer adsorption capacity, K is the Langmuir constant (which is directly related to Henry's constant), and P is the partial pressure of adsorbate. The correlation of the Langmuir fit is easily checked by plotting P/q vs. P which yields a straight line with a slope of $1/q_m$ (Gregg and Sing, 1982). The quality of the fit is based on the linearity of the line (linear = good fit, curved = poor fit).

Brunauer, Emmett, and Teller (BET method) (1938) have extended the Langmuir isotherm equation to evaluate multilayer adsorption and determine the surface area of solid materials. For the first layer of adsorption, the basic Langmuir assumptions are applied. For subsequent layers, the rate of adsorption is taken to be proportional to the fraction of the lowest layer still vacant and the rate of desorption is taken to be proportional to the amount present in that layer. In addition, the heat of adsorption for all layers except the first is assumed to be equal to the heat of liquefaction of the adsorbed gas. Summing over infinite numbers of adsorbed layers yields equation 35

(35) $$\frac{P}{V(P_o - P)} = \frac{1}{V_m C} + \frac{(C-1)P}{V_m V P_o}$$

where V= volume of gas adsorbed at pressure P

V_m = volume of gas adsorbed in monolayer

P_o = saturation pressure of adsorbate gas at the experimental temperature

C = a constant related experimentally to the heats of adsorption and liquefaction of the gas by equation 36

(36) $$C = e^{\frac{(q_1 - q_l)}{RT}}$$

where q_1 = heat of adsorption of first layer

q_l = heat of liquefaction of adsorbed gas on all other layers

R = gas constant

When the BET equation is a good fit, a plot of $P/V(P_o-P)$ versus P/P_o gives a straight line, the slope and intercept of which can be used to evaluate V_m and C. If the average area occupied by an adsorbed molecule is known, the surface area can be calculated from V_m. Since the cross-sectional area per adsorbed molecule of nitrogen has been well established, it is the most commonly used gas for BET analysis.

Many adsorbents have heterogeneous adsorption sites with inhomogeneous adsorption energetics. The Langmuir constants, which are only empirical nonlinear least squares fit derived values, provide no real insight into the physical nature of the adsorbent surface (Toth, 1971; Satterfield, 1991; Ruthven, 1984, 1991), and as a result, alternative adsorption isotherm equations, derived assuming a heterogeneous surface, have been developed (Toth, 1971, 1997; Honin and Reyerson, 1951; Knaebel, 1995; Do and Do, 1997).

The Toth isotherm equation 37, a basic extension of the Langmuir model, can be

(37) $$q = q_m \frac{KP}{\left(1 + KP^t\right)^{1/t}}$$

used to fit adsorption data and estimate the heterogeneity of the surface of the adsorbent (Toth, 1971; Myers and Valenzuela, 1989). The Toth isotherm incorporates a unitless heterogeneity fitting parameter (t), which ranges from $0 < t < 1$. When t = 1, the Toth equation reverts to the basic Langmuir, and the fit suggests that the surface of the adsorbent is homogeneous. On the other hand, as the values of t approach zero, the heterogeneity of

the adsorbent surface increases. The Toth isotherm has been used to fit ethylene adsorption data collected on activated carbon (Ray and Box, 1950; Lewis et al., 1950), silica gel (Lewis et al., 1950), and zeolites (Hyun and Danner, 1982; Kaul, 1987). Toth fitting parameters from these selected studies are listed in Table 17.

Table 17. Toth Isotherm Fitting Parameters for Ethylene Adsorption on Activated Carbon, Silica gel, and Zeolites

material	b, atm^{-1}	t	q, mmol/g
activated carbon[a]	0.118	0.5988	7.34
silica gel[b]	0.627	0.845	2.54
zeolites[c]	0.044	0.687	3.19

[a] Ray and Box, 1950.
[b] Lewis et al., 1950.
[c] Kaul, 1987.

The Unilan isotherm equation 38, based on the distribution of energies among

(38) $$q = \frac{q_m}{2s} Ln\left(\frac{c + Pe^{+s}}{c + Pe^{-s}}\right)$$

adsorption sites, can also be used to evaluate surface heterogeneity (Honig and Reyerson, 1951, Myers and Valenzuela, 1989; Knaebel, 1995; Yang, 1987). The distribution function for the energy of adsorption is statistically derived by comparing the fraction of sites occupied to experimentally collected isoteric heats of adsorption (Sips, 1950; Honig and Reyerson, 1952). In the Unilan equation 40, s is the heterogeneity parameter, which generally falls in the range of 0-7 (Myers and Valenzuela, 1989). As with the Toth equation, the Unilan equation reverts back to the basic Langmuir when s = 0, dictating that the surface is homogeneous. On the other hand, as the value of s increases, the heterogeneity of the adsorbent surface is said to increase. The fitting parameter c is an arbitrary constant which provides a rough measure of the heat of adsorption of the first monolayer. The Unilan isotherm has been used to fit ethylene adsorption collected on activated carbon (Ray and Box, 1950; Lewis et al., 1950), silica gel (Lewis et al., 1950),

and zeolites (Hyun and Danner, 1982; Kaul, 1987). Unilan fitting parameters from these selected studies are listed in Table 18.

Table 18. Unilan Isotherm Fitting Parameters for Ethylene Adsorption on Activated Carbon, Silica gel, and Zeolites

material	c, atm^{-1}	s	q_m ,mmol/g
activated carbon[a]	96	0.067	16.44
silica gel[b]	72.9	5.6	8.1
zeolites[c]	0.165	1.9	3.0

[a] Ray and Box, 1950.
[b] Lewis et al. 1950.
[c] Kaul, 1987.

Selecting Adsorption Isotherms

Knaebel (1995) reported that selecting the most appropriate isotherm equation is not a well defined process. He mentions that engineers commonly believe that any isotherm fitting the general trend of the adsorption data is acceptable. Althought the most simple isotherm equation is typically the best choice for fitting the data. Additionally, parameters must be added to reflect non-ideal sufaces and adsorption behaviors (i.e. as is the case with the Toth and Unilan equations described above). Knaebel (1995) stresses these points by using four different isotherm equations to fit the adsorption of water vapor on silica gel. Results show that three equations fit the data reasonably well.

Do and Do (1997) and Rudzinski et al. (1997), in agreement with Knaebel (1995), have stressed that constants or parameters of an adsorption isotherm equation should reflect the heterogeneity of the surface of the adsorbent, and the interactions between adsorbates. Rudzinski et al. (1997) noted that isotherm parameters commonly lack correlation with these adsorption properties. Hence, fitting parameters from different adsorption isotherm equations must be used cautiously to infer information concerning adsorbent structure and adsorption interactions.

Experimental Techniques for Collecting Adsorption Data

Adsorption isotherms are collected using gravimetric methods, chromatographic methods, constant-volume methods, and dynamic methods (Yang, 1987). A more in-depth review of techniques for measuring adsorption was presented in Chapter I; only a short description follows. In gravimetric methods, the total amount of absorbed phase is measured using a microbalance. Chromatographic methods involve analyses of breakthrough curves. In constant volume (static) methods, the amount and composition of the absorbed phase are approximated by the difference in the amount and composition of the gas phase mixture, before and after adsorption. Gas phase mixture amounts are calculated using P-V-T relationships, and gas phase compositions are usually determined using gas chromatography. In dynamic (flow) methods, the adsorbent is loaded to equilibrium and the absorbate mixture is quantitatively desorbed by evacuation and/or heating and trapped in liquid nitrogen cooled or evacuated vessels. The total amount and composition of the adsorbed mixture is measured directly, using P-V-T relationships and gas chromatography, respectively. The adsorption isotherm is typically plotted with adsorption capacity, measured in ml/g or mmol/g, on the ordinate and partial pressure of the gas stream at constant temperature on the abscissa.

Ag(I) Exchanged Amberlyst 15 Resin

As reported by Yang and Kikkinides (1995) and shown in Chapter IV, unexchanged Amberlyst 15 resin adsorbs equal quantities of ethylene and ethane. Based on these results, Yang and Kikkinides assumed the unexchanged sites of the Amberlyst 15 resin were homogeneous and physisorbed both ethylene and ethane. Yang and Kikkinides (1995) reported that a 51.7% Ag(I) exchanged Ambertlyst 15 resin selectively adsorbs ethylene (1.15 mmol/g) over ethane (0.125 mmol/g) (Yang and Kikkinides, 1995). In addition to physisorption on the remaining unexchanged sites, Yang and Kikkinides postulated Ag(I) exchanged sites of the Amberlyst 15 resin were heterogeneous and

selectively chemisorbed olefin. Extended Huckel Molecular Orbital (EHMO) calculations (Yang and Kikkinides, 1995) on the interaction of ethylene with the silver salt of benzenesulfonic acid were conducted to support the chemisorption assertion. Based on the Dewar-Chatt Duncanson (Chatt and Duncanson, 1953; Dewar, 1951) bonding model, the EHMO calculations attributed 16% of the interaction to π-backbonding and 84% of the interaction to sigma donation. The calculations also provided a theorectial heat of ethylene adsorption (29.7 kcal/mol). Based on these results, Yang and Kikkinides predicted chemisorbed the most prominent interaction on the 51.7% Ag(I) exchanged Amberlyst 15 resin.

Using these assumptions, Yang and Kikkinides (1995) developed isotherm equation 39,

$$q = \frac{q_{mp} K_p P}{1 + K_p P} + \frac{q_{mc}}{2s} \ln \frac{1 + K_c P e^{s}}{1 + K_c P e^{-s}} \tag{39}$$

where q_m is the monolayer adsorption capacity, q is the adsorption capacity, K is the Langmuir constant, P is the partial pressure of adsorbate, and s is a heterogeneity parameter. The first portion of the equation, derived from the Langmuir model, represented ethylene physisorbed on the homogeneous unexchanged sites of the Ag(I) exchanged Amberlyst 15 resin. The second portion of the equation, derived from the Unilan model, represented ethylene chemisorbed on heterogeneous Ag(I) exchanged sites of the Amberlyst 15 resin.

Using Marquardt nonlinear regression methods, equation 40 was used to

$$s = \frac{\sqrt{3}\sigma}{RT} \tag{40}$$

nonlinear least squares fit ethylene adsorption data collected on 51.7% Ag(I) exchanged Amberlyst 15 resin (Yang and Kikkinides, 1995). For the fit, the heterogeneity parameter s was empirically estimated with equation 42, where σ is the square root of the variance of

the uniform energy distribution. A value of 3.5 appeared reasonable based on previous reports (Myers and Valenzuela, 1989). Based on the constructed bonding model, constraints were placed upon the physical adsorption contributions (q_{mp} and b_p). Since 48.3% of the acidic sites of the Amberlyst 15 resin were unexchanged, q_{mp} was constrained to 48.3% of the q_{mp} value obtained for ethylene adsorbed on the non-exchanged sites of the Amberlyst 15 resin. In addition, the b_p value obtained for adsorption on non-exchanged sites of the Amberlyst 15 resin was used as an upper b_p value. Hence, q_{mc} and b_c were the only true fitting parameters. The fitting parameters used by Yang and Kikkinides (1995) to characterzie ethylene adsorption on the 51.7% Ag(I) exchanged Amberlyst 15 resin are presented in Table 16.

Using equation 39 and the same constraints, Yang et al. (1997) have also fit ethylene adsorption data collected on 50.2% Ag(I) exchanged Amberlyst 15 resin and 34.5% Ag(I) exchanged Amberlyst 35 resin. The resulting fitting parameters are listed in Tables 20 and 21.

Table 19. Yang and Kikkinides Isotherm Fitting Parameters for Ethylene Adsorption on 51.7% Ag(I) Exchanged Amberlyst 15 Resin[a]

adsorbent	temp, °C	q_{mp}, mmol/g	b_p, 1/atm	q_{mc}, mmol/g	b_c , 1/atm	s
C_2H_4/resin	25	0.267	1.22			
C_2H_4/Ag resin	25	0.102	0.911	1.46	3.07	3.5

[a] Yang and Kikkinides, 1995.

Table 20. Yang and Kikkinides Isotherm Fitting Parameters for Ethylene Adsorption on 50.2% Ag(I) Exchanged Amberlyst 15 Resin[a]

adsorbent	temp, °C	q_{mp}, mmol/g	b_p, 1/atm	q_{mc}, mmol/g	b_c, 1/atm	s
C_2H_4/Ag resin	25	0.197	20.75	1.674	1.725	3.5

[a] Yang et al. 1997.

Table 21. Yang and Kikkinides Isotherm Fitting Parameters for Ethylene Adsorption 34.5% Ag(I) Exchanged Amberlyst 35 Resin[a]

adsorbent	temp, °C	q_{mp}, mmol/g	b_p, 1/atm	q_{mc}, mmol/g	b_c, 1/atm	s
C_2H_4/resin	25	0.253	8.9			
C_2H_4/Ag resin	25	0.250	13.29	2.338	1.267	3.5

[a] Yang et al. 1997.

Experimental Results

Curve Fits

The results of the Langmuir, Toth, Unilan, and Yang and Kikkinides curve fits of the ethylene adsorption isotherm of the 61% Ag(I) exchanged Amberlyst 15 resin are overlayed in Figure 62. As shown, all four isotherm equations reasonably fit the ethylene adsorption isotherm.

The Langmuir correlation plot is presented in Figure 63. As shown, the correlation plot is linear (i.e. correlation coeffieint of 1.0). As noted by Ruthven (1991), the linearity of the plot indicates a high quality fit between the Langmuir equation and adsorption isotherm.

The nonlinear least square fitting parameters of the Yang and Kikkinides, Langmuir, Toth, and Unilan isotherm fits are presented in Tables 22, 23, 24, and 25. In addition to the resulting parameters, the inital guesses and constraints, used in the curve fits, are listed in the Tables.

Initial guesses, similar to those reported by Yang and Kikkinides (1995), were used in obtaining the curve fit with the Yang and Kikkinides isotherm equation, and constraints were set extremly high. As shown, the q_m and q_c fitting parameters agree with previous adsorption fits of Ag(I) exchanged Amberlyst 15 and 35 resins (Yang and Kikkinides, 1995; Yang et al., 1997), while the b_p and b_c fitting parameters differ by over 20. This variation can be attributed to different algorithms, since different fitting programs were used and the fitting parameters only make the data converge. The value of the heterogeneity fitting parameter (s), slightly larger than previous reports (Yang and Kikkinides, 1995; Yang et al. 1997), suggests that the surface sites of the 61% Ag(I) exchanged Amberlyst 15 resin are heterogeneous.

The Langmuir, Toth, and Unilan curve fits were obtained using extremely high constraints. While structural interpertation cannot be inferred from the Langmuir parameters, the heterogeneity parameters of the Toth and Unilan fits suggest that the surface sites of the 61% Ag(I) exchanged Amberlyst 15 resin are homogeneous.

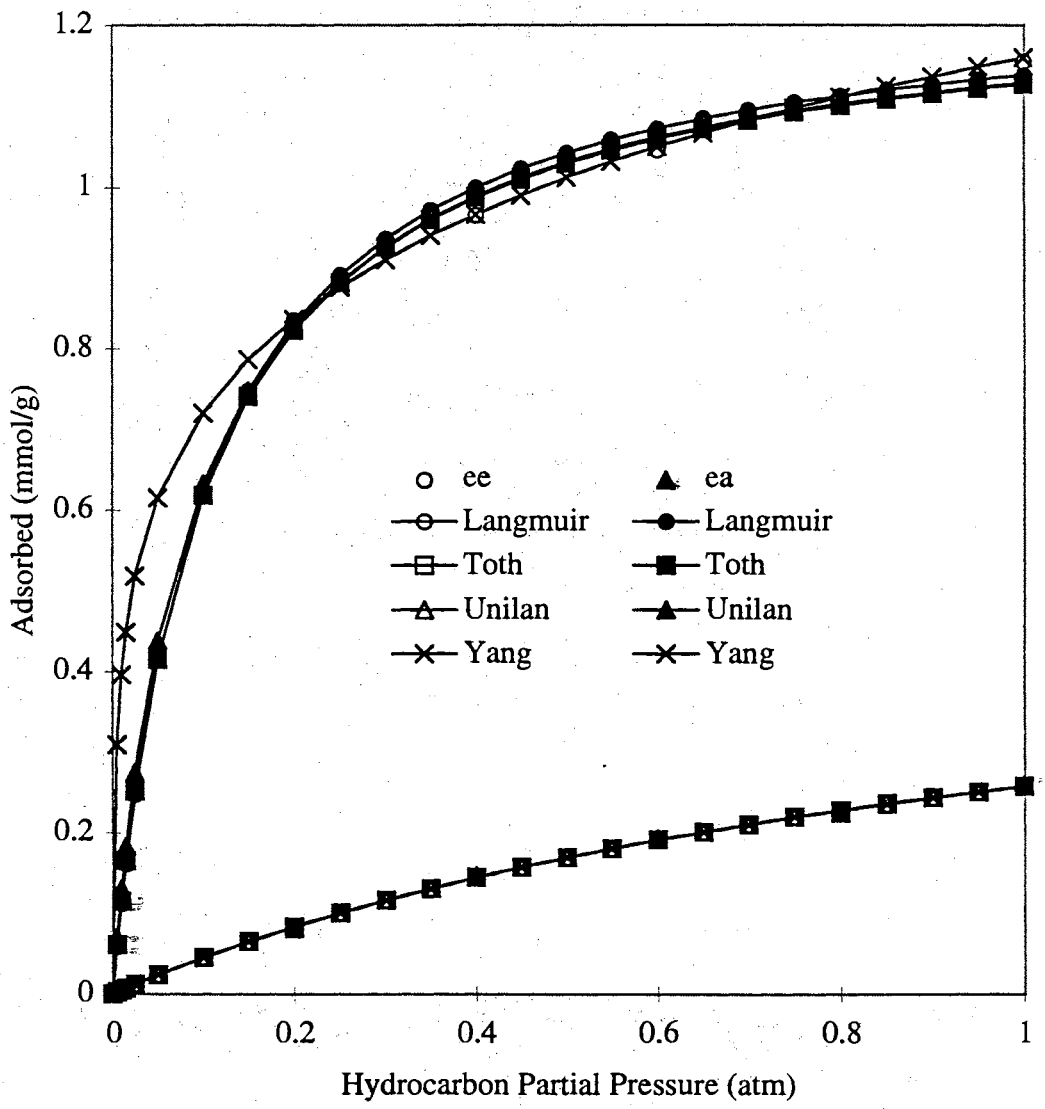

Figure 62. Curve fits of ethylene adsorption on 61% Ag(I) exchanged Amberlyst 15 resin.

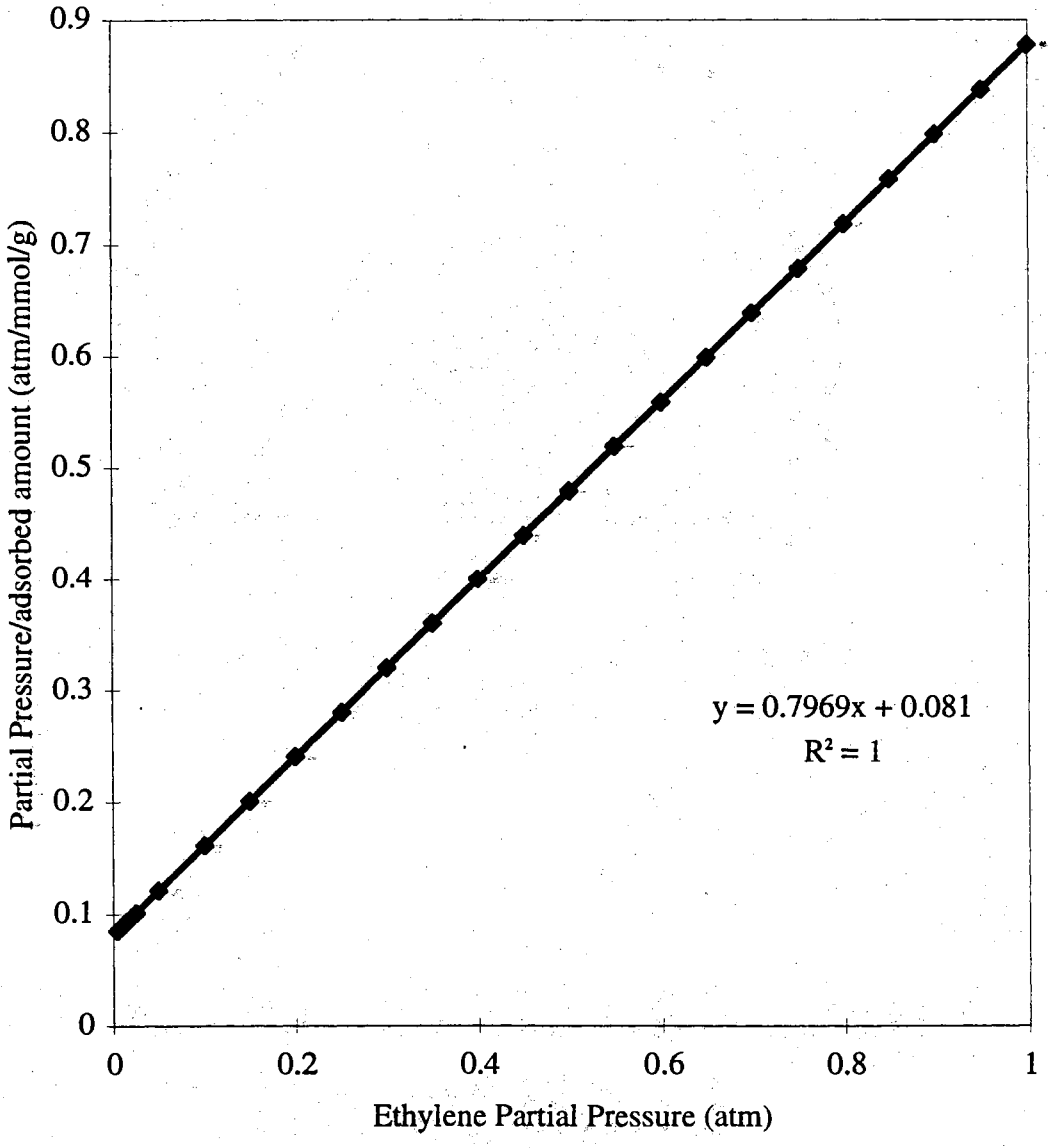

Figure 63. Langmuir isotherm correlation plot.

Table 22. Yang and Kikkinides Isotherm Fitting Parameters for Ethylene Adsorption on 61% Ag(I) Exchanged Amberlyst 15 Resin

adsorbent	temp, °C	q_{mp}, mmol/g	b_p, 1/atm	q_{mc}, mmol/g	b_c, 1/atm	s
initial guess	25	0.540	0.912	1.0	1.0	3.5
constraint	25	1.0	0.912	10	10	11.0
C_2H_4/Ag resin	25	0.343	0.912	1.446	7.89	5.4

Table 23. Langmuir Isotherm Fitting Parameters for Ethylene Adsorption on 61% Ag(I) Exchanged Amberlyst 15 Resin

adsorbent	temp, °C	q_m , gmol/kg	b, 1/atm
initial guess	25	2.0	0.2
constraint	25	10.0	1.0
C_2H_4/resin	25	0.2664	0.4534
C_2H_4/Ag resin	25	1.25	0.107

Table 24. Toth Isotherm Fitting Parameters for Ethylene Adsorption on 61% Ag(I) Exchanged Amberlyst 15 Resin

adsorbent	temp, °C	q_m , gmol/kg	t	b, 1/atm
initial guess	25	1.25	1.0	0.2
constraint	25	10.0	10.0	10.0
C_2H_4/resin	25	0.2664	0.9667	0.4417
C_2H_4/Ag resin	25	1.25	0.9621	0.1064

Table 25. Unilan Isotherm Fitting Parameters for Ethylene Adsorption on 61% Ag(I) Exchanged Amberlyst 15 Resin

adsorbent	temp, °C	q_m, gmol/kg	s	c, atm^{-1}
initial guess	25	1.25	1.0	1.0
constraints	25	10.0	10.0	10.0
C_2H_4/resin	25	0.2664	0.6520	0.4509
C_2H_4/Ag resin	25	1.25	1.0062	0.0983

Physisorbed and Chemisorbed Fractions of Ethylene

Using equation 39, the quantities of physisorbed and chemisorbed ethylene on the 51.7% Ag(I) exchanged Amberlyst 15 resin were respectfully calculated. The respective fractions were evaluated by separating equation 39 into the Langmuir and Unilan components and evaluating each equation separately using the fitting parameters reported by Yang and Kikkinides (1995). The calculated results are presented in Table 26.

Table 26. Physisorbed and Chemisorbed Fractions of Ethylene on 51.7% Ag(I) Exchanged Amberlyst 15 Resin

pressure, atm	ethylene physisorbed, mmol/g	ethylene chemisorbed, mmol/g	total adsorbed, mmol/g
0.00	0.000	0.000	0.000
0.20	0.016	0.637	0.653
0.40	0.027	0.776	0.801
0.60	0.034	0.857	0.893
0.80	0.043	0.915	0.958
1.00	0.049	0.961	1.01

As shown, the calcuations using the Unilan portion of equation 39 suggest that over 95% of the total ethylene capacity of the 51.7% Ag(I) exchanged Amberlyst 15 resin is chemisorbed on the proposed heterogeneous sites, while the Langmuir portion of equation 39 indicates less than 5% of the ethylene is physisorbed on the proposed homogeneous sites of the Amberlyst 15 resin.

Discussion

The Yang and Kikkinides, Langmuir, Toth and Unilan isotherm equations all reasonably fit the ethylene adsorption isotherm of the 61% Ag(I) exchanged Amberlyst 15 resin. In agreement with Knaebel (1995), the fits indicate that the simpler isotherm equations can be used to fit ethylene adsorption on the 61% Ag(I) exchanged Amberlyst 15 resin.

Yang and Kikkinides proposed that the ethylene was adsorbed on two sites (i.e. unexchanged and Ag(I) exchanged sites) of the Ag(I) exchanged Amberlyst 15 resin. The olefin adsorption data in Chapter IV, collected on the high Ag(I) exchanged Amberlyst 15 resins, agree with the different sites. The data show that the olefin adsorption capacities of Amberlyst 15 resins dramatically increase after Ag(I) exchange suggesting the Ag(I) must facilitate different active sites which adsorb olefin. In contrast, olefin adsorption data, collected on the low Ag(I) exchanged Amberlyst 15 resins, are not consistent with the two site model. The adsorption data show that low Ag(I) exchanged Amberlyst 15 resins have unexpectedly large ethylene adsorption capacities. For example, data indicate that 7% Ag(I) exchanged Amberlyst 15 resin adsorbs 0.82 mmol/g of ethylene corresponding to an ethylene/Ag(I) mole ratio of 2.5. As stated in Chapter IV, nitrogen adsorption data, mercury porosimetry data, and EDXAS profiles indicate the large adsorption capacity is not a result of physical modifications of the resin bead. Therefore, as described in Chapter IV, the data suggest that the Ag(I) exchanged Amberlyst 15 resin have an additional Ag(I) exchanged active site which more efficiently adsorbs olefin at low Ag(I) loading. Based on these results, the two site model does not adequately represent the olefin adsorption on this proposed third Ag(I) exchanged active site.

The Yang and Kikkinides isotherm equation, suggesting that over 95% of the ethylene is chemisorbed on 51.7% Ag(I) exchanged Amberlyst 15 resin, is inconsistent with the heats of olefin adsorption and DRIFTS-HTEC spectra of the Ag(I) exchanged Amberlyst 15 resins. The heats of ethylene adsorption of the 7% and 61% Ag(I)

exchanged Amberlyst 15 resins are 10 kcal/mol. According to Yang (1987), the 10 kcal/mol heats of ethylene adsorption, which fall below typical chemisorption values (15 kcal/mol), do not indicate that ethylene is chemisorbed on the Ag(I) exchanged Amberlyst 15 resins. The DRIFTS-HTEC spectra of ethylene exposed 61% Ag(I) exchanged Amberlyst 15 resin do not show ethylene bands in the 1450-1623 cm^{-1} region. Activated ethylene bands in this region have routinly been assigned to olefin chemisorbed on Ag(I) (Noltes et al., 1970; Scott, 1972; Nagakura and Hosoya, 1963; Yates et al., 1966); thus, the DRIFTS-HTEC spectra do not indicate that ethylene is chemisorbed on the Ag(I) exchanged Amberlyst 15 resin. Based on these data, the Yang and Kikkinides isotherm equation does not accurately represent ethylene adsorption on the Ag(I) exchanged Amberlyst 15 resin. This conclusion is most logical since the two site model, which was used to derive the Yang and Kikkinides isotherm equation, is also inconsistent with experimental data.

As discussed in the background, inferring active site homogeneity from fitting parameters is a common practice (Gregg and Sing, 1982; Ruthven, 1991; Rudzinski et al., 1997; Knaebel, 1995, Brunauer et al., 1940). Based on this precedence, the heterogeneity fitting parameters of the Toth and Unilan isotherm equations suggest the active sites of the 61% Ag(I) exchanged Amberlyst 15 resin are homogeneous. In contrast, the heterogeneity fitting parameter of the Yang and Kikkinides isotherm equation suggests the active sites of the 61% Ag(I) exchanged Amberlyst 15 resin are heterogeneous. As suggested by Rudzinski, the significance of the fitting parameters are commonly questionable. In accord, the fitting parameters support Rudzinski's assertion, and unfortunately provide no evidence to distinguish heterogeneity of the active sites of the Ag(I) exchanged Amberlyst 15 resin.

Conclusion

The Yang and Kikkinides, Langmuir, Toth and Unilan isotherm equations are all shown to fit the ethylene adsorption isotherm of the 61% Ag(I) exchanged Amberlyst 15 resin. Therefore, in agreement with Knaebel (1995), the simpler isotherm equations can be used to fit ethylene adsorption on the 61% Ag(I) exchanged Amberlyst 15 resin.

Heats of adsorption, adsorption data, and DRIFTS-HTEC spectra of Ag(I) exchanged Amberlyst 15 resins conclusively indicate that the two site model, proposed by Yang and Kikkinides, and the Yang and Kikkinides isotherm equation do not adequately represent ethylene adsorption on Ag(I) exchanged Amberlyst 15 resin.

As suggested by Rudzinski, the heterogeneity fitting parameters of the Toth, Unilan, and Yang and Kikkinides isotherm equations provide no conclusive evidence to distinguish the heterogeneity of the active sites of the Ag(I) exchanged Amberlyst 15 resin.

CHAPTER VI

OLEFIN ADSORPTION CAPACITIES AND SPECTROSCOPIC CHARACTERIZATION OF Ca(II), Na(I), and Ni(II) EXCHANGED AMBERLYST 15 RESINS

Summary

In Chapter IV, spectroscopic and adsorption data showed that ethylene was physisorbed on the Ag(I) exchanged Amberlyst 15 resins. As discussed in Chapter I, exchanging the sodium cation of zeolites with calcium, magnesium, or potassium increased ethylene adsorption capacities and olefin/paraffin selectivities by physisorption interactions (dispersion forces). Preliminary economic analysis of 61% Ag(I) exchanged Amberlyst resins had indicated that the high cost of silver might limit industrial application of those materials in olefin separation and recovery. Amberlyst 15 resins exchanged with alternative metal cations could offer considerable cost advantages over Ag(I) if high olefin adsorption capacities and olefin/paraffin selectivities could be achieved. In addition, spectroscopic characterization of the Ca(II) and Na(I) exchanged Amberlyst 15 resins might provide valuable information about the active sites for ion exchange and olefin adsorption on the Amberlyst 15 resins.

In Chapter VI, the ethylene adsorption capacities of Ca(II), Na(I), and Ni(II) exchanged Amberlyst 15 resins, measured in single component streams by TGA, are reported. DRIFTS spectra of the Ca(II) and Na(I) exchanged Amberlyst 15 resins are presented and discussed. The adsorption data indicate that the Ca(II) and Na(I) exchanged Amberlyst 15 resins, having very poor adsorption capacities, offer no economic advantage over Ag(I) exchanged Amberlyst 15 resins. In addition and in agreement with data in Chapter III, the DRIFTS spectra of the Ca(II) and Na(I) exchanged Amberlyst 15 resins indicate; (1) the sulfonate groups are the active sites for cation exchange on the Amberlyst 15 resin; (2) the cation exchange reorganizes the hydration structure of the Amberlyst 15 resins; and (3) the Amberlyst 15 resins contain residual moisture.

Background

Analysis of Industrial Process using Ag(I) Exchanged Amberlyst 15 Resin

Preliminary cost analysis of the 51.7% Ag(I) exchanged Amberlyst 15 resin in an industrial olefin separation process attributed over 56% of the process cost solely to Ag(I) (Lemmons, 1997). Due to the high cost of $AgNO_3$ (estimated from Aldrich, 1997), it was concluded that the adsorption process using 51.7% Ag(I) exchanged Amberlyst 15 resin would not be economically feasible.

Olefin Adsorption on Cation Exchanged Zeolites

The separation of ethylene and propylene from gas streams using modified zeolites has been investigated by Schoeller and Mueller (1986). By ion exchanging zeolites with K^+, Ba^{2+}, and Mg^{2+} ions, olefin separations were obtained by adsorption and by blocking the transport of alkanes through the zeolite. Based on breakthrough curves, retention times for ethane and ethylene at 25 °C were 3 min and 15 min, respectfully, for the Mg^{2+} zeolite. In the separation tests, the olefin was desorbed by heating to temperatures between 293 and 500 K while flowing nitrogen gas through the system. Olefin loadings per gram of adsorbent were shown to depend on the exchanged ions and were 1.35 mmol/g for K^+, 1.71 mmol/g for Ba^{2+}, and 1.93 mmol/g for Mg^{2+}.

Triebe et al. (1996) investigated the utility of Ca^{2+} exchanged zeolites to separate olefins from paraffin streams. Separation studies on Ca^{2+} zeolite showed that olefin/paraffin adsorption ratios, reported as ratios of Henry's law constants, ranged from 100 to 1100. The authors reported a heat of ethylene adsorption on the Ca^{2+} zeolite of 13.9 kcal/mol and attributed the separation to physisorption interaction between the π-bond of the olefin and the divalent Calcium sites in the zeolite.

Infrared Spectroscopy of Sulfonated Polystyrene Resins and Polystyrene-Divinylbenzene Resins

Infrared spectroscopy studies of cation exchanged polystyrenesulfonic acid resins (Zundel, 1969; Bazuin and Fan, 1995; Burford et al. 1994) and polystyrene-divinylbenzene resins (Bartholin et al., 1981) were reviewed in Chapter III. For reference, a compiled list of infrared band assignments from Chapter III are provided in Tables 27 and 28.

Table 27. Infrared Band Assignments of Polystyrenesulfonic Acid and its Salts[a,b,c]

vibration	moiety	band, cm^{-1}
-O-H stretch	Water	3700-2500
=C-H stretch	Phenyl	3065, 3030
-C-H anti, sym stretches	Backbone	2928, 2856
H-O-H scissor	Water	1690-1640
-C-H skeleton	Phenyl	1601, 1495, 1413
-C-H scissor	Backbone	1451
-S=O antisym. stretch	$-SO_3H$	1350
-S-O antisym. stretch	$-SO_3^-$	1200 (split)
-S=O sym. stretch	$-SO_3H$	1172
-S-O sym. stretch	$-SO_3^-$	1134
-C-H in-plane skeleton	Phenyl	1128
-C-H in-plane skeleton	Phenyl	1097
-S-O sym. stretch	$-SO_3^-$	1034
-C-H in-plane bend	Phenyl	1011-1001
-S-O stretch	$-SO_3H$	907
-C-H out-of-plane bend	Phenyl	838
-C-H out-of-plane bend	Phenyl	777
-C-C ring vibration	Phenyl	671

[a] Zundel, 1969.
[b] Bazuin and Fan, 1995.
[c] Burford et al., 1994.

Table 28. Infrared Band Assignments of Polystyrene-Divinylbenzene Resin[a]

vibration	moiety	band, cm^{-1}
-C=C	Vinyl	1680-1630
H-O-H	Water	1600-1602
-C-C, -C-H	Phenyl	1600-1602
-C-C	Phenyl	1510
-C-C	Phenyl	1492
-C-C	Phenyl	1484-1488
-C-C	Phenyl	1451
-C-C	Phenyl	1443
-C-H	Vinyl	1410
-C-H	Phenyl	1026
=C-H	Phenyl	1015-1018
=C-H	Vinyl	990-985
-C-H	Phenyl	905
-C-H	Phenyl	838, 830
-C-H	Phenyl	795-797
-C-H	Phenyl	760

[a] Bartholin et al., 1981.

Experimental Results

Adsorption and Desorption of Ethylene

Ethylene adsorption and desorption isotherms of the Ca(II) exchanged Amberlyst 15 resin are presented in Figure 64. The data were collected at RT and 1 atm using the TGA. As illustrated, the Ca(II) exchanged Amberlyst 15 resin adsorbs 0.43 mmol/g of ethylene at RT and 1 atm. The desorption isotherm shows that the Ca(II) exchanged Amberlyst 15 resin irreversibly adsorbs 22% of the ethylene at RT.

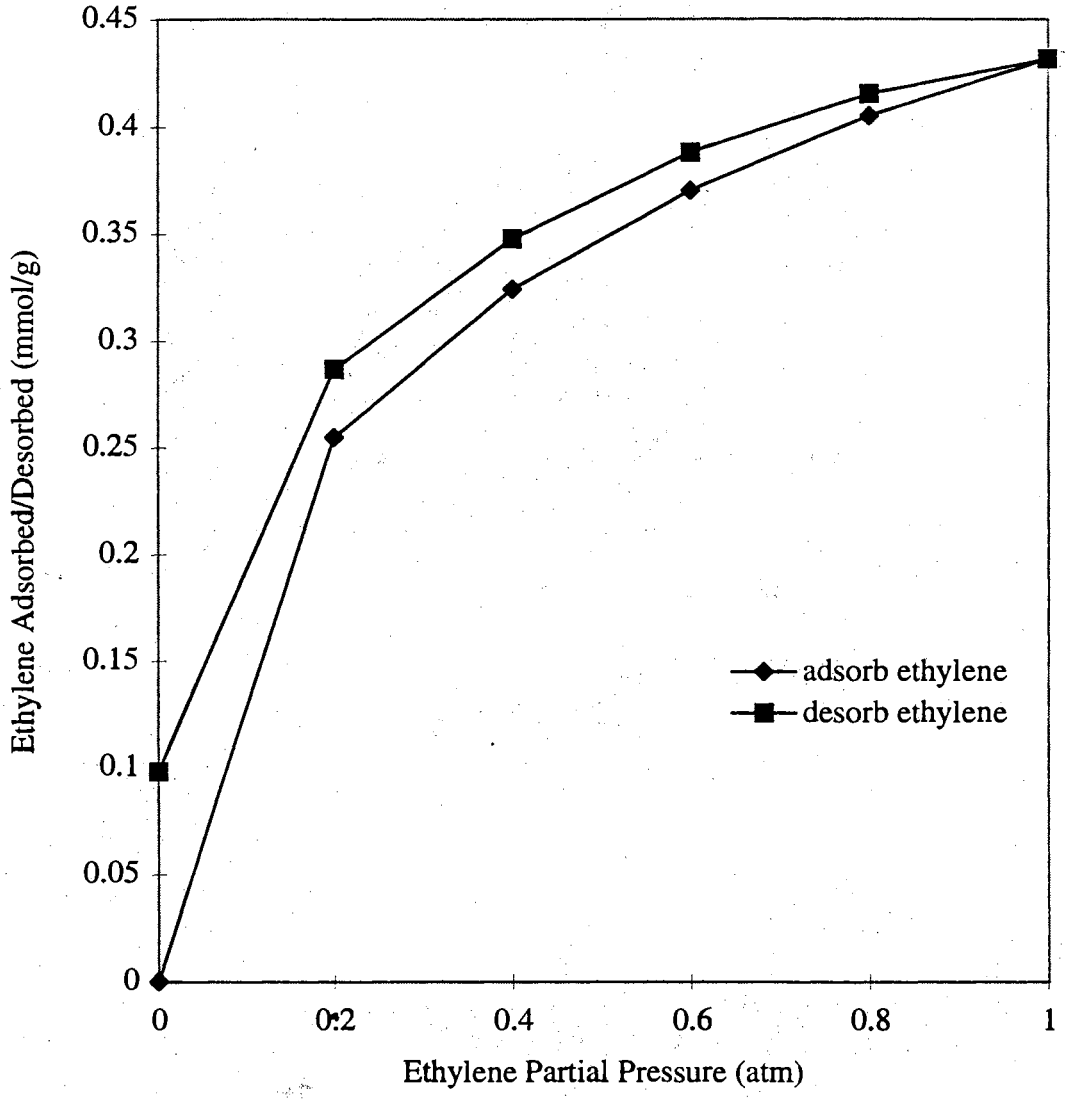

Figure 64. Ethylene adsorption and desorption isotherms of Ca(II) exchanged Amberlyst 15 resin.

Ethylene adsorption of the Ni(II) and Na(I) exchanged Amberlyst 15 resins is presented in Table 29. The data were collected at RT and 1 atm using the TGA. As shown, the Ni(II) exchanged Amberlyst 15 resin adsorbed 0.32 mmol/g of ethylene, and the Na(I) exchanged Amberlyst 15 resin adsorbed 0.25 mmol/g of ethylene. Due to the poor adsorption capacities, complete isotherms were not collected on the Ni(II) and Na(I) exchanged Amberlyst 15 resin.

Table 29. Adsorption of Ethylene on Na(I) and Ni(II) Exchanged Amberlyst 15 Resins

adsorbent	ethylene partial pressure, atm	temperature, °C	ethylene adsorbed, mmol/g
Na(I) resin	1.0	25	0.25
Ni(II) resin	1.0	25	0.32

DRIFTS Spectra

The DRIFTS spectrum of the Ca(II) exchanged Amberlyst 15 resin is presented in Figure 65 and bands are assigned based on previous reports (Zundel, 1969; Bazuin and Fan, 1995; Burford et al., 1994). In the spectrum of the Ca(II) exchanged Amberlyst 15 resin, the bands of polystyrene-divinylbenzene, listed of the Table 28, are observed. Strong and intense bands, assigned to the OH stretch and HOH scissor vibration of water, are respectfully observed at 3428 cm^{-1} and 1640 cm^{-1}. A band centered at 1200 cm^{-1} (split at 1217 cm^{-1} and 1178 cm^{-1}) and a band 1350 cm^{-1}, respectfully assigned to the antisymmetric S-O stretch of the sulfonate anion and antisymmetric S=O stretch of the sulfonic acid, are observed. A band assigned to the in-plane bend of the phenyl is observed at 1011 cm^{-1}.

The DRIFTS spectrum of the Na(I) exchanged Amberlyst 15 resin is presented in Figure 66 and bands are assigned based on previous reports (Zundel, 1969; Bazuin and Fan, 1995; Burford et al., 1994). In the spectrum of the Na(I) exchanged Amberlyst 15 resin, the bands of polystyrene-divinylbenzene, listed of the Table 28, are observed. Strong bands, assigned to the OH stretch and HOH scissor vibration of water, are respectfully observed at 3480 cm^{-1} and 1640 cm^{-1}. A band centered at 1200 cm^{-1} (split at

1217 cm^{-1} and 1189 cm^{-1}) and a band 1350 cm^{-1}, respectfully assigned to the antisymmetric S-O stretch of the sulfonate anion and antisymmetric S=O stretch of the sulfonic acid, are observed. A band assigned to the in-plane bend of the phenyl is observed at 1010 cm^{-1}. In contrast to the DRIFTS spectrum of the Ca(II) exchanged Amberlyst 15 resin, a band, assigned to the S-O stretch of sulfonic acid, is observed at 906 cm^{-1}.

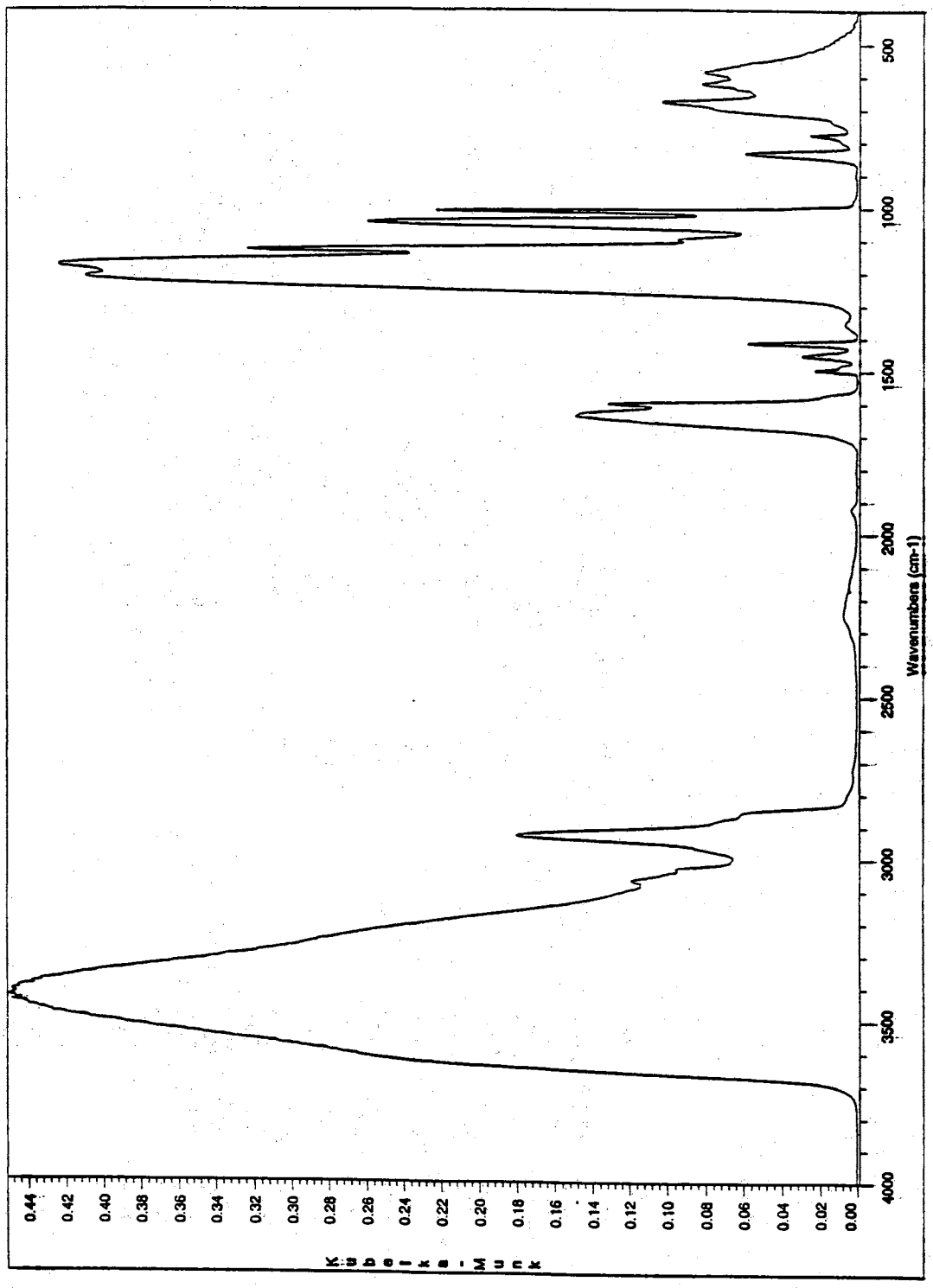

Figure 65. DRIFTS spectrum of Ca(II) exchanged Amberlyst 15 resin.

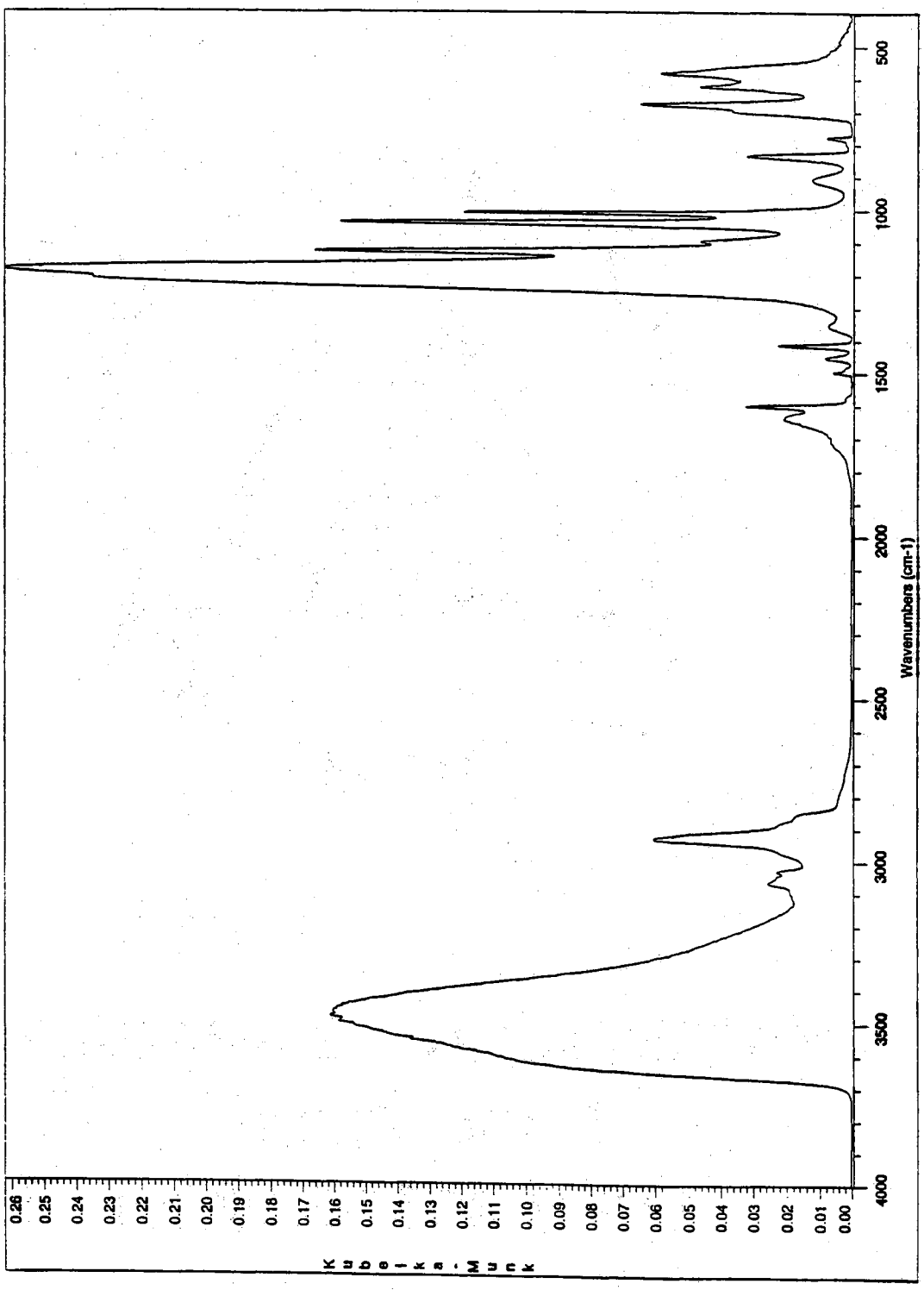

Figure 66. DRIFTS spectrum of Na(I) exchanged Amberlyst 15 resin.

Discussion

Data show that the Ca(II) exchanged Amberlyst 15 resin adsorbs an additional 0.25 mmol/g of ethylene when compared to the 0.18 mmol/g of ethylene adsorbed by the unexchanged Amberlyst 15 resin. Compared to the olefin adsorbents discussed in Chapter I, the adsorption capacity of the Ca(II) exchanged Amberlyst 15 resin is greater than the adsorption capacity of the activated carbon supported copper(I) chloride (Hirai et al., 1988) but less than the other olefin adsorbents. Thus, the Ca(II) exchanged Amberlyst 15 resin offers little economic incentive.

Data show that the Ni(II) and Na(I) exchanged Amberlyst 15 resins, respectively, adsorb an additional 0.14 mmol/g of ethylene and 0.07 mmol/g of ethylene than the unexchanged Amberlyst 15 resin. However, the adsorption capacities of the Ni(II) and Na(I) exchanged Amberlyst 15 resins fall far below that of Ca(II) exchanged Amberlyst 15 resin and the previously reported olefin adsorbents. Thus, the Ni(II) and Na(I) exchanged Amberlyst 15 resin offer no additional economic incentive.

Band changes in the DRIFTS spectra of the Ca(II) and Na(I) exchanged Amberlyst 15 resins indicate that the exchange removes the acidic proton of the sulfonate groups. For example, in both spectra, the intensity of the bands at 906 cm-1 and 1350 cm-1, respectfully assigned to the S-O stretch and S=O antisymmetric stretch of the sulfonic acid, decrease. As described previously by Zundel (1969) and Bazuin et al. (1996), the decrease in intensity of these bands indicates that the exchange displaces the acidic proton of the sulfonic acid. As observed in the Ca(II) exchanged Amberlyst 15 resin, cation exchange is observed to completely remove the 906 cm-1 band. In accord with Zundel (1969), this indicates the Ca(II) exchange leaves no unexchanged sulfonate sites. This is easily rationalized since the selectivity coefficient for Ca(II)-H replacement is 2 times higher than that of Ag(I)-H and 4 times higher than that of Na(I)-H.

Band changes in the DRIFTS spectra of the Ca(II) and Na(I) exchanged Amberlyst 15 resins indicate that the cation interacts with the oxygen of the sulfonate anion. For

example, when compared with the DRIFTS spectrum of the unexchanged Amberlyst 15 resin, the DRIFTS spectra of the Ca(II) and Na(I) exchanged Amberlyst 15 resin show split bands, centered at 1200 cm^{-1}. In agreement with Zundel (1969) the split of the 1200 cm^{-1} band, assigned to the symmetric stretch of the S-O bond of the sulfonate anion interacting with the metal cation, indicates the metal cations are attached to the oxygen of the sulfonate anion.

Consistent with Zundel (1969) and Bazuin and Fan (1996) and the conclusions based on the DRIFTS spectra of the Ag(I) exchanged Amberlyst 15 resins in Chapter III, these changes in the sulfonate bands, observed in the DRIFTS spectra of the Ca(II) and Na(I) exchanged Amberlyst 15 resins, indicate that the active sites for cation exchange on the Amberlyst 15 resins are the sulfonate groups.

The infrared bands observed in the DRIFTS spectra of the Ca(II) and Na(I) exchanged Amberlyst 15 resins indicate that cation exchange reorganizes the hydration structure of the Amberlyst 15 resin. For example, when compared with the broad and continuos water bands in the DRIFTS spectra of the unexchanged Amberlyst 15 resin, the isolated OH bands of water, observed in both spectra, indicate reorganization of the hydration structure around the metal cations. In accord with the postulated structures reported by Zundel (1969), the isolated OH bands of water imply that the hydration structure of the Amberlyst 15 is more organized after cation exchange and that the structure may consist of water molecules which are bound to cation and hydrogen bonded to surrounding unexchanged sulfonate groups. DRIFTS spectra of the Ag(I) exchanged Amberlyst 15 resins in Chapter III indicated similar results.

The infrared bands observed in the DRIFTS spectra of the Ca(II) and Na(I) exchanged Amberlyst 15 resins indicate that the Amberlyst 15 resins retain significant quantities of moisture. For example, in both spectra very intense water bands are observed in the OH stretching and HOH scissor vibration regions indicating significant moisture content. These results are consistent with DRIFTS spectra of the Ag(I) exchanged

Amberlyst 15 resins in Chapter III which indicate that the Ag(I) exchanged Amberlyst 15 resins also have a high moisture content.

Conclusion

When compared with the unexchanged Amberlyst 15 resin, the Ca(II), Na(I), and Ni(II) exchanged Amberlyst 15 resins show enhanced ethylene adsorption capacities. However, the capacities are only moderate when compared with the 1.15 mmol/g ethylene adsorption capacity of the Ag(I) exchanged Amberlyst 15 resin and the olefin adsorption capacities of the soluble and solid olefin adsorbents. As a result, the alternative cation exchanged Amberlyst 15 resins, having very poor adsorption capacities, offer no economic advantage over Ag(I) exchanged Amberlyst 15 resins. In addition and in agreement with data in Chapter III, the DRIFTS spectra of the Ca(II) and Na(I) exchanged Amberlyst 15 resins indicate the following; (1) the sulfonate groups are the active sites for cation exchange on the Amberlyst 15 resin; (2) the cation exchange reorganizes the hydration structure of the Amberlyst 15 resins; and (3) the Amberlyst 15 resins contain residual moisture.

CHAPTER VII

PROPOSED ACTIVE SITE(S) FOR OLEFIN ADSORPTION ON Ag(I) EXCHANGED AMBERLYST 15 RESINS

Summary

In Chapter III, DRIFTS and NMR spectra indicate that the sulfonate groups are the active sites for Ag(I) exchange on the Amberlyst 15 resin. Nitrogen adsorption data, mercury porosimetry data, and SEM images indicate that the structural properties of the Amberlyst 15 resin are not modified by Ag(I) exchange. EDXAS profiles show that Ag(I) is homogeneously distributed within the Amberlyst 15 resin bead. In Chapter IV, adsorption studies indicate the following; (1) Ag(I) exchanged Amberlyst 15 resins selectively adsorb ethylene over ethane, (2) ethylene adsorption capacities fall at high Ag(I) loading but are surprisingly high at low Ag(I) loading, corresponding to ethylene/Ag(I) mole ratios greater than 2.5, and (3) ethylene is not chemisorbed at low Ag(I) loading; only a small amount of ethylene is chemisorbed at high Ag(I) loading. Heats of ethylene adsorption and DRIFTS-HTEC spectra provide no evidence for chemisorption of olefin. In Chapter V, curve fits and fitting parameters indicate the proposed two site adsorption model of Yang and Kikkinides isotherm equation inadequately represents ethylene adsorption on the Ag(I) exchanged Amberlyst 15 resin.

In Chapter VII, a model compound study is reported with respect to alternative sites for Ag(I) interaction on Amberlyst 15 resin. Active sites and a model for ethylene adsorption on Ag(I) exchanged Amberlyst 15 resins are proposed. The model compound study provides no evidence for Ag(I) interactions with unsaturated systems of the Amberlyst 15 resin, and the proposed active site model for olefin adsorption is consistent with spectroscopic analysis and adsorption studies.

Experimental Approach

In Chapter VII, nuclear magnetic resonance spectroscopy (NMR) is used to characterize possible interactions of Ag(I) (i.e. from silver trifluoroacetate) with *p*-toluenesulfonic acid and 4-styrenesulfonic acid sodium salt. These compounds were chosen because each represents a monomer unit of the Amberlyst 15 resin.

Background

Macroreticular Polystyrene-Divinylbenzene Ion Exchange Resin

According to Albright (1986), Guyot (1988), Kressman et al. (1962, 1963a, 1963b, 1964), and Kunin et al. (1962), macroreticular polystyrene-divinylbenzene ion exchange resins, illustrated in Figure 67, typically contain greater than 5% divinylbenzene (DVB) crosslinking, and depending on preparation conditions (i.e. temperature, dilutents, extraction of dilutent, drying, DVB content), the macroreticular resins consist of agglomerates of micro-gel spheres which are linked together forming continuous pore channels.

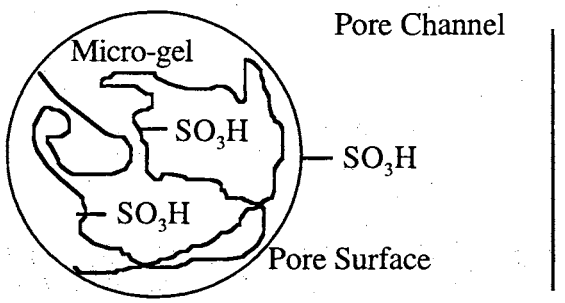

Figure 67. Macroreticular polystyrene-divinylbenzene ion exchange resin.

In macro-resins, the micro-gel spheres, similar to conventional polystyrene-divinylbenzene resins, consist of a high degree of divinylbenzene crosslinking, contain the majority of exchange sites, and retain a smaller fraction of the moisture content. On the other hand, the pore channels of macro-resins range from 20-1000 nm, contain fewer exchange sites, and

retain a larger fraction of the moisture content (Albright, 1986; Kressman et al., 1963a, 1963b, 1964).

Alternative Sites for Ag(I) Interaction on Polystyrene and Sulfonated Polystyrene-Divinylbenzene Resins

Donovan and Mowat (1995) studied polystyrene and Ag(I) doped polystyrene by matrix-assisted laser desorption/ionization (MALDI) and time-of-flight mass spectrometry. Comparison of the mass spectra of samples showed that polystyrene peaks narrowed and were split into doublets after the addition of Ag(I). Based on reported binding energies (230 kJ/mol) between benzene and Ag(I) (Afzaal and Freiser, 1994), which were evaluated by Fourier transform ion cyclotron resonance mass spectrometry, Donovan and Mowat (1995) attributed spectral changes to the formation of Ag(I)-polystyrene adducts.

Gregor (1951) evaluated alkali metal-H^+ selectivity coefficients of conventional sulfonated polystyrene-divinylbenzene resins (Dowex 50). Results indicated that selectivity coefficients decreased with decreasing water content and increasing cation exchange. Based on these conclusions, variations in selectivity coefficients were attributed to osmotic pressure changes which resulted from different hydrated ionic volumes (i.e. size of the ion hydration sphere).

Bonner and Rhett (1953) evaluated Ag(I)-Na(I)-H^+ selectivity coefficients of conventional sulfonated polystyrene-divinylbenzene resins (Dowex 50) using Ag(I) radioactive tracer techniques. Analyses indicated that Ag(I)-H^+ selectivity coefficients progressively increased with decreasing water content. Based on these results and the fact that the hydration sphere of Ag(I) is smaller than that of H^+, Bonner et al. (1956) negated the previously proposed osmotic pressure theory (Gregor, 1951).

Hogfeldt et al. (1958), in studying single beads of conventional sulfonated polystyrene-divinylbenzene resins (Dowex 50) from the same lot, reported that selectivity coefficients varied from bead to bead. Based on these results and previous theories (Boyd and Myers, 1956; Bonner et al., 1956), Hogfeldt et al. (1958) suggested the resin beads

have different types of exchange sites which are distributed differently in different beads.

In an attempt to explain variations in the selectivity coefficients of sulfonated polystyrene-divinylbenzene resin beads, a physical model and a chemical model for the chemically different exchange sites were proposed (Hogfeldt et al., 1958). The physical model was based on a continuum of chemically different exchange sites which varied from bead to bead and within a bead. These chemically different sites were proposed to result from variations in the physical properties (i.e. density, porosity, etc.) and bead structures. The chemical model, illustrated in Figure 68 and also recently proposed by Sastre et al. (1997), was based on two distinct and chemically different exchange sites, one exchange site located on polystyrene and the other on divinylbenzene.

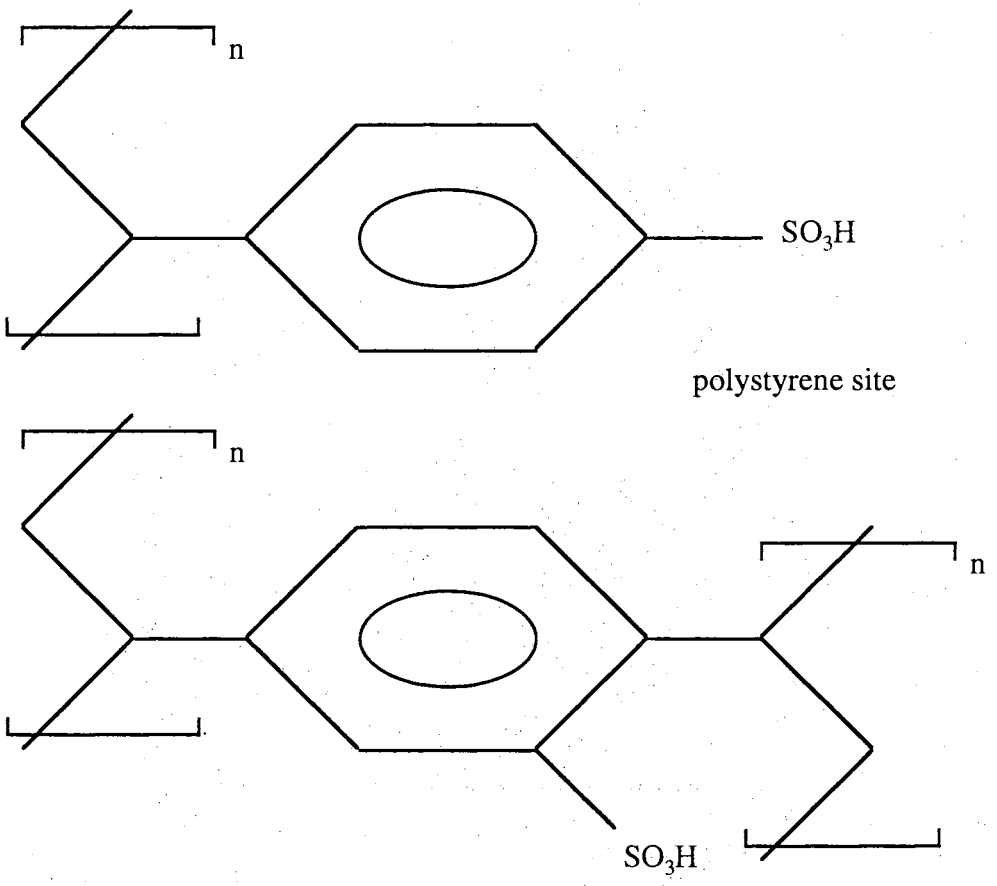

Figure 68. Proposed chemical exchange sites of sulfonated polystyrene-divinylbenzene resin.

Hogfeldt et al. (1958) suggested that if the chemical model were correct, there should exist a correlation between the amount of divinylbenzene and the fraction of the two exchange sites. Based on the physical and chemical models, Hogfeldt et al. (1958) theoretically calculated Ag(I)-H^+ selectivity coefficients of sulfonated polystyrene-divinylbenzene (10%) resin. Calculations, based on the physical model, showed a continuous distribution of selectivity coefficients that ranged from 2.5 to 420. Calculations, based on the chemical model, ascribed 10% of the resin capacity to the divinylbenzene sites with a selectivity coefficient of 224 and 90% to the polystyrene site with a selectivity coefficient of 4. Based on these results, the authors concluded both models fit the experimental data well and suggested additional research was needed to differentiate between the models.

Ag(I)-Olefin Complexes

As discussed in Chapters I and IV, Ag(I) interacts with olefins through the formation of a π-bond. Dewar (1951), Chatt and Duncanson (1953) explained the π-bond using the following scenario. The olefin donates electron density from its π-orbital into the empty s orbital of the metal, and the filled d orbital of the metal donates electron density back (i.e. backbonding) into the empty anti-bonding orbital of the olefin.

As reviewed in Chapter IV, π-bonds between olefins and transition metals have been characterized by infrared spectroscopy (Noltes et. al., 1970; Scott, 1973; Tsai and Quinn, 1969; Brandt, 1959; Nagakura and Hosoya, 1963; Yates et al., 1966; Busca et al., 1992; Nagendrappa and Devaprabhakara, 1968), and interactions between unsaturated systems and Ag(I) have been evaluated using proton nuclear magnetic resonance spectroscopy (Schug and Martin, 1962). Upon coordination to transition metals, the infrared data indicated that the symmetry of the C=C olefin bond is disturbed, shifting the infrared C=C vibrational band of the olefin to lower wavenumber. The proton NMR spectra showed that the olefinic protons shift downfield upon complexation with Ag(I). For example, NMR spectra showed that the olefin protons of cyclohexene shift 0.69 ppm downfield and those of benzene shift 0.21-0.87 ppm downfield upon complexation with Ag(I). Based on these spectral results, donation of electron density from the olefin into the π-bond was predicted to dominate the olefin-Ag(I) interaction.

Many surface studies have evaluated the orientation of olefin when bonded to surface-supported transition metals (Albert et al., 1982; Carr et al., 1985; Bao, 1995). The main consensus of those studies is that one olefin lies parallel to the surface of the metal in order to accommodate proper overlap of the π-orbitals. As noted here and in Chapter I, the Dewar, (1951) Chatt, and Duncanson (1953) bonding model and previous olefin

adsorption studies also limit olefin/metal ratios of supported transition metal olefin adsorbents to 1. However, in a review on Ag(I)-olefin complexes in solution, Tsai and Quinn (1969) described studies in which olefin/Ag(I) ratios exceeded 1. For example, a $(C_{10}H_{10})_3AgBF_4$ aqueous solution complex was fully characterized and shown to have an olefin/Ag(I) ratio of 3 (Quinn, 1968). In the complex, the olefin molecules were found to be trigonally positioned about the Ag(I) atom. The authors suggested that the closed d shell of the Ag(I) ion formed higher olefin/Ag(I) mole ratio complexes because the closed d shell allowed the smallest differences between the destabilization introduced by replacement of the waters of hydration with olefin and the stabilization introduced by charge delocalization from olefin to metal.

Experimental Results

^{1}H NMR Spectra of Model Compounds

The ^{1}H NMR spectrum of *p*-toluenesulfonic acid in 80% acetonitrile-d_3/20% deuterium oxide is presented in Figure 69. In the spectrum, an AA'XX' splitting pattern of the phenyl protons is observed. The solvent proton and the methyl protons, having no nearest neighbors, are observed as singlets.

The ^{1}H NMR spectrum of Ag(I) exposed *p*-toluenesulfonic acid in 80% acetonitrile-d_3/20% deuterium oxide is presented in Figure 70. In the spectrum, the phenyl and vinyl proton resonances are unaffected by Ag(I) cation, and no new resonances are observed. However, the solvent proton is observed to shift upfield.

The ^{1}H NMR spectrum of 4-styrenesulfonic acid sodium salt in 80% acetonitrile-d_3/20% deuterium oxide is presented in Figure 71. In the spectrum, an AA'XX' splitting pattern of the phenyl protons is observed. In addition, an ABX splitting pattern of the vinyl protons is observed. The solvent proton, having no nearest neighbors, is observed as an intense signal.

The ^{1}H NMR spectrum of the Ag(I) exposed 4-styrenesulfonic acid sodium salt in 80% acetonitrile-d_3/20% deuterium oxide is presented in Figure 72. In the spectrum, the phenyl and vinyl proton resonances are unaffected by Ag(I) cation, and no new resonances are observed. However, the solvent proton is observed to shift downfield.

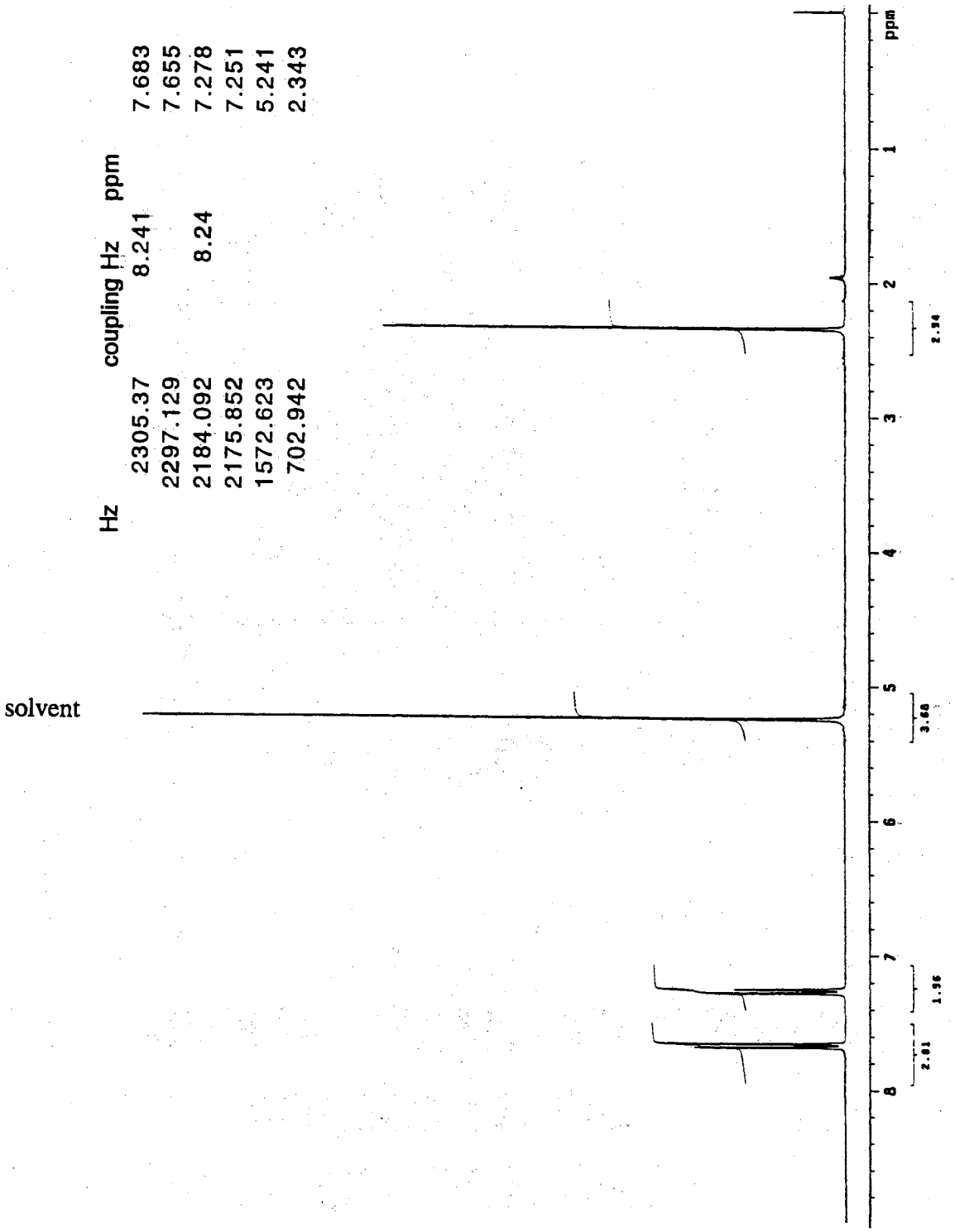

Figure 69. ^{1}H NMR spectrum of *p*-toluenesulfonic acid in 80% acetonitrile-d_3/20% deuterium oxide.

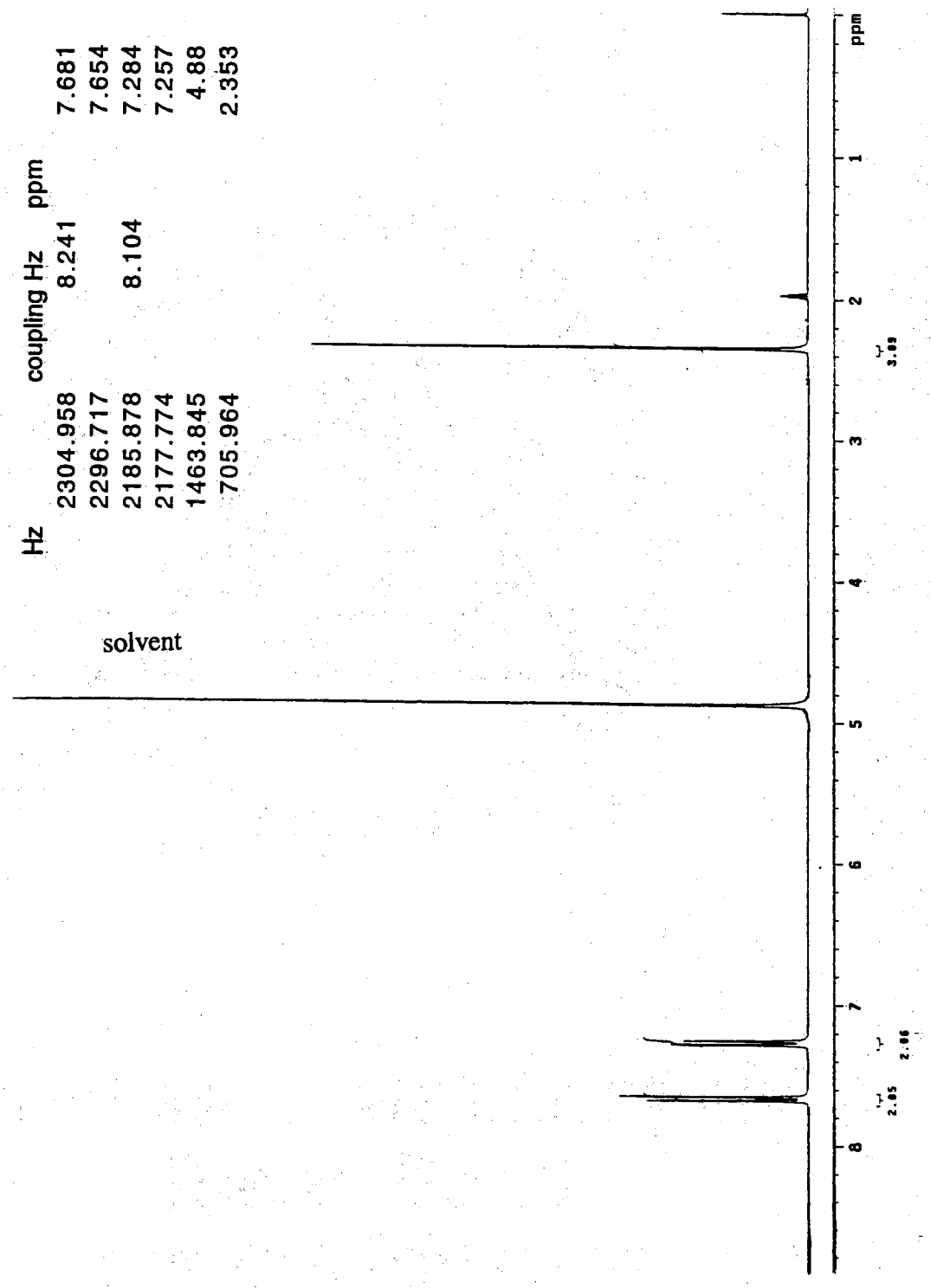

Figure 70. ^{1}H NMR spectrum of Ag(I) exposed *p*-toluenesulfonic acid in 80% acetonitrile-d_3/20% deuterium oxide.

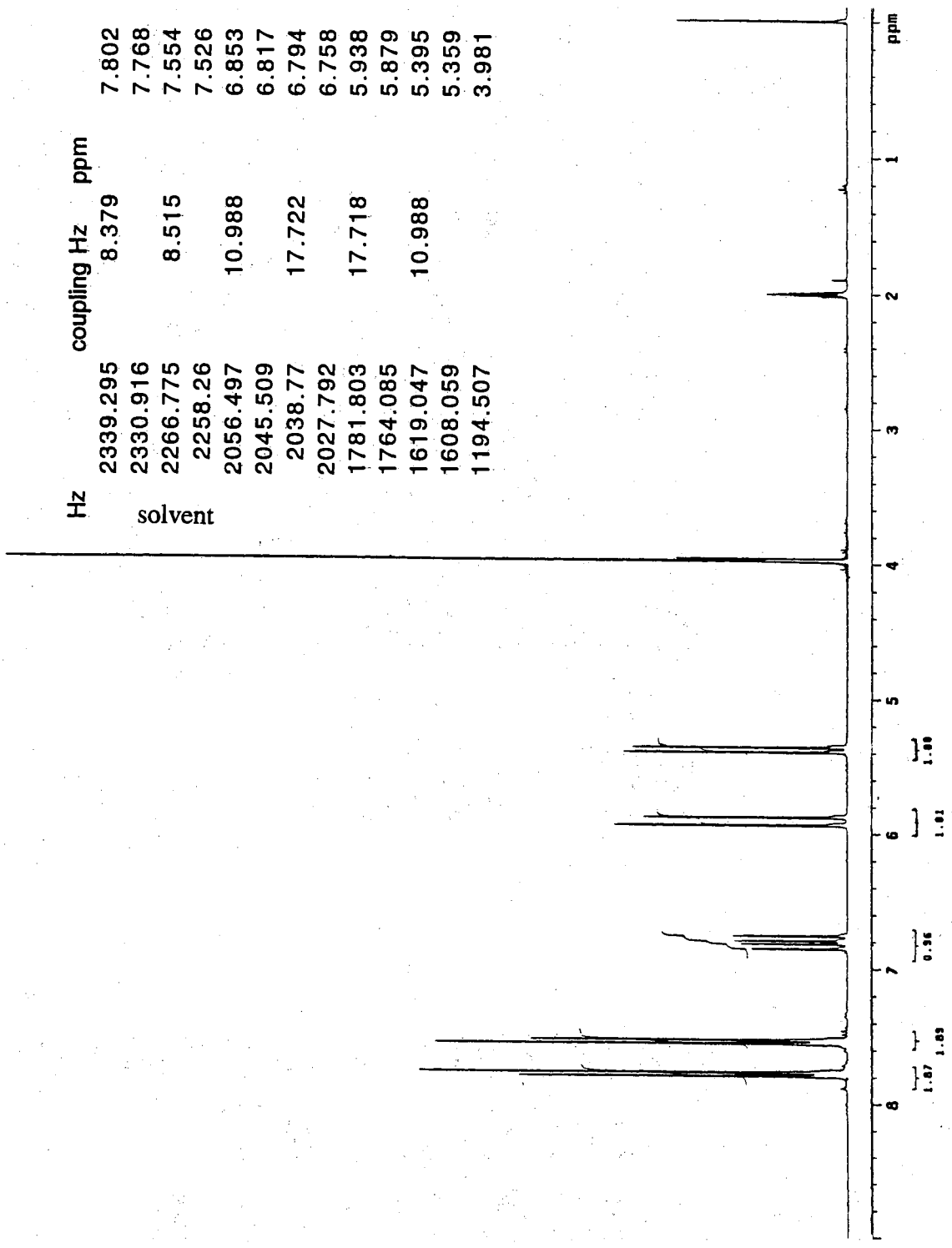

Figure 71. ^{1}H NMR spectrum of 4-styrenesulfonic acid sodium salt in 80% acetonitrile-d_3/20% deuterium oxide.

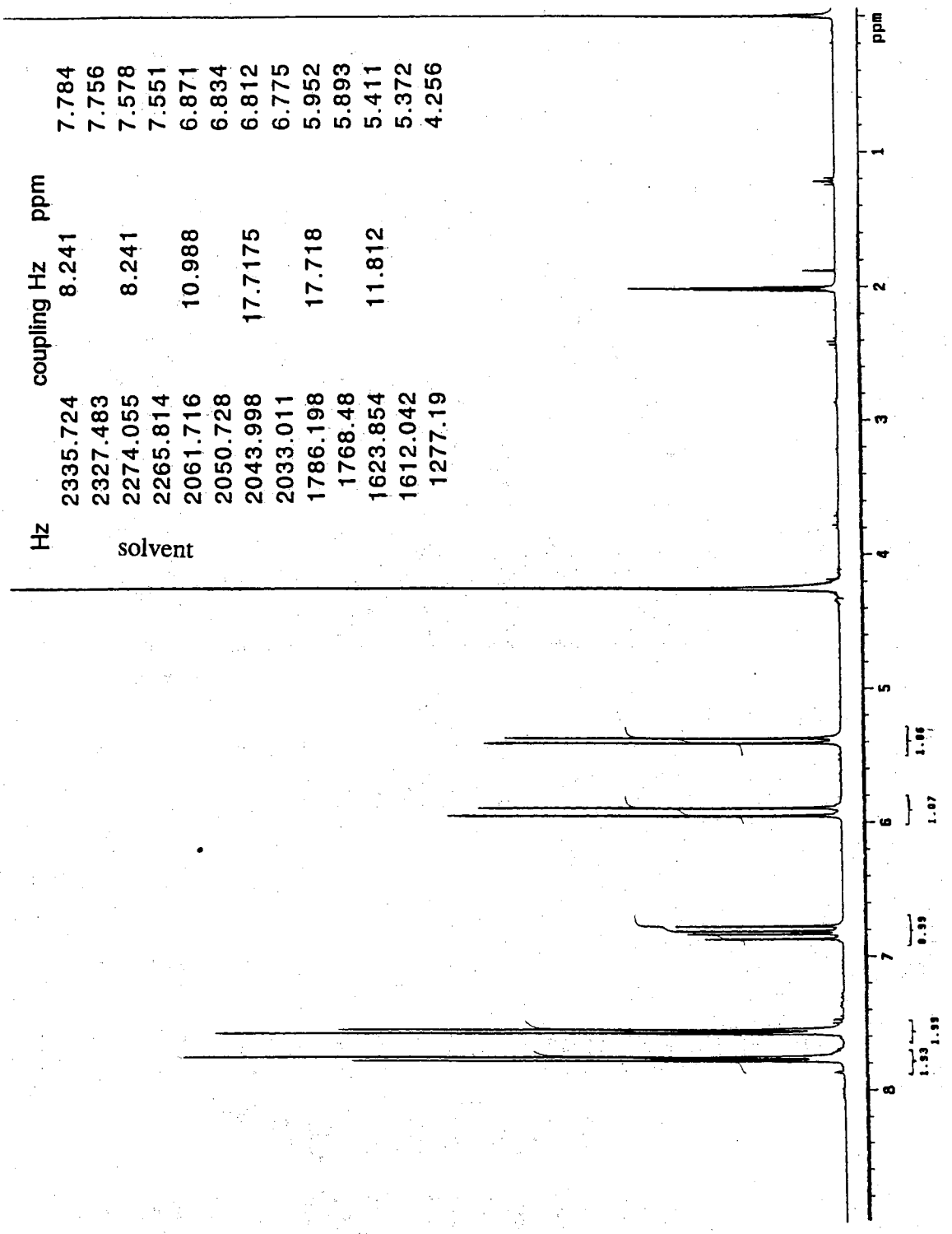

Figure 72. ^{1}H NMR spectrum of Ag(I) exposed 4-styrenesulfonic acid sodium salt in 80% acetonitrile-d_3/20% deuterium oxide.

^{13}C NMR Spectra of Model Compounds

The ^{13}C NMR spectrum of *p*-toluenesulfonic acid in 80% acetonitrile-d_3/20% deuterium oxide is presented in Figure 3. In the spectrum, five different resonances, which represent the five chemically distinct carbons of *p*-toluenesulfonic acid, are observed.

The ^{13}C NMR spectrum of Ag(I) exposed *p*-toluenesulfonic acid in 80% acetonitrile-d_3/20% deuterium oxide is presented in Figure 74. In the spectrum, the five carbon resonances are unaffected by Ag(I) cation and no new resonances are observed.

The ^{13}C NMR spectrum of 4-styrenesulfonic acid sodium salt in 80% acetonitrile-d_3/20% deuterium oxide is presented in Figure 75. In the spectrum, six different resonances, which represent the six chemically distinct carbons of the compound, are observed.

The ^{13}C NMR spectrum of Ag(I) exposed 4-styrenesulfonic acid sodium salt in 80% acetonitrile-d_3/20% deuterium oxide is presented in Figure 76. In the spectrum, the six carbon resonances are unaffected by Ag(I) cation and no new resonances are observed.

For reference, the ^{13}C spectrum of silver trifluoroacetate in 80% acetonitrile-d_3/20% deuterium oxide is provided in Figure 77. In the spectrum, the upfield resonance of the CF_3 and the downfield resonance of the carbonyl are split into a quartet due to F coupling. In addition, the carbon resonances of acetonitrile are observed at 1.3 and 119 ppm (Kegley and Pinhas, 1986) in all the ^{13}C NMR spectra.

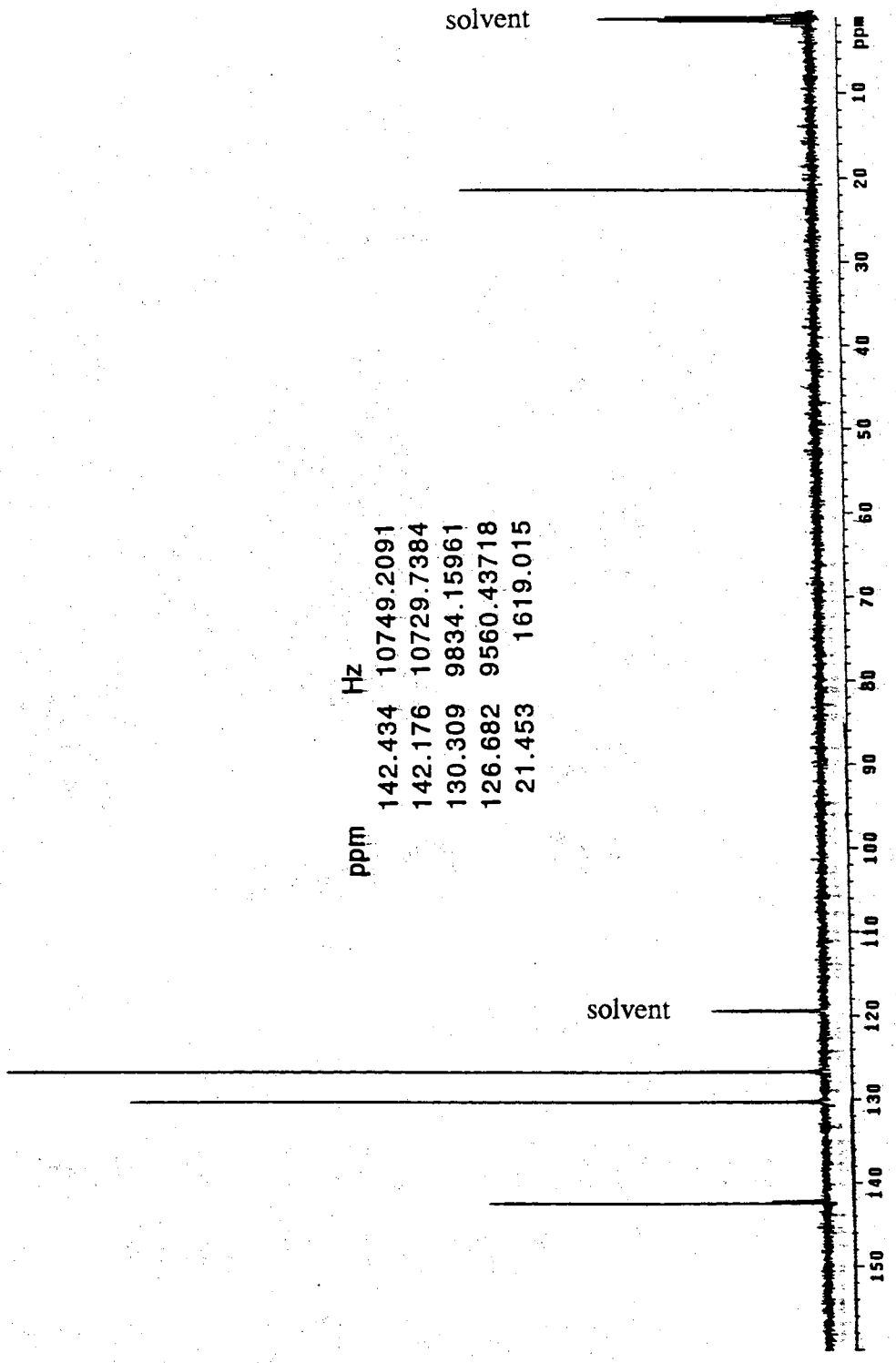

Figure 73. ^{13}C NMR spectrum of *p*-toluenesulfonic acid in 80% acetonitrile-d_3/20% deuterium oxide.

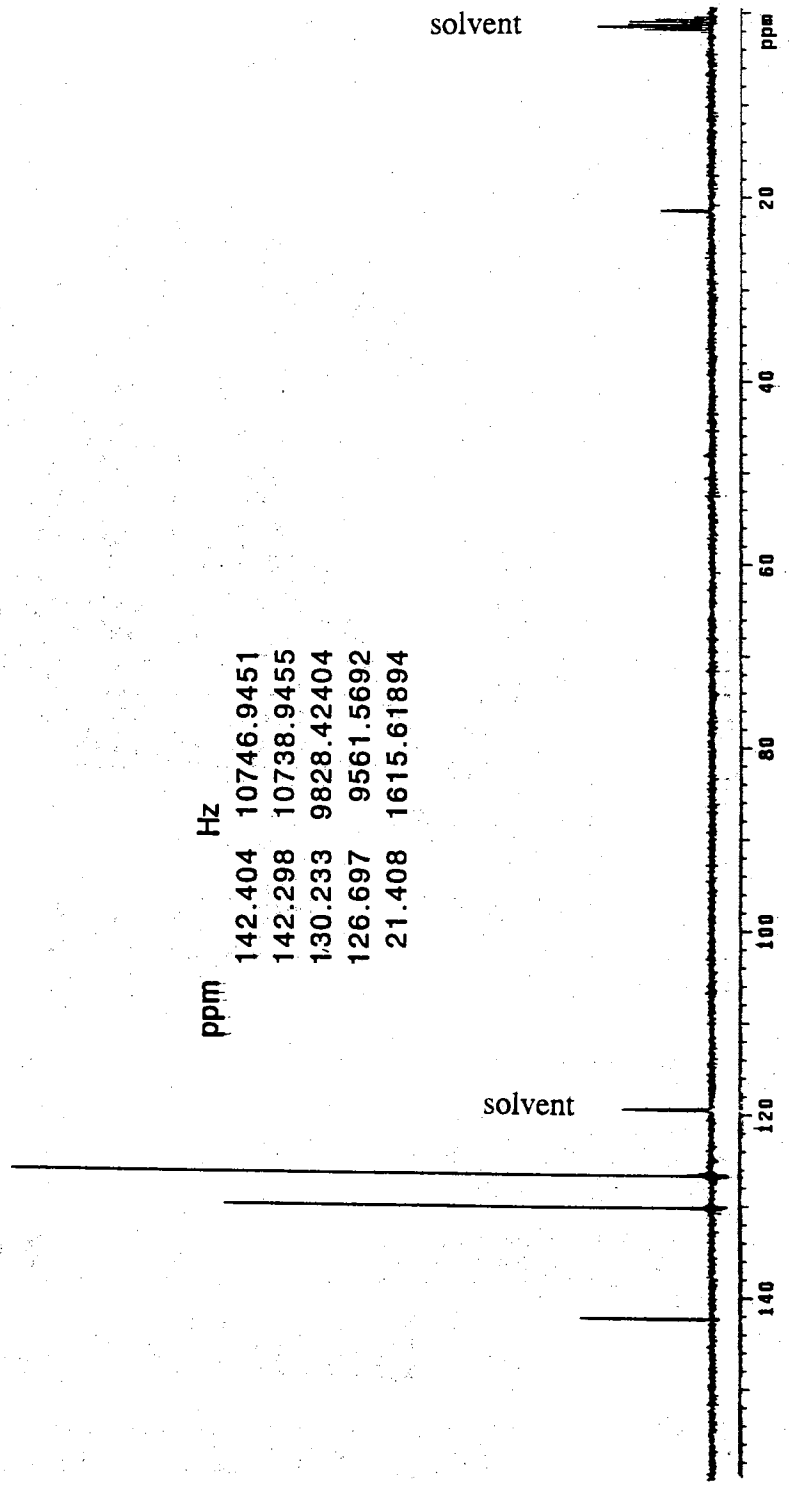

Figure 74. ^{13}C NMR spectrum of Ag(I) exposed *p*-toluenesulfonic acid in 80% acetonitrile-d_3/20% deuterium oxide.

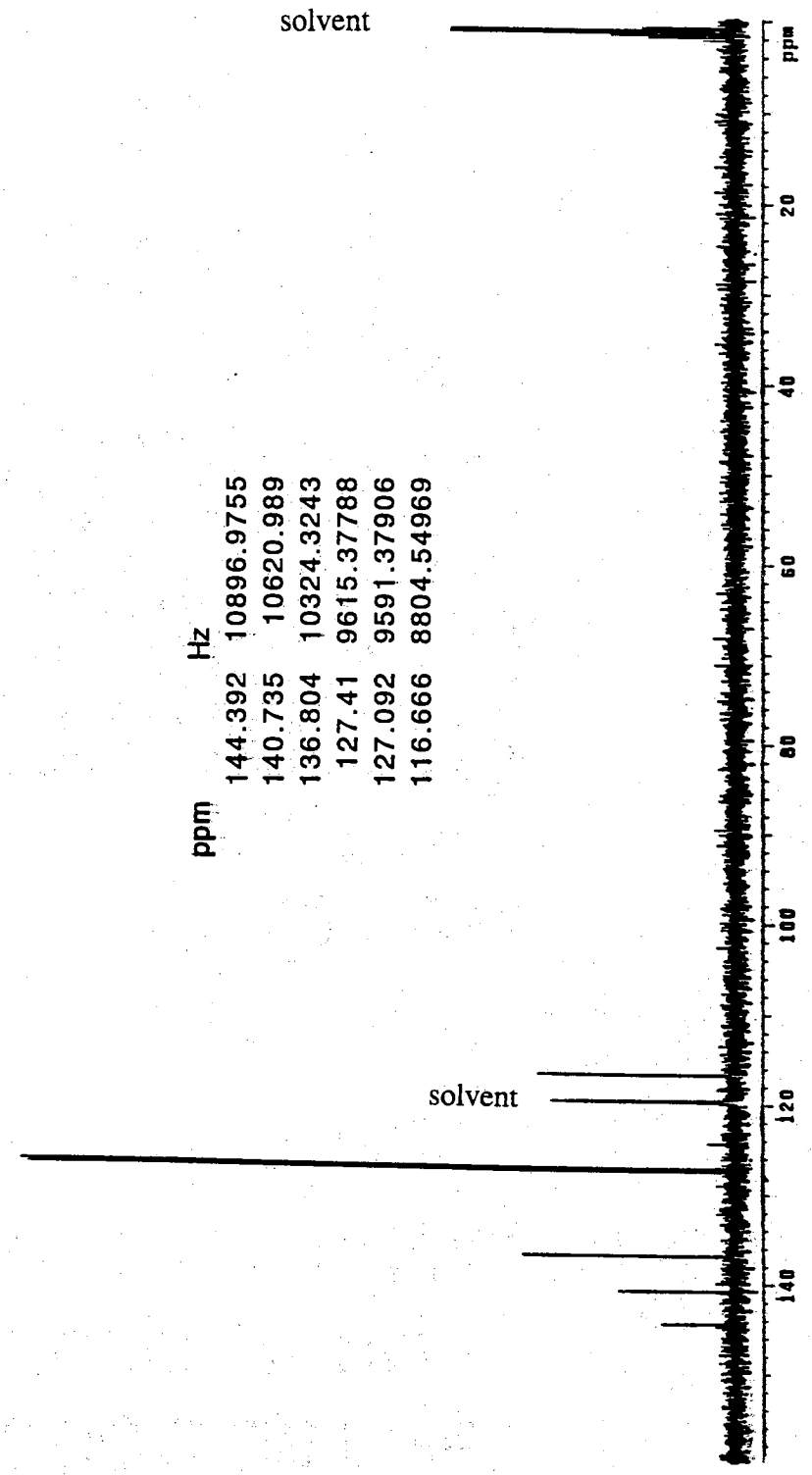

Figure 75. ^{13}C NMR spectrum of 4-styrenesulfonic acid sodium salt in 80% acetonitrile-d_3/20% deuterium oxide.

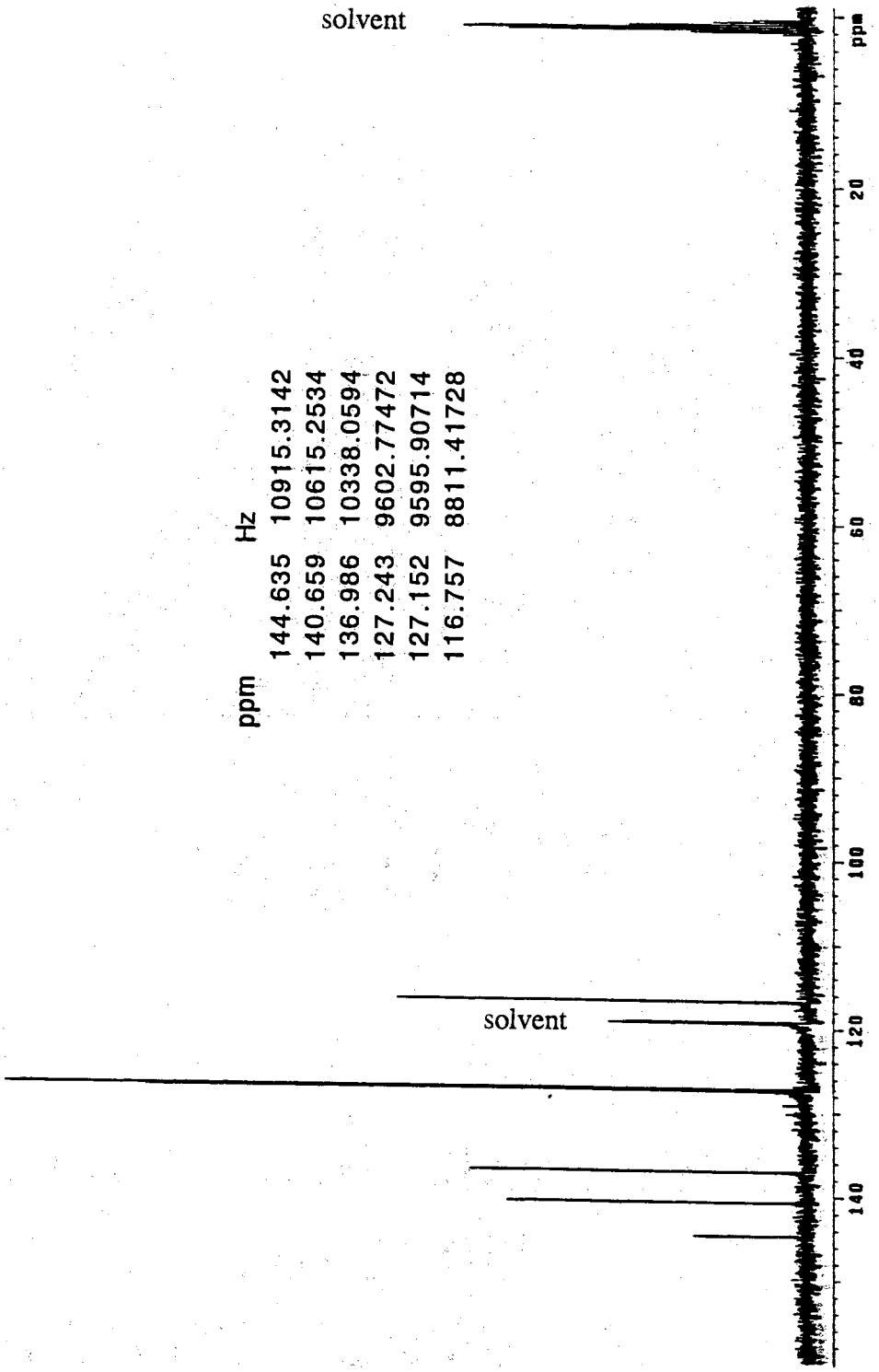

Figure 76. ^{13}C NMR spectrum of Ag(I) exposed 4-styrenesulfonic acid sodium salt in 80% acetonitrile-d_3/20% deuterium oxide.

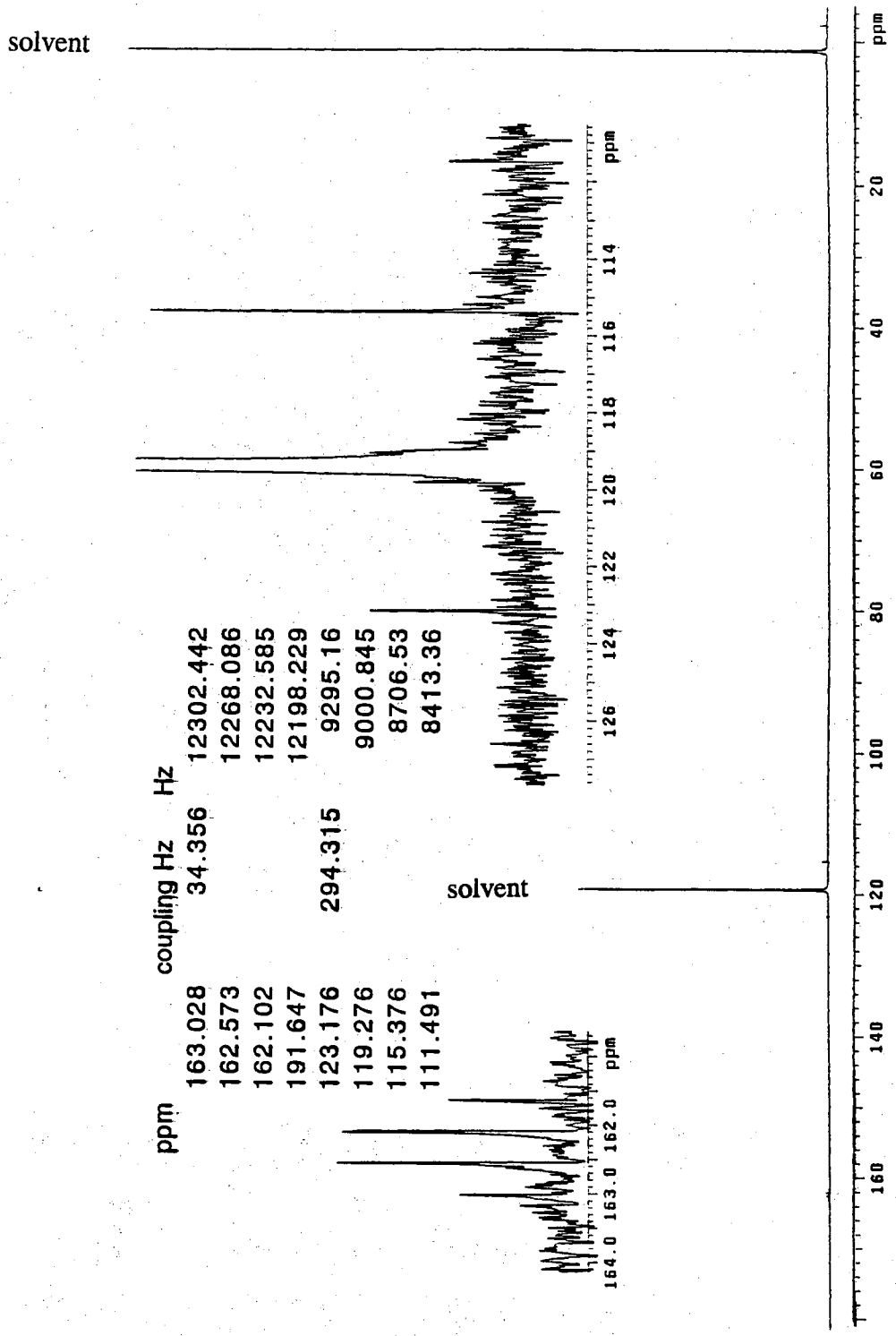

Figure 77. ^{13}C NMR spectrum of silver trifluoroacetate in 80% acetonitrile-d_3/20% deuterium oxide.

Discussion

As reported in Chapter IV, the ethylene/ethane adsorption data, collected on Ag(I) exchanged Amberlyst 15 resins as a function of Ag(I) loading and binary stream composition, show obvious adsorption trends. For example, ethylene/Ag(I) mole ratios, which exceed 2 at low Ag(I) loadings, fall below 1 at Ag(I) loadings higher than 29 % of the exchange capacity of the Amberlyst 15 resin. The ethylene/ethane selectivities increase at higher Ag(I) loadings and show an increased temperature dependence at higher Ag(I) loadings. The ethane adsorption capacities decrease at higher Ag(I) loadings. The quantities of irreversibly adsorbed ethylene also increase at higher Ag(I) loadings. These adsorption trends strongly indicate that Ag(I) exchanged Amberlyst 15 resins have different types of Ag(I) exchanged sites which have different affinities for ethylene. For example, adsorption sites, which weakly adsorb multiple ethylene molecules, are prevalent at low Ag(I) loading, and other adsorption sites, which more strongly adsorb one or fewer ethylene molecules, are prevalent only at high Ag(I) loading. Based on these results, the following discussions introduce, support, and/or disregard hypotheses which explain the adsorption trends of Ag(I) exchanged Amberlyst 15 resins.

Donovan and Mowat (1995) and Schug and Martin (1962) suggested that Ag(I) interacts with benzene rings of polystyrene. Based on these results, it is suggested that Ag(I) interacts with unsaturated groups of Amberlyst 15 resins, and the unsaturated-Ag(I) sites promote adsorption of ethylene. In disagreement with this suggestion, our ^{1}H and ^{13}C NMR spectra show no preferential interaction of Ag(I) with the unsaturated systems of the model compounds. These observations are in agreement with DRIFTS and NMR data in Chapter III which indicate no change in the unsaturated systems of the Amberlyst 15 resin after Ag(I) exchange, and that the Amberlyst 15 resin does not contain a significant quantity of unpolymerized vinyl groups. Therefore, the possibility that ethylene is adsorbed on Ag(I)-unsaturated sites is not consistent with experimental results.

Dixit and Yadav (1996) showed that the structure of Amberlyst 15 resin can be physically altered by alkylation reaction, and that these alterations drastically affect the transport of molecules into and within the polymer network. Based on these results, it is suggested that Ag(I) exchange may facilitate structural changes in the Amberlyst 15 resin, and these structural changes may selectively trap and/or retain olefin in discrete locations within polymer networks. In disagreement with this suggestion, nitrogen adsorption, mercury porosimetry, and SEM images, collected on unexchanged and Ag(I) exchanged resin beads, indicate that Ag(I) exchange does not modify the physical properties or structure of the Amberlyst 15 resin, and that the physical properties do not vary from bead to bead. Furthermore, hydrated Ag(I) cation has a smaller hydration sphere than H^+ and a higher selectivity coefficient (Bonner and Rhett, 1953; Helfferich, 1962) allowing for improved diffusion of hydrated Ag(I) into and within the Amberlyst 15 resin bead. The diffusion of hydrated Ag(I) into and through the resin beads is supported by previous diffusion studies (Boyd and Soldano, 1954) and EDXAS images and DRIFTS spectra in Chapter III, which indicate that hydrated Ag(I) is homogeneously dispersed within the structure of the Ag(I) exchanged Amberlyst 15 resin bead. Based on these results, the hypothesis that ethylene is adsorbed in pockets and/or trapped in restricted areas of the Amberlyst 15 resin created by Ag(I) exchange is not consistent with experimental results.

Since physical modifications of the Amberlyst 15 resin structure and alternative sites for Ag(I) interaction on the Amberlyst 15 resin do not facilitate the adsorption trends of Ag(I) exchanged Amberlyst 15 resins, and DRIFTS and NMR data show that sulfonate sites are the sole sites for ion exchange on Amberlyst 15 resins, an alternative hypothesis for the adsorption trends of Ag(I) exchanged Amberlyst 15 resins is that Amberlyst 15 resins have different sulfonate exchange sites which preferentially exchange hydrated Ag(I) cation resulting in Ag(I) site which have different affinities for ethylene. For example, at low Ag(I) loadings, hydrated Ag(I) cations on preferred exchange sites weakly adsorb

multiple ethylene molecules, while at high Ag(I) loadings, hydrated Ag(I) cations on less preferred exchange sites more strongly adsorb one or fewer ethylene molecules.

Literature precedence for different exchange sites on both conventional and macroreticular sulfonated polystyrene-divinylbenzene ion exchange resins exists. For example, Gregor (1951), Bonner and Rhett (1953), Bonner et al. (1956), Boyd and Myers (1956), Hogfeldt et al. (1958) and Saster et al. (1997) experimentally observed different cation selectivity coefficients for resin beads. Based on these observations, the authors attributed the different selectivity coefficients to a distribution of different exchange sites within the resin beads. Based on their results and the adsorption trend of the Ag(I) exchanged Amberlyst 15 resin, it is suggested that the higher selectivity coefficients represent exchange sites which preferentially exchange hydrated Ag(I) cations at lower Ag(I) loadings resulting in the adsorption of more than one ethylene molecule. By analogy, the lower selectivity coefficients represent exchange sites which subsequently exchange hydrated Ag(I) cations at higher Ag(I) loadings resulting in the adsorption of one or fewer ethylene molecules.

These assertions are rationalized by combining acid/base chemistry, electrostatic interaction strengths, and the adsorption trends of Ag(I) exchanged Amberlyst 15 resins. For example, the preferred exchange sites should be more acidic (i.e. weaker conjugate base). Therefore, electrostatic interactions between preferred exchange sites and Ag(I) cations should be weak, allowing the Ag(I) cations to retain positive charge. On the other hand, the less preferred exchange sites should be less acidic (i.e. stronger conjugate base). Therefore, electrostatic interactions between the less preferred exchange sites and Ag(I) cations should be stronger, resulting in donation of negative charge to Ag(I) cations and displacement of positive charge from Ag(I) cations. Based on these electrostatic interactions, it is suggested that hydrated Ag(I) cations on preferred exchange sites (i.e. sites at low Ag(I) loadings), which retain significant positive charge, readily accept additional electron density from more than one ethylene molecule. In contrast, hydrated

Ag(I) cations on less preferred exchange sites (i.e. sites at higher Ag(I) loadings) only accept limited electron density from one or fewer ethylene molecules due to build up of negative charge. These electronic interactions are in accord with spectroscopic studies which show that olefins primarily donate electron density to Ag(I) cations (Noltes et. al., 1970; Scott, 1973; Tsai and Quinn, 1969; Brandt, 1959; Nagakura and Hosoya, 1963; Yates et al., 1966; Busca et al., 1992; Nagendrappa and Devaprabhakara, 1968; Schug and Martin, 1962). In conclusion, the experimental adsorption data and literature reports conclusively support different types of Ag(I) exchanged sites on the Amberlyst 15 resin. Based on this conclusion, the discussions that follow speculate on the local environments and locations of the different exchange sites within the macroreticular Amberlyst 15 resin bead.

Tasi and Quinn (1969) reviewed Ag(I)-olefin complexes in aqueous solution and reported that $(C_{10}H_{10})_3AgBF_4$, a spectroscopically characterized solution complex, has an olefin/Ag(I) ratio of 3 (Quinn, 1968). In contrast, surface bonding models (Dewar, 1951; Chatt and Duncanson, 1953), surface studies (Albert et al., 1982; Carr et al., 1985; Bao, 1995), and adsorption studies on surface supported adsorbents (Yang and Kikkinides, 1995; Yang et al., 1997; Hirai et al., 1985; Blytas, 1990; Keller, 1990; Doyle, 1988; Komiyama, 1989; Tabler, 1985) have yet to report and/or predict olefin/metal ratios greater than 1. Analogous to these results and models and in agreement with the adsorption trends of Ag(I) exchanged Amberlyst 15 resins, it is suspected that Ag(I) cations on preferred exchange sites (i.e. lower Ag(I) loading) must behave like Ag(I) in solution while Ag(I) cations on less preferred exchange sites (i.e. higher Ag(I) loading) must behave like Ag(I) on a surface. This solution/surface analogy is in accord with DRIFTS spectra of Ag(I) exchanged Amberlyst 15 resins presented in Chapter III which show that the extent of hydration decreases with increasing Ag(I) loading.

As reported, macroreticular resins are primarily composed of a gel phase, which consists of interconnected micro-gel spheres that form pore channels within the polymer

bead. (Albright, 1986; Kunin et al., 1962). The gel phase is high in divinylbenzene concentration, contains the majority of the exchange sites, and retains less moisture content, while pore surfaces in the channels contain fewer exchange sites and retain the majority of the moisture content. Based on reported selectivity coefficients (Helfferich, 1962), the exchange sites in the gel phase adsorb Ag(I) preferentially over exchange sites in the pore surface. This is rationalized by the fact that the gel phase contains the majority of exchange sites, and that exchangeable protons in the gel phase, which are more acidic and less stable, are preferentially displaced. In conclusion, the gel phase is believed to contain both the preferred and less preferred exchange sites of the Amberlyst 15 resin.

Hogfeldt et al. (1958) and more recently Saster et al. (1997), based on different selectivity coefficients of both conventional and macroreticular resin beads and curve fitting analyses, suggested an alternative explanation for different selectivity coefficients. Hogfeldt et al. (1958) and Saster et al. (1997), based solely on curve fits, attributed higher selectivity coefficients to exchange sites on divinylbenzene and lower selectivity coefficients to exchange sites on polystyrene. Based on these assertions, Hogfeldt et al. (1958) suggested that the different selectivity coefficients should correlate with the percent of divinylbenzene crosslinking. Since the divinylbenzene content of Amberlyst 15 resin is 20%, and the adsorption trends of Ag(I) exchanged Amberlyst 15 resins indicate that the less preferred adsorption sites begin to dominate at 20-30% of the exchange capacity, correlation of the divinylbenzene content and adsorption trends suggests that hydrated Ag(I) cations on preferred divinylbenzene exchange sites (i.e. lower Ag(I) loading) adsorb more than one ethylene molecule. By analogy, hydrated Ag(I) cations on less preferred polystyrene exchange sites (i.e. higher Ag(I) loading) adsorb one or fewer ethylene molecules. Alternatively, due to possible steric interactions between ethyl groups and sulfonate groups of divinylbenzene, steric effects of divinylbenzene exchange sites may also promote differences between Ag(I) exchanged sites of divinylbenzene and polystyrene since steric interactions between sulfonate and substituents are not possible on exchange

sites of polystyrene. Although the two chemically distinct exchange sites are in agreement with the high concentration of divinylbenzene in the gel phase of the Amberlyst 15 resin, literature support for these two distinct exchange sites is limited.

In conclusion, the experimental data indicate that Amberlyst 15 resins have different types of exchange sites that preferentially exchange Ag(I) cation resulting in Ag(I) sites which have different affinities for ethylene adsorption. While many theories have been suggested to explain the different exchange sites, the experimental data provide no conclusive evidence to specifically identify and/or differentiate the best theory, exact locations, local environments, or possible steric interactions of the different types of exchange sites within the Amberlyst 15 resin. Therefore, in Chapter VIII additional studies are suggested to characterize the location and local environments of different exchange sites within the Amberlyst 15 resin bead.

Conclusion

Model compound studies show that Ag(I) does not preferentially interact with unsaturated systems of the Amberlyst 15 resins, ruling out possible Ag(I)-unsaturated sites for ethylene adsorption on the Ag(I) exchanged Amberlyst 15 resins. The experimental data indicate that ethylene is not physisorbed in pockets or trapped in isolated areas of the resin created during Ag(I) exchange. In agreement with previous reports on macroreticular ion exchange resins, the experimental data indicate that Ag(I) exchanged Amberlyst 15 resins have different exchange sites which preferentially exchange Ag(I) cation resulting in Ag(I) sites which have different affinities for ethylene.

CHAPTER VIII

FUTURE STUDIES

Summary

Since a commercially viable olefin adsorbent and/or olefin adsorption process is not available, the work conducted in this study was initially proposed as a collaborative effort between chemists and engineers to develop a more efficient and economical adsorbent and adsorption process for the separation of olefins from paraffin streams. The chemistry goals were to; (1) develop and/or identify a potentially applicable adsorbent; (2) characterize the adsorption properties of the adsorbent under conditions representative of industrial process; and (3) identify avenues to reduce costs and improve the adsorption capacity and olefin/paraffin selectivity of the adsorbent. The engineering goals were to use the adsorption results to develop technical and economic models for an adsorption process that were compatible with the selected adsorbent and could be incorporated into commercial units which produce olefin-containing streams.

As reported in this study, the chemistry goals have been attained. For example, binary adsorption and olefin/paraffin selectivity data have been collected which indicate that Ag(I) exchanged Amberlyst 15 resins selectively adsorb ethylene over ethane. In addition, experimental results, presented in this study, suggest that Ag(I) exchanged Amberlyst 15 resins have different Ag(I) exchanged active sites. The data show that Ag(I) exchanged active sites, prevalent at low Ag(I) loading, efficiently adsorb olefin, while Ag(I) exchanged active sties, prevalent at high Ag(I) loading, inefficiently adsorb olefin. Since preliminary cost analyses indicate high Ag(I) exchanged Amberlyst 15 resins exceed industrial costs, the more efficient low Ag(I) exchanged active sites should provide a route for designing improved and more economical olefin adsorbents. However, additional studies are needed to further evaluate these active sites and eventually exploit their use in the development of improved and more economical olefin adsorbents. The engineering

tasks, which will asses the commercial viability of the adsorbent, are currently in initial stages of development.

In Chapter VIII, the engineering studies, which will be performed using the temperature dependent binary adsorption data collected on the Ag(I) exchanged Amberlyst 15 resin, are briefly described. Additional studies are proposed to evaluate olefin adsorption on Ag(I) exchanged Amberlyst 15 resins under conditions more representative of industrial processes and further characterize the different Ag(I) exchanged active sites of Ag(I) exchanged Amberlyst 15 resins.

Adsorption

Using the temperature dependent binary adsorption data, reported in this study, the engineers will: (1) develop mathematical adsorption models, based on pressure swing and/or temperature swing processes; (2) develop a practical adsorber bed and adsorber unit; and (3) use process simulators such as ASPEN PLUS™ and SPEEDUP™ to optimize the adsorber unit and make preliminary estimates of the energy savings, waste reductions, and costs of replacing existing technologies with the alternative adsorption process. Results will indicate adsorbent improvements (i.e. stability, adsorption capacity, selectivity, regenerability, etc.) and adsorber unit design changes, both of which are needed to redesign the adsorbent, adsorber model, and/or adsorber unit to meet industrial requirements.

Since most industrial separation processes operate in streams containing more than two components, olefin adsorption capacities and olefin/paraffin selectivities of the Ag(I) exchanged Amberlyst 15 resin in more complex streams would provide additional adsorbent information for better adsorber unit design. Based on these assumptions, the MDA has been further designed and used to measure adsorption in a ternary stream composed of 20% ethylene, 10% ethane, and 70% nitrogen. Preliminary studies have shown the ethylene/ethane selectivities dramatically drop in nitrogen streams. Based on

these experimental results, further evaluations of the MDA and adsorption in ternary streams are suggested.

Ag(I) Active Exchange Sites

As described in the summary, experimental data in this study support different Ag(I) exchanged active sites for olefin adsorption on Ag(I) exchanged Amberlyst 15 resins but do not differentiate the local environment or location of these sites within the resin beads. To differentiate and further evaluate the structure and electronic properties of these Ag(I) exchanged sites, the following studies are suggested.

Measuring the olefin adsorption capacities and olefin/Ag(I) ratios of Ag(I) exchanged resins crosslinked with different amounts of divinylbenzene should test the theory that olefin adsorption on Ag(I) exchanged Amberlyst 15 resins is related to Ag(I) exchanged active sites of divinylbenzene. Increasing ethylene adsorption capacities and ethylene/Ag(I) mol ratios with increasing amounts of divinylbenzene at constant Ag(I) exchange would support the suggestion that the more active Ag(I) exchanged sites are associated with divinylbenzene.

Measuring olefin adsorption capacities and olefin/Ag(I) ratios of Ag(I) exchanged sulfonated polystyrene resins, which are crosslinked with fluorinated divinylbenzene, should describe the electronic properties of the divinylbenzene sulfonate exchange sites. Due to the electron withdrawing characteristics of fluorine, the $-SO_3H$ groups on the divinylbenzene would be much more acidic and exchange more readily. This should increase the quantity of Ag(I) exchanged active sites on the divinylbenzene rings of the polymer. Since ethylene adsorption capacities and olefin/Ag(I) ratios of the Amberlyst 15 resins at low Ag(I) loadings may be attributed to Ag(I) exchanged sites of divinylbenzene, increased ethylene adsorption capacities and ethylene/Ag(I) mol ratios at lower Ag(I) loadings on the fluorinated divinylbenzene resin would support the role of the Ag(I)-divinylbenzene sites in olefin adsorption.

Studies have shown that platinum and nickel bind olefin more strongly than Ag(I) and provide greater infrared band shifts (70-250 cm^{-1}) assigned to the vibrational stretch of the C=C of ethylene (Collman et al., 1987; Elschenbroich and Salzer, 1992). Based on these observations, it is proposed that infrared data be collected on ethylene exposed Pt and Ni exchanged Amberlyst 15 resins. The infrared specta should provide electronic evidence for two chemically different exchange sites or a continuum of chemically different exchange sites. For example, if two different bands of ethylene appear shifted to lower wavenumber, the two bands will support the chemically different metal exchanged sites within the resin.

BIBLIOGRAPHY

Abrams, I. M. U. S. Patent 2 844 546, 1958; *Chem. Abstr.* **1958**, *52*, 20779h.

Ackley, M. W. Ph. D. Thesis, State University of New York at Buffalo, 1991.

Ackley, M. W.; Yang, R. T. *A. I. Ch. E.* **1991**, *37*(11), 1645.

Adams B. A.; Holmes, E. L. *J. Soc. Chem. Ind.* **1935**, *54*, 1T.

Afzaal, S.; Freiser, B. S. *Chem. Phys. Letters* **1994**, *218*, 254.

Albert, M. R.; Sneddon, L. G.; Eberhardt, W.; Greuter, F.; Gustafasson, T.; Plummer, E. W. *Surface Science* **1982**, *120*, 19.

Albright, R. L.; Yarnell, P. A. *Encyclopedia of Polymer Science and Engineering*; John Wiley and Sons: New York, 1987; p 341, Vol. 8.

Albright, R. L. *Reactive Polymers* **1986**, *4*, 155.

Alexandratos, S. D.; Strand, M. A.; Quillen, D. R.; Walder, A. J. *Macromolecules* **1985**, *18*, 829.

Bao, S.; Hofmann, P.; Schindler, K. M.; Fritzsche, V.; Bradshaw, A. M.; Woodruff, D. P.; Casado, C.; Asensio, M. C. *Surface Science* **1995**, *323*, 19.

Bartholin, M.; Boissier, G.; Dubois, J. *J. Makromol. Chem.* **1981**, *182*, 2075.

Bazuin, C. G.; Fan, X. *Macromolecules* **1995**, *28*, 8209.

Blytas, G. C. *Separation and Purification Technology*; Li, N. N.; Calo, J. M., Eds.; Marcel Dekker: New York, 1992; Chapter 2.

Bonner, O. D.; Holland, V. F.; Smith, L. L. *J. Phys. Chem.* **1956**, *60*, 1102.

Bonner, O. D.; Rhett, V. *J. Phys. Chem.* **1953**, *57*, 254.

Bonner, O. D.; Payne, W. *J. Phys. Chem.* **1954**, *58*, 183.

Bonner, O. D. *J. Phys. Chem.* **1955**, *59*, 2978.

Boyd, G. E.; Myers, G. E. *J. Phys.Chem.* **1956**, *60*, 521.

Boyd, G. E.; Soldano, B. A. *J. Am. Chem. Soc.* **1954**, *75*(24), 6091.

Brandt, P. *Acta Chem. Scand.* **1959**, *13*, 1639.

Breck, D. W. *Zeolite Molecular Sieves*; Malabar: Florida, 1984.

Brunauer, S.; Deming, L. S.; Deming, W. S.; Teller, E. *J. Am. Chem. Soc.* **1940**, *62*, 1723.

Brunauer, S.; Emmet, P. H.; Teller, E. *J. Am. Chem. Soc.* **1938**, *60*, 309.

Burford, R. P.; Fane, A. G.; Byun, S. *J. Appl. Polym. Sci.* **1994**, *52*(2), 825.

Busca, G.; Lorenzelli, V.; Ramis, G.; Saussey, J.; Lavalley, J. C. *J. Mol. Struct.* **1992**, *267*, 315.

Buss, E. *Gas Sep. Purif.* **1995**, *9*(3), 189.

Carr, R. G.; Sham, T. K.; Eberhardt, W. E. *Chem. Phys. Lett.* **1985**, *113*, 63.

Cen, P. L. *A. I. Ch. E.* **1990** *36*(5), 789.

Chatt, J.; Duncanson, L. A. *J. Chem. Soc.* **1953**, 2939.

Choudhary V. R.; Mayadevi, S. *Separation Science and Technology* **1993**, *28*(8), 1595.

Chrones, J. *Hydrocarbon Process. Pet. Refin.* **1961**, *40*, 179.

Collins, J. J. *Chem. Eng. Prog.* **1968**, *64*(8), 66.

Collman, J. P.; Hegedus, L. S.; Norton, J. R.; Finke, R. G. *Principles and Applications of Organotransition Metal Chemistry*; University Science Books: California, 1987.

Corte H.; Netz, O. Br. Patent 1 036 239, 1966; *Chem. Abstr.* **1966**, *65*(6), 20310a.

D'Alelio, G. U. S. Patent 2 366 007, 1944; *Chem. Abstr.* **1945**, *39*(2), 4418.

Danner, R. P.; Chol, E. C. *Ind. Eng. Chem. Fundam.* **1978**, *17*(4), 248.

Davis, B. H. *Applied Catalysis* **1984**, *10*, 185-198.

Devaprabhakara, D.; Nagendrappa, G. *J. Organomet. Chem.* **1968**, *15*, 225.

Dewar, M. J. S. *Bull. Soc. Chim. France* **1951**, C79, 18.

Diamond, R. M. *J. Am. Chem. Soc.* **1955**, *77*, 2978.

Dixit, A. B.; Yadav, G. D. *Reactive and Functional Polymers* **1996**, *31*, 237.

Do, D. D.; Do, H. D. *Chem. Eng. Sci.* **1997**, *52*(2), 297.

Donovan, R. J.; Mowat, I. A. *Rapid Communications in Mass Spectrometry* **1995**, *9*, 82.

Doyle, G.; Ho, W. S.; Savage, D. W.; Pruett, R. L. *Ind. Eng. Chem. Res.* **1988**, *27*, 334-337.

Drake, L. B. U. S. Patent 2 764 562, 1955; *Chem. Abstr.* **1957**, *51*(2), 3875f.

Dyer, A.; Hudson, M. J.; Williams, P. A. *Ion Exchange Processes Advances and Applications*; Royal Society of Chemistry: Cambridge, 1993.

Eldridge, B. *Ind. Eng. Chem. Res.* **1993**, *32*, 2208.

Elschenbroich, C.; Salzer, A. *Organometallics*; ZCH: New York, 1992; Vol. 2.

Emmrich, G. *Advances in the Separation of C4 Hydrocarbons: Separation of Paraffinic and Olefinic C4 Hydrocarbons*; Krupp Koppers Tech. Publ. 1986.

Fontana F. *Memorie Mat. Fis. Soc. Ital. Sci.* **1777**, 1, 679.

Ford, W. T.; Periyasamy, M.; McEnroe, F. J. *J. Polym. Sci. Part A Polym. Chem.* **1989a**, *27*, 2387.

Ford, W. T.; Periyasamy, M.; Mohanraj, S.; McEnroe, F. J. *J. Polym. Sci. Part A Polym. Chem.* **1989b**, *27*, 2345.

Gans, R. *Jahrb. Preuss. Geol. Landesanstalt (Berlin)* **1905**, *26*, 179.

Gates, B. C. *Catalytic Chemistry*; John Wiley & Sons: New York, 1992.

Gordon, J. *J. Phys. Chem.* **1962**, *66*, 1150.

Gregg, S. J.; Sing, K. S. W. *Adsorption, Surface Area and Porosity*; Academic Press: New York, 1982.

Gregor, H. P. *J. Am.Chem.Soc.* **1951**,*73*, 642.

Guyot, A. *Synthesis and Separations using Functional Polymers*; Sherrington, D. C.;

Hodge, P., Eds.; John Wiley and Sons: New York, 1988; p 1.

Harm, F. German Patent 95 447, 1896.

Helfferich, F. *Ion Exchange*; McGraw Hill Book Co.: New York, 1962.

Herzberg, G. *Molecular Spectra and Molecular Structure*; Van Nostrand Reinhold: New York, 1945.

Hirai, H.; Kurima, K.; Wada, K.; Komiyama, M. *Chemistry Letters* **1985**, 1513-1516.

Hirai, H.; Kominyama, M.; Wada, K. U. S. Patent 4 747 855, 1988; *Chem. Abstr.* **1985**, *103*(3), 392341, 113.

Hogfeldt, E. *Arkiv Kemi* **1958**, 491.

HogFeldt, E.; Ekedahl, E.; Sillen, L. G. *Acta Chem. Scand.* **1950**, *4*, 1471.

Honig, J. M.; Reverson, L. H. *J. Phys. Chem.* **1952**, *56*, 140.

Hyun, S. H.; Danner, R. P. *J. Chem. Eng. Data* **1982**, *27*, 196.

Iler, R. K. *The Chemistry of Silica*; Wiley: New York, 1979.

Jackson, L. W. M.S. Thesis, Oklahoma State University, 1974.

Jain, A. K.; Jasra, R. V.; Bhat, S. G. T. *Separation Science and Technology* **1990**, *25*(4), 489.

Jakes, J.; Doskocilova, D.; Schneider, B. *Journal of Magnetic Resonance* **1978**, *29*, 79.

Jenson, V. G.; Jeffreys, G. V. *Mathematical Methods in Chemical Engineering*; Academic Press: New York, 1963, 356.

Joyner, L. G.; Emmett, P. H. *J. Am. Chem. Soc.* **1948**, *70*, 2353.

Kaul, B. K. *Ind. Eng. Chem. Res.* **1987**, *26*, 928.

Kayser, H. *Wied. Ann.* **1881**, *14*, 451.

Kegley, S. E.; Pinhas, A. R. *Problems and Solutions in Organometallic Chemistry*; University Science Books: Mill Valley, California, 1986.

Keller, G. E.; Marcinkowsky, A. E.; Verma, S. K.; Williamson, K. D. *Separation and Purification Technologies*; Li, N. N.; Calo, J. M., Eds.; Marcel Dekker: New York, 1992; Chapter 3.

Kitchener, J. A. *Ion Exchange Resins*; John Wiley and Sons: New York, 1957.

Knaebel, K. *Chem. Engineering* **1995**, 92.

Komiyama, M. *Chem. Eng. Technol.* **1989**, *12*, 356-357.

Kressman, T. R. E.; Tye, F. L. Br. Patent 726 918, 1955; *Chem. Abstr.* **1955**, *49*(4), 11209b.

Kressman, T. R. E.; Millar, J. R.; Smith, D. G.; Marr, W. E. *J. Chem. Soc.* **1964**, 2741.

Kressman, T. R. E.; Millar, J. R.; Smith, D. G.; Marr, W. E. *J. Chem. Soc.* **1963a**, 2779.

Kressman, T. R. E.; Millar, J. R.; Smith, D. G.; Marr, W. E. *J. Chem. Soc.* **1963a**, 219.

Kulvaranon, S.; Findley, M. E.; Liapis, A. I. *Ind. & Eng. Chem. Res.* **1990**, *29*, 106.

Kumar, R.; Prausnittz, J. M.; King, C. J. *Advan. Chem. Ser.*; ACS: Washington D. C., 1972; p 115.

Kunin, R.; Kun K. A. *J. Polym. Sci. Part A-1* **1968**, *6*, 2689.

Kunin, R.; Meitzner, E. F.; Oline, J. A.; Fisher, S. A.; Frisch, N. *Ind. Eng. Chem. Res. Dev.* **1962**, *1*(2), 140.

Langmuir, I. *J. Am. Chem. Soc.* **1918**, *40*, 1361.

Lemmons, D. Ph. D. Thesis, Oklahoma State University, in progress.

Lewis W. K.; Gilliland, E. R.; Chertow, B.; Milliken, W. *J. Am. Chem.Soc.* **1950a**, *72*, 1157.

Lewis, W. K.; Gilliland, E. R.; Chertow, B.; Milliken, W. *J. Am. Chem. Soc.* **1950b**,*72*, 1160.

Lide, D. R. *CRC Handbook of Chemistry and Physics* ; CRC Press: Boston, 1990; Ed. 71.

Linlin, G.; Qinlin, G.; Youchang, X.; Youqi, T. *Scientia Sinica Series B* **1984**, *25*(5), 445.

Lukchis, G. M. *Chem. Eng.* **1973**, *111*, 83.

McCash, E. M. *Vacuum* **1990**, *40*, 423.

MacZura, G.; Goodboy, K. P.; Koenig, J. J. *Kirk-Othmer Encyclopedia of Chem. Tech.*; Wiley-Interscience: New York, 1977; Vol. 2, Ed. 3.

Mathias, P. M.; Orhan, T.; Li, J.; Kumar, R.; Moyer, J. D.; Schork, J. M. *Gas Sep. Pruif.* **1996**, *10*(3), 149.

Myers A. L.; Valenzuela, D. P. *Adsorption Equilibrium Data Handbook*; Prentice Hall: New Jersey, 1989.

Nagakura, S.; Hosoya, H. *J. Am. Chem. Soc.* **1964**, *37*(2), 249.

Noltes, G.; Leusink, A. J.; Van Der Kerk, J. M.; Beverwijk, C. D. M. *Organomet. Chem. Review. A* **1970**, *5*, 215.

Nyberg, C.; Tengstal, C. G.; Andersson, S.; Holmes, M. W. *Chem. Phys. Lett.* **1982**, *87*, 87.

Olah G. A.; Beal, D. A.; Olah, J. A. *J. Org. Chem.* **1976**, *41*, 1627.

Pearch, G. K. U. S. Patent 4 717 398, 1988; *Chem. Abstr.* **1986**, *104*(3), 34463j, 9.

Pitochelli, A. R. *Ion Exchange Catalyst and Matrix Effects*; Rohm and Haas, 1980.

Pretsch, E.; Clerc, T.; Seibl, J. *Spectral Data for Structure Determination of Organic Compounds*; Springer-Verlag: New York, 1983.

Quinn, H. W. *Can J. Chem.* **1968**, *46*, 117.

Ray, G. C.; Box E. O. *Ind. Eng. Chem.* **1950**, *42*, 1315.

Rudzinski, W.; Dominko, A.; Wojciechowski, B. W. *Chemical Engineering Journal* **1996**, *64*, 85.

Ruthven, D. M. *Kirk Othmer Encyclopedia of Chemical Technology*; John Wiley & Sons: New York, 1991; p 493, Ed. 4, Vol. 1.

Ruthven, D. M. *Principles of Adsorption and Adsorption Processes*; John Wiley & Sons: New York, 1984.

Satterfield, C. N. *Heterogenous Catalysis in Industrial Practice*; McGraw-Hill Inc: New York, 1991.

Scheele C. W. *Chemical Observations on Air and Fire* **1780**, 182.

Schoeller, R.; Mueller, U. *Adsorption Science and Technology* **1986**, *3*, 167.

Scott, J. G. V. *Spectrochimica Acta* **1973**, *29*, 559.

Sherrington, D. C.; Law, R. V.; Snape, C. E. *Macromolecules* **1997**, *30*(10), 2368.

Sherrington, D. D.; Snape, C. E.; Law, R. V. *Ind. Eng. Chem. Res.* **1995**, *34*(8), 2740.

Shu, C. M.; Kulvaranon, S.; Findley, M. E.; Liapis, A. I. *Separations Technology* **1990**, *1*, 18.

Sips, R. *J. Chem. Phys.* **1950**, *18*, 1024.

Smith, P. B.; Martin, S. J.; Sammler, R. L.; Wilson, L.; Marks, M. J.; Harris, W. I.; O'Connor, P. J.; Cutie, S. S. *Macromolecules* **1996**, *29*, 7872.

Somorjai, G. A. *Introduction to Surface Chemistry and Catalysis*; John Wiley and Sons: New York, 1994.

Stobaugh, R. B. *Hydrocarbon Process. Pet. Refin.* **1966**, *45*, 188.

Sunderrajan, S.; Freeman, B. D.; Pinnau, I . *Polymeric Materials: Science and Engineering* **1997**, *77*, 267.

Tabler, D. C. Phillips Petroleum Company, Report 10052-85, 1985.

Tamon, H.; Kitamura, K.; Okazaki, M. *A. I. Ch. E.* **1996**, *42*(2), 422.

Thompson, H. S. *J. Roy. Agr. Sco. Engl.* **1850**, *11*, 68.

Tooper, E. B.; Wirth, L. F. *Ion Exchange Technology*; Nachod F. C.; Schubert J., Eds.; Academic Press: New York, 1956; p 7.

Toth, J. *Acta. Chim. (Budapest)* **1971**, *69*(3), 311.

Toth, J. *J. Colloid and Interface Science* **1997**, *185*, 228.

Triebe, R. W.; Tezel, F. H.; Khulbe, K. C. *Gas. Sep. Purif.* **1996**, *10*(1), 81-84.

Quinn, H. W.; Tsai, J. H. *Advances in Inorganic Chemistry and Radiochemistry: Olefin Complexes of the Transition Metals*; Academic Press: New York, **1969**; Vol. 12, p 217.

Tucher, W. *Oil Gas J.* **1959**, *57*, 94.

Van Ness, H. C. *I & E C Fundamentals* **1969**, *8*(3), 464.

Vansant, E. F. *Separation Technology*; Elsevier: New York, 1994; p 413.

Vickers, T. J.; Wang, H.; Mann, C. K. *Applied Spectroscopy* **1995**, *49*(1), 127.

Way, J. T. *J. Roy. Agr. Soc. Engl.* **1850**, *11*, 313.

Wheaton, R. M.; Hatch, M. J. *Ion Exchange*; Marinsky, J., Ed.; Marcel Dekker: New York, 1969; Vol. 2.

Wuchter, R. B. U. S. Patent 3 791 996, 1974; *Chem. Abstr.* **1973**, *79*(5), 79747m, 44.

Xie, Y.; Bu, N.; Liu, J.; Yang, G.; Qiu, J.; Yang, N.; Tang, Y. U. S. Patent 4 917 711, 1990; *Chem. Abstr.* **1988**, *109*(6), 95234k, 113.

Yang, R. T. *Gas Separation by Adsorption Processes*; Butterworths: Boston, 1987.

Yang, R. T.; Cheng, L. S. *Adsorption* **1995**, *1*, 61-75.

Yang, R. T. ; Chue, K.; Kim, J.; Cho, S.; Han, S.; Wu, Z. *Ind. Eng. Chem. Res.* **1997**, *36*, 2749-2756.

Yang, R. T.; Kikkinides, E. S. *A. I. Ch. E.* **1995**, *42*(3), 509.

Yates, D. J. C.; Carter, J. L.; Lucchesi, P. J.; Elliott, J. J.; Kevorkian, V. *Phy. Chem.* **1966**, *70*(4), 1126.

Yasuda, H.; Tamai, H.; Ikeuchi, M.; Kojima, S. *Adv. Mater.* **1997**, *9*(1), 55.

Youchang, X.; Naifang, Y.; Yingjun, L; Youqi, T. *Scientia Sinica Series B* **1983**, *26*(4), 337.

Zundel, G. *Hydration and Molecular Interation*; Academic Press: New York, 1969.

APPENDIX A

THERMAL GRAVIMETRIC ANALYSIS SUPPLEMENTS

Calculations

Table 30. Ethylene Adsorption on 61% Ag(I) Exchanged Amberlyst 15 Resin

ethylene	helium	vacuum weight	mixture weight	buoyancy correction	ethylene uptake	ethylene uptake
mole fraction	mole fraction	mg	mg	mg	mg	mmol/g
0	1	53.96	53.96	0	0	0
0.2	0.8	53.96	55.194	0.031	1.265	0.83576796
0.4	0.6	53.96	55.365	0.057	1.462	0.96592313
0.6	0.4	53.96	55.458	0.086	1.584	1.04652684
0.8	0.2	53.96	55.528	0.113	1.681	1.11061339
1	0	53.96	55.574	0.135	1.749	1.15554005

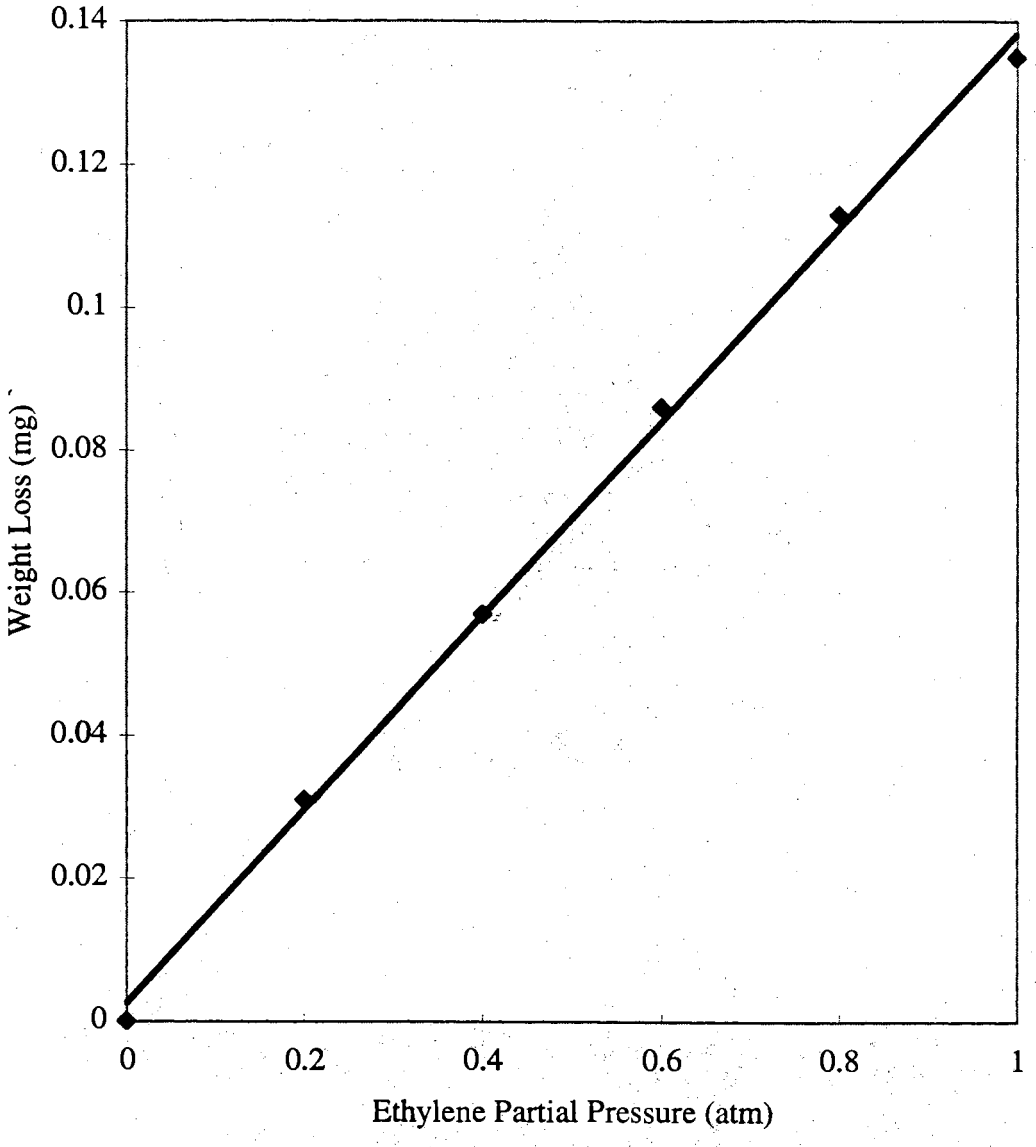

Figure 78. Ethylene buoyancy correction.

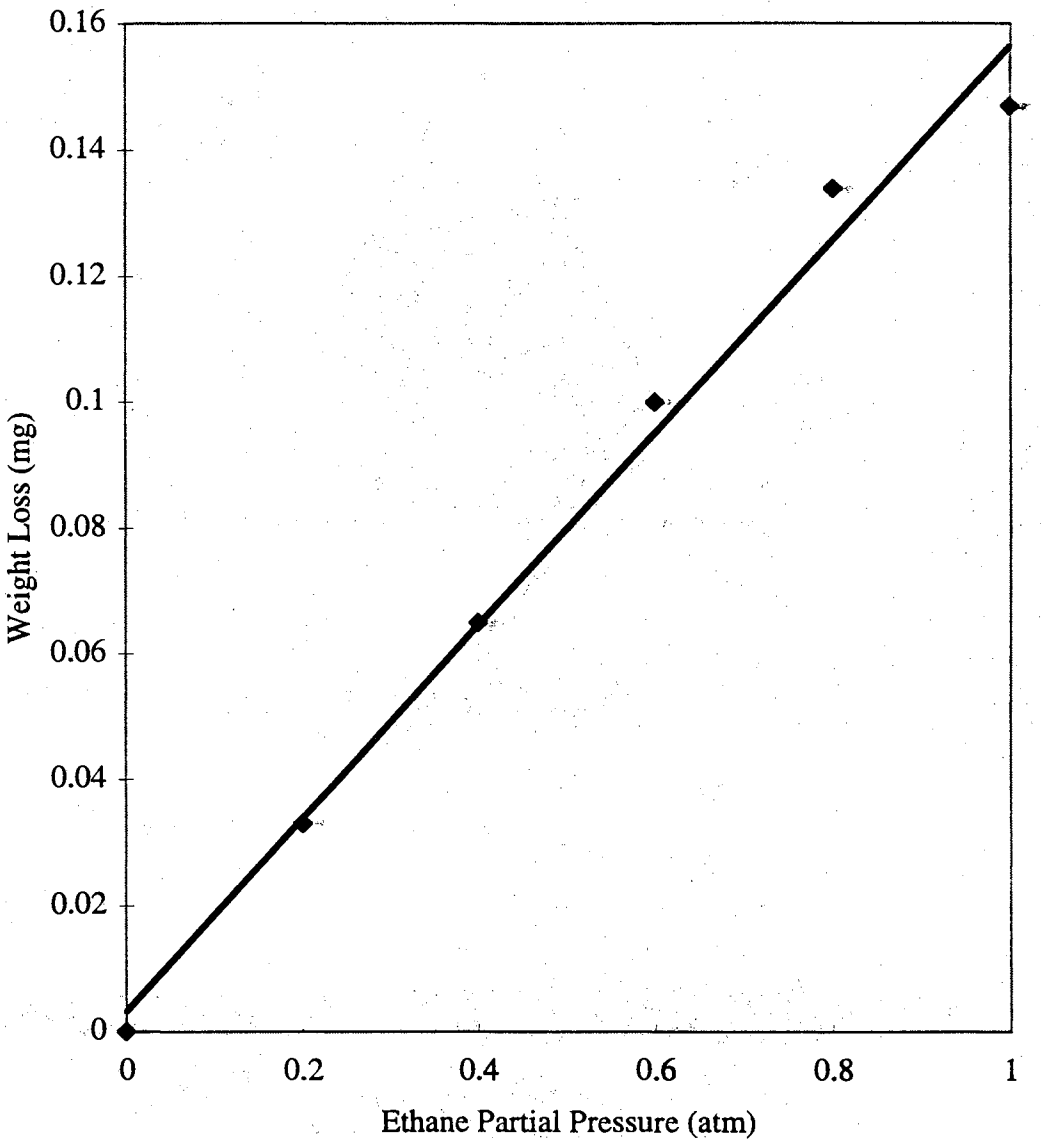

Figure 79. Ethane buoyancy correction.

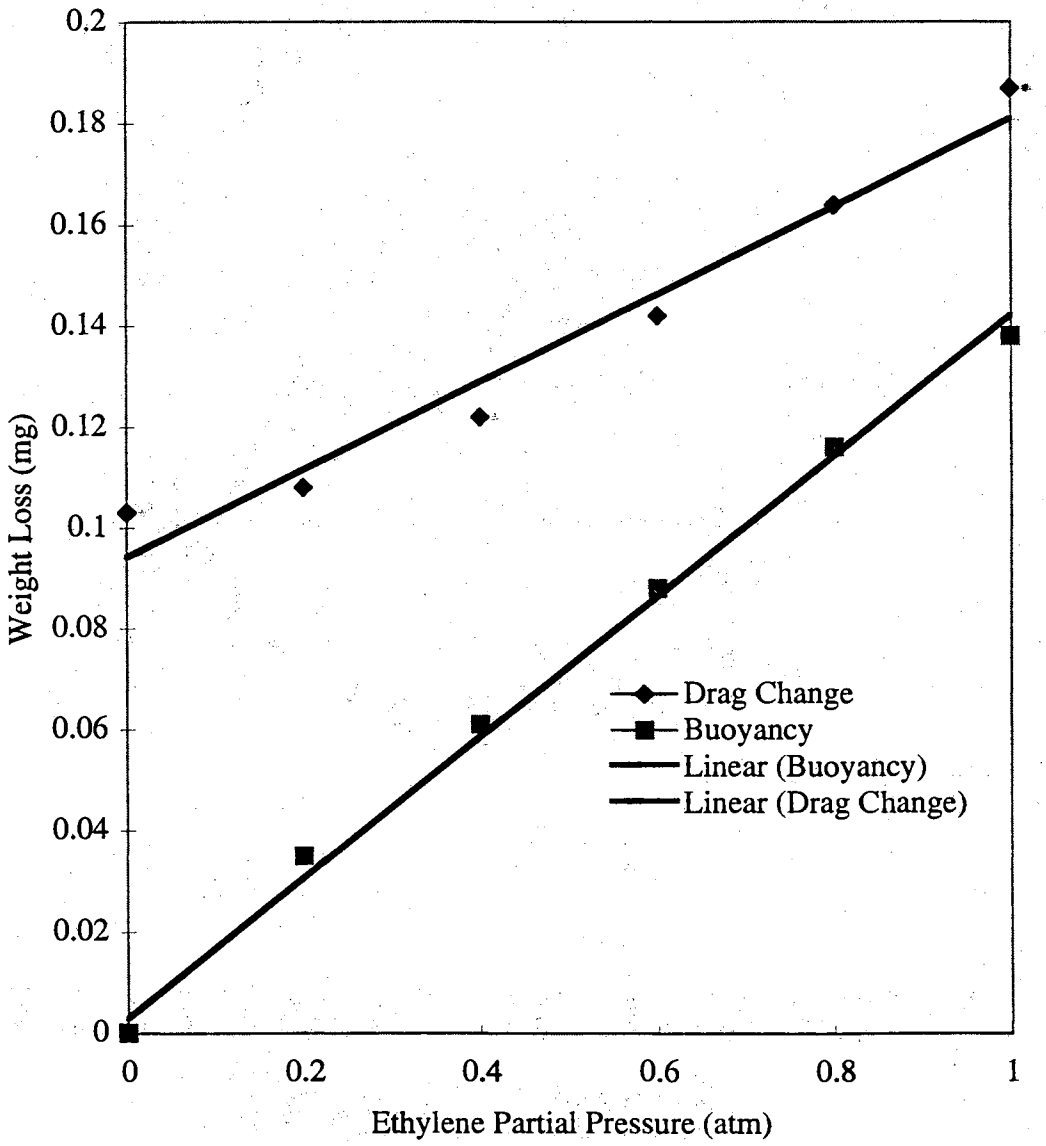

Figure 80. Ethylene drag and buoyancy corrections.

APPENDIX B

MULTICOMPONENT DESORPTION ANALYZER SUPPLEMENTS

Calculations

Table 31. Void Space of 185.39 mg of 61% Ag(I) Exchanged Amberlyst 15 Resin in MDA Loop

1st trial						
atm press.	atm press.	trap press.	trap press.	trap vol.	loop vol.	total loop vol.
mm Hg	atm	psi	atm	mL	mL	mL
747.3	0.98329	0.24	0.01633	4.8496	80.546	80.545965
747.3	0.98329	0.18	0.01225	4.8496	60.409	140.95544
747.3	0.98329	0.13	0.00885	4.8496	43.629	184.5845
747.3	0.98329	0.1	0.0068	4.8496	33.561	218.14532
747.3	0.98329	0.09	0.00612	4.8496	30.205	248.35006
747.3	0.98329	0.07	0.00476	4.8496	23.493	271.84263
747.3	0.98329	0.05	0.0034	4.8496	16.78	288.62304
747.3	0.98329	0.02	0.00136	4.8496	6.7122	295.33521
2nd trial						
747.3	0.98329	0.23	0.01565	4.8496	77.19	77.189884
747.3	0.98329	0.18	0.01225	4.8496	60.409	137.59936
747.3	0.98329	0.13	0.00885	4.8496	43.629	181.22842
747.3	0.98329	0.1	0.0068	4.8496	33.561	214.78924
747.3	0.98329	0.07	0.00476	4.8496	23.493	238.28181
747.3	0.98329	0.06	0.00408	4.8496	20.136	258.41831
747.3	0.98329	0.05	0.0034	4.8496	16.78	275.19872
747.3	0.98329	0.04	0.00272	4.8496	13.424	288.62304
747.3	0.98329	0.02	0.00136	4.8496	6.7122	295.33521

Table 32. Composition of Binary Inlet Stream

run #	time	ethene	ethane	ethene	ethane	ethene
	min	% comp	% comp	gc area	gc area	mole cal.
1	10	20	80	40078	149208	1.303E-07
2	20	20	80	40078	149208	1.303E-07
3	30	20	80	40078	149208	1.303E-07
4	40	20	80	40078	149208	1.303E-07
total	40	20	80	40078	149208	1.303E-07

ethane	ethene	ethane
mole cal.	%	%
4.366E-07	22.9822	77.0178
4.366E-07	22.9822	77.0178
4.366E-07	22.9822	77.0178
4.366E-07	22.9822	77.0178
4.366E-07	22.9822	77.0178

Table 33. Total Gas Desorbed from 61% Ag(I) Exchanged Amberlyst 15 Resin.

press.	pressure.	volume	mixture
psia	atms	L	mole
5.34	0.36336665	0.00484965	7.2795E-05
0.97	0.06600480	0.00484965	1.3223E-05
0.54	0.03674494	0.00484965	7.3613E-06
0.44	0.02994032	0.00484965	5.9981E-06
7.29	0.49605672	0.00484965	9.9377E-05

Table 34. Composition of Gas Mixture Desorbed from 61% Ag(I) Exchanged Amberlyst 15 Resin.

ethene	ethane	ethene	ethane	ethene	ethane
gc area	gc area	mole cal.	mole cal.	%	%
65148	13674	1.863E-07	6.034E-08	75.5314	24.4686
12767	514	6.930E-08	2.885E-08	70.6055	29.3945
0	0	4.079E-08	0	100	0
0	0	4.079E-08	0	100	0
77915	14188	2.148E-07	6.157E-08	77.7194	22.2806

Table 35. Gases Desorbed from 61 % Ag(I) Exchanged Amberlyst 15 Resin

ethene	ethane
mole	mole
5.4983E-05	1.7812E-05
9.3362E-06	3.8868E-06
7.3613E-06	0
5.9981E-06	0
7.7236E-05	2.2142E-05

Table 36. Gases in Void Space of Loop Packed with 61% Ag(I) Exchanged Amberlyst 15 Resin

volume	atm press.	mixture	ethene	ethane
L	atm	mole	mole	mole
0.000298	1.003634	1.237E-05	2.843E-06	9.527E-06
0.000298	1.003634	1.237E-05	2.843E-06	9.527E-06

Table 37. Gases Adsorbed on 61% Ag(I) Exchanged Amberlyst 15 Resin

ethene	ethene total	ethane	ethane total
mole	mole	mole	mole
5.2140E-05	5.2140E-05	8.2846E-06	8.2846E-06
9.3362E-06	6.1476E-05	3.8868E-06	1.2171E-05
7.3613E-06	6.8838E-05	0	1.2171E-05
5.9981E-06	7.4836E-05	0	1.2171E-05
7.4393E-05	7.4393E-05	1.2615E-05	1.2615E-05

resin wt.	ethylene	ethane
g	mmol/g	mmol/g
0.19254	0.27080144	0.04302788
0.19254	0.31929119	0.06321511
0.19254	0.35752374	0.06321511
0.19254	0.38867618	0.06321511
0.19254	0.38637468	0.06551661

Table 38. Ethylene/Ethane Adsorption Ratio and Selectivity of 61 % Ag(I) Exchanged Amberlyst 15 Resin

adsorption ratio	ethylene	ethane	selectivity
	mole frac.	mole frac.	
6.293626639	0.22982169	0.77017831	21.0911983
5.050868100	0.22982169	0.77017831	16.9264666
5.655668807	0.22982169	0.77017831	18.9532744
6.148469382	0.22982169	0.77017831	20.6047474
5.897354341	0.22982169	0.77017831	19.7632108

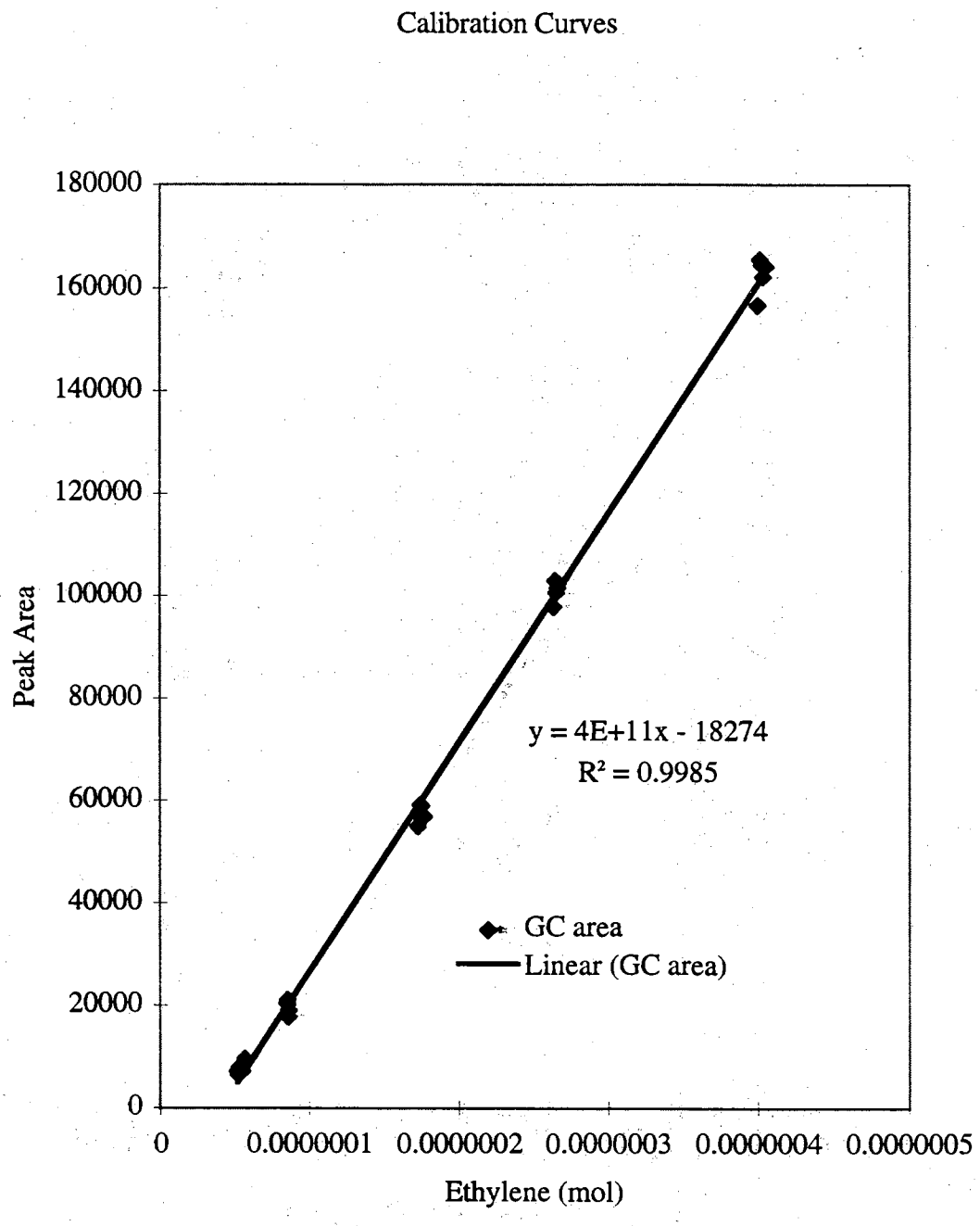

Figure 81. Ethylene calibration curve.

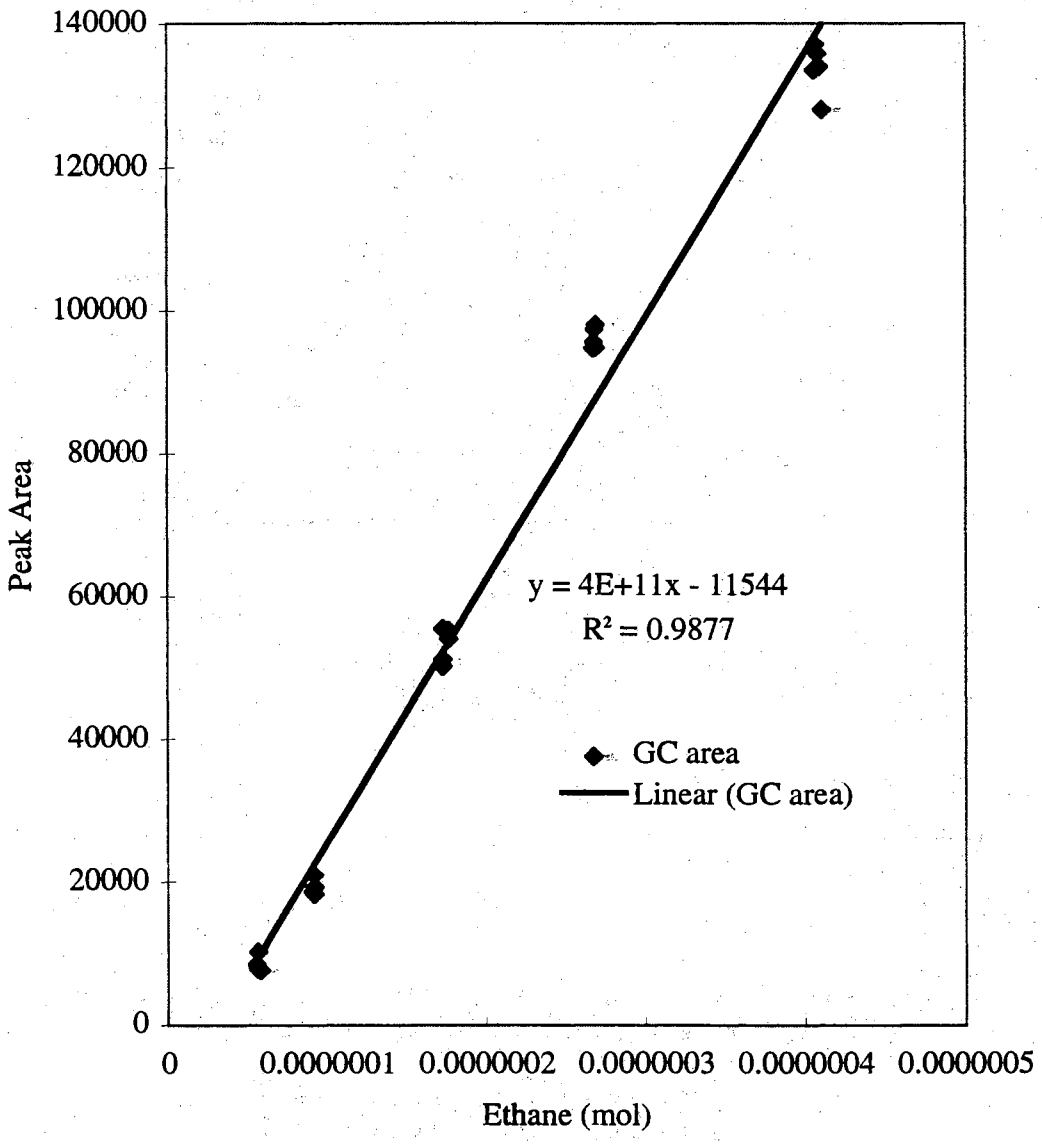

Figure 82. Ethane calibration curve.

VITA

James Earl Graham

Candidate for the Degree of

Doctor of Philosophy

Thesis: EVALUATION OF ADSORBENTS FOR THE SEPARATION OF OLEFINS FROM MULTICOMPONENT PROCESS STREAMS

Major Field: Chemistry

Biographical:

Personal Data: Born in Calico Rock, Arkansas, on November 5, 1970 the son of Vernon and Lola F. Graham. Married in Batesville, Arkansas, on July 2, 1994 to Tammy D. Meitzen.

Education: Graduated from Heber Springs High School, Heber Springs, Arkansas, in May 1989; received Bachelor of Science degree in Chemistry from Lyon (Arkansas) College, Batesville, Arkansas, in May 1993. Completed the requirements for the Doctor of Philosophy degree with a major in Chemistry at Oklahoma State University in May 1998.

Experience: Employed by Wal Mart during high school; employed by Lyon (Arkansas) College as a teaching assistant, mentor, community activity chairman, residence hall assistant, and counselor during undergraduate career; employed by Arkansas Eastman as a development lab technician in the summer of 1992; employed by Oklahoma State University Chemistry Department as a research and teaching assistant from 1993 to present.

Professional Memberships: American Chemical Society, Chi Beta Phi, Tau Kappa Epsilon.